UNIVERSITÀ
DEGLI STUDI
DI PADOVA

Sede Amministrativa: Università degli Studi di Padova
Dipartimento di Biologia

SCUOLA DI DOTTORATO DI RICERCA IN BIOSCIENZE E BIOTECNOLOGIE
INDIRIZZO: GENETICA E BIOLOGIA MOLECOLARE DELLO SVILUPPO
CICLO XXVIII

Investigating the role of extracellular matrix in regulating signaling pathways and embryonic development

Direttore della Scuola: Ch.mo Prof. Paolo Bernardi
Coordinatore d'indirizzo: Ch.mo Prof. Rodolfo Costa
Supervisore: Ch.mo Prof. Paolo Bonaldo

Dottoranda: Valeria Trapani

Index

Abstract ..... **I**

Riassunto ..... **III**

Chapter I

1. Introduction **1**

1.1. The extracellular matrix **1**

1.1.1. The extracellular matrix functions 1

1.1.2. The extracellular matrix components 3

1.1.2.1. The elastic fibers 7

1.1.2.1.1. The Emilin/Multimerin family 8

1.1.2.1.1.1. The Emilin/Multimerin family in mouse 9

1.1.2.1.1.2. The Emilin/Multimerin family in zebrafish 10

1.1.2.1.2. Emilin3 12

1.2. The notochord **14**

1.2.1. The notochord functions 14

1.2.1.1. Structural function of the notochord 14

1.2.1.2. Signaling function of the notochord 15

1.3. The Hedgehog signaling pathway **16**

1.3.1. Modulation of the Hedgehog signaling activity 16

1.3.1.1. Biosynthesis of Hedgehog ligands 17

1.3.1.2. Secretion and propagation of Hedgehog ligands 17

1.3.1.3. Modulation of the Hedgehog signal reception 17

1.3.1.4. Intracellular transduction of the Hedgehog signal 18

1.3.1.5. Hedgehog target genes 19

1.3.2. The Hedgehog signaling in zebrafish 19

1.3.2.1. Zebrafish Hedgehog genes and mutants 19

1.3.2.2. Hedgehog signaling in zebrafish development 21

1.4. Structural and signaling alterations after ablation of peri-notochordal basement membrane proteins **22**

Emilin3 is required for notochord sheath integrity and interacts with Scube2 to regulate notochord-derived Hedgehog signals **27**

The notochord: structure and functions **51**

References **77**

Chapter II

1. Introduction 91

1.1. Collagen VI 91

1.1.1. Collagen VI chain structure 91

1.1.2. Collagen VI structure and assembly 93

1.1.3. Collagen VI functions and tissue distribution 93

1.1.3.1. Collagen VI function in skeletal muscle 94

1.1.3.1.1. Collagen VI null mouse model and therapeutic approaches to ameliorate muscle phenotype 96

1.1.3.2. Collagen VI function in nervous system 98

1.1.4. Collagen VI in zebrafish animal model 100

1.2. The CRISPR/Cas9 genome editing technology 103

1.2.1. Generation of loss-of-function frameshift mutations in zebrafish using CRISPR/Cas9 105

1.2.1.1. Cas9 modification 106

1.2.1.2. Single-guide RNA design 106

1.2.1.3. *In vivo* introduction and identification of Cas9–sgRNA-induced Indels 108

2. Materials and methods 111

2.1. Database searches and bioinformatic analysis 111

2.2. Zebrafish husbandry and embryo manipulations 111

2.3. Microinjection 112

2.3.1. Morpholino oligonucleotides 112

2.3.2. *In vitro* mRNA synthesis 113

2.4. Plasmid constructions 114

2.4.1. Agarose gel electrophoresis 114

2.4.2. Restriction digestion 114

2.4.3. Dephosphorylation 115

2.4.4. Column DNA purification 115

2.4.4.1. DNA extraction from agarose gel 115

2.4.4.2. Purification of DNA by Centrifugation 115

2.4.5. Ligation 116

2.4.6. Heat shock transformation 116

2.4.7. Purification of plasmid DNA 116

2.4.7.1. MiniPrep 116

2.5. Quantitative RT-PCR (qRT-PCR) 117

2.6. Whole-mount *in situ* hybridization 118
2.6.1. Preparation of antisense digoxigenin (DIG) labelled RNA probes 118
2.6.2. Preparation of embryos 119
2.6.3. Pre-hybridization treatments and hybridization 119
2.6.4. Post-hybridization washes 120
2.6.5. Staining 120
2.6.6. Imaging 121
2.6.7. Vibratome sectioning 121
2.7. Western blot analysis 121
2.8. Whole mount immunofluorescence 122
2.9. Birefringence assay 122
2.10. Evans blue dye (EBD) injection 123
2.11. Analysis of motor axons defects 123
2.12. CRISPR/Cas9-mediated mutagenesis protocol 123
2.12.1. Target site selection 123
2.12.2. Generation of sgRNA 123
2.12.3. Generation of Cas9 mRNA 125
2.12.4. Injection of Cas9 mRNA and sgRNA 125
2.12.5. Determination of somatic indel frequency 126

3. Results 129
3.1. Characterization of the zebrafish genes coding for collagen VI chains 129
3.1.1. Conserved synteny for zebrafish Collagen VI genes 130
3.1.2. Zebrafish collagen VI chains share high structural similarities with their mammalian counterparts 130
3.2. Expression pattern of zebrafish Collagen VI chains during development 131
3.3. Knockdown of *col6a1* gene leads to developmental defects 132
3.3.1. Efficacy of morpholinos-mediated knock-down of *col6a1* gene in zebrafish embryos 132
3.3.2. Analysis of macroscopic phenotypic alterations of *col6a1* morphants 132
3.3.3. Muscle development is affected in collagen VI morphant embryos 133
3.3.3.1. Knockdown of *col6a1* interferes with muscle integrity 133
3.3.3.2. Collagen VI ablation affects myofibers and myosepta development 134

3.3.3.3. *col6a1* knockdown causes contraction-induced myofibers detachment..... 135
3.3.4. Neuromuscular development is affected in collagen VI morphant embryos..... 135
3.3.4.1. *col6a1* knockdown leads to primary motor neuron defects and abnormal AchRs patterning..... 135
3.3.5. Collagen VI knockdown results in alterations of Wnt and BMP signaling pathways..... 136
3.4. Generation of a *col6a1* null zebrafish line with CRISPR/Cas9 technology..... 137
4. Discussion..... 141
5. Figures..... 147
References..... 187

Abstract

During my PhD I was involved in different projects exploiting the zebrafish animal model in order to analyse the role of extracellular matrix proteins in regulating signaling pathways.

In particular, in the first period of my PhD, I focused my attention on the *in vivo* function of Emilin3 in zebrafish animal model, with the aim of fully understanding the biological role of this extracellular matrix glycoprotein, both in embryonic development and in tissue homeostasis. In particular, I have contributed to *in vivo* studies, using several genetic approaches. These results demonstrated that Emilin3, a component of the peri-notochordal basement membrane, is required not only for the proper maturation of the notochord, but also for the regulation of Hedgehog signals derived from the notochord itself. Moreover, I also contributed to *in vitro* experiments that allowed us to understand how Emilin3 limits Hedgehog signals secreted by the notochord. We found that Emilin3 is able to interact with Scube2, a secreted factor that acts in a permissive way in the generation of Hedgehog ligand gradients. In this context, I generated several deletion constructs of Emilin3 and Scube2, which allowed us to determine the specific action of Emilin3, revealing that this extracellular matrix protein is able to interact with the EGF motifs of Scube2. Overall, this study revealed that the interaction between Emilin3 and Scube2 within the peri-notochordal basement membrane is essential for the proper notochord patterning activity. Such results were published in a full article in *Development* (Corallo *et al*., 2013). Alongside this work, my increasing interest on notochord patterning and functions led me to contribute to two review manuscripts on this subject (Corallo *et al.*, *Cell Mol Life Sci* 2015; Corallo *et al.*, *J Cell Sci,* in preparation).

Since the second year of my PhD, I independently started new functional studies in zebrafish focused on the role of Collagen VI during embryonic development. Mutations of Collagen VI genes in humans are causative for different forms of inherited muscle diseases, including Bethlem myopathy and Ullrich dystrophy. Previous work carried out in Collagen VI knockout (*Col6a1*$^{-/-}$) mice revealed a crucial role for this extracellular matrix component in tissues homeostasis, and in particular in skeletal muscles, and demonstrated that ablation of Collagen VI has a remarkable impact on cell survival and organelle turnover. Indeed, these studies showed that collagen VI deficiency is causative for the myopatic syndrome of the

mouse model and patients, characterized by spontaneous apoptosis, organelles alterations and deficient autophagy in muscle fibers. Although past work demonstrated that Collagen VI is broadly and dynamically expressed in a large number of tissues during embryonic development and postnatal life, no study until now ever assessed which roles Collagen VI plays during development and whether and how this major extracellular matrix component is regulating signaling pathways. Therefore, the aim of this part of my PhD work was to investigate which signaling pathways and tissues are affected by ablation of Collagen VI, in particular during embryonic development and using zebrafish as a model organism.

Towards this aim, I first carried out a characterization of the structure, organization and gene expression of Collagen VI chains in zebrafish. These information were the basis for further functional studies. By means of morpholino-mediated Collagen VI knockdown in different transgenic reporter zebrafish lines, I identified not only an alteration of muscle fibers development, but also an axonal growth defect of motor neurons in Collagen VI morphant embryos. In addition, knockdown of Collagen VI led to variations in Wnt and BMP signals during embryogenesis, thus suggesting a possible correlation between the developmental defects and the signaling pathway alterations caused by Collagen VI knockdown. Finally, I successfully applied the CRISPR/Cas9 technology for *in vivo* site-specific mutagenesis, generating a zebrafish *col6a1* VI null line that represents a valuable tool for the thorough understanding of the functions of Collagen VI during development and in regulating signaling pathways.

Riassunto

Durante i tre anni di dottorato ho preso parte a diversi progetti, in cui ho utilizzato l'organismo modello di zebrafish per capire il ruolo di diverse proteine della matrice extracellulare nel regolare le vie di trasduzione del segnale.

Il mio primo progetto di dottorato ha riguardato lo studio di funzione della proteina della matrice extracellulare Emilina3 nel modello animale di zebrafish, al fine di comprendere appieno il ruolo biologico di questa glicoproteina nello sviluppo embrionale e nell'omeostasi tissutale.

In particolare ho contribuito agli esperimenti *in vivo*, sfruttando tecniche di *forward genetic*, che dimostrano come Emilina3, componente della matrice extracellulare che sta attorno alla notocorda, è necessaria non solo per la corretta maturazione della notocorda ma anche e per la regolazione dei segnali di Hedgehog derivanti dalla notocorda stessa. Inoltre, ho contribuito agli esperimenti *in vitro* che hanno permesso di comprendere come Emilina3 limiti i segnali di Hedgehog secreti dalla notocorda: questa proteina è in grado di interagire e sequestrare un fattore secreto che agisce in maniera permissiva nel rilascio dei ligandi di Hedgehog, Scube2. In questo contesto, ho generato diversi costrutti di Emilina3 e Scube2, deleti nei loro diversi domini, necessari per saggi di legame *in vitro* che hanno permesso di comprendere che Emilina3 è in grado di interagire specificatamente con le ripetizioni EGF di Scube2. Nel complesso, questo studio ha stabilito per la prima volta come l'interazione tra Emilina3 e Scube2 nella membrana basale della notocorda è fondamentale per la corretta attività di *patterning* della notocorda stessa. Tali ricerche sono state oggetto di pubblicazione (Corallo *et al.*, *Development* 2013). A margine di questo lavoro, le attività di documentazione e studio delle più recenti scoperte riguardo la notocorda hanno portato all'elaborazione di due *reviews* sull'argomento (Corallo *et al.*, *CMLS* 2015; Corallo *et al.*, *JCS* in preparazione).

A partire dal secondo anno di dottorato, ho utilizzato il modello animale di zebrafish per avviare in maniera indipendente studi funzionali, volti a comprendere il ruolo del collagene VI durante lo sviluppo embrionale. Numerosi studi precedentemente effettuati dal nostro gruppo sui topi privi di collagene VI (*Col6a1* knockout) hanno rivelato un ruolo cruciale di tale componente della matrice extracellulare nell'omeostasi dei tessuti, ed in particolare di quello muscolare. Tali studi dimostrano che il deficit di collagene VI determina l'insorgenza di una

sindrome miopatica a carico dei muscoli, caratterizzata da apoptosi spontanea, alterazioni agli organelli e deficit di autofagia nelle fibre muscolari. Analoghe alterazioni sono state evidenziate nei muscoli dei pazienti affetti da miopatia di Bethlem e distrofia di Ullrich, due patologie umane legate a mutazione dei geni codificanti per il collagene VI. Il mio progetto è nato da queste premesse: l'obiettivo è comprendere appieno, in assenza del collagene VI, quali alterazioni tissutali e molecolari avvengono utilizzando l'organismo modello di zebrafish

In particolare, ho condotto una caratterizzazione della struttura, dell'organizzazione genica e dell'espressione delle catene del collagene VI nell'organismo modello di zebrafish. Tutte queste informazioni sono alla base per studi funzionali. In particolare, attraverso il silenziamento genico mediato da morfolino del collagene VI in diverse linee transgeniche reporter di zebrafish, ho iniziato a indagare quali vie di segnalazione e tessuti sono affetti dall'assenza di questa importante componente della matrice extracellulare. In particolare ho individuato non solo un'alterazione dello sviluppo delle fibre muscolari, ma anche un difetto di crescita assonale dei motoneuroni negli embrioni morfanti per il collagene VI. Inoltre, ho anche osservato un'alterazione nelle vie di segnale di Wnt e BMP; e in futuro si prospetta di trovare una correlazione tra le alterazioni di sviluppo dei tessuti e quelle delle vie di segnale. In parallelo, ho applicato con successo la nuova tecnica di mutagenesi sito-specifica CRISPR/Cas9, generando una linea di zebrafish priva di collagene VI, al fine di confermare ed estendere i risultati ottenuti. Questi studi sono di particolare rilievo, in quanto per la prima volta indagano alterazioni finora sconosciute dei meccanismi molecolari legati a deficit di collagene VI, aprendo così la strada ad ulteriori studi nei pazienti affetti da patologie legate al collagene VI.

Chapter I

1. Introduction

1.1. The extracellular matrix

The extracellular matrix (ECM) is the dynamic and multifaceted space composed of secreted macromolecules, proteins and polysaccharides, produced by different cell types that are locally assembled into an organised three-dimensional network in which cells are layered and anchored to form specialized tissues and organs (Hay, 1981). The ECM is synthesized and secreted by embryonic cells from the two-cell stage and it is a component of the environment of all cell types, although the composition of the ECM and the spatial relationships between cells and ECM differ between tissues (Adams and Watt, 1993).

1.1.1. The extracellular matrix functions

Distinct groups of ECM molecules are able to fulfill multiple functions, thus playing a crucial role for tissue homeostasis. First, the ECM provides the architectural framework for tissues. Indeed, through physical cell-matrix interactions, it imparts positional information as well as specific physical properties, such as resilience and elasticity, necessary for tissue integrity. For instance, ECM proteins define tissue boundaries and organize cell layers by means of basement membranes. Moreover, the ECM functions as adhesive substrate for migration of different cell types. In the interstitial spaces, the ECM provides the structural

framework needed to promote and, in some cases, restrict cell movements. Moreover, the ECM can sense and transduce mechanical signals. In particular, it activates intracellular signaling through interaction with cell surface receptors, engages cytoskeletal machinery and synergize with growth factor signaling. The role of ECM in cell adhesion and cell signaling via surface receptors, such as integrins, has received much attention (Hynes, 2002; Berrier and Yamada, 2007; Legate *et al*., 2009). This "sensing" of embedded information in the ECM via specialized receptors at the cell surface can have a profound influence on cell behaviors by affecting not only adhesive functions but also cell polarity, migration and other intracellular signals that regulate cell survival, proliferation and differentiation. ECM signals are arguably at least as important as soluble signals in governing these processes (Hynes, 2009). Remarkably, short and long range physical forces generated as a consequence of morphogenetic movements can also alter the availability of cell-interactive and other functional domains embedded within the ECM and regulate cellular response to the extracellular environment. More recently, the biomechanical properties of the matrix, such as stiffness and deformability, have also been recognized to provide inputs for cells behavior (Discher *et al*., 2009; Geiger *et al*., 2009; Dupont *et al*., 2011).

As a matter of fact, the ECM is also able to situate, concentrate, sequester and store growth factors and other signaling molecules. The consequence of such interactions may be to restrict or promote access of ligands to related cell-surface receptors, as well as to allow spatio-temporal modulation of factor release and organization of morphogen gradients. Indeed, soluble factors can be maintained in the ECM, which acts as a reservoir, or – in the presence of appropriate forces or after proteolytic degradation – be released from the matrix for the subsequent binding to their cell surface receptors (McCawley and Matrisian, 2001). For instance, many growth factors (*e.g.* fibroblast growth factors and vascular endothelial growth factors) bind avidly to heparin and heparan sulfate, a component of several matrix proteoglycans (PGs), which in this way act as a reservoir and may assist in establishing stable gradients of growth factors. It is also recognized that growth factors can be released from the ECM by degradation of ECM proteins or of the glycosaminoglycan components of PGs. In this way, the ECM facilitates crosstalk between growth factor receptors and ECM receptors. Indeed, the ECM is able to present growth factors to their receptors and allow spatial distribution of ECM-bound surface molecules. On the other hand, some growth factors bind to their

signaling receptors with heparan sulfate as a cofactor. The binding of fibroblast growth factor to its receptor depends on the simultaneous binding to heparan sulfate chains (Mohammadi *et al*., 2005), and transforming growth factor-β (TGF-β) ligands bind first to integral membrane PGs that "present" these ligands during signaling (Shi and Massague, 2003). Moreover, several ECM proteins contain receptor binding motifs, such as the RGD sequence (adhesive Arg-Gly-Asp), that can be either openly exposed, acting as ligands for canonical growth factor receptors, or hidden within any given matrix molecule (Davis *et al*., 2000). The latency of cryptic endogenous signaling motifs of ECM proteins or bound signaling molecules is regulated by proteinases, such as matrix metalloproteinases (MMPs) (Davis *et al*., 2000; Nagase and Woessner, 1999). Intrinsic domains of ECM proteins, such as the repeated epithelial growth factor (EGF)-like domains present in laminins (Schenk *et al*., 2003) and tenascins (Swindle *et al*., 2001), can bind cell surface receptors and modulate their signaling by acting as solid phase ligands (Engel, 1989), or can be fragmented and released by proteolysis (for instance, by MMPs) and presented as soluble ligands.

ECM protein networking has a crucial role in modulating cell behaviour and homeostasis. In parallel, abnormalities in ECM structure and composition and the establishment of a modified cross-talk between altered ECM proteins and cells have been linked to an increasing number of pathologies, such as tumorigenesis, inflammation processes, and neuromuscular diseases (Tsang *et al*., 2010; Hubmacher and Apte, 2013). Mutant and knockout animal models for ECM molecules provide a valuable tool for translational studies and for the mechanistic understanding of human diseases linked to ECM defects. The deeper understanding of diverse biological activities and properties of the ECM components will be crucial for developing novel targeted therapeutic interventions for disease treatment.

1.1.2. The extracellular matrix components

In keeping with its various functions, the ECM has a complex molecular composition. Matrix proteins are large and complex with multiple distinct domains, and are highly conserved among different taxa. Many ECM proteins have dozens of individually folded domains, but the functions of only few of these domains were elucidated in detail until now. The matrix is composed by major groups of secreted macromolecules with disparate evolutionary origins. The vertebrate genomes have hundreds of different genes coding for ECM proteins. Many of these genes are ancient, such as those composing basement membranes (type IV collagen, laminins,

nidogen, perlecan, and type XV/XVIII collagens), which are found in most metazoans. However, many vertebrate ECM proteins and genes evolved much more recently, during evolution of the deuterostome lineage, and that expansion includes not only the expansion of preexisting families (for example, laminins and collagens) but also novel proteins (*e.g.*, fibronectins and tenascins) (Whittaker *et al*., 2006).

The ECM is mainly composed of fibrous proteins (typically collagens, fibronectin, elastin, and fibrillins) that allow mechanical strength and flexibility, embedded in a gel-like polysaccharide ground substance. In addition to fibrous structural proteins (*e.g.* collagens, elastin), glycosaminoglycans and proteoglycans, the ECM contains adhesion proteins (*e.g*. fibronectin, laminins, fibrillins) that link components of the matrix both to one another and to the cell surface. The differences between these major types of ECM result from variations on this general theme. ECM components also include enzymes able to modify these molecules, such as lysyl oxidase, and proteinases, such as the matrix metalloproteinases.

Glycosaminoglycans (GAGs) are linear unbranched heteropolysaccharides that contain repeating disaccharides composed mainly of N-acetylated hexosamines (N-acetyl-D-galactosamine or N-acetyl-D-glucosamine) and D-/L-hexuronic acid (D-glucuronic acid or L-iduronic acid). These molecules have remarkable physical properties provided by the abundance of carboxyl, hydroxyl and sulfate groups that define individual GAGs (*e.g.*, chondroitin-, dermatan-, keratan- and heparan-sulfates). With the exception of the non-sulfated GAG hyaluronan (HA), all sulfated GAGs are covalently linked to different core proteins to form proteoglycans (PGs). HA does, however, assemble with aggregating PGs and these interactions are critical for the formation of pericellular matrices. The transmembrane receptor for HA, CD44, also participates in the assembly of the pericellular matrix and the subsequent propagation of cell signals. Proteoglycans can contain between one to several hundred of GAGs chains attached usually to serine residues of a core protein. A variety of core proteins (ranging from 10 to >500 kDa) have been identified, rendering the proteoglycans a complex and heterogeneous group of macromolecules (Silbert and Sugumaran, 1995). Due to their high content of charged polysaccharides, GAGs and proteoglycans bind positively charged ions and trap water molecules to form hydrated gels, thus providing mechanical support to the ECM. This trapping of water in the interstitial spaces, in which GAGs reside, can open up pathways promoting the invasion and migration of cells. This mechanism has been suggested for HA, which is correlated with cancer metastasis and initiation

of cell migration (Toole, 2001). Besides acting in this way as structural components, both extracellular and cell-surface proteoglycans bind also several growth factors and other types of secreted proteins (*e.g.* proteases and protease inhibitors). Thus, proteoglycans can also contribute to the regulation of the metabolites and cell signaling (Scott, 2001; Hardingham *et al*., 1992). Indeed, the regulated expression of enzymes involved in GAG assembly can have important developmental consequences (Camenisch *et al*., 2000; Spicer *et al*., 2002).

ECM glycoproteins include different types of collagens as well as a large variety of non-collagenous proteins, such as laminins, tenascins, and fibronectin. Collagens are the most abundant fibrous proteins in the animal kingdom, constitutes up to 30% of the total protein mass of a multicellular animal and are mainly synthesized and secreted by fibroblasts. The most distinctive feature of all collagens is the triple-helical organization of their α-chain subunits, which contributes to the unique physical properties of these ECM proteins. In vertebrates, the collagen superfamily is composed of 28 different collagen types, which on the whole are the product of about fifty distinct α-chain polypeptides encoded by separate genes (Gordon and Hahn, 2010). Collagens are made of three polypeptide α chains that contain one or more regions with Gly-X-Y repeats, where the X and Y positions are frequently occupied by proline and 4-hydroxyproline, respectively. This repeating structure forms stable, rod-like, trimeric coiled coils, which can vary in lengths. The α-chains assemble in homo- or hetero-trimeric fashions to form triple helical structures (Ricard-Blum, 2011; Brodsky and Persikov, 2005). Based on the type of polymeric assemblies, the collagen superfamily can be divided into at least six different subgroups, with different three-dimensional structure and tissue distribution: *i)* fibril-forming collagens, such as types I, II, III, V, XI, XXIV, and XXVII; *ii)* fibril-associated collagens with interrupted triple helix (FACITs), such as types IX, XII, XIV, XVI, XIX, XX, XXI and XXII; *iii)* membrane-associated collagens with interrupted triple helices (MACITs), which include types XIII, XVII, XXIII, XXV; *iv)* beaded microfilaments (collagen type VI, XXVI, and XXVIII); *iv)* multiple triple-helix domains and interruptions (multiplexin), such as types XV and XVIII; *v)* anchoring fibrils (collagen type VII); and *vi)* network-forming collagens (types IV, VIII, and X) (Ricard-Blum, 2011). The organization, distribution and density of collagen fibrils and networks vary among different tissues, influencing the direction and magnitude of forces to which a given tissue is subjected. Collagens provide structural strength to all forms of matrices, including the strong fibers of tendons, the organic matrices

of bones and cartilages, the laminar sheets of basement membranes, the viscous matrix of the vitreous humor, and the interstitial ECM of the dermis and of capsules around organs. Beside forming fibrils or network-like structures that function in limiting the distension and thus providing the integrity of tissues, collagens fulfill a variety of other biological functions such as cell adhesion, growth, differentiation, motility and migration, thus playing a crucial role in supporting tissue development and maintaining the proper structure and function of different organs (Rozario and DeSimone, 2010).

In addition to collagens and proteoglycans, matrices contain about 200 different non-collagenous glycoproteins, which are represented by several protein families with diverse origins (Naba *et al*., 2012). Moreover, elastic fibers provide recoil to tissues that undergo repeated stretch (see description below). These proteins have many different functions, including the structural organization of ECM and cell adhesion. Indeed, these non-collagenous glycoproteins contain domains responsible for binding to a variety of other ECM proteins, polysaccharides, cell surface proteins and signaling molecules, such as growth factors and hormones. The bound growth factors can serve as reservoirs that can be released (*e.g.*, by proteolysis) or can be presented as solid-phase ligands by the ECM proteins (Hynes, 2009). Many of these ECM molecules are composed of multiple chains each encoded by distinct (*e.g.*, laminin trimers) or single (*e.g*., fibronectin dimers) genes. Further variation in protein sequence, structure and function can occur through alternative splicing of expressed transcripts, as in the case of fibronectin, depending on the developmental stage and the tissue-specific expression (Astrof *et al*., 2007; DeSimone *et al*., 1992; Ffrench-Constant and Hynes, 1989). The best-studied ECM glycoproteins are laminins (Yurchenco, 2011) and fibronectins (Schwarzbauer and DeSimone, 2011). Laminins comprise a family of cross-shaped, heterotrimeric extracellular glycoproteins and are the major components of the basal lamina of many different tissues, with >10 different possible trimeric combinations. Laminins are composed of a central α-chain, with a varying number of globular regions, and two chains (β- and γ-) with helical and globular regions. The trimeric proteins interconnect cell membranes and ECM molecules, binding also each other to form sheets in the basal lamina (Colognato and Yurchenco 2000). The structures of these glycoproteins are well known and exemplify the typical multimodular domain structure and the multimeric forms of ECM proteins. Another category of molecules is able to connect cells to ECM and to modulate interactions with plasma membrane receptors. These

are termed matricellular proteins or multifunctional adhesive proteins, such as thrombospondins and tenascins (Tsang *et al*., 2010; Hubmacher and Apte, 2013).

1.1.2.1. The elastic fibers

In order to fulfill their proper functions, different organs need to be elastic and flexible. These physical characteristics have been essentially required among multicellular organisms and maintained during evolution. Elastic fibers are ECM assemblies that give resiliency to the connective tissues, permitting long-range deformability and passive recoil without energy input. Importantly, elastin stretch is crucially limited by tight association with collagen fibrils, which impart tensile strength and limit tissue stretching and damage (Wise and Weiss, 2009). Elastic fibers are assembled in the early stages of the development and are very stable with very low or absent turnover. In adults, damaged elastic fibers are often repaired improperly and do not function normally (Wagenseil and Mecham, 2007). Elastic fibers are present within tissues as large networks composed of two discrete components, an amorphous core made of elastin, and peripheral microfibrils associated with the amorphous core. Genesis of elastic fibers involves deposition of tropoelastin (the soluble precursor of mature elastin) on a preformed template of fibrillin-rich microfibrils (Davis and Mecham, 1998). Secreted tropoelastin molecules assemble into fibers and become highly cross-linked to one another via their lysine residues by members of the lysyl oxidase enzyme family, which include lysyl oxydase (LOX), lysyl oxidase-like (LOXL)-1, -2 and -3, and LOXC (Borel *et al*., 2001; Lucero and Kagan, 2006). Mature elastic fibers are thus a complex network formed by an inner core of amorphous cross-linked elastin and an outer microfibrillar mantle, which are also essential for the integrity of the elastic fiber itself (Wise and Weiss, 2009). The main structural components of elastic-fiber-associated microfibrils are cysteine-rich glycoproteins of large size (~350 kDa), called fibrillins (fibrillin-1, -2, and -3) (Sakai *et al*., 1986, Zhang *et al*., 1994). Nevertheless, a large spectrum of different elastic-fibers-associated-molecules has been identified in the past years. Other components of microfibrils are microfibril-associated protein (MFAP)-1, -3 and -4 (Lausen *et al*., 1999) and microfibril-associated glycoproteins (MAGP)-1 and -2 (Hatzinikolas and Gibson, 1998), which are localized to the beaded region of microfibrils and play an important role as bridging molecules during elastic fiber assembly (Wagenseil and Mecham, 2007; Mecham and Gibson, 2015). Other molecules that co-localize with microfibrils are Latent TGF-β Binding Protein (LTBP)-1, -2, -3 and -4 (Gibson *et al*., 1995; Giltay *et*

al., 1997), fibulins, which participate in the formation of elastic fibers and are required for the proper assembly of mature elastic fibers (Papke and Yanagisawa, 2014), and Emilins (described in detail below).

1.1.2.1.1. The Emilin/Multimerin family

The "Emilin/Multimerin" family comprises five proteins, namely Emilin1, Emilin2, Emilin3, Multimerin1 and Multimerin2. The primary structure of these ECM proteins is composed by an N-terminal EMI domain, followed by a long central region with a high probability of forming coiled-coil structures, and a C-terminal region with high similarity to the globular C1q (gC1q) domain (Hayward *et al*., 1995; Doliana *et al*., 2000a, 2001; Christian *et al*., 2001). The EMI domain spans about 80 amino acids and is characterized by the presence of highly conserved cysteine residues located at regular positions (Doliana *et al*., 2000b). Moreover, the EMI domain is always located in a single copy at the N-terminal portion of the mature protein. The positions of the seven cysteine residues in the EMI domain are conserved: distances between C1 and C2, C5 and C6, and C6 and C7 are absolutely conserved, whereas minimal gaps are present between C2, C3 and C4 (Doliana *et al*., 2000). It has been demonstrated that the EMI domain of Emilin1 binds pro-TGF-β1, thereby preventing its proteolytic processing into the mature and active cytokine (Zacchigna *et al*., 2006). The gC1q domain was shown to be essential for the cell adhesion properties of Emilin1, and it was proposed that this domain is involved in the supramolecular organization and self-assembly of Emilin1 into multimers (Colombatti *et al*., 2000, Mongiat *et al*., 2000; Spessotto *et al*., 2003). Conversely, Emilin3 is the only protein of the family that lacks the gC1q domain in its C-terminal region (Leimeister *et al*., 2002; Doi *et al*., 2004). The roles of the Emilin/Multimerin proteins are far from being fully understood. The *in vivo* biological function of mammalian Emilins/Multimerins remains largely unknown, and until now only the phenotype of Emilin1 knockout mice was characterized in detail (Zacchigna *et al*, 2006). Emilin1 null animals show subtle structural alterations of the elastic fibers of the cells in the wall of large blood vessels (Zanetti *et al*., 2004). Notably, it has been demonstrated that Emilin1 null mice are affected by arterial hypertension due to increased TGF-β signaling in the vascular wall, consistent with the finding that Emilin1 is a regulator of TGF-β processing and activation. In addition, Emilin1 null mice display defects in the lymphatic system and skin (Danussi *et al*., 2008; Danussi *et al*., 2011). As the EMI domain of Emilin1 was found to interact with both elastin and fibulin-5 (Zanetti *et al*., 2004), it is possible that Emilin1 can stabilize

interactions among components of the elastic fibers by enabling them to attach properly to the cells. Emilin1 may regulate elastogenesis, by stabilizing the molecular interactions between elastic fibers components. Moreover, Emilin1 interacts with α4β1 and α9β1 integrins and may connect cells to elastic fibers by providing them with specific cell adhesion properties (Danussi *et al*., 2013). *In vitro* and *in vivo* studies pointed out that Emilin2 is an extracellular pro-apoptotic factor, a role that is exerted through a direct binding to death receptors (Mongiat *et al*., 2007). More recently, a significant antitumoral *in vivo* effect was also reported for Emilin2 (Mongiat *et al*., 2010).

1.1.2.1.1.1. The Emilin/Multimerin family in mouse

Previous work investigated the expression pattern of some Emilin/Multimerin genes during murine embryonic and postnatal development. A common hallmark of different members of the Emilin/Multimerin family is their abundance throughout the cardiovascular system and in the mesenchymal compartment of various organs (Braghetta *et al*., 2002, 2004; Leimeister *et al*., 2002). These studies in mice showed that individual Emilin/Multimerin genes have distinct expression patterns, although their territories of expression appear largely overlapping and the possibility of functional redundancy and mutual compensation was proposed (Braghetta *et al*., 2004). Among them, Emilin1 displays the most abundant and broad expression (Braghetta *et al*., 2002). *In situ* hybridization data showed that during mouse development Emilin3 has a dynamic expression pattern (Schiavinato *et al*., 2012), which only partially overlaps with that of other Emilin/Multimerin genes (Braghetta *et al*., 2004). Expression of Emilin3 in mouse was first detected at embryonic day (E) 8.5 in the tail bud region (Schiavinato *et al*., 2012), a structure known to contain a multipotent stem cell population (Wilson *et al*., 2009). This peculiar expression during early embryogenesis was never observed for other Emilin/Multimerin genes and is in full agreement with what was observed in early zebrafish embryos for Emilin3 ortholog genes (Milanetto *et al*., 2008; described in detail below). At later developmental stages, and similarly to Emilin1, expression of Emilin3 becomes prominent in mesenchymal condensations where differentiation is taking place, such as branchial arches and limb buds (Braghetta *et al*., 2002). As the development proceeds, Emilin3 becomes restricted to more specific sites or disappears. For instance, Emilin3 is strongly expressed in the skeletal primordia, but when differentiation proceeds, the expression becomes confined to the perichondrium. The conspicuous expression of Emilin3 in the developing mouse skeleton is in

agreement with previous reports (Leimeister *et al*., 2002) and with studies in zebrafish where expression of Emilin3 orthologs was found in the cartilage primordia of the developing craniofacial skeleton (Milanetto *et al*., 2008). At early developmental stages, Emilin3 is strongly expressed in the esophageal buds, whereas at later stages, the expression is confined to myenteric cells. In the central nervous system, Emilin3 is transiently expressed from E10.5 to E12.5 at the level of the ventricular zone o the midbrain, where neuronal differentiation takes place (Corbin *et al*., 2008). The levels of Emilin3 transcripts in different organs decrease with age, and in the adult, only a few tissues still express the mRNA (Schiavinato *et al*., 2012).

1.1.2.1.1.2. The Emilin/Multimerin family in zebrafish

The zebrafish genome contains eight Emilin/Multimerin genes that are the orthologs of mammalian genes coding for Emilin1, Emilin2, Multimerin2, and Emilin3. Each gene is present in two duplicated paralogs, in agreement with the proposed genomic duplication occurred in teleosts during evolution (Christoffels *et al*., 2004). The only mammalian Emilin/Multimerin gene for which no ortholog was found in *Danio rerio* is the one coding for Multimerin1 (Milanetto *et al*., 2008). Genomic information, as derived by query of the GenBank database, indicated that these zebrafish paralogs are located in different chromosomes but share conserved synteny among them and with their human homologues (Milanetto *et al*., 2008). Bioinformatic analysis revealed that the predicted structural features of zebrafish Emilin/Multimerin proteins are highly conserved with those of their mammalian orthologs, showing similar domain structures and sequences. They all possess an EMI domain at the N-terminal end, followed by a long central region with high probability of forming coiled coil structures. In particular, the EMI domain of all the zebrafish Emilin/Multimerin proteins contains the seven conserved cysteines and other conserved amino acid residues, except for Emilin3a which lacks the second cysteine, the same residue that is also missing in mammalian Multimerin1 (Doliana *et al*., 2000b). Moreover, zebrafish Emilin/Multimerin proteins end with a globular C1q domain, except for Emilin3a and Emilin3b, in agreement with their mammalian counterparts.

As observed also in the mouse, zebrafish Emilin/Multimerin genes are abundantly expressed in the cardiovascular system (Milanetto *et al*., 2008). Briefly, *emilin1a* and *emilin1b* have similar but not identical expression patterns during zebrafish development. At early developmental stages (5- to 25-somite), the

expression of both zebrafish *emilin1* genes is restricted to distinct territories of the central nervous system, whereas at late somitogenesis (24 hours post-fertilization, hpf) expression in the nervous system decreases and the two transcripts are mostly expressed by blood vessels, particularly in the caudal vein, in the heart, and mesenchymal cells of various organs (Milanetto *et al*., 2008). At all stages of zebrafish development, the expression of both zebrafish *emilin2* genes is mainly found in the heart and in the developing blood vessels of head and trunk. In particular, *emilin2a* is first detected in the lateral plate mesoderm, in clusters of macrophages within the yolk, and subsequently in the circulatory system and in the dermis of trunk and tail. At 48 hpf, *emilin2a* transcript become restricted to the atrium of the developing heart. Besides its expression in the cardiovascular system, at 15 somites *emilin2b* is also detectable in few areas of the central nervous system. This particular expression of *emilin2b* in the central nervous system is no longer detectable after 24 hpf, when the labelling becomes maintained only in vascular structures such as the heart, the dorsal aorta, the cephalic blood vessels, the primordial hindbrain channel, the intersegmental blood vessels, and the caudal vein. At 48 hpf, besides expression in vascular structures, *emilin2a* transcripts become detectable in the heart at the level of atrium. Similarly to *emilin2a*, expression of *emilin2b* transcript is abundant in the cardiovascular system, but at the 15-somite stage *emilin2b* shows also a peculiar expression in few specific territories of the central nervous system. At later stages (40-48 hpf), *emilin2b* expression is maintained only in the heart and in the circulatory system of the head (Milanetto *et al*., 2008). Concerning the two zebrafish paralog genes coding for Multimerin2 (*mmrn2a* and *mmrn2b*), at 24 hpf *mmrn2a* is expressed in the heart, in the caudal vein, in the posterior retina, in the most anterior part of the floor plate, and in the fin buds. At this stage, *mmrn2a* transcript is also detected in a region of the anterior gut where the intestinal bulb will form. At 48 hpf, *mmrn2a* is expressed in the circulatory system of the head, in the heart, in the anterior floor plate, and in the prospective intestinal bulb. At 22 hpf, *mmrn2b* is expressed in the heart, in the inner side of the otic vesicle, in the ependymal cells lining the ventricles of midbrain and hindbrain and in the most posterior somites. At 48 hpf, *mmrn2b* transcript is found in the posterior somites and in the mesenchyme of pectoral fins (Milanetto *et al*., 2008).

The two zebrafish *emilin3* genes display the most peculiar expression pattern during zebrafish development, in agreement with the distinct protein structure of

Emilin3 and its classification in a different family. At all examined stages of zebrafish development, *emilin3a* and *emilin3b* have a very similar pattern of expression, which never includes cardiovascular structures. This is a remarkable difference from the other Emilin/Multimerin genes, supporting the different role of this divergent Emilin family member. At early stages (starting from 5- to 15-somite), *emilin3a* is markedly expressed in the tail bud at the level of the notochord, with prominent labelling of an area corresponding to the chordoneural hinge, a structure containing a multipotent stem cell population. In embryos at 20-somite embryos, labelling for *emilin3a* in the notochord becomes stronger with a characteristic postero-anterior gradient. At 24 hpf, expression in the notochord decreases and becomes restricted to the most posterior region, where the floor plate, the chordoneural hinge, and the hypochord are also stained. At 48 hpf, expression in the notochord and floor plate disappears and *emilin3a* transcripts becomes evident in the cartilage elements of branchial arches and craniofacial developing skeleton (Milanetto *et al*., 2008). The pattern of expression of the zebrafish *emilin3* genes is fully in agreement with that of their murine ortholog. In fact, during mouse embryogenesis *Emilin3* mRNA is first detected in the tail bud and in the primitive gut, and at later stages it becomes abundant in the developing gonads and in the osteogenic mesenchyme. Moreover, as for zebrafish, also the murine *Emilin3* is never expressed in the cardiovascular system (Schiavinato *et al*, 2012).

1.1.2.1.2. Emilin3

As already mentioned, two major features make Emilin3 a peculiar member within the Emilin/Multimerin family of secreted proteins. First, Emilin3 is not expressed in any region of the cardiovascular system where all the other Emilins/Multimerins are abundant. Second, despite a high degree of conservation of global protein organization with the other Emilins/Multimerins (*i.e.* the presence of one EMI domain at the N-terminal end and a large region with high propensity for forming coiled coil structures), Emilin3 is lacking the C-terminal gC1q domain that is present in all other members of the family. Data banks mining and mRNA analysis showed that murine Emilin3 is the only gene of the family that can undergo alternative splicing, generating two differently spliced mature mRNAs coding for two protein isoforms that were named Emilin3L and Emilin3S (Schiavinato *et al*., 2012). Emilin3S is a shorter form that lacks the first 141 bp of the fourth exon. At least three coiled-coil motifs are predicted in the C-terminal region of Emilin3. The further characterization of the biochemical properties of Emilin3 (Schiavinato *et al*.,

2012), revealed that Emilin3 is able to form disulfide-linked oligomers: the smallest Emilin3 oligomers have a mobility consistent with homotrimer formation but Emilin3 predominantly exists as higher order oligomers. Moreover, the authors show that neither the gC1q domain nor the EMI domain is strictly necessary for the assembly of Emilin3, thus suggesting that the coiled coil regions with their flanking cysteine residues must be important for this process (Schiavinato *et al*., 2012). Another interesting property of this protein is that Emilin3 binds heparin with high affinity and that this binding is mediated by the EMI domain. This new function of the EMI domain may be responsible for the interaction of Emilin3 with the heparan sulfate moiety of specific ECM and cell surface proteoglycans, such as perlecan, syndecans, and glypican, and/or secreted growth factors. Notably, among the extracellular proteins known to bind heparin/heparan sulfate chains, there are several elastic fibers-associated proteins, such as tropoelastin (Broekelmann *et al*., 2005), Fibrillin-1 (Cain *et al*., 2005), latent TGF-β binding proteins (Kantola *et al*., 2008; Parsi *et al*., 2010), and various members of the TGF-β superfamily (Rider *et al*., 2006). The cysteine-rich EMI domain was already found to work as a self-interacting module (Doliana *et al*., 2000) and as a protein-protein interaction domain as in the case of the binding to pro-TGF-β1. In this regards, Emilin3 appears to be very effective in inhibiting the activity of pro-TGF-β1 as well as pro-TGF-β2 and -3. Although this activity largely relies upon the EMI domain, the precise molecular mechanisms involved in then *in vivo* regulation of TGF-β activity by Emilin proteins remain to be understood (Schiavinato *et al*., 2012).

1.2. The notochord

The notochord is an embryonic midline structure common to all members of the phylum Chordata, providing both mechanical and signaling cues to the developing embryo (Corallo *et al*., 2015). In vertebrates, the notochord arises from the dorsal organizer. The organizer appears during gastrulation and has an essential role in the induction of the embryonic axis. In teleosts, the dorsal organizer (named embryonic shield) gives rise to three different germ layers: the floor plate, the notochord and the hypochord (Shih and Fraser, 1996; Harlan *et al*., 1997; Saùde *et al*., 2000).

1.2.1. The notochord functions

1.2.1.1. Structural function of the notochord

As a midline cylinder-like axis, the notochord plays an important structural role. The inner cells of the notochord form large fluid-filled intracellular vacuoles that occupy most of the cell volume. The outer cells are responsible for secreting ECM proteins to form a thick extracellular tri-layered peri-notochordal sheath, which provides stiffness and rigidity, essential for the axial structure (Stemple, 2005; Corallo *et al*., 2015). Indeed, the pressure exerted from notochord vacuoles against the extracellular sheath generate turgor in the notochord, giving its characteristic rod-like appearance, and providing stiffness and mechanical strength that are essential for the proper elongation of embryos and for the locomotion of invertebrate chordates and many vertebrate species (Adams *et al*., 1990). In this way, the notochord provides a structural role since it serves as the hydrostatic skeleton of the embryo during development, driving the elongation of the antero-posterior axis before spine morphogenesis (Adams *et al*., 1990; Ellis *et al*., 2013). In some vertebrate clades, such as the Agnatha (lampreys), and in primitive fish, such as sturgeons, the notochord persists throughout life. In higher vertebrates, while the notochord completely regresses during embryogenesis in the correspondence of the vertebral bodies (or centra), small areas of notochord tissue persist in the center of the intervertebral discs and notochord cells condense to form the nucleus pulposus (Smits and Lefebvre, 2003). Consistent with its structural role in vertebrate development, the notochord shares many features with cartilage and is likely to represent a primitive form of cartilage. There is, however, one clear difference between chondrogenesis and notochord formation. Chondrocytes normally secrete a highly hydrated ECM, which provide cartilage with its main structural properties. Conversely, while notochord cells produce a thick basement membrane sheath, they

retain hydrated material in large vacuoles (Adams *et al*., 1990; Coutinho *et al*., 2004; Parsons *et al*., 2002).

1.2.1.2. Signaling function of the notochord

Besides its essential structural role, the notochord plays another key function during embryogenesis. In fact, positioned centrally in the embryo with respect to both the dorsal-ventral and left-right axes, the notochord produces secreted factors that instruct surrounding ectodermal, mesodermal and endodermal tissues to acquire specific differentiated fates. In this way, the notochord is essential for specifying ventral fates in the central nervous system, controlling aspects of left-right asymmetry, inducing pancreatic fates, regulating the arterial versus venous identity of the major axial blood vessels, and specifying a variety of cell types in the somites (Corallo *et al*., 2015). One of the main signals secreted by the notochord is the Hedgehog (Hh) family of proteins. The Hedgehog signaling pathway is a central regulator of embryonic development, controlling the patterning of its adjacent tissues (Currie and Ingham, 1996; Ericson *et al*., 1996; Lewis and Eisen, 2001).

1.3. The Hedgehog signaling pathway

The Hedgehog (Hh) signaling pathway plays critical roles in embryonic growth and patterning in organisms ranging from insects to mammals, and also functions post-embryonically in tissue homeostasis (Beachy *et al*., 2004; Varjosalo and Taipale 2008). Furthermore, inappropriate activity of the Hh signaling pathway has been linked with birth defects and with cancer growth arising sporadically or in genetically predisposed individuals (Beachy *et al*., 2004; Teglund and Toftgard 2010). Originally identified through genetic analysis in *D. melanogaster*, the components of the Hh signaling pathway were functionally characterized also in vertebrate species (principally in mouse, human and zebrafish), revealing a high level of conservation across the eumetazoa. The sonic Hh (Shh) ligand is a secreted signaling protein that acts through at least two proteins, Patched (Ptc) and Smoothened (Smo). Ptc negatively regulates Hh signaling by inhibiting Smo. Hh binding to Ptc relieves the inhibition and allows Smo to transduce the signal (Ingham and McMahon, 2001). Then, Smo instructs a cytoplasmic complex that includes a divergent kinesin (Cos2) and several protein kinases needed to stop production of the transcriptional repressor (CiR/GliR) and begin production of the transcriptional activator (CiA/GliA). Vesicular trafficking, phosphorylation, dimerization and reassortment within the regulatory complex are all involved in translating Hh concentrations into transcriptional responses (Cohen, 2003; Choudhry *et al*., 2014). The execution of the wide repertoire of processes controlled by the same Hh ligands depends upon the ability of the organism to modulate the properties of the signaling system in different developmental contexts. A hallmark of Hh signaling is its ability to act over a long range and control distinct cell fates as a function of Hh concentration, thus generating gradients and transducing different thresholds of Hh to elicit distinct developmental outcomes. In addition to signaling strength, signaling duration is also important for shaping developmental outcomes.

1.3.1. Modulation of the Hedgehog signaling activity

Sophisticated molecular mechanisms have evolved to control the biosynthesis, secretion, and propagation of Hh ligands and ensure the formation of tissue-appropriate activity gradients. In addition, the final shape of the Hh activity gradients is further regulated by feedback mechanisms.

1.3.1.1. Biosynthesis of Hedgehog ligands

The core of the diverse spatio-temporal responses of Shh signaling pathway is based on a Shh gradient, which is likely to be generated by lipid modification of membrane-anchored Shh and its movement within the morphogenetic field. During biosynthesis, the full-length Hh precursor undergoes autocleavage to release an N-terminal fragment (Hh-N) with a cholesterol moiety covalently linked to its C-terminus (Porter *et al*., 1996). Cholesterol modification is essential for the formation of a steep gradient because it increases the affinity of Hh for cell membranes and restricts its free dispersal (Burke *et al*., 1999; Li *et al*., 2006). Hh-N is further palmitoylated near its N-terminus by the acyltransferase Skinny Hedgehog (Ski, HHAT in humans) (Chamoun *et al*., 2001; Lee and Treisman, 2001; Buglino and Resh 2008). Although such dual lipid modification of Hh proteins can promote their retention in the plasma membranes of cells, cholesterol coupling has been shown to be crucial for the long-range activity of Hh proteins (Lewis *et al*., 2001). Thus, coupling to cholesterol is critical for the controlled movement of Hh protein through assemblies of cells, allowing the appropriate spatial profile of signaling activity to be established (Burke *et al*., 1999).

1.3.1.2. Secretion and propagation of Hedgehog ligands

After the release in the extracellular space, Hh-N is "multimerized" to become dual lipid-modified Hh (M-Hh-N), which makes the Hh ligand soluble and diffusible thus enabling long range signaling (Zeng *et al*., 2001). Actually, Dispatched (Disp), a transmembrane protein that is structurally related to Ptc (Burke *et al*., 1999), act to promote the assembly of Hh protein into multimeric micelle-like complexes or its incorporation into lipoprotein particles. Both of these entities have been proposed to facilitate the movement of Hh molecules away from secreting cells, a process that also seems to require interaction between the lipid-modified protein and heparan sulphate proteoglycans (HSPGs). Variation in the composition and levels of the latter between tissues could provide an additional mechanism for the context dependent modulation of Hh signaling. How HSPGs facilitate Hh movement is not understood, but it may involve dynamic Hh-HSPGs interactions (Bornemann *et al*., 2004; Han *et al*., 2004a).

1.3.1.3. Modulation of the Hedgehog signal reception

Another important means of controlling the range of Hh signaling is through the establishment of a negative-feedback loop: Hh causes upregulation of the expression

of its transmembrane receptor Ptc and, in vertebrates, a second membrane-spanning Hh-binding protein, Hip (Hh-interacting protein), which sequesters the signal and increase its receptor-mediated endocytosis (Ochi *et al*., 2006). In this way, Hh-responding cells can attenuate the spreading of the signal, an effect that can be tuned by modulating both the rate of endocytosis and the strength of the transcriptional response of the Ptc and Hip genes to Hh pathway activity. On the other hand, the binding of Hh to responding cells is facilitated by the transmembrane proteins Cdo and Boc (iHog and boi in *Drosophila*) (Lum *et al*. 2003a; Tenzen *et al*. 2006; Yao *et al*. 2006). These proteins act positively in the pathway, binding to Hh via conserved fibronectin repeats (Yao *et al*. 2006) and increasing Hh association with its signaling receptor Ptc (Tenzen *et al*. 2006; Yao *et al*. 2006). The expression levels of Cdo and Boc are down-regulated in response to Hh signaling, thus resulting in another negative feedback that limits pathway activity.

1.3.1.4. Intracellular transduction of the Hedgehog signal

Unusually for a signal receptor, Ptc is not activated in response to ligand binding but rather is suppressed by its interaction with Hh. In its unbound state, Ptc represses the activity of another transmembrane protein, Smo, a divergent member of the G-protein-coupled receptor superfamily, an obligate step for the transduction of Hh signals across the plasma membrane and into the cell. Thus, Hh activates Smo by binding to and inactivating Ptc. Once activated, Smo promotes the expression of Hh target gene expression by modulating the activity of members of the Gli family of transcription factors (Choudhry *et al*., 2014). In *Drosophila*, a single Gli protein, known as Ci (Cubitus interruptus), controls Hh target gene expression. Ci is bifunctional and has both a transcriptional activator domain and a transcriptional repressor domain that flank the central sequence-specific DNA-binding domain composed of five zinc fingers (Chen *et al*., 1999). In the absence of Hh pathway activity, the C-terminal activation domain is cleaved from the protein, yielding a truncated form that enters the nucleus and represses target gene transcription. Activation of Smo blocks Ci processing, allowing the full-length form of the protein to accumulate, enter the nucleus and activate target genes. In vertebrates, these opposing activities of Ci are distributed between three related Gli proteins; only two of these undergo cleavage in a manner analogous to the *Drosophila* Ci protein, while the third, Gli1, acts exclusively as an activator that amplifies the transcriptional response once it is initiated. The Hh signal cellular response depends on both level

of ligand exposure and the individual Gli genes expressed (Cohen, 2003). The relative levels of Gli activator and repressor activities present in a cell determine which Hh target genes are expressed. In this way, different levels of Hh signaling activity can elicit distinct patterns of gene expression and hence distinct cell identities.

1.3.1.5. Hedgehog target genes

At the molecular level, the diverse cellular responses are affected by the induction of different sets of target genes. Among the genes regulated by the Hh signaling are those encoding other secreted signaling proteins, including bone morphogenetic protein 4 (BMP4) (Astorga and Carlsson, 2007), fibroblast growth factor 4 (FGF4) (Laufer et al., 1994), and vascular endothelial growth factor (VEGF) (Pola *et al*., 2001), as well as genes coding for proteins involved in cell growth and division (*e.g*., N-Myc) (Oliver *et al*., 2003) and many transcription factors that are essential for animal development, including members of the MyoD/Myf, Pax, Nkx, Dbx, and Irx families (Pierani *et al*., 1999; Gustafsson *et al*., 2002; Jacob and Briscoe 2003; Vokes *et al*., 2007). The broad range of genes regulated by Hh signals is only beginning to be discovered. A number of expression profiling studies have identified several novel target genes (Xu *et al*., 2006; Vokes *et al*., 2007), and genome-wide *in silico* analyses identified 42 conserved enhancer modules with two or more Gli sites in the human genome (Hallikas *et al*. 2006). The genes that are induced by Hh in many tissues, in turn, are generally involved in positive and negative feedback loops to the pathway itself and include Gli1, Ptc, and Hip. As Ci and the Gli proteins act as repressors in the absence of Hh and activators in its presence, many of the target genes also behave similarly, being repressed in the absence of Hh and induced in its presence.

1.3.2. The Hedgehog signaling in zebrafish

1.3.2.1. Zebrafish Hedgehog genes and mutants

Sonic Hedgehog (Shh) is one of three Hh family members expressed in axial midline structures of the zebrafish embryo, the others being the Indian Hedgehog paralogue Echidna Hedgehog (Ehh), which is expressed in the notochord (Currie and Ingham, 1996) and the Shh paralogue, Tiggy-winkle Hedgehog (Twhh), which is expressed in the overlying floor plate of the neural tube (Ekker *et al*., 1995). Analysis of the role of Hh signaling in the zebrafish embryo has been greatly facilitated by the availability of mutants affecting several components of the Hh

pathway, as well as by the ability to knockdown specific gene functions by injection of morpholino antisense oligonucleotides into the early embryo. In zebrafish, forward genetic screenings have pointed out mutant alleles in genes coding for several orthologs and in addition have led to the identification of two genes not previously implicated in the Hh signaling pathway. Mutants in Hh pathway components were identified initially on the basis of shared phenotypic traits involving midline structures (Brand *et al*., 1996; van Eeden *et al*., 1996). In some, though not all cases, mutant embryos display a defect in the formation of the horizontal myoseptum, resulting in the loss of the characteristic chevron shape of each somite, which instead adopts a more U-shaped conformation. For this reason, these mutants were designated the ''you-shaped'' class, a classification from which several derive their names (*you, you-too, sonic-you*) (van Eeden *et al*., 1996). The activity of Shh itself is reduced or abolished by *sonic you* (*syu*) mutations, of which there are three alleles. One of these is a deletion of the entire transcription unit, while the other two are base substitutions in the coding region and at a splice donor junction (Schauerte *et al*., 1998). The function of Smo is inactivated in *slow muscle omitted* (*smu*) mutants. The smu^{b641} allele is associated with a substitution within the predicted second transmembrane domain, while the smu^{b577} allele is associated with a substitution in the extracellular domain between the fourth and fifth transmembrane domains (Chen *et al*., 2001). The function of zebrafish Disp1 is inactivated by two mutant alleles at the *chameleon* (*con*) locus, both of which introduce premature termination codons into the coding region (Nakano *et al*., 2004). In the zebrafish, Gli1 is inactivated by *detour* (*dtr*) mutant alleles. Among three alleles identified, the weakest allele dtr^{tm276} is associated with an amino acid substitution whilst the dtr^{ts269} and the dtr^{te370} both introduce premature termination codons into the coding region (Karlstrom *et al*., 2003). Mutant alleles at the *you-too* (*yot*) locus introduce premature termination codons downstream of the zinc finger domain of the Gli2 coding region, giving rise to truncated forms of the protein that lack the C-terminal activation domain but retain the repressor domain N-terminal to the DNA binding motif (Karlstrom *et al*., 1999). In addition to these mutations in the well-established components of the pathway, analysis of zebrafish midline mutants has identified two previously uncharacterized proteins that modulate the activity of the pathway in different ways. The *iguana* (*igu*) locus encodes the zebrafish orthologue of DZIP, a zinc-finger coiled-coil domain protein of previously unknown function, which appears to act by regulating nuclear-cytoplasmic shuttling of the Gli

proteins (Wolff *et al*., 2004; Sekimizu *et al*., 2004). The *you* locus, by contrast, encodes an extracellular protein of the EGF-CUB family, homologous to mouse Scube2. Analysis of the *you* phenotype suggests that zebrafish Scube2 is involved in extracellular transport or stability of the Hh proteins (Woods *et al*., 2005).

1.3.2.2. Hedgehog signaling in zebrafish development

Previous studies revealed that Hh signaling is required to specify the fate of individual cells of the zebrafish myotome and neural tube (Krauss *et al*., 1993; Currie and Ingham, 1996; Blagden *et al*., 1997; Du *et al*., 1997; Schauerte *et al*., 1998). In zebrafish, during the first stages of somitogenesis (about 10 hpf), notochord-derived Hedgehog proteins induce medial paraxial mesoderm – also known as adaxial cells which express the Hh receptors *patched1* (*ptc1*) and *patched2* (*ptc2*) – to become slow twitch muscle fibers (Currie and Ingham, 1996; Blagden *et al*., 1997; Du *et al*., 1997; Lewis *et al*., 1999; Drapeau *et al*., 2002). Once induced, most of the adaxial cells migrate to the surface of the myotome and differentiate into so-called Superficial Slow Fibers (SSFs). However, a minority remains medially located and differentiates into another type of slow muscle fiber called Muscle Pioneers (MPs), which produce the horizontal myosepta. Both types of fiber express the slow isoform of the Myosin Heavy Chain (MyHC). In addition, MPs express two members of *engrailed* genes, *eng1* and *eng2* (Hatta *et al*., 1991). Subsequently, the remaining muscle progenitors in each somite differentiate into fast muscle cells that express the fast MyHC isoform. A subset of fast muscle cells located close to the notochord, the so-called Medial Fast Fibers (MFFs), also express the Eng protein, though at lower level than MPs (Roy *et al*., 2001; Wolff *et al*., 2003). The specification of the different muscle cell identities is dependent on the level, range and timing of Shh signaling (Wolff *et al*., 2003).

Several factors are thought to regulate the response of muscle to Hh (Wolff *et al*., 2003), although mechanisms that restrict Hh signaling to adaxial cells and that produce graded Hh levels to specify slow muscle and muscle pioneer fates are still poorly understood.

1.4. Structural and signaling alterations after ablation of peri-notochordal basement membrane proteins

The peri-notochordal basement membrane is composed of a variety of ECM molecules that interact to facilitate the anchorage of notochordal cells. Although the precise molecular composition of the notochord sheath is still partially unknown, several proteins have been characterized as essential constituents of this structure among different species. Actually, the peri-notochordal basement membrane is normally composed of three different laminar layers. Closest to the cell membrane, there is a single inner layer that mainly contains laminins and corresponding to a true basement membrane (Parsons *et al*., 2002). Next, there is the intermediate fibrillar layer, which is composed of dense collagen fibers oriented in one parallel direction around notochord cells, and finally the outer granular layer, which is oriented perpendicularly to the middle layer (Scott and Stemple, 2005).

Several studies in zebrafish showed that ablation of key ECM components of the notochord sheath results in severe notochord structural and molecular defects in the developing embryo. Those studies have suggested that the formation of the extracellular sheath, in addition to the structural support, is involved in the differentiation process of notochordal cells, and their reciprocal interactions are fundamental for the normal development and activity of the notochord itself (Parsons *et al*., 2002; Gansner *et al*., 2007, 2008; Gansner and Gitlin, 2011; Pagnon-Minot *et al*., 2008; Christiansen *et al*., 2009; Mangos *et al*., 2010, Yamamoto *et al*., 2010; for a full report of zebrafish models with notochord-related phenotypes linked to the loss of extracellular sheath components see Corallo *et al*., 2015).

In the first period of my PhD work I was involved in the analysis of the *in vivo* function Emilin3, exploiting the zebrafish model. By using a novel specific antibody, we demonstrated that Emilin3 is localized in the basement membrane that surrounds the notochord. Moreover, we observed that the concurrent knockdown of both Emilin3 paralogs (*emilin3a* and *emilin3b*) leads to a marked distortion of the notochord, a disorganization of the medial layer of the peri-notochordal sheath, and a persistent expression of the early chordamesoderm marker *col2a1*. Strikingly, the patterning activity of the notochord is also affected by Emilin3, as revealed by increased Hh signaling in Emilin3-depleted embryos and decreased Hh signaling in embryos overexpressing Emilin3 in notochord cells. In this context, I took part to

both the knockdown and overexpressing experiments, subsequently analysing – by *in situ* hybridization and immunofluorescence – the expression of several Hh target genes. Moreover, I actively contributed to the generation of a plasmid carrying the full-length murine Emilin3 cDNA under the control of a promoter that confers notochord-specific expression. Furthermore, I generated different constructs, necessary for *in vitro* binding assay experiments, which allowed unveiling the mechanism through which Emilin3 regulates notochord-derived Hh ligands.

Taken together, our data suggest that Emilin3 is required for the proper maturation of the notochord and that this component of peri-notochordal ECM sheath is important for the correct regulation of notochord-derived Hh signaling. We found that Emilin3 is able to interact with the EGF repeats of Scube2, a secreted permissive factor that act non-cell autonomously in the release of lipidated Shh from producing cells. Based on these finding, we propose that Emilin3 and Scube2 interaction in the notochord sheath is crucial for the proper notochord patterning activity. This model supports the concept that ECM plays an important role for tuning the Hh activity arising from the notochord.

Alongside this experimental work, my increasing knowledge on notochord patterning and functions allowed me to play an active role in the review entitled "The notochord: structure and function" published in *Cellular and Molecular Life Science* journal.

Chapter I

Emilin3 is required for notochord sheath integrity and interacts with Scube2 to regulate notochord-derived Hedgehog signals

© 2013. Published by The Company of Biologists Ltd | Development (2013) 140, 4594-4601 doi:10.1242/dev.094078

RESEARCH ARTICLE

Emilin3 is required for notochord sheath integrity and interacts with Scube2 to regulate notochord-derived Hedgehog signals

Diana Corallo[1,*], Alvise Schiavinato[1,*], Valeria Trapani[1], Enrico Moro[1], Francesco Argenton[2] and Paolo Bonaldo[1,‡]

ABSTRACT

The notochord is a transient and essential structure that provides both mechanical and signaling cues to the developing vertebrate embryo. In teleosts, the notochord is composed of a core of large vacuolated cells and an outer layer of cells that secrete the notochord sheath. In this work, we have identified the extracellular matrix glycoprotein Emilin3 as a novel essential component of the zebrafish notochord sheath. The development of the notochord sheath is impaired in Emilin3 knockdown embryos. The patterning activity of the notochord is also affected by Emilin3, as revealed by the increase of Hedgehog (Hh) signaling in Emilin3-depleted embryos and the decreased Hh signaling in embryos overexpressing Emilin3 in the notochord. *In vitro* and *in vivo* experiments indicate that Emilin3 modulates the availability of Hh ligands by interacting with the permissive factor Scube2 in the notochord sheath. Overall, this study reveals a new role for an EMILIN protein and reinforces the concept that structure and function of the notochord are strictly linked.

KEY WORDS: Extracellular matrix, EMILIN, Notochord, Hedgehog, Scube2, Zebrafish

INTRODUCTION

EMILINs (elastin microfibril interface located proteins) are extracellular matrix (ECM) glycoproteins belonging to the EMILIN/multimerin family. Emilin1, the founding member of this family, was originally identified as an ECM component associated with microfibrils in blood vessels (Bressan et al., 1993). Emilin3 contains the characteristic cysteine-rich EMI domain at the N-terminal end, followed by a region forming three coiled-coil structures at the C-terminal end (Schiavinato et al., 2012). At variance with the other EMILIN/multimerin proteins, Emilin3 is not expressed in the cardiovascular system and it lacks the C-terminal gC1q domain, which is involved in cell attachment and integrin binding (Spessotto et al., 2003; Danussi et al., 2011). Emilin3 expression during mouse development is particularly abundant in the perichondrium of developing bones (Leimeister et al., 2002; Doi et al., 2004; Schiavinato et al., 2012). We have previously found that eight EMILIN/multimerin genes are present in the zebrafish genome in four pairs of duplicated paralogs (Milanetto et al., 2008). Thus, Emilin3 is present in zebrafish with two genetic paralogs that we termed *emilin3a* and *emilin3b*. Similarly to the murine Emilin3 ortholog, the two zebrafish paralogs are not expressed in the cardiovascular system, whereas they are abundantly expressed in the notochord and in the chordoneural hinge until 24 hpf, and in cartilage primordia of the developing craniofacial skeleton at 48 hpf (Milanetto et al., 2008).

In the present study, we focused on the role of the two zebrafish Emilin3 genes during notochord development. During the early phases of embryonic development, until the segmentation stage, the notochord is distinguishable from adjacent tissues by the expression of specific genes, such as *shh*, *ehh* and *col2a1* (Yan et al., 1995; Currie and Ingham, 1996). As the notochord develops, expression of these early-transcribed genes is turned off and notochord cells differentiate in two different cell populations, an outer sheath layer and an inner vacuolated cell layer. The choice between these two fates is determined by Notch signals (Yamamoto et al., 2010). The outer cell layer is responsible for the synthesis of the notochord sheath, a thick peri-notochordal basement membrane that is composed of several ECM proteins, whereas the inner cells contain large intracellular vacuoles. Recently, the nature of these vacuoles was elegantly identified as lysosome-related organelles (Ellis et al., 2013). Both the notochord sheath and the vacuolated cells are essential for conferring the proper stiffness and rigidity to the notochord (Stemple, 2005).

Several studies in zebrafish showed that the formation of a notochord sheath is closely linked to the differentiation of notochord cells, and their reciprocal interactions are fundamental for the proper development and function of the notochord itself (Parsons et al., 2009; Pagnon-Minot et al., 2008; Mangos et al., 2010; Yamamoto et al., 2010). Here, we provide evidence that Emilin3 is a novel component of the notochord sheath that plays an essential role for the correct organization and the proper function of this structure. Moreover, we found that Emilin3 has a physiological role for limiting notochord-derived Hh signals, a function entailing the interaction of Emilin3 with the secreted protein Scube2.

RESULTS

Emilin3 is a novel essential component of the notochord sheath

To study Emilin3 protein distribution in the zebrafish embryo, we carried out whole-mount immunofluorescence with a polyclonal Emilin3 antibody. At 20 hpf, a specific signal was present throughout the notochord with a distinct posteroanterior gradient, whereas no labeling was detected in embryos at eight somites (data not shown; see also supplementary material Fig. S5D). At 24 hpf, Emilin3 became restricted to the notochord sheath, as confirmed by colocalization with collagen II. In agreement with mRNA expression data (Milanetto et al., 2008), labeling of the notochord sheath was lost at 48 hpf, indicating that Emilin3 undergoes a rapid turnover in the ECM and may fulfill a temporally restricted function during notochord development (Fig. 1A).

To investigate the role of Emilin3 during notochord development, we injected one- to two-cell-stage zebrafish embryos

[1]Department of Biomedical Sciences, University of Padova, I-35121 Padova, Italy.
[2]Department of Biology, University of Padova, I-35121 Padova, Italy.
*These authors contributed equally to this work

‡Author for correspondence (bonaldo@bio.unipd.it)

Received 15 January 2013; Accepted 27 August 2013

RESEARCH ARTICLE Development (2013) doi:10.1242/dev.094078

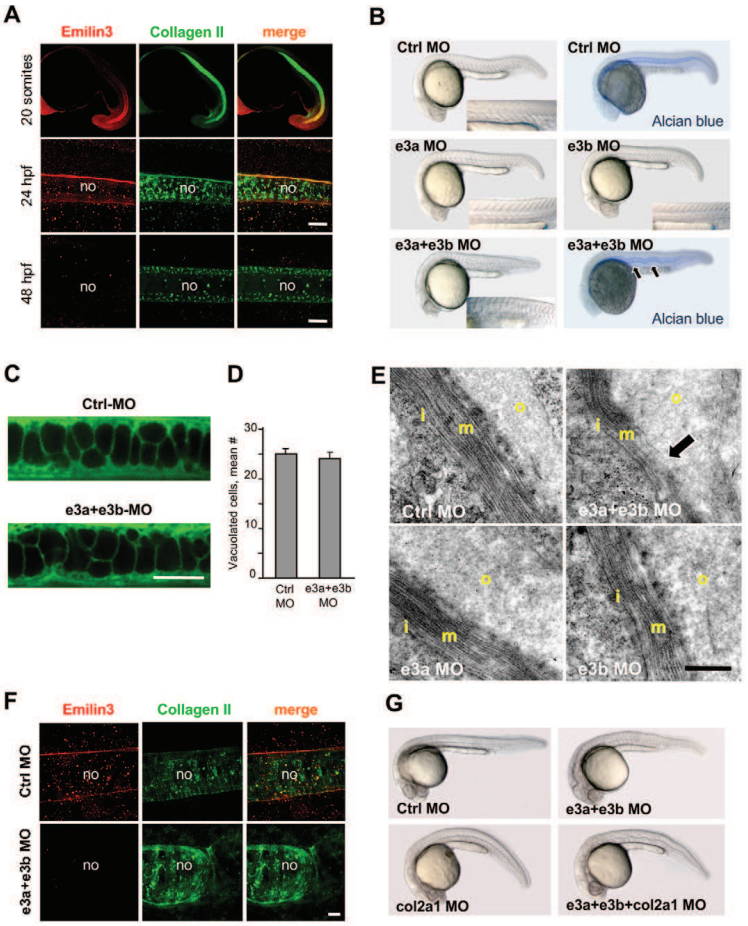

Fig. 1. Emilin3 is an essential component of the notochord sheath. (A) Lateral views of zebrafish embryos after immunofluorescence for Emilin3 and collagen II. Scale bars: 30 µm. (B) Lateral views of 24 hpf injected embryos. (C) BODIPY TR Ceramide staining of notochord cells in 24 hpf injected embryos. Scale bar: 50 µm. (D) Quantification of the mean number of vacuolated cells within the trunk region of control and treated notochord (not significantly different, *n*=10). Data are mean+s.e.m. (E) Transmission electron micrographs of the notochord sheath in transverse trunk sections of 30 hpf injected embryos. The arrow points at the medial layer of the notochord basement membrane, which is thinner and partially disorganized in Emilin3 double morphants. Scale bar: 500 nm. (F) Immunofluorescence for Emilin3 and collagen II in 24 hpf injected embryos. Scale bar: 10 µm. (G) Lateral views of 24 hpf injected embryos. col2a1 MO, *col2a1* morpholino; Ctrl MO, control morpholino; e3a MO, *emilin3a* morpholino; e3b MO, *emilin3b* morpholino; i, inner layer; m, medial layer; no, notochord; o, outer layer.

with antisense morpholino oligonucleotides targeting the splice sites between the first exon and the first intron of *emilin3a* and *emilin3b* genes. Co-injection of the two morpholinos resulted in the knockdown of the corresponding transcripts and proteins (supplementary material Fig. S1A,B), leading to a distinct distortion of the notochord with partial loss of the V-shaped conformation of somites and shortening of the main axis (Fig. 1B). Embryos injected with translation-blocking morpholinos for *emilin3a* and *emilin3b* showed a similar phenotype, and the same result was found in mixed experiments where a splice-blocking morpholino for one paralog was co-injected with a translation-blocking morpholino for the other paralog (supplementary material Fig. S1C; supplementary material Table S1). Injection of morpholinos targeting only one paralog did not cause a similar phenotype, even when injected at double concentration (Fig. 1B; supplementary material Table S1). As a further control, we performed p53 knockdown and found that co-injection of p53 morpholino was ineffective in rescuing the phenotypic defects induced by Emilin3 depletion (supplementary material Fig. S1D). Two different mechanisms could be inferred for the notochord phenotype of Emilin3 double morphants: (1) an increased pressure generated inside the notochord; or (2) a disruption of the sheath organization.

Quantification of total and vacuolated notochord cells in control and Emilin3 double morphant embryos did not reveal any significant difference, suggesting that Emilin3 deficiency is not grossly perturbing the morphology and commitment of notochord cells (Fig. 1C,D; supplementary material Fig. S2). Notch signaling is known to regulate the fate choice between vacuolated and non-vacuolated notochord cells (Yamamoto et al., 2010). Using the Tg_Hbb:EGFP Notch reporter zebrafish line (Parsons et al., 2009), we did not detect any major difference of Notch signaling activity in notochord cells of control and Emilin3 double morphant embryos (supplementary material Fig. S3).

RESEARCH ARTICLE

Development (2013) doi:10.1242/dev.094078

We next investigated the structure of the notochord sheath by electron microscopy. At 30 hpf, in Emilin3 double morphants, but not in Emilin3 single morphants, the medial layer of the notochord basement membrane was not properly organized and many fibers appeared interrupted, whereas the outer and inner layers appeared normal (Fig. 1E). The medial and inner layers of the notochord sheath are thought to consist of collagen and laminin, respectively (Stemple, 2005). *In situ* hybridization and immunofluorescence showed that collagen II was more abundant in Emilin3-depleted embryos at both 24 and 48 hpf (Fig. 1F; supplementary material Fig. S4A,B), whereas laminin labeling was normal (supplementary material Fig. S4C). To exclude the possibility that the phenotype of Emilin3 morphants could be caused by an upregulation of collagen II, we performed concurrent knockdown of *emilin3a*, *emilin3b* and *col2a1*. Knockdown of *col2a1* caused ventral body curvature as expected (Mangos et al., 2010), whereas simultaneous knockdown of the three genes resulted in the overlap of the two phenotypes (Fig. 1G). Altogether, these data reveal that Emilin3 is essential for the normal structure of the notochord sheath.

Emilin3 knockdown results in the upregulation of Hh signaling

Next, we investigated whether knockdown of Emilin3 could affect notochord patterning activity, a process that is largely mediated by the secretion of Hh ligands (Stemple, 2005). Expression of *ptc1* (*ptch2* – Zebrafish Information Network), which is transcriptionally regulated by Hh signaling (Concordet et al., 1996), was strongly increased in the trunk of 24 hpf Emilin3 morphants and this effect was completely blocked by treatment with 100 µM cyclopamine, an inhibitor of Hh signaling, but was unaffected by p53 (Tp53 – Zebrafish Information Network) knockdown (Fig. 2A; supplementary material Fig. S5A,B). To assess whether *ptc1* upregulation was specifically due to Emilin3 ablation, we analyzed *ptc1* expression at eight somites, a stage where Emilin3 proteins are not yet present in the sheath. Consistently, at this stage, *ptc1* was not differently expressed in Emilin3 morphants (supplementary material Fig. S5C,D).

Next, we generated the Tg12x_Gli zebrafish line, which express the mCherry reporter under the transcriptional regulation of Gli1 (see Materials and methods). We co-injected *emilin3a* and *emilin3b* morpholinos in Tg12x_Gli embryos and investigated expression of the transgene at 24 hpf. Notably, Emilin3 morphants displayed a remarkable increase of transgene expression (Fig. 2A), as also confirmed by qPCR experiments (Fig. 2B). We investigated the expression of other genes that respond to notochord-derived Hh signals in different embryonic structures. Expression of *nkx2.2a*, *tbx20* and *myoD1* was consistently increased in Emilin3-depleted embryos (Fig. 2C). Similarly, *olig2*, *vegf* and *eng2a* were upregulated (supplementary material Fig. S6A). Overexpression of Hh ligands by notochord cells can lead to hyperactivation of the Hh pathway (Yamamoto et al., 2010). At 20 somites, *shh* and *ehh*, the only two Hh ligands produced in the notochord, were not

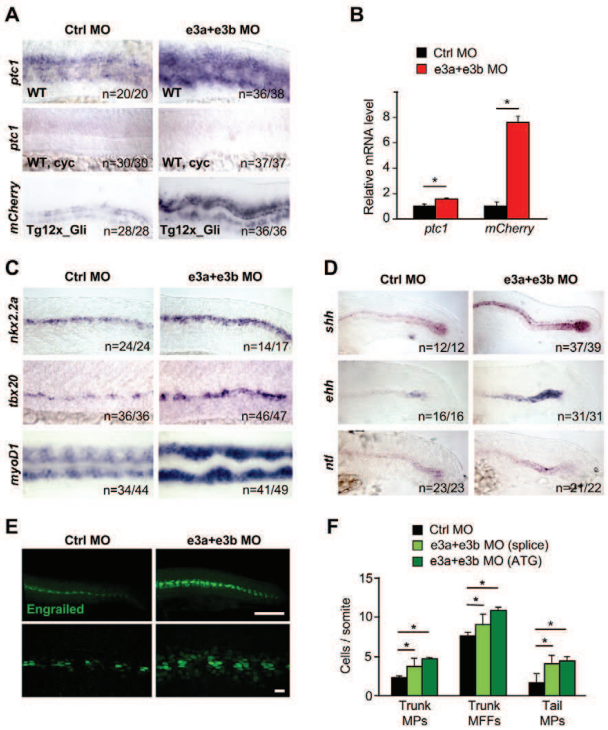

Fig. 2. Hh signaling is upregulated in Emilin3 morphant embryos. (A) Wild-type (WT) and Tg12x_Gli embryos were treated with 100 µM cyclopamine (cyc) and probed at 24 hpf by *in situ* hybridization for *ptc1* or *mCherry*. (B) qRT-PCR for *ptc1* and *mCherry* transcripts in Emilin3 morphant and control embryos (**P*<0.05; *n*=30). (C) *In situ* hybridization for *nkx2.2a*, *tbx20* and *myoD1* in 24 hpf injected embryos. All images are lateral views, except for bottom panels (dorsal views). (D) *In situ* hybridization for *shh*, *ehh* and *ntl* in 24 hpf injected embryos. (E) Immunofluorescence for engrailed in 24 hpf injected embryos. Scale bars: 150 µm. (F) Quantification of engrailed-positive cells at 24 hpf (**P*<0.05; *n*=10). Data are mean+s.e.m. Ctrl MO, control morpholino; e3a MO, *emilin3a* morpholino; e3b MO, *emilin3b* morpholino; e3a+e3b MO, *emilin3a* + *emilin3b* morpholinos; MPs, muscle pioneers; MFFs, medial fast fibers.

Development

RESEARCH ARTICLE Development (2013) doi:10.1242/dev.094078

differently expressed in Emilin3 morphants when compared with control embryos (data not shown), whereas at 24 hpf they were upregulated in the distal part of the notochord (Fig. 2D). Therefore, the sole upregulation of *shh* and *ehh* did not explain the increased Hh activity in Emilin3 morphants. Moreover, expression of *ntl* and of the notochord-unrelated gene *fgf8* was not affected, thus excluding a developmental delay (Fig. 2D; supplementary material Fig. S6B).

We quantified engrailed-positive cells and found that both muscle pioneers (MPs) and medial fast fibers (MFFs) were significantly increased in Emilin3 morphants (Fig. 2E,F). It is known that engrailed expression in the zebrafish myotome is negatively regulated by BMP signaling (Du et al., 1997; Dolez et al., 2011), and high levels of Hh activity can prevent the accumulation of activated Smads in the medial part of the myotome (Maurya et al., 2011). Consistently, we found that expansion of the engrailed-positive domain in Emilin3 morphants was paralleled by a reduction of the pSmad1/5/8 domain in the medial part of the myotome. Treatment with low doses of cyclopamine was sufficient to rescue pSmad distribution in the somites of Emilin3 morphants, indicating that Hh pathway is primarily affected by Emilin3 knockdown (supplementary material Fig. S7A). To exclude the possibility that the observed effect on Hh signaling could be mediated by the pro-TGFβ inhibitory activity of Emilin3 (Schiavinato et al., 2012), we treated morphant embryos with two different selective inhibitors of TGFβ type I receptors, SB431542 and LY364947. Neither of these inhibitors was effective in decreasing *ptc1* expression, and pharmacological inhibition of TGFβ activity also exacerbated notochord distortion in Emilin3 morphants (supplementary material Fig. S7B).

Emilin3 overexpression leads to downregulation of Hh target genes

To investigate whether upregulation of the Hh pathway was directly caused by Emilin3 deficiency or was a broader effect caused by disruption of the notochord sheath, we analyzed *ptc1* expression in *emilin3a* and *emilin3b* single morphants. Interestingly, albeit to a lesser extent than in Emilin3 double morphants, *ptc1* expression was increased in the trunk of single morphants (Fig. 3A). To further assess the role of Emilin3 in notochord-derived Hh signaling, we generated a pCS-twhh-mEmilin3 construct carrying murine full-length *Emilin3* cDNA under the control of a promoter that confers notochord-specific expression (Du et al., 1997). Embryos injected with this construct developed normally but at 24 hpf they displayed mild notochord defects and a shorter axis, when compared with embryos injected with a control pCS-twhh-β-gal construct (Fig. 3B). Notably, embryos injected with pCS-twhh-mEmilin3 showed impaired *myoD1* expression, together with reduced number of engrailed-positive cells. Emilin3 overexpression in the notochord did not influence *ehh* transcription, indicating that expression of Hh ligands by notochord cells was not grossly affected (Fig. 3B,C). Moreover, injection of the pCS-twhh-mEmilin3 construct also rescued the effects of morpholino-mediated ablation of Emilin3 both on notochord development and Hh signaling (supplementary material Fig. S8).

Emilin3 functionally interacts with Scube2

As Emilin3 paralogs are expressed by notochord cells with a pattern closely similar to that of Hh ligands, we speculated that Emilin3 could influence the rate of synthesis and/or release of Hh proteins. Interestingly, when Emilin3 and Shh were transiently co-expressed in HEK293T cells, the amount of Shh released in media was

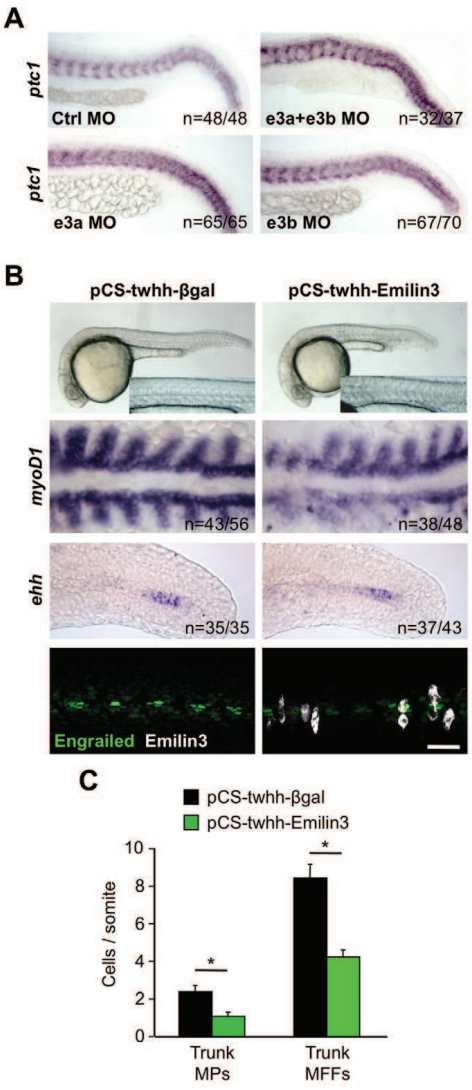

Fig. 3. Overexpression of Emilin3 affects notochord patterning activity. (A) Lateral views of 24 hpf embryos probed for *ptc1*. Embryos were injected with the indicated morpholinos. (B) Wild-type embryos were injected with the indicated constructs at 50 ng/µl and photographed at 24 hpf (upper panels), or probed by *in situ* hybridization for *myoD1* at eight somites and for *ehh* at 24 hpf (middle panels), or by immunofluorescence for engrailed and Emilin3 at 24 hpf (lower panels). Scale bar: 50 µm. (C) Quantification of engrailed-positive cells in 24 hpf embryos injected as in B (*P<0.05; n=15). Data are mean+s.e.m. Ctrl MO, control morpholino; e3a+e3b MO, *emilin3a* + *emilin3b* morpholinos; MPs, muscle pioneers; MFFs, medial fast fibers.

Development

RESEARCH ARTICLE

Development (2013) doi:10.1242/dev.094078

reduced (Fig. 4A). This effect was not dependent on the EMI domain and it was lost when Emilin3 was co-expressed with ShhN, a form of Shh lacking cholesterol modification (Fig. 4B,C). Co-immunoprecipitation experiments failed to reveal any interaction between Emilin3 and Shh (Fig. 4D). Therefore, we hypothesized that Emilin3 could interact with a factor secreted by HEK293T and involved in Shh release. To test this hypothesis, we used conditioned media derived from HEK293T transfected with empty vector or with Emilin3 construct to stimulate the release of Shh from stably transfected Shh-293 cells. Interestingly, the conditioned medium derived from mock-transfected cells strongly increased Shh release compared with fresh medium, whereas medium from Emilin3-transfected cells induced a much lower rate of Shh release (supplementary material Fig. S9).

Recent studies demonstrated a role for the secreted protein Scube2 in Shh release (Creanga et al., 2012; Tukachinsky et al., 2012). We therefore investigated whether Emilin3 could interact with Scube2. When HEK293T cells were co-transfected with Emilin3 and FLAG-tagged Scube2, Emilin3 was co-precipitated with Scube2 from media (Fig. 4E). Similarly, FLAG-tagged Scube2 was efficiently immunoprecipitated by HA-tagged Emilin3 (supplementary material Fig. S10A). This interaction was confirmed by *in vitro*-binding experiments and did not require the EMI domain or the coiled-coil region of Emilin3 (Fig. 4F,G). A similar *in vitro*-binding experiment showed that the EGF repeats of Scube2 are sufficient for Emilin3 binding (supplementary material Fig. S10B). To investigate whether the interaction of Emilin3 with Scube2 has any functional significance, we treated transfected HEK293T cells with conditioned media derived from Scube2-transfected cells. Notably, treatment with Scube2-conditioned media, as well as Scube2 co-transfection, were able to rescue the effect of Emilin3, whereas treatment with soluble heparin was ineffective (Fig. 4H; supplementary material Fig. S10C-E). We also prepared conditioned media derived from HEK293T transiently transfected with Scube2 alone or in combination with Emilin3, and found that the latter was less effective in releasing Shh from 293-Shh cells (Fig. 4I).

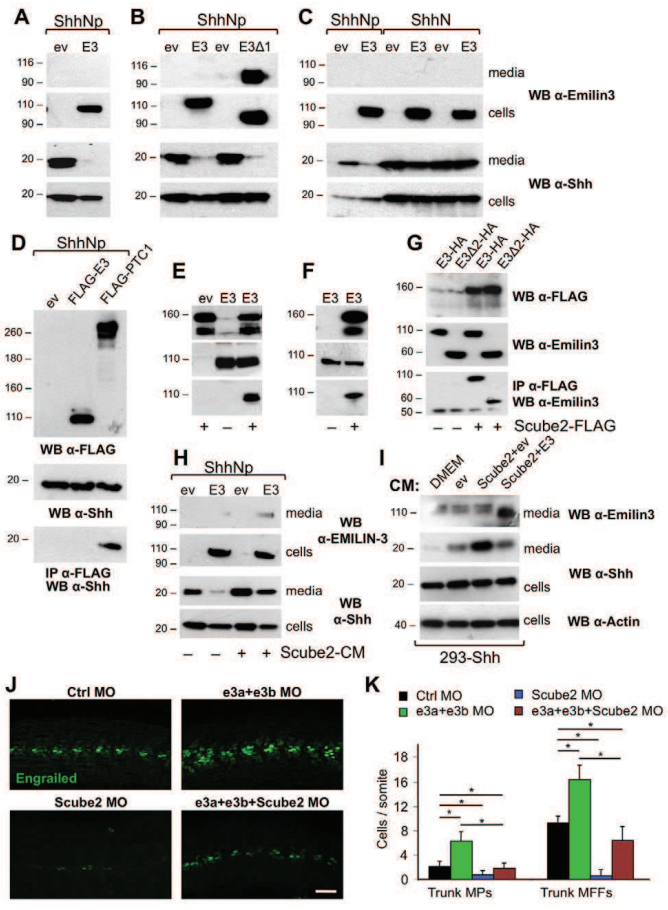

Fig. 4. Emilin3 functionally interacts with Scube2. (A-C) HEK293T were transiently co-transfected with the indicated constructs. Conditioned serum-free media and cell lysates were analyzed by western blot. (D) Cell lysates of HEK293T transfected with the indicated plasmids were analyzed by western blot or subjected to immunoprecipitation. (E-G) HEK293T were either co-transfected (E,G) or separately transfected (F) with the indicated plasmids. Media (E,F) and cell lysates (G) were analyzed by western blot or subjected to immunoprecipitation. (H) Transfected HEK293T were incubated for 24 hours with conditioned media derived from control or Scube2-transfected cells. (I) Stably transfected 293-Shh cells were incubated for 6 hours with fresh medium (DMEM) or with conditioned media derived from HEK293T co-transfected with the indicated plasmids. Media and cell lysates were analyzed by western blot. (J) Lateral views of 24 hpf embryos injected with the indicated morpholinos and immunostained for engrailed. Scale bar: 50 μm. (K) Quantification of engrailed-positive cells in injected embryos (**P*<0.05; *n*=6). Data are mean+s.e.m. CM, conditioned media; E3, murine full-length Emilin3; E3Δ1, murine Emilin3 lacking the EMI domain; E3Δ2, murine Emilin3 lacking the EMI domain and the coiled-coil region; ev, empty vector; IP, immunoprecipitation; PTC1, human FLAG-patched-1; WB, western blot; Ctrl MO, control morpholino; e3a+e3b MO, *emilin3a* + *emilin3b* morpholinos; Scube2 MO, Scube2 morpholino; MPs, muscle pioneers; MFFs, medial fast fibers.

RESEARCH ARTICLE Development (2013) doi:10.1242/dev.094078

Finally, to investigate whether the interaction of Emilin3 with Scube2 was relevant *in vivo*, we injected embryos with morpholinos directed against *emilin3a*/*emilin3b* and *scube2*, as well as their combination. Emilin3 knockdown resulted in a robust increase of both MFFs and MPs, whereas Scube2 morphants lacked engrailed-positive cells as expected (Woods and Talbot, 2005). Interestingly, although co-injection of the three morpholinos resulted in the overlap of the two phenotypes (supplementary material Fig. S11A), the number of engrailed-positive cells was rescued almost to wild-type levels in triple morphants (Fig. 4J,K). qRT-PCR experiments showed that Scube2 expression was slightly, albeit not significantly, upregulated in Emilin3-depleted embryos (supplementary material Fig. S11B). Overall, these results support a physiological role for Emilin3 in limiting the activity of Scube2 on the release of Hh ligands by notochord cells.

DISCUSSION

In this work, we provided the first *in vivo* functional characterization of Emilin3, revealing both structural and functional roles for notochord development in zebrafish. Electron microscopy showed that Emilin3 is required for proper structural organization of the peri-notochordal basement membrane. In the absence of Emilin3, the sheath is not resistant enough to withstand the pressure generated by vacuolization of notochord cells, and this defect provides an explanation for the notochord distortion we observed in Emilin3 morphants.

Interestingly, the notochord phenotype of Emilin3 double morphant embryos is similar to that described for other ECM components. In particular, the ultrastructural alterations we found in the medial layer of the notochord sheath are reminiscent of those described for the zebrafish *gulliver* mutants, which carry a missense mutation in the globular C1q domain of the *col8a1* gene (Gansner and Gitlin, 2008). Intriguingly, unlike other EMILIN proteins, this domain is missing in Emilin3. It has been shown that the globular C1q domain is involved in the supramolecular organization of EMILINs by interacting with the EMI domain (Doliana et al., 2000), thus suggesting the possibility that Emilin3 and collagen VIII are interacting partners in the medial layer of the notochord sheath.

Our data also support previous findings, which indicated that defects in the notochord sheath can influence the gene expression pattern of notochord cells. However, at odds with what is observed in other models of notochord disruption (Parsons et al., 2002; Pagnon-Minot et al., 2008; Yamamoto et al., 2010), we found that *col2a1* and Hh ligands are not co-regulated. Indeed, in Emilin3 double morphants, *col2a1* expression is upregulated throughout the length of the notochord, whereas *shh* and *ehh* are overexpressed only in the expression field of *emilin3a* and *emilin3b*, at the level of the chordoneural hinge. Conversely, laminin mutants and collagen XV morphants display a similar upregulation of *col2a1* and *ehh* throughout the notochord (Parsons et al., 2002; Pagnon-Minot et al., 2008). This implies that notochord cells can respond to extracellular signals in a region-specific way.

The second function we report here for Emilin3 concerns the regulation of notochord-derived Hh signals. We show that Emilin3 interacts with Scube2 in the extracellular environment. Recently, Scube2 has been identified as a secreted, permissive factor, acting non-cell autonomously in the release of lipidated Shh from producing cells (Creanga et al., 2012; Tukachinsky et al., 2012). Scube2 is a multi-domain protein, with a signal peptide sequence at the N-terminal end followed by nine EGF repeats, one spacer region, three cysteine-rich motifs and one CUB domain at the C-terminal end. The CUB domain was found to interact with Shh and its presence is required for the activity of Scube2 on Shh release (Creanga et al., 2012; Tukachinsky et al., 2012). Our finding that Emilin3 is able to interact with the EGF repeats of Scube2 supports the hypothesis that this region of the protein may be important for targeting Scube2 to the ECM and fine-tuning its localization and activity in the extracellular milieu. We therefore propose that Emilin3 deficiency disturbs notochord sheath formation and causes abnormal localization and/or activity of Scube2 in the extracellular milieu, thus leading to increased Hh signals (Fig. 5). It is tempting to speculate that Emilin3, similar to Emilin1, associates with fibrillin microfibrils in the ECM, and thus the Scube2/Emilin3 interaction may represent a novel mechanism by which microfibrils control tissues homeostasis. Overall, our data indicate that the ECM endows a novel level of regulation for Hh signals through Scube2, and we propose that Emilin3 and Scube2 interaction in the notochord sheath is crucial for the proper notochord patterning activity.

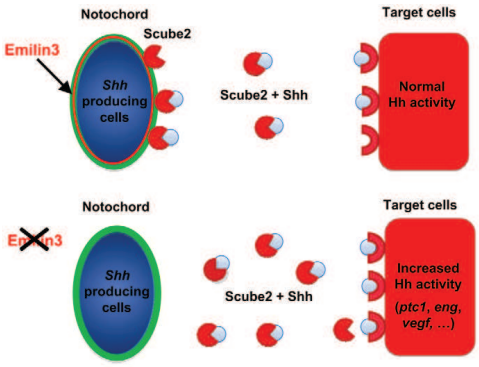

Fig. 5. Hypothetical model of Emilin3 and Scube2 interaction in the notochord sheath. Emilin3 is located in the extracellular matrix of the notochord sheath and interacts with Scube2, a secreted factor that mediates the release of lipid-modified Hh ligand. In wild-type embryos, Emilin3 ensures the integrity and function of the notochord sheath, which is necessary for proper notochord patterning activity. Emilin3 deficiency results in the disruption of the notochord sheath and affects Scube2 localization and activity in the extracellular milieu, thus leading to increased Hh signals.

MATERIALS AND METHODS

Zebrafish lines

Wild-type (AB/TU) zebrafish were maintained as described previously (Westerfield, 1995). For the generation of the *Tg(12xGli-HSVTK:nlsmCherry)ia10* zebrafish line (Tg12x_Gli), a cassette containing twelve multimerized Gli1-binding sites was isolated from the 12GLI-RE-TKO-luc construct (Kogerman et al., 1999) and ligated with the Herpes simplex virus thymidine kinase minimal promoter in the p5E-MCS Tol2 5′ entry vector. Positive clones were sequenced in both strands and recombined with a middle entry vector carrying the *mCherry* open reading frame and a 3′ entry vector carrying a SV40 poly-A tail. Entry plasmids were finally recombined into the pTol2 destination vector as previously described (Kwan et al., 2007). A total of 25 pg of Tol2 recombinant plasmids and 25-50 pg of *in vitro* synthesized transposase mRNA (Kawakami et al., 2004) were co-injected into zebrafish embryos at the one- to two-cell stage. Microinjected embryos were raised to adulthood and outcrossed to wild-type fish. Six out of 30 screened fish were identified as founders for the reporter line. The *Tg(EPV.TP1-Mmu.Hbb:EGFP)ia12* zebrafish line (Tg_Hbb:EGFP) has been previously described (Parsons et al., 2009).

RESEARCH ARTICLE Development (2013) doi:10.1242/dev.094078

Zebrafish embryo injection

Sequences of the morpholinos used in the study are reported in supplementary material Table S2. All morpholinos were splice blocked, except where indicated. Morpholinos were dissolved in 1×Danieu's buffer and injected at the doses reported in supplementary material Table S1. p53 morpholino (Robu et al., 2007) and Scube2 morpholino (Woods and Talbot, 2005) were injected at 6 ng/embryo and 2 ng/embryo, respectively. For DNA microinjection, linearized DNA was dissolved in deionised H_2O to a final concentration of at 50 ng/µl (Du et al., 1997), except where indicated. Murine *Emilin3* cDNA was cloned into the pCS-twhh-βgal vector (Du et al., 1997).

Pharmacological treatments

Cyclopamine hydrate (Sigma) was dissolved in DMSO and embryos were incubated at the indicated concentrations beginning at shield stage until fixation at 24 hpf. LY364947 (Zhou et al., 2011) and SB431542 (Ho et al., 2006) (Sigma) were dissolved in DMSO and diluted into embryo medium to a final concentration of 30 µM and 100 µM, respectively, and embryos were incubated with these compounds from 8 hpf until fixation at 24 hpf. Embryos incubated with DMSO were used as control.

Probes and plasmids

For *in situ* hybridization experiments, the used riboprobes were: *emilin3a* and *emilin3b* (Milanetto et al., 2008), *col2a1* (Yan et al., 1995), *ntl* (Schulte-Merker et al., 1994), *shh* (Krauss et al., 1993), *ehh* (Currie and Ingham, 1996), *ptc1* (Concordet et al., 1996), *nkx2.2a* (Barth and Wilson, 1995), *tbx20* (Ahn et al., 2000), *vegf* (Liang et al., 1998), *olig2* (Park et al., 2002), *eng2a* (Ekker et al., 1992), and *fgf8* (Reifers et al., 1998). The cDNA constructs for murine full-length Emilin3 and EMILIN-3Δ1, which lacks amino acid residues 54-189, have been described previously (Schiavinato et al., 2012). Murine EMILIN-3Δ2 cDNA construct, which lacks both the EMI domain (amino acid residues 54-189) and the coiled-coil region (amino acid residues 534-758), was prepared by PCR using the EMILIN-3Δ1 construct as a template and the following primers: SP6 (forward) and 5′-CTAAGCGTAATCTGGAACATCGTATGGGTACCAGGCCTTCACCTC-TGC-3′ (reverse). The EMILIN-3-HA cDNA construct was generated by adding the human influenza hemagglutinin (HA) tag sequence at the C-terminal end of murine full-length Emilin3. Murine full-length Shh, ShhN and Scube2 cDNAs were obtained by PCR and cloned into the pCS2+ vector. The Scube2-FLAG construct was generated by adding the FLAG tag sequence at the C-terminal end of murine Scube2. The EGF-FLAG construct, encompassing amino acids 1-479 of murine Scube2, was generated by PCR using the Scube2 full-length construct as a template with the following primers: 5′-GGTTGCATGCTGATGGGAGA-3′ (forward) and 5′-TTCTCGAGTCACTTGTCATCGTCGTCCTTGTAGTCTGACGAGA-GGTGAATGCC-3′ (reverse, coding for the FLAG tag sequence). The PCR product was then subcloned into the pCS2 vector. All constructs were sequenced prior to use.

Immunohistochemistry and BODIPY labeling

Immunohistochemical staining of whole zebrafish embryos was performed essentially as described previously (Dolez et al., 2011). Used antibodies were: monoclonal anti-engrailed (4D9, DSHB; 1:10 dilution); monoclonal anti-collagen II (II-II6B3, DSHB; 1:400); rabbit polyclonal anti-laminin (L9393, Sigma; 1:200); rabbit polyclonal anti-phospho-Smad1/Smad5/Smad8 (9511, Cell Signaling; 1:100); rabbit polyclonal anti-Emilin3 (Schiavinato et al., 2012; 1:500); mouse monoclonal anti-β-Catenin (C7207, Sigma; 1:500). Nuclei were stained with Hoechst (Invitrogen). Where indicated, embryos were stained with 100 µM BODIPY TR Ceramide (Invitrogen) in E3 medium for 2 hours. All embryos were imaged with a Leica SP5 confocal microscope.

Electron microscopy

Embryos were prepared essentially as described previously (Parsons, 2002) and ultrathin sections were viewed on a Zeiss 902 electron microscope.

RNA analysis

Total RNA was extracted from pools of 30 embryos using TRIzol Reagent (Invitrogen) as recommended by the manufacturer and 1 µg of RNA was used for cDNA synthesis, using the M-MLV Reverse Transcriptase kit (Invitrogen). The efficacy of splice-blocking morpholinos was tested by RT-PCR using the following primers: 5′-ACGTGCTGAAATTGGTGGA-3′ (*emilin3a*, forward); 5′-GGAACAGCTTGACCTTCGAG-3′ (*emilin3a*, reverse); 5′-ACTCAAGCAAGCTGGACCAT-3′ (*emilin3b*, forward); 5′-CCTTGTGTGTGGAGCGACA-3′ (*emilin3b*, reverse). Expression of *nlsmCherry*, *ptc1* and *scube2* transcripts was analyzed by real-time qualitative RT-PCR using the SYBR Green Realtime PCR Master Mix in an ABI PRISM 7900HT System (Applied Biosystems). Expression of *gapdh* was used as normalizer in each sample and triplicate PCR reactions were carried out. Primers used were: 5′-GTGGAGTCTACTGGTGTCTTC-3′ (*gapdh*, forward); 5′-GTGCAGGAGGCATTGCTTACA-3′ (*gapdh*, reverse); 5′-GAAGGTGACCAAGGGCGGCC-3′ (*nlsmCherry*, forward); 5′-CTGGGTCACGGTCACCACGC-3′ (*nlsmCherry*, reverse); 5′-CTTCAGTCGCCAAGGTCTTC-3′ (*ptc1*, forward); 5′-CCGATCAATCC-CATCATACC-3′ (*ptc1*, reverse); 5′-GCAAGGCTTTTTCCTGAGTG-3′ (*scube2*, forward); 5′-TTACCATGGTTGCAGGTCAA-3′ (*scube2*, reverse).

Cell culture and transfection

HEK293T were grown in DMEM supplemented with 10% FBS (Invitrogen) and transfected with LT-1 (Mirus). The next day cells were washed and incubated in serum-free medium. For the preparation of Scube2-conditioned medium, cells were transfected and kept in DMEM supplemented with 2% FBS for 72 hours. Stably transfected HEK-293 (293-Shh) cells were generated by transfection with the murine full-length Shh cDNA subcloned into the pcDNA3.1+ vector, followed by selection with G418 (Invitrogen) at a concentration of 400 µg/ml.

Western blot and immunoprecipitation

Cells and conditioned media were harvested 24 hours (western blot) or 72 hours (immunoprecipitation) after incubation in serum-free medium. Cells were lysed in ice-cold lysis buffer [25 mM Tris (pH 7.5), 150 mM NaCl, 2.5 mM EDTA, 10% glycerol, 1% Nonidet P-40] supplemented with proteases inhibitor (Roche) and media were TCA precipitated. Immunoprecipitation, SDS-PAGE and western blot were performed as previously described (Schiavinato et al., 2012). Used antibodies were: rabbit polyclonal anti-Emilin3 (Schiavinato et al., 2012), rabbit polyclonal anti-Shh (Santa Cruz), mouse monoclonal anti-FLAG (Sigma) and mouse monoclonal anti-HA (Sigma).

Statistical analysis

Data are expressed as mean±s.e.m. Statistical significance was determined by unequal variance Student's *t*-test. $P<0.05$ was considered significant.

Acknowledgements

We thank Walter Giuriati for help with electron microscopy. We are grateful to Professor Mats Paulsson and Dr Raimund Wagener for Emilin3 antibody and for critical reading of the manuscript.

Competing interests

The authors declare no competing financial interests.

Author contributions

D.C. and A.S. conceived and performed the majority of the experiments, and analyzed data. V.T. performed experiments and analyzed data. E.M. and F.A. provided zebrafish transgenic lines, contributed new reagents/analytic tools. P.B. and A.S. designed the study, analyzed data and wrote the paper. All authors discussed the results and commented on the manuscript.

Funding

This work was supported by grants from the University of Padova and the Italian Ministry of University and Research.

Supplementary material

Supplementary material available online at
http://dev.biologists.org/lookup/suppl/doi:10.1242/dev.094078/-/DC1

Development

RESEARCH ARTICLE Development (2013) doi:10.1242/dev.094078

References

Ahn, D. G., Ruvinsky, I., Oates, A. C., Silver, L. M. and Ho, R. K. (2000). tbx20, a new vertebrate T-box gene expressed in the cranial motor neurons and developing cardiovascular structures in zebrafish. *Mech. Dev.* **95**, 253-258.

Barth, K. A. and Wilson, S. W. (1995). Expression of zebrafish nk2.2 is influenced by sonic hedgehog/vertebrate hedgehog-1 and demarcates a zone of neuronal differentiation in the embryonic forebrain. *Development* **121**, 1755-1768.

Bressan, G. M., Daga-Gordini, D., Colombatti, A., Castellani, I., Marigo, V. and Volpin, D. (1993). Emilin, a component of elastic fibers preferentially located at the elastin-microfibrils interface. *J. Cell Biol.* **121**, 201-212.

Concordet, J. P., Lewis, K. E., Moore, J. W., Goodrich, L. V., Johnson, R. L., Scott, M. P. and Ingham, P. W. (1996). Spatial regulation of a zebrafish patched homologue reflects the roles of sonic hedgehog and protein kinase A in neural tube and somite patterning. *Development* **122**, 2835-2846.

Creanga, A., Glenn, T. D., Mann, R. K., Saunders, A. M., Talbot, W. S. and Beachy, P. A. (2012). Scube/You activity mediates release of dually lipid-modified Hedgehog signal in soluble form. *Genes Dev.* **26**, 1312-1325.

Currie, P. D. and Ingham, P. W. (1996). Induction of a specific muscle cell type by a hedgehog-like protein in zebrafish. *Nature* **382**, 452-455.

Danussi, C., Petrucco, A., Wassermann, B., Pivetta, E., Modica, T. M., Del Bel Belluz, L., Colombatti, A. and Spessotto, P. (2011). EMILIN1-α4/α9 integrin interaction inhibits dermal fibroblast and keratinocyte proliferation. *J. Cell Biol.* **195**, 131-145.

Doi, M., Nagano, A. and Nakamura, Y. (2004). Molecular cloning and characterization of a novel gene, EMILIN-5, and its possible involvement in skeletal development. *Biochem. Biophys. Res. Commun.* **313**, 888-893.

Dolez, M., Nicolas, J. F. and Hirsinger, E. (2011). Laminins, via heparan sulfate proteoglycans, participate in zebrafish myotome morphogenesis by modulating the pattern of Bmp responsiveness. *Development* **138**, 97-106.

Doliana, R., Bot, S., Bonaldo, P. and Colombatti, A. (2000). EMI, a novel cysteine-rich domain of EMILINs and other extracellular proteins, interacts with the gC1q domains and participates in multimerization. *FEBS Lett.* **484**, 164-168.

Du, S. J., Devoto, S. H., Westerfield, M. and Moon, R. T. (1997). Positive and negative regulation of muscle cell identity by members of the hedgehog and TGF-beta gene families. *J. Cell Biol.* **139**, 145-156.

Ekker, M., Wegner, J., Akimenko, M. A. and Westerfield, M. (1992). Coordinate embryonic expression of three zebrafish engrailed genes. *Development* **116**, 1001-1010.

Ellis, K., Bagwell, J. and Bagnat, M. (2013). Notochord vacuoles are lysosome-related organelles that function in axis and spine morphogenesis. *J. Cell Biol.* **200**, 667-679.

Gansner, J. M. and Gitlin, J. D. (2008). Essential role for the alpha 1 chain of type VIII collagen in zebrafish notochord formation. *Dev. Dyn.* **237**, 3715-3726.

Ho, D. M., Chan, J., Bayliss, P. and Whitman, M. (2006). Inhibitor-resistant type I receptors reveal specific requirements for TGF-beta signaling in vivo. *Dev. Biol.* **295**, 730-742.

Kawakami, K. (2004). Transgenesis and gene trap methods in zebrafish by using the Tol2 transposable element. *Methods Cell Biol.* **77**, 201-222.

Kogerman, P., Grimm, T., Kogerman, L., Krause, D., Undén, A. B., Sandstedt, B., Toftgård, R. and Zaphiropoulos, P. G. (1999). Mammalian suppressor-of-fused modulates nuclear-cytoplasmic shuttling of Gli-1. *Nat. Cell Biol.* **1**, 312-319.

Krauss, S., Concordet, J. P. and Ingham, P. W. (1993). A functionally conserved homolog of the Drosophila segment polarity gene hh is expressed in tissues with polarizing activity in zebrafish embryos. *Cell* **75**, 1431-1444.

Kwan, K. M., Fujimoto, E., Grabher, C., Mangum, B. D., Hardy, M. E., Campbell, D. S., Parant, J. M., Yost, H. J., Kanki, J. P. and Chien, C. B. (2007). The Tol2kit: a multisite gateway-based construction kit for Tol2 transposon transgenesis constructs. *Dev. Dyn.* **236**, 3088-3099.

Leimeister, C., Steidl, C., Schumacher, N., Erhard, S. and Gessler, M. (2002). Developmental expression and biochemical characterization of Emu family members. *Dev. Biol.* **249**, 204-218.

Liang, D., Xu, X., Chin, A. J., Balasubramaniyan, N. V., Teo, M. A. L., Lam, T. J., Weinberg, E. S. and Ge, R. (1998). Cloning and characterization of vascular endothelial growth factor (VEGF) from zebrafish, *Danio rerio*. *Biochim. Biophys. Acta* **1397**, 14-20.

Mangos, S., Lam, P. Y., Zhao, A., Liu, Y., Mudumana, S., Vasilyev, A., Liu, A. and Drummond, I. A. (2010). The ADPKD genes pkd1a/b and pkd2 regulate extracellular matrix formation. *Dis. Model. Mech.* **3**, 354-365.

Maurya, A. K., Tan, H., Souren, M., Wang, X., Wittbrodt, J. and Ingham, P. W. (2011). Integration of Hedgehog and BMP signalling by the engrailed2a gene in the zebrafish myotome. *Development* **138**, 755-765.

Milanetto, M., Tiso, N., Braghetta, P., Volpin, D., Argenton, F. and Bonaldo, P. (2008). Emilin genes are duplicated and dynamically expressed during zebrafish embryonic development. *Dev. Dyn.* **237**, 222-232.

Pagnon-Minot, A., Malbouyres, M., Haftek-Terreau, Z., Kim, H. R., Sasaki, T., Thisse, C., Thisse, B., Ingham, P. W., Ruggiero, F. and Le Guellec, D. (2008). Collagen XV, a novel factor in zebrafish notochord differentiation and muscle development. *Dev. Biol.* **316**, 21-35.

Park, H. C., Mehta, A., Richardson, J. S. and Appel, B. (2002). olig2 is required for zebrafish primary motor neuron and oligodendrocyte development. *Dev. Biol.* **248**, 356-368.

Parsons, M. J., Pollard, S. M., Saude, L., Feldman, B., Coutinho, P., Hirst, E. M. and Stemple, D. L. (2002). Zebrafish mutants identify an essential role for laminins in notochord formation. *Development* **129**, 3137-3146.

Parsons, M. J., Pisharath, H., Yusuff, S., Moore, J. C., Siekmann, A. F., Lawson, N. and Leach, S. D. (2009). Notch-responsive cells initiate the secondary transition in larval zebrafish pancreas. *Mech. Dev.* **126**, 898-912.

Reifers, F., Böhli, H., Walsh, E. C., Crossley, P. H., Stainier, D. Y. R. and Brand, M. (1998). *Fgf8* is mutated in zebrafish acerebellar (ace) mutants and is required for maintenance of midbrain-hindbrain boundary development and somitogenesis. *Development* **125**, 2381-2395.

Robu, M. E., Larson, J. D., Nasevicius, A., Beiraghi, S., Brenner, C., Farber, S. A. and Ekker, S. C. (2007). p53 activation by knockdown technologies. *PLoS Genet.* **3**, e78.

Schiavinato, A., Becker, A. K., Zanetti, M., Corallo, D., Milanetto, M., Bizzotto, D., Bressan, G., Guljelmovic, M., Paulsson, M., Wagener, R. et al. (2012). EMILIN-3, peculiar member of elastin microfibril interface-located protein (EMILIN) family, has distinct expression pattern, forms oligomeric assemblies, and serves as transforming growth factor β (TGF-β) antagonist. *J. Biol. Chem.* **287**, 11498-11515.

Schulte-Merker, S., Hammerschmidt, M., Beuchle, D., Cho, K. W., De Robertis, E. M. and Nüsslein-Volhard, C. (1994). Expression of zebrafish goosecoid and no tail gene products in wild-type and mutant no tail embryos. *Development* **120**, 843-852.

Spessotto, P., Cervi, M., Mucignat, M. T., Mungiguerra, G., Sartoretto, I., Doliana, R. and Colombatti, A. (2003). beta 1 Integrin-dependent cell adhesion to EMILIN-1 is mediated by the gC1q domain. *J. Biol. Chem.* **278**, 6160-6167.

Stemple, D. L. (2005). Structure and function of the notochord: an essential organ for chordate development. *Development* **132**, 2503-2512.

Tukachinsky, H., Kuzmickas, R. P., Jao, C. Y., Liu, J. and Salic, A. (2012). Dispatched and scube mediate the efficient secretion of the cholesterol-modified hedgehog ligand. *Cell Reports* **2**, 308-320.

Westerfield, M. (1995). *The Zebrafish Book*. Eugene, OR: University of Oregon Press.

Woods, I. G. and Talbot, W. S. (2005). The you gene encodes an EGF-CUB protein essential for Hedgehog signaling in zebrafish. *PLoS Biol.* **3**, e66.

Yamamoto, M., Morita, R., Mizoguchi, T., Matsuo, H., Isoda, M., Ishitani, T., Chitnis, A. B., Matsumoto, K., Crump, J. G., Hozumi, K. et al. (2010). Mib-Jag1-Notch signalling regulates patterning and structural roles of the notochord by controlling cell-fate decisions. *Development* **137**, 2527-2537.

Yan, Y. L., Hatta, K., Riggleman, B. and Postlethwait, J. H. (1995). Expression of a type II collagen gene in the zebrafish embryonic axis. *Dev. Dyn.* **203**, 363-376.

Zhou, Y., Cashman, T. J., Nevis, K. R., Obregon, P., Carney, S. A., Liu, Y., Gu, A., Mosimann, C., Sondalle, S., Peterson, R. E. et al. (2011). Latent TGF-β binding protein 3 identifies a second heart field in zebrafish. *Nature* **474**, 645-648.

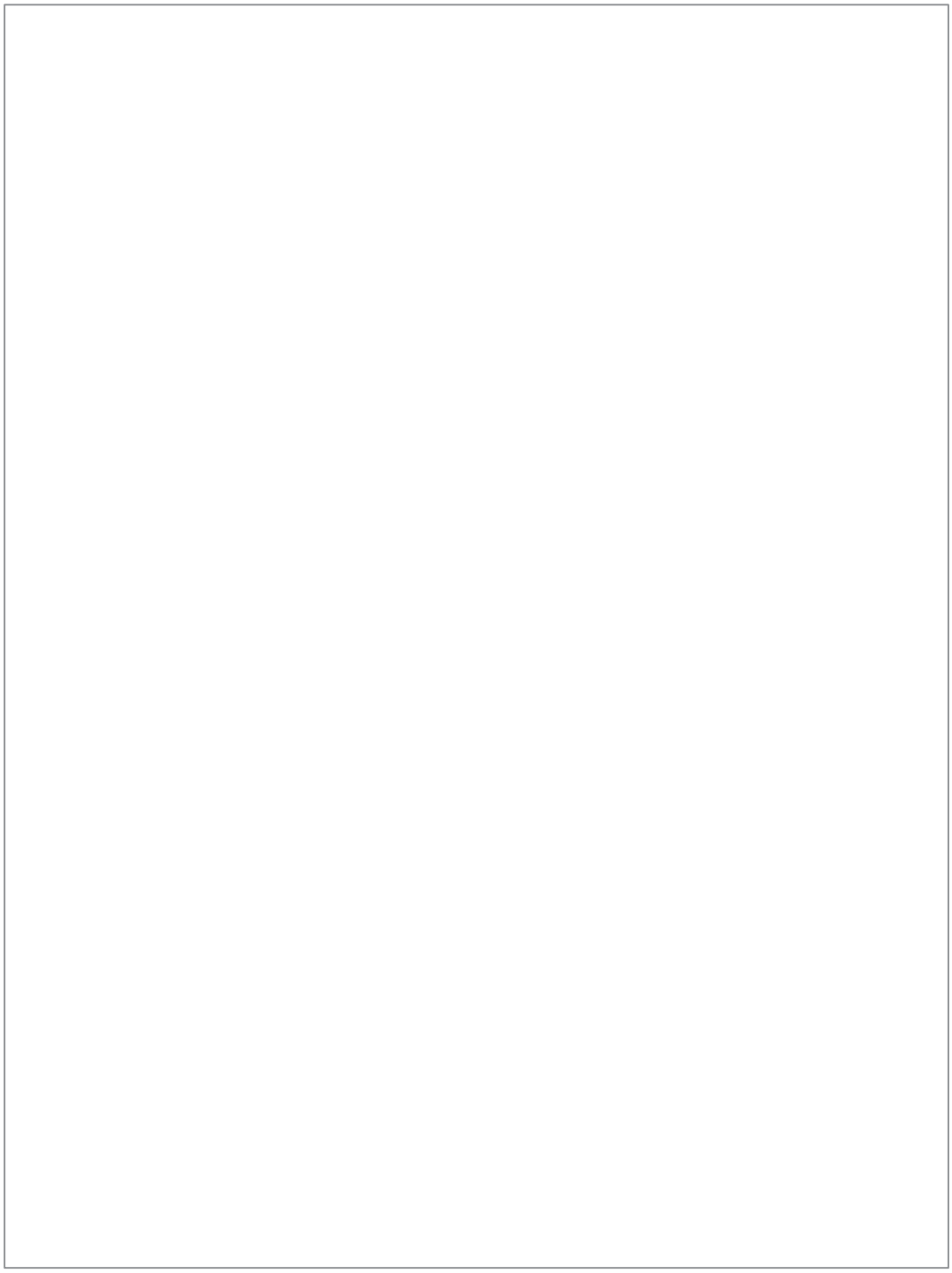

Figure S1

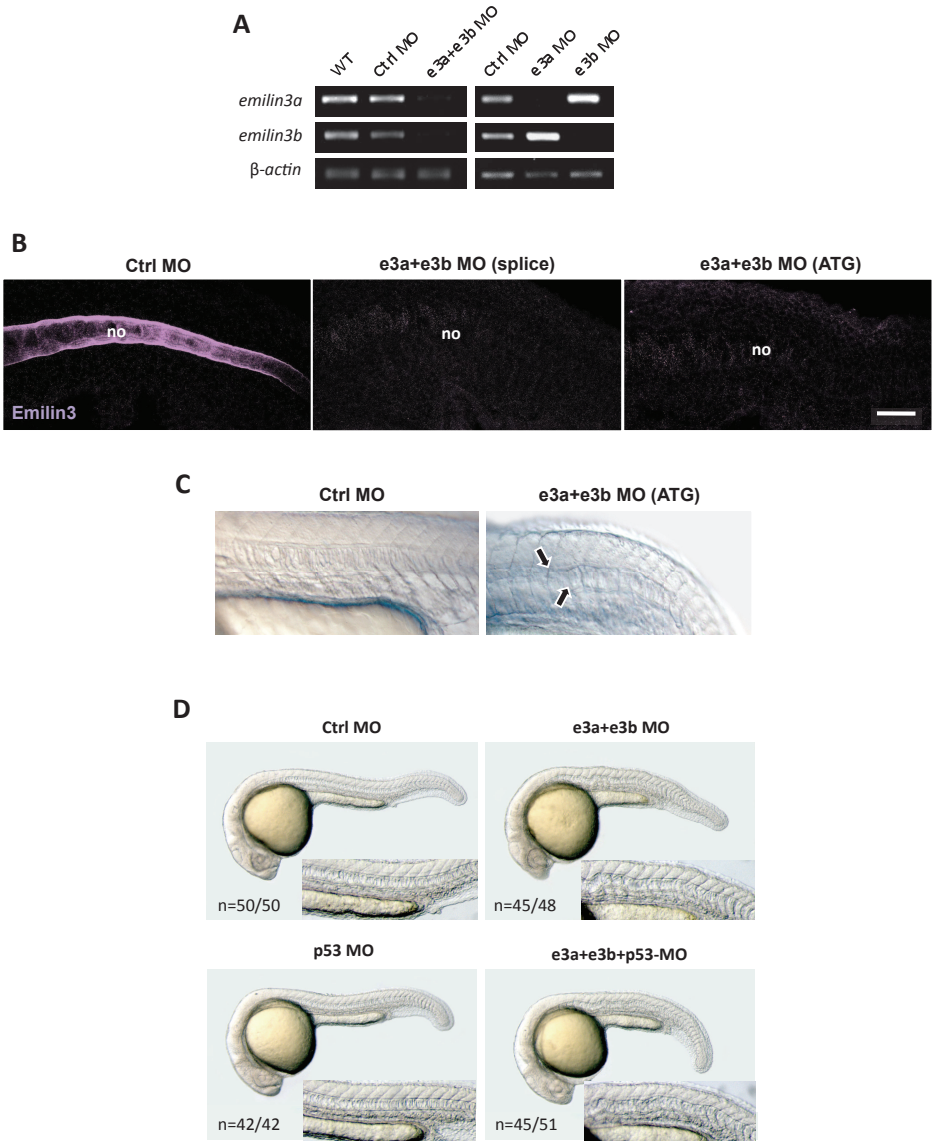
A
WT
Ctrl MO
e3a+e3b MO
Ctrl MO
e3a MO
e3b MO
emilin3a
emilin3b
β-actin
B
Ctrl MO
e3a+e3b MO (splice)
e3a+e3b MO (ATG)
no
no
no
Emilin3
C
Ctrl MO
e3a+e3b MO (ATG)
D
Ctrl MO
e3a+e3b MO
n=50/50
n=45/48
p53 MO
e3a+e3b+p53-MO
n=42/42
n=45/51

Figure S2

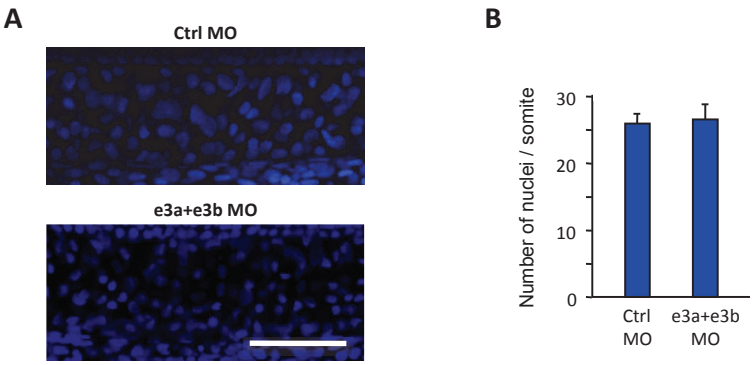
A
Ctrl MO
e3a+e3b MO
B
Number of nuclei / somite
30
20
10
0
Ctrl MO
e3a+e3b MO

Figure S3

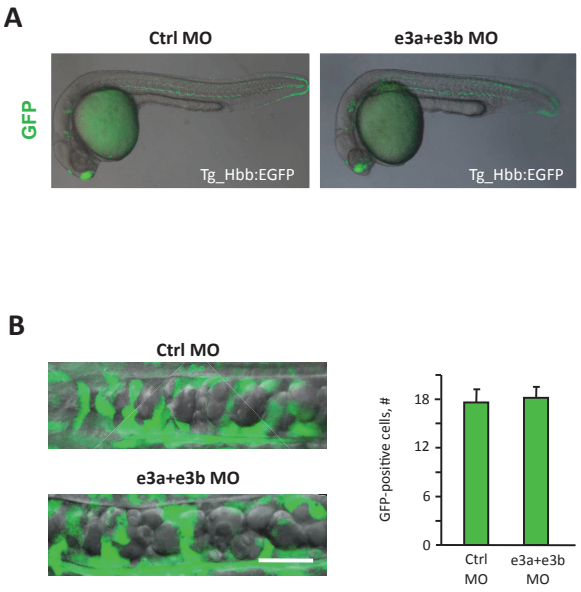
A
Ctrl MO
e3a+e3b MO
GFP
Tg_Hbb:EGFP
Tg_Hbb:EGFP
B
Ctrl MO
e3a+e3b MO
GFP-positive cells, #
18
12
6
0
Ctrl MO
e3a+e3b MO

Figure S4

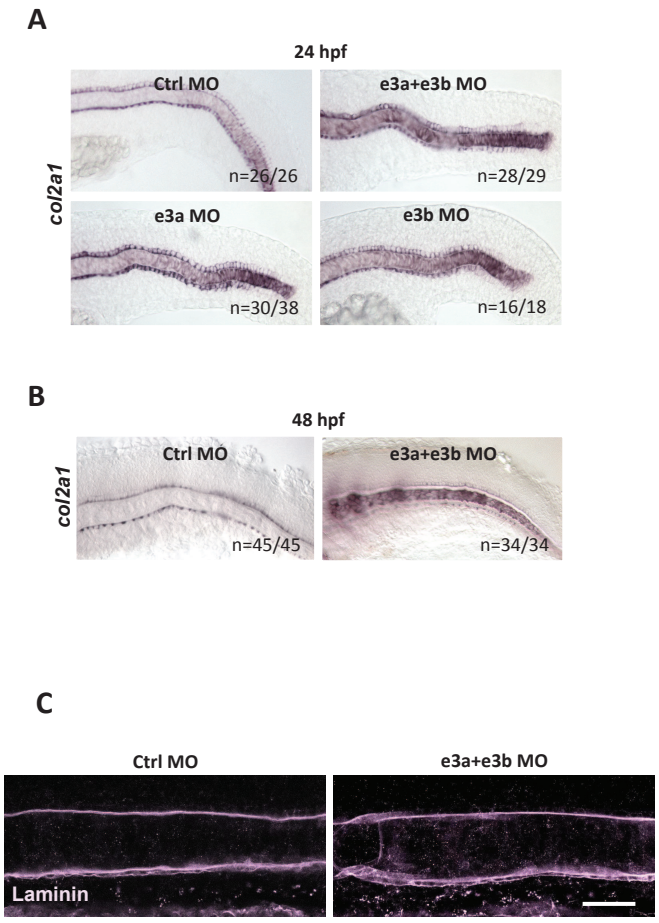
A
24 hpf
Ctrl MO
e3a+e3b MO
col2a1
n=26/26
n=28/29
e3a MO
e3b MO
n=30/38
n=16/18
B
48 hpf
Ctrl MO
e3a+e3b MO
col2a1
n=45/45
n=34/34
C
Ctrl MO
e3a+e3b MO
Laminin

Figure S5

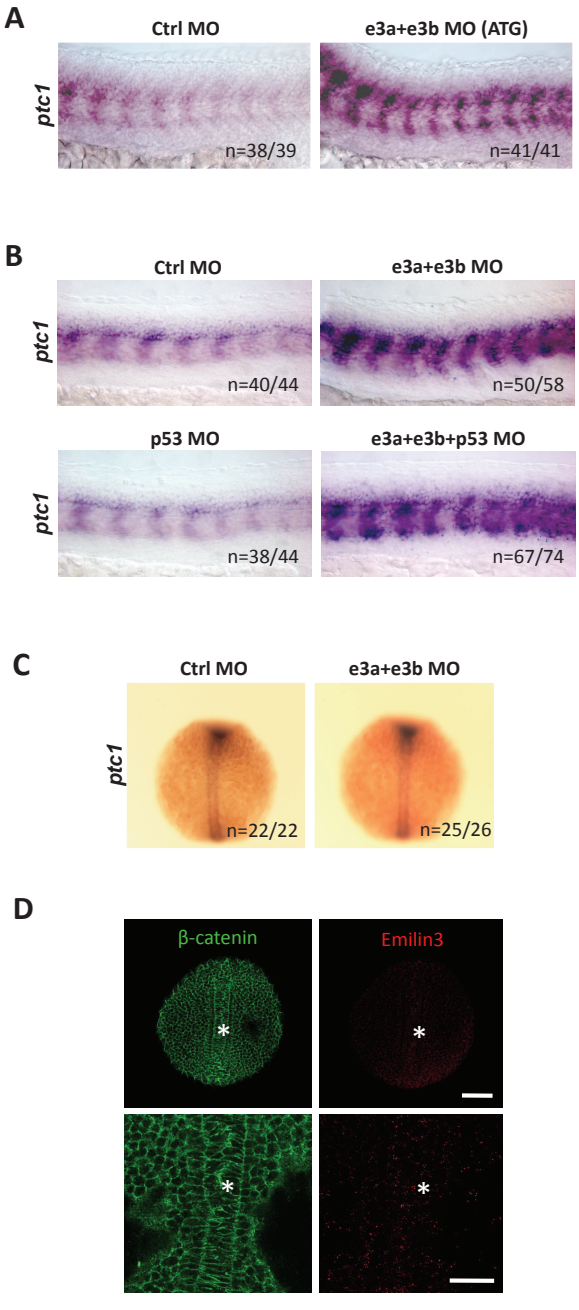
A
Ctrl MO
e3a+e3b MO (ATG)
ptc1
n=38/39
n=41/41
B
Ctrl MO
e3a+e3b MO
ptc1
n=40/44
n=50/58
p53 MO
e3a+e3b+p53 MO
ptc1
n=38/44
n=67/74
C
Ctrl MO
e3a+e3b MO
ptc1
n=22/22
n=25/26
D
β-catenin
Emilin3

Figure S6

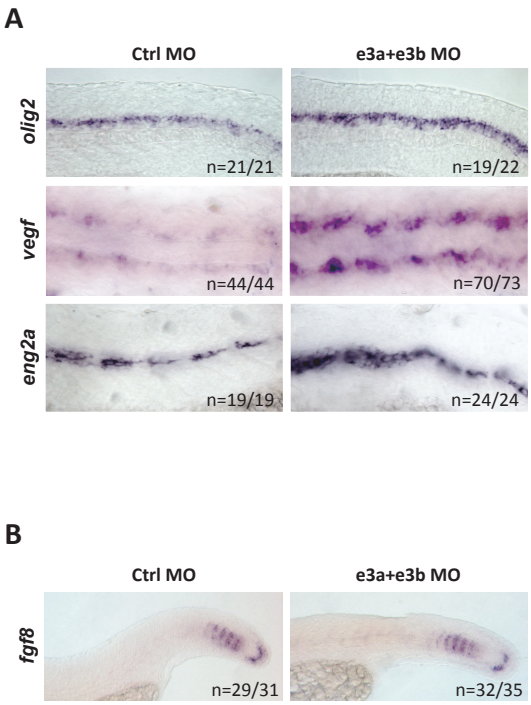
A
Ctrl MO
e3a+e3b MO
olig2
n=21/21
n=19/22
vegf
n=44/44
n=70/73
eng2a
n=19/19
n=24/24
B
Ctrl MO
e3a+e3b MO
fgf8
n=29/31
n=32/35

Figure S7

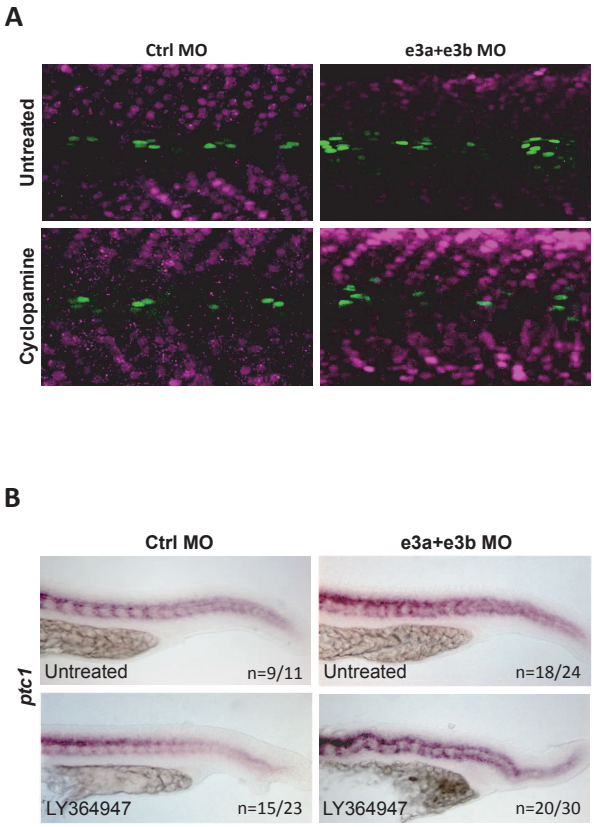
A
Ctrl MO
e3a+e3b MO
Untreated
Cyclopamine
B
Ctrl MO
e3a+e3b MO
ptc1
Untreated
n=9/11
Untreated
n=18/24
LY364947
n=15/23
LY364947
n=20/30

Figure S8

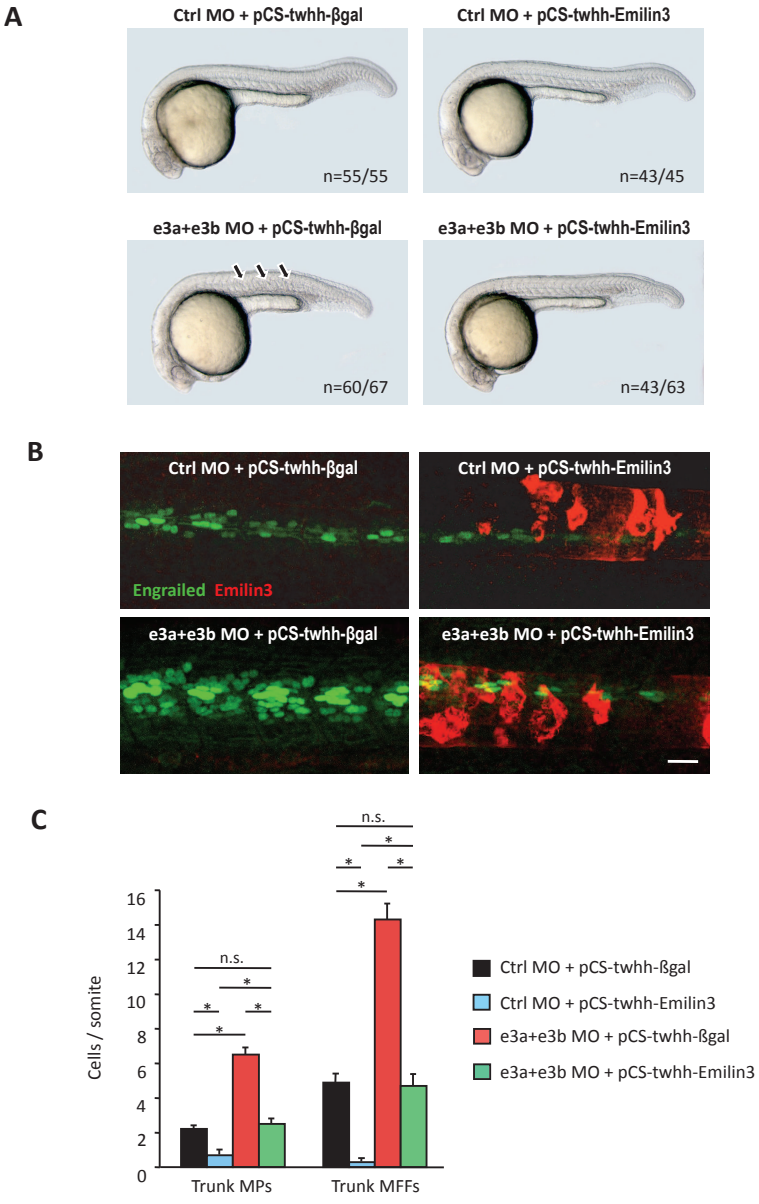
A
Ctrl MO + pCS-twhh-βgal
Ctrl MO + pCS-twhh-Emilin3
n=55/55
n=43/45
e3a+e3b MO + pCS-twhh-βgal
e3a+e3b MO + pCS-twhh-Emilin3
n=60/67
n=43/63
B
Ctrl MO + pCS-twhh-βgal
Ctrl MO + pCS-twhh-Emilin3
Engrailed Emilin3
e3a+e3b MO + pCS-twhh-βgal
e3a+e3b MO + pCS-twhh-Emilin3
C
Cells / somite
16
14
12
10
8
6
4
2
0
n.s.
*
Trunk MPs
Trunk MFFs
Ctrl MO + pCS-twhh-ßgal
Ctrl MO + pCS-twhh-Emilin3
e3a+e3b MO + pCS-twhh-ßgal
e3a+e3b MO + pCS-twhh-Emilin3

Figure S9

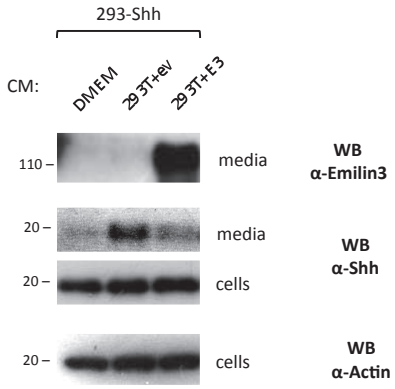
293-Shh
CM:
DMEM
293T+ev
293T+E3
110 –
media
WB
α-Emilin3
20 –
media
20 –
cells
WB
α-Shh
20 –
cells
WB
α-Actin

Figure S10

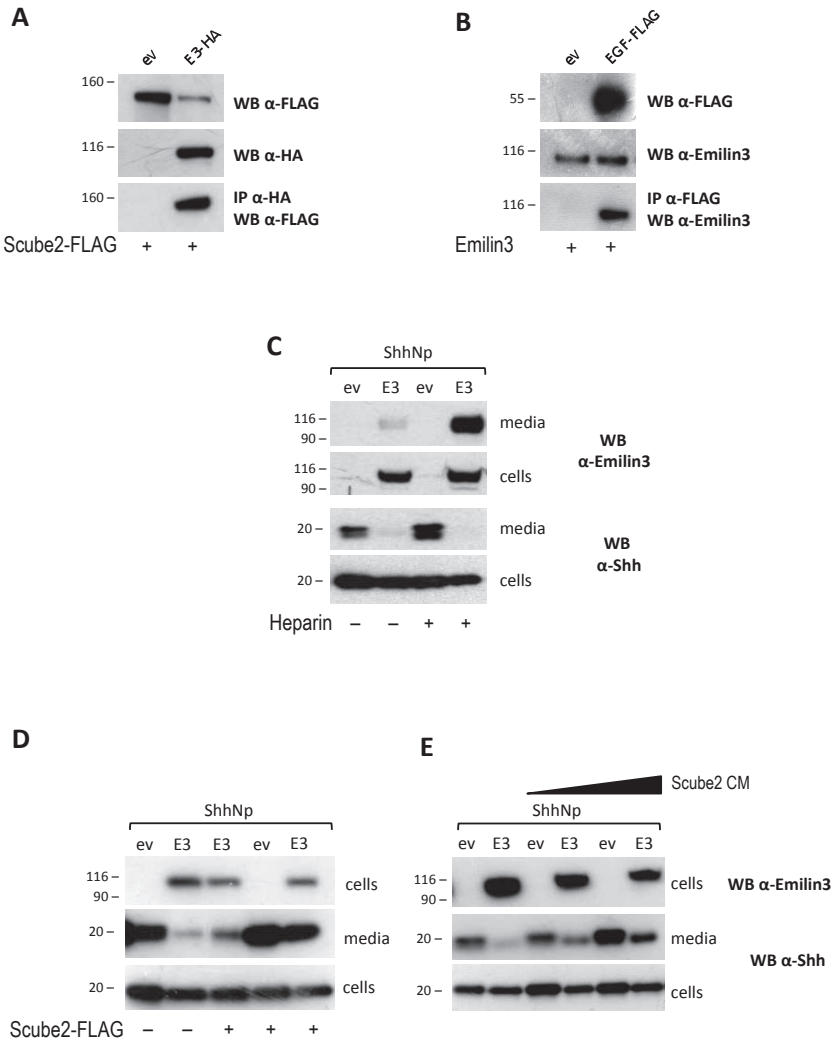
A
ev
E3-HA
160 –
WB α-FLAG
116 –
WB α-HA
160 –
IP α-HA
WB α-FLAG
Scube2-FLAG + +
B
ev
EGF-FLAG
55 –
WB α-FLAG
116 –
WB α-Emilin3
116 –
IP α-FLAG
WB α-Emilin3
Emilin3 + +
C
ShhNp
ev E3 ev E3
116 –
90 –
media
cells
WB
α-Emilin3
20 –
media
cells
WB
α-Shh
Heparin – – + +
D
ShhNp
ev E3 E3 ev E3
116 –
90 –
cells
20 –
media
20 –
cells
Scube2-FLAG – – + + +
E
Scube2 CM
ShhNp
ev E3 ev E3 ev E3
116 –
90 –
cells
WB α-Emilin3
20 –
media
WB α-Shh
20 –
cells

Figure S11

A

B

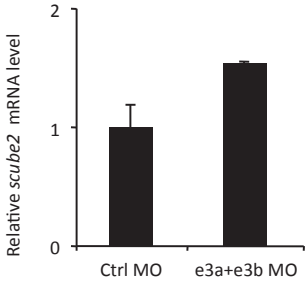

Table S1

Type of morpholino	Dose (ng)	Embryos examined	Phenotype		
			Normal	Notochord defects	Radialized embryos
Ctrl	4	153	151 (99%)	0 (0%)	2 (1%)
e3a (splice)	2	63	61 (97%)	1 (1.5%)	1 (1.5%)
e3a (splice)	4	68	50 (74%)	17 (25%)	1 (1%)
e3b (splice)	2	63	58 (92%)	3 (5%)	2 (3%)
e3b (splice)	4	63	54 (86%)	7 (11%)	2 (3%)
e3a (splice) + e3b (splice)	4 + 4	80	3 (5%)	58 (92%)	2 (3%)
	2 + 2	231	33 (14%)	195 (84%)	3 (2%)
	0.5 + 0.5	55	61 (97%)	1 (1.5%)	1 (1.5%)
e3a (ATG)	2	69	51 (74%)	17 (24%)	1 (2%)
e3b (ATG)	2	51	38 (75%)	13 (25%)	0 (0%)
e3a (ATG) + e3b (ATG)	2 + 2	106	12 (11%)	94 (89%)	0 (0%)
Ctrl	3.5	40	37 (92%)	0 (0%)	3 (8%)
e3a (splice)	2	63	61 (97%)	1 (1.5%)	1 (1.5%)
e3b (ATG)	1.5	42	42 (100%)	0 (0%)	0 (0%)
e3a (splice) + e3b (ATG)	2 + 1.5	62	27 (44%)	33 (53%)	2 (3%)

Table S2

Type of morpholino	Sequence
e3a MO (splice)	5′ –TTACTCATGGATACTTACTTGTGCC– 3′
e3b MO (splice)	5′ –TAGCGTTTACTTACTTATGATGCCC– 3′
col2a1 MO (splice)	5′ –TGAAAAACTCCAACTTACGGTCATC– 3′
e3a MO (ATG)	5′ –TGCAAAATCTTCTCC AGTAGCATGA– 3′
e3b MO (ATG)	5′ –ACGGAAATGCAAGAATCCACCTCAT– 3′
scube2 MO (ATG)	5′ –GCCGTACAGTCCAAACAGCTCCCAT– 3′
p53 MO (ATG)	5′ –GCGCCATTGCTTTGCAAGAATTG– 3′
Ctrl MO	5′ –CCTCTTACCCTAGTTACAATTTATA– 3′

Chapter I

The notochord: structure and function

Cellular and Molecular Life Sciences

Cell.Mol.Life Sci.
Volume 72
No. 16, 2015
Pages 2989 – 3200
August 2015, 2nd issue
ISSN 1420-682X

Cellular and Molecular Life Sciences

Cell.Mol.Life Sci. | Volume 72 | No. 16 | 2015 | pp. 2989 – 3200 | August 2015, 2nd issue

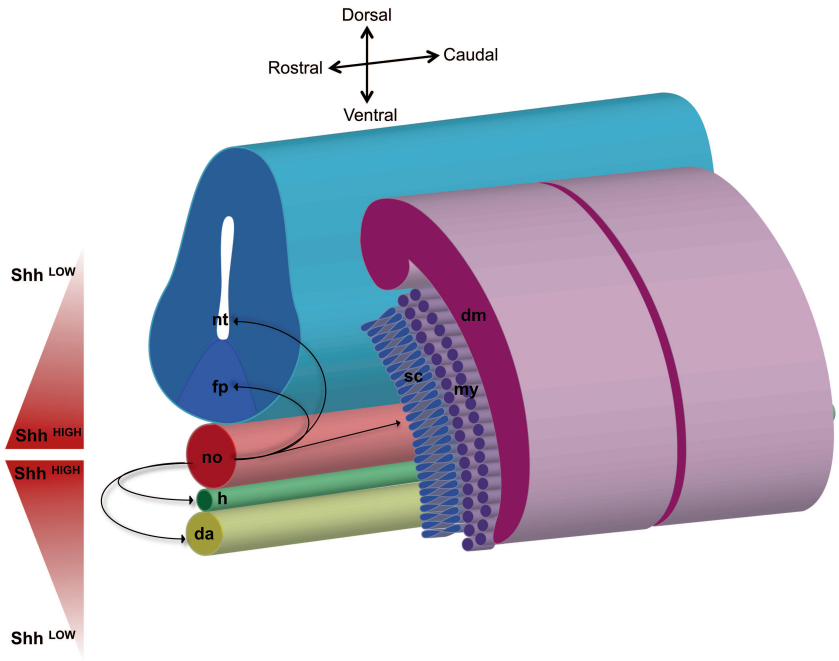

Springer

Cell. Mol. Life Sci.
DOI 10.1007/s00018-015-1897-z

Cellular and Molecular Life Sciences

REVIEW

The notochord: structure and functions

Diana Corallo[1] · Valeria Trapani[1] · Paolo Bonaldo[1]

Received: 12 February 2015 / Revised: 23 March 2015 / Accepted: 26 March 2015
© Springer Basel 2015

Abstract The notochord is an embryonic midline structure common to all members of the phylum Chordata, providing both mechanical and signaling cues to the developing embryo. In vertebrates, the notochord arises from the dorsal organizer and it is critical for proper vertebrate development. This evolutionary conserved structure located at the developing midline defines the primitive axis of embryos and represents the structural element essential for locomotion. Besides its primary structural function, the notochord is also a source of developmental signals that patterns surrounding tissues. Among the signals secreted by the notochord, Hedgehog proteins play key roles during embryogenesis. The Hedgehog signaling pathway is a central regulator of embryonic development, controlling the patterning and proliferation of a wide variety of organs. In this review, we summarize the current knowledge on notochord structure and functions, with a particular emphasis on the key developmental events that take place in vertebrates. Moreover, we discuss some genetic studies highlighting the phenotypic consequences of impaired notochord development, which enabled to understand the molecular basis of different human congenital defects and diseases.

Keywords Notochord · Vacuoles · Peri-notochordal basement membrane · Signaling · Nucleus pulposus · Chordomas

✉ Paolo Bonaldo
bonaldo@bio.unipd.it

[1] Department of Molecular Medicine, University of Padova, Viale G. Colombo 3, 35131 Padua, Italy

Introduction

The notochord is the most prominent feature of chordates, which originated more than 550 million years ago. Indeed, the phylum *Chordata* is named after this structure. Many examples in literature describe the evolutionary origin of this distinct chordate character in the history of metazoan evolution, first studied by Alexander Kowalevsky more than 150 years ago [1, 2] (for a review, see [3–5]). A recent study on the polychaete worm *Platynereis dumerilii* proposed an earlier evolutionary origin in the most recent common ancestor of chordates and annelids [6]. This work challenged the previous view that considered the notochord as an evolutionary innovation of chordates.

In vertebrates, the notochord arises from the dorsal organizer. The organizer appears during gastrulation and has an essential role in the induction of the embryonic axis. In particular, the organizer mediates the dorsal patterning to the mesoderm, regulates the movements of the ectoderm and mesoderm, and finally provides signals necessary for the induction of the neuroectoderm along the antero-posterior axis [7, 8]. In teleosts, the dorsal organizer (named embryonic shield) gives rise to three different germ layers: the floor plate, the notochord and the hypochord [9, 10]. In particular, the notochord precursor, called "chordamesoderm", begins as a rod of stacked cells that converge at the embryonic midline and express specific markers, such as *echidna hedgehog* (*ehh*), *sonic hedgehog* (*shh*), *collagen II* (*col2a1*), and *no tail* (*ntl*) [11]. During the segmentation stage, the expression of these early marker genes is turned off and chordamesoderm cells differentiate into two distinct cell subpopulations, through a Notch-dependent mechanism [12]—an outer sheath layer and an inner vacuolated cell layer. The outer cells secrete a thick extracellular peri-notochordal basement membrane

Published online: 02 April 2015

composed of several extracellular matrix proteins, whereas inner cells form large fluid-filled intracellular vacuoles that occupy most of the cell volume (Fig. 1). The notochordal sheath and vacuoles have been described in all analyzed vertebrate species, corroborating the essential role of these components during embryonic development [13, 14]. Indeed, the pressure exerted by notochord vacuoles on the peri-notochordal basement membrane endows this structure with a characteristic stiffness and mechanical strength. In this way, a hydrostatic skeleton is generated during development, driving the elongation of the antero-posterior axis before spine morphogenesis [15, 16]. The biogenesis of vacuolated cells was recently clarified in zebrafish, and it has been suggested that these vacuoles are lysosome-related organelles originating through an H^+-ATPase-dependent acidification and Rab32 function [16]. Beyond its structural role, the notochord plays critical functions for developing embryos. In fact, it is also a source of secreted growth factors, such as Sonic hedgehog (Shh), which instruct surrounding tissues to acquire specific differentiated fates.

In this review, we will highlight both the mechanical and signaling role of the notochord, emphasizing the studies performed in zebrafish, one of the major animal models used for the examination of this structure. We will provide an overview of evidences explaining the influence of the notochord on the patterning and maintenance of different neighboring tissues. In the past, elegant mechanistic and genetic studies highlighted that the notochord is a key structural and molecular component of the developing embryo. In more recent studies, some of the molecular mechanisms underlying notochord morphogenesis and function were thoroughly dissected. The full knowledge of notochord structure and function in vertebrates during both early development and late-life stages may enable to better understand different human congenital vertebral defects.

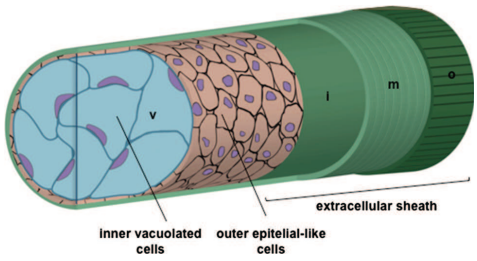

Fig. 1 Structure of the zebrafish notochord and its surrounding sheaths. This cartoon illustrates notochord structure of inner vacuolated cells surrounded by an epithelial-like sheath of cells. Around these cells, a peri-notochordal BM is present. This extracellular sheath is composed of three parts: the inner (*i*) basal lamina, surrounded by a medial (*m*) layer of collagen fibrils that run parallel to the notochord, and an outer (*o*) granular layer of loosely organized matrix that is mostly oriented in a perpendicular manner to the notochord. The peri-notochordal sheath counteracts the pressure generated from vacuoles (*v*), providing the rigidity and the correct stiffness of this structure

The peri-notochordal basement membrane

Basement membranes (BM) are complex structures composed of different extracellular proteins situated in close contact with cells at various locations in the body. Ultrastructural analysis revealed significant differences in the organization of BMs among different organs [17]. Moreover, there is a large hetereogeneity in the molecular composition of BMs [18, 19], as well as in the mutual interactions and the supramolecular organization of different BM components. The composition of BM together with the repertoire of matrix receptors defines the specificity of cellular responses [20]. The morphology of the peri-notochordal BM is similar among different species, such as teleosts, amphibians and chicken [21]. The peri-notochordal BM is normally composed of three different laminar layers. The single inner layer, in close proximity to the plasma membrane, mainly contains laminins. The intermediate layer is composed of dense collagen fibers oriented in one parallel direction around notochord cells, and distal to this there is an outer layer of fibers oriented in an orthogonal direction [22–24]. This tension-resisting sheath contains vacuolated cells under pressure, resembling the hydrostatic skeleton of different organisms (e.g. worms, herbaceous plants). Biomechanical studies in *Xenopus laevis* revealed that the role of the notochord sheath in constraining the shape and size of the notochord during development is influenced by the orientation of the sheath fibers [15]. This suggests that the complex fiber architecture of the notochord is related to its peculiar mechanical function.

Work in zebrafish showed that the formation of a notochord sheath is closely linked to the differentiation of notochord cells, and their reciprocal interactions are fundamental for the proper development and function of the notochord itself [12, 22, 25–27]. The fine interplay between cell–cell and cell–matrix interactions during notochord morphogenesis has been elegantly described in *X. laevis*, uncovering the function of the transmembrane receptor dystroglycan in laminin assembly, cell polarization and vacuole differentiation [28]. The cytoskeletal integrity and the correct stiffness of these cells are essential characteristics that provide resistance to the increasing pressure generated by inflating vacuoles, leading to body axis elongation [28]. In mice, several mutations that specifically

affect the development of the notochord have been identified (for a review, see [29]). Mutational studies in zebrafish embryos led to a more comprehensive understanding of notochord development and function. Here we report and discuss previous works describing notochord-related phenotypes due to the loss of different notochord components.

Mutants with early specification defects of the axial mesoderm

The relationships between the dorsal organizer activity and the formation of a mature notochord have been extensively characterized, providing valuable information on the genetic basis of axis formation and notochord development. During early gastrulation, different cellular rearrangements and inductive gene expression patterns promote the transition from the dorsal organizer to chordamesoderm. Analysis of different zebrafish mutant lines revealed two essential loci as key factors for this transition: *bozozok* (*boz*) and *floating head* (*flh*).

The zebrafish *flh* gene encodes a homeodomain transcription factor, homologous to *Not* genes of *Xenopus* and chick [30–32], which is expressed in the dorsal organizer and notochord during early development [31]. *flh* mutant embryos entirely lack notochord, which is substituted with muscle tissue in the midline [31, 33]. Thus, *flh* acts to promote notochord development and repress muscle development in axial mesodermal cells by antagonizing *spadetail* (*spt*), a T-box transcription factor normally required for proper morphogenesis and fate specification of trunk somitic muscle cells [34, 35]. Indeed, loss of *spt* function rescues many aspects of the *flh* mutant phenotype. *spt*/*flh* double mutant embryos develop an anterior notochord, a nearly complete floor plate and do not form ectopic midline muscle, indicating that *flh* normally antagonizes *spt* function in the developing midline mesoderm. The data obtained from studies in zebrafish and *Xenopus* embryos suggest that *flh*/*Not* genes are necessary and sufficient to maintain notochordal fate along the entire antero–posterior body axis [31, 36, 37]. Conversely, in mouse embryos, the role of *Not* appears to be different. Loss of *Not* function does not affect notochord development in the anterior body axis, but results in abnormal notochord formation in the posterior trunk. This suggests that the role of individual components of the genetic hierarchy governing notochord development vary between different vertebrate species [38].

The zebrafish *boz* gene encodes for a homeodomain protein named Dharma, previously described for its ability to induce axis formation in the zebrafish embryo [39]. *boz* mutants display a reduction or a complete loss of the dorsal organizer, with consequent loss of the organizer-derived dorsal midline structures including notochord, prechordal mesendoderm, hypocord and floor plate [40]. Interestingly, the phenotype of *boz* mutants strongly resembles the one observed after mechanical removal of the embryonic shield, indicating that perturbing in different ways the shield signaling center may cause the same consequences [1]. Moreover, expression of several genes in the embryonic shield is decreased or absent in *boz* mutants, whereas analysis of endodermal marker, such as *axial*, showed that only the dorsal mesodermal tissue is affected [40]. At the onset of gastrulation, expression of the notochord-specific *flh* gene is almost absent in *boz* embryos [40]. For these reasons, since the embryonic shield does not form in *boz* mutants and expression of dorsal-specific genes is affected before the shield stage, activity of the Dharma protein is required at the blastula stages for the formation of a complete organizer.

A systematic mutation analysis of early zebrafish development revealed another gene, named *momo* (*mom*), which is required for early notochord formation [41]. In *mom* mutants, the notochord fails to form in the trunk region but appears normal in the tail region. Notably, only one mutated allele of *mom* has been isolated and its phenotype is not fully penetrant, suggesting that the isolated allele is not a null mutation. *mom* embryos with a strong phenotype display some similarities with the *flh* mutants, suggesting that *flh* and *mom* have a common role in early specification of the axial mesoderm [41].

Fibronectin is an abundant component of the extracellular matrix throughout the body and it is also found in the peri-notochordal basement membrane of mouse, zebrafish and frog [28, 42, 43]. Despite grossly normal cell fate specification, as well as differentiation and migration of diverse embryonic lineages, fibronectin mutant fish, mouse and frog embryos display severe defects in the overall embryonic morphogenesis and in particular in the formation of somites from somite precursors, differentiation of heart from cardiac precursors, and morphogenesis of the notochordal plate into the notochord [44–49].

Mutants with early notochord defects

In *no tail* (*ntl*) and *doc* (*doc*) mutants chordamesoderm cells are present in the trunk but then fail to differentiate into a mature notochord. In particular, although *ntl* mutants develop a BM, the tail does not form and the notochord is completely absent in the most posterior region of the trunk, leading to the fusion of the somites [50]. *ntl* is orthologous to *Brachyury*, a well-known gene previously characterized in mouse and *Xenopus* models [50–53]. *ntl* encodes for a putative transcription factor that is transiently expressed in both notochord and tail and it is essential for development of both domains [50, 53–58]. Loss of *Brachyury*/*ntl*

function appears to disrupt morphogenesis of mesoderm during gastrulation in both mouse and zebrafish [59, 60] suggesting that *ntl* plays an early role in cell fate choice at the dorsal midline to antagonize floor plate development and promoting the notochord formation. Moreover, experiments conducted in *ntl/flh* double mutants revealed that these two proteins cooperate during chordamesoderm differentiation with a predominant effect of *ntl* on *flh*.

In addition to *ntl*, in *doc* mutants the chordamesoderm fail to differentiate in most parts of the embryo, despite the formation of a peri-notochordal BM. In *doc* mutants notochord cells fail to form normal vacuoles and mutant embryos show a reduction of the main axis. The analysis of *ntl* expression in *doc* mutants and the similarities of the two mutant phenotypes suggest that *doc* is required for the maintenance of *ntl* expression after gastrulation, which in turn is necessary for the differentiation of the chordamesoderm into notochord [41].

Mutants with late notochord defects

Several studies mostly exploited in zebrafish revealed that the BM is not only an essential structural component of the notochord, but it is also required for its right morphogenesis [23]. Although the precise molecular composition of this structure is still partially unknown, during the final stages of notochord development, several proteins have been characterized as essential constituents of the peri-notochordal BM.

Laminins are a family of heterotrimeric extracellular glycoproteins and are the major components of basal lamina of many different tissues. Laminins are composed of a central α-chain, with a varying number of globular regions, and two chains (β- and γ-) with helical and globular regions. The trimeric proteins interconnect cell membranes and extracellular matrix molecules and also bind to each other to form sheets in the basal lamina [61]. The first genetic alterations causing abrogation of notochord sheath formation were identified in the laminin β1 and laminin γ1 genes in the zebrafish [22]. *Lamc1* null mouse embryos die too early (E5.5) to study the role of laminin γ1 in notochord sheath formation in this model [62]. In *grumpy* (*gup*) and *sleepy* (*sly*) zebrafish mutants, in which the zygotic supply of the laminin β1 or γ1 chain is disrupted, laminin 1 protein (or other laminin isoforms containing the β1 or γ1 chain) is absent in the whole embryo, causing at least two types of defects. First, electron microscopy analysis showed a disorganization and loss of the three layers of peri-notochordal BM. This phenotype indicates that laminin 1 is an essential component of this structure and it might serve as a scaffold for the normal organization of other BM components [22]. Moreover, notochord cells fail to form proper vacuoles resulting in a significant shortening of the main embryonic axis, in agreement with the fact that the BM has to sustain the hydrostatic pressure generated from vacuolated cells. Finally, in *grumpy* (*gup*) and *sleepy* (*sly*) mutants, where laminin β1 or γ1 chains are disrupted, notochord cells do not differentiate, as revealed by the persistent notochordal expression of early expressed genes, such as collagen type II (*col2a1*), Sonic hedgehog (*shh*) and Echidna hedgehog (*ehh*). This phenotype suggests that signals coming from BM proteins are required for notochord differentiation and survival, albeit the molecular mechanisms underlying this process are still unknown. Transplantation experiments provided the link between laminin deposition and notochord differentiation: when *gup* or *sly* mutant shields were transplanted to wild-type hosts, a resulting secondary axis was formed with phenotypically normal notochord. Therefore, laminin β1 and laminin γ1 can non-autonomously rescue notochord differentiation. Moreover, wild-type shield cells transplanted into mutant hosts also form normal notochords. Hence, functional laminin chains can be supplied to the notochord from either autonomous or non-autonomous cell sources [22].

The zebrafish locus *bashful* (*bal*) encodes for laminin α1 [63]. Mutants lacking this laminin chain display a weaker phenotype compared to *gup* and *sly* mutants, since only the anterior region of the notochord fails to form. Interestingly, while laminin 1 immunoreactivity is totally ablated in *gup* and *sly* mutants, *bal* mutant embryos display laminin 1 deposition in the posterior notochord. This data suggests that other laminin isoforms have a redundant role in posterior notochord development. Indeed, knockdown of laminin α4 and α5 chains by injection of antisense morpholino oligonucleotides (MOs) in *bal* null embryos results in a more severe notochord phenotype, comparable to the one observed in *gup* and *sly* mutants [63]. In particular, in laminin α4-MO injected *bal* mutant embryos vacuoles fail to inflate properly, *ehh* expression is abnormally persistent and laminin 1 immunoreactivity is severely reduced. Injection of laminin α5-MO in *bal* mutants leads to the same abnormal and persistent expression of *ehh* along the notochord, concurrently with failure of cellular inflation and loss of laminin immunoreactivity. Taken together, these results pointed to a redundant role for laminin 411 (also called laminin 8) and laminin 511 (also called laminin 10) in chordamesoderm differentiation and BM assembly [63].

Together with laminins, other extracellular matrix proteins localized in the peri-notochordal BM have an essential role during notochord development. Collagens, the most abundant extracellular matrix proteins, are composed of three polypeptide α-chains coiled around each other to form the triple helical configuration. Depending upon the collagen type, the molecule can be composed of either three identical α-chains

(homotrimers), or two or three different α-chains (heterotrimers). Collagens assemble into different types of extracellular matrix structures such as fibrils (e.g., collagen types I–III), networks (e.g., collagen type IV) and microfilaments (e.g., collagen type VI) [64]. Characterization of one recessive lethal mutant, named Gulliver (gul), revealed a new role for the alpha 1 chain of type VIII collagen (*col8a1*) in notochord morphogenesis [65]. *gul* mutant embryos display notochord distortion accompanied by a disorganization of collagen fibers only in the medial layer of the notochord sheath. Interestingly, notochord cells form inflated vacuoles and survive, despite the accumulation of protein aggregates in the rough endoplasmic reticulum. It is reasonable to speculate that the undulated shape of the notochord in *gul* mutants may be due to the defective peri-notochordal BM architecture that is not able to sustain the hydrostatic pressure generated from vacuolated cells. In addition to *col8a1*, MO-mediated knockdown of the alpha 1 chain of type XV collagen (*col15a1*) revealed a new role for this extracellular matrix protein as an essential component of the peri-notochordal BM. In *col15a1*-depleted embryos notochord differentiation is impaired, as suggested by the reduction of the mean size of vacuoles and persistent expression of the two chordamesodermal markers *col2a1* and *ehh*. Moreover, all the three layers of the peri-notochordal BM appear affected and highly disorganized in *col15a1*-depleted embryos, with a lower number of less dense collagen fibers in the medial and outer layers and a disruption of the inner layer [25]. A key role for type XXVII collagen (*col27a1a* and *col27a1b* paralogs) in notochord morphogenesis has been also identified [66]. Both *col27a1a* and *col27a1b* show a dynamic expression in the notochord, closely similar to that displayed by *col2a1*. Single knockdown of *col27a1a* or double knockdown of both paralogs leads to a notochord curvature at early developmental stages, together with abnormal cellular clumping along the notochord sheath and protein accumulation beside notochord cell membranes. These results suggest that loss of *col27a1a* and *col27a1b* leads to a weak peri-notochordal sheath that is unable to withstand the pressure generated by vacuolated cells within the notochord [66].

A similar (but not identical) phenotype has been observed after the concurrent knockdown of *loxl1* and *loxl5b*, two lysyl oxidase-coding genes expressed in the developing notochord [67]. Lysyl oxidases are copper-dependent enzymes that catalyze the crosslinking of elastin and collagens, thus stabilizing the extracellular matrix and maintaining notochord sheath integrity. MO-mediated knockdown of *loxl1* or *loxl5b* does not result in notochord distortion, whereas *loxl1*/*lox5b* double morphants recapitulate the kinked notochord observed also with chemically induced copper deficiency [67]. This finding indicates that these two enzymes have overlapping functions during notochord development. Interestingly, inhibition of lysyl oxidases activity by pharmacological treatments or genetic ablation of *loxl1* and *loxl5b* does not affect the peri-notochordal BM deposition and organization, consistent with the concept that lysyl oxidase inhibition alters the final stages of notochord sheath deposition and organization [67]. In addition, the impaired lysyl oxidase activity appears to prevent the differentiation of vacuolated cells, as suggested from the persistent expression of *col2a1*. One explanation for this sustained *col2a1* expression might come from a general loss of notochord strength and stiffness. Hence, it is likely that the BM is required to sense or to transduce a notochord differentiation signal, although a precise mechanistic explanation is still missing. All reported data provide an interesting model for studying the relationships between BM organization, nutritional deficiencies and copper metabolism disorders, in agreement with the essential role of copper for notochord structural organization [68]. For example, copper deficiency results in severe developmental abnormalities. This is most clearly illustrated by Menkes disease (OMIM #309400), a rare X-linked disorder of copper metabolism [69]. Interestingly, as Menkes disease models and to study the effects of developmental copper deprivation, zebrafish *calamity* (*cal*) and *catastrophe* (*cto*) mutants represent a valuable tool for high-throughput chemical screenings [68, 70].

A forward genetic screen for mutants displaying notochord sensitivity to lysyl oxidase inhibition pointed out a role for the extracellular matrix protein fibrillin-2 in notochord morphogenesis [71]. Fibrillin-2 mutants (*puff daddy*) and morphant embryos display notochord distortion with a marked reduction of the peri-notochordal BM outer layer size, while the other two layers appear normally organized. Moreover, as observed also in *col2a1*-depleted embryos [67], fibrillin-2 mutants are sensitized to lysyl oxidases inhibition obtained by *loxl5b* MO-mediated knockdown or by pharmacological treatment. This sensitivity may be caused in part by an impaired ability to bind and recruit lysyl oxidases at their correct site of action during notochord formation, as already described in knockout mice for other microfibril-associated proteins such as elastin and fibulin-5 [72].

More recently, a similar phenotype has been described for Emilin3, a glycoprotein of the extracellular matrix localized in the peri-notochordal BM at early stages of zebrafish development [27]. The concurrent knockdown of both Emilin3 paralogs (*emilin3a* and *emilin3b*) leads to a marked distortion of the notochord associated with a significant shortening of the main embryonic axis. Moreover, fibers of the medial layer of the peri-notochordal BM are

disorganized and frequently disrupted in Emilin3 morphant embryos, whereas the outer and inner layers appear normal. Interestingly, quantification of total and vacuolated notochord cells in control and Emilin3 depleted embryos did not reveal any significant difference, suggesting that Emilin3 deficiency is not grossly perturbing the morphology and differentiation of notochord cells [27]. Although the phenotype is not as severe as in laminin mutants, also in Emilin3 double morphants the early chordamesodermal marker *col2a1* is persistently expressed, supporting the concept that defects in the notochord sheath can influence the gene expression pattern of notochord cells. However, in contrast to other models of notochord disruption, *shh* and *ehh* are overexpressed only in the expression field of *emilin3a* and *emilin3b* paralogs, at the level of the chordoneural hinge [27]. Conversely, laminin mutants and collagen XV morphants display a similar upregulation of *col2a1* and *ehh* in the notochord [22, 25]. This implies that notochord cells might respond to extracellular signals in a region-specific manner.

In addition to the genetic mutants and morphant models showing defects in later notochord formation, three other mutants have been characterized for their defects during the formation of a mature notochord. *Sneezy* (*sny*), *happy* (*hap*) and *dopey* (*dop*) loci encode the α, β and β′ subunits of the zebrafish coatomer complex [73]. This complex consists of seven subunits that in association with the small GTPase Arf1 form the vesicular coat of COPI vesicles. Coatomer complex is essential for the maintenance of the Golgi apparatus and the control of retrograde vesicular transport machinery. Hence, in the absence of COPI function, the normal transport of proteins from endoplasmic reticulum and Golgi is disrupted (for a review, see [74]). During chordamesoderm differentiation there is an elevated secretory activity and a higher demand for coatomer function in the notochord. For this reason, the mRNA expression is specifically upregulated during the transition from the chordamesoderm to the notochord [73]. Loss of COPI function in *sny, hap* and *dop* mutants produce almost identical morphological defects, including a shortening of the main axis due to the loss of notochord cell differentiation. This defect is confirmed by the persistent expression of the chordamesoderm markers *shh* and *col2a1* and the generation of vacuoles that fail to fully inflate and undergo to apoptosis [73]. Moreover, electron microscopy showed that, while the innermost layer of the peri-notochordal BM is correctly deposited and display normal levels of laminin 1 immunoreactivity, the medial layer is mostly disrupted [73]. Shield transplantation experiments showed that the medial layer of the peri-notochordal BM derives only from the chordamesoderm and, in contrast to the inner layer, cannot be supplied by exogenous sources [73]. These findings indicate that the notochord has a strict requirement for coatomer function in order to undergo its correct development and organization.

A number of other mutations were isolated in zebrafish, leading to a variety of other late notochord defects. For example, in *crash test dummy* (*ctd*), *zickzack* (*ziz*), *quasimodo* (*qam*), *kinks* (*kik*) and *wavy tail* (*wat*) mutants, the common phenotype is an undulated notochord along the body axis [41, 75].

Taken together, these studies in zebrafish mutant and morphant models highlighted the importance of the correct deposition and organization of the peri-notochordal BM during notochord development. First, the peri-notochordal BM is important for the elongation of the embryonic axis, conferring the proper rigidity to the developing embryo. Alterations of this structure may prevent the mechanical support needed to withstand the hydrostatic pressure originated from vacuoles. Although the various studies discussed here support the concept that the peri-notochordal BM is necessary for notochord differentiation, it remains unclear what is the relationship between the inability to form an extracellular sheath and the failure to differentiate. It is reasonable to speculate that loss of the BM may lead to loss of BM-associated signals, including gene expression, apoptosis, proliferation and regulation of growth factors. The analysis of other notochord mutants will be useful to obtain additional insights into the mechanism of signaling related to the BM and the notochord. The ability to knockdown candidate genes of interest using MOs had an important role in the application of the zebrafish as a model system. However, MOs can induce p53-dependent apoptosis [76–78], and several off-target phenotypes were described in a recent systematic phenotypic analysis of a large number of morphant embryos [79]. These shortcomings strongly raise the concept of reconsidering the use of antisense-based technology for characterization of gene function. The application of programmable site-specific nucleases or the recently developed CRISPR/Cas9 technology for in vivo targeted gene disruption may provide a much better option to characterize gene function during development.

Notochord signaling

In addition to its structural function, the notochord is also an important source of signals that are essential for patterning the adjacent tissues [23, 80]. In the sections below, we will discuss the experimental evidence indicating that the notochord is a source of key signaling molecules for the surrounding ectodermal, mesodermal and endodermal derived tissues (Fig. 2).

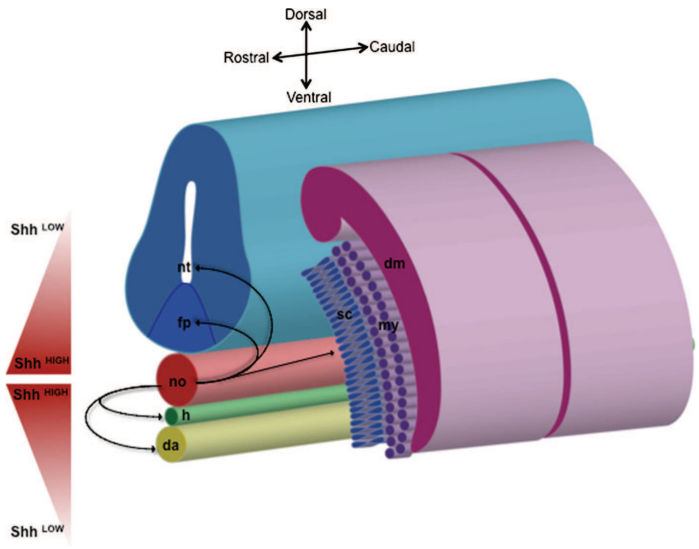

Fig. 2 Schematic diagram of transverse sections of a vertebrate embryo depicting notochord signaling to adjacent tissues. The notochord (*no*) secretes Shh, represented by *arrows* in the figure. This signal is responsible for patterning the ventral neural tube (*nt*). In particular, the notochord is able to induce the differentiation of the floor plate (*fp*), and they both represent a continuing source of ventralizing signals within the neural tube. The notochord is also important for somite differentiation, where Shh concentration gradients differentially pattern dorsal–ventral somitic fates. Very low levels of Shh signal to maintain the dermomyotome (*dm*); slightly higher levels induce both loss of dermomyotomal markers and activation of myogenic differentiation (myotome, *my*); finally, higher levels of Shh cause the loss of myotomal markers and the induction of sclerotome (*sc*). Notochord signaling is also critical for the development of the hypochord (*h*) and of the dorsal aorta (*da*)

Notochord signals for ectoderm development

The ectoderm is divided into three major domains: the outer ectoderm (mainly the epidermis), the neural tube (brain and spinal cord), and the neural crest (peripheral neurons, pigment, facial cartilage). During vertebrate embryonic development, signals from the dorsal organizer or its derivative, the notochord, are responsible for ectodermal commitment to a neuronal lineage.

Patterning the neural tube

Patterning of the neural tube is perhaps the best characterized role for the notochord during embryonic development. The vertebrate nervous system arises from the neural plate, a sheet of neuroepithelial cells that overlies the axial mesoderm. As development proceeds, the neural plate folds to form the neural tube, which in turn will form the spinal cord and the brain. At this stage, a dorsoventral polarity is established: cells in the dorsal half generate different neurons that relay sensory signals, whereas cells in the ventral half generate distinct classes of motor neurons and ventral interneurons that participate in the coordination of motor output (for a review, see [81]). Pioneering observations and embryological manipulations in chick and amphibians indicated that the notochord has a key role in establishing the dorsoventral polarity of the spinal cord [82, 83]. The notochord-secreted protein Shh was found to be the signal required and sufficient for patterning the ventral neural tube. The importance of Shh is confirmed by the loss of ventral neurons in embryos in which Shh signaling was either biochemically or genetically blocked [84–88]. Shh is initially secreted by the notochord and is able to induce the differentiation of the floor plate, a specialized group of neuroepithelial cells in the ventral portion of spinal cord [83, 89–91]. Then, floor plate cells express themselves *shh*, conferring the capability to specify both floor plate and motor neuron cellular fates, thus establishing a continuing source of a ventralizing signal within the neural tube. Evidences indicate that the minimal amount of Shh sufficient to induce the differentiation of each neuronal class in vitro correlates with the distance of Shh from its source of synthesis in vivo [88]. Thus, neurons generated in progressively more

ventral regions of the neural tube require higher Shh concentrations for their induction [88]. Moreover, the generation of an engineered mouse that produces fluorescently labelled Shh from the endogenous locus provided new insights into the possible mechanism of in vivo Shh signal distribution during neural tube patterning [92]. This study supports a model wherein a graded signaling response to notochord-derived Shh activates a long-range patterning process in the ventral neural tube. Indeed, when patterning begins, Shh ligand is first detected at the apical region of ventral midline cells and then is progressively extended to the dorsal region. Moreover, the temporal gradient of Shh ligand accumulation is similar to the in vitro profile of Shh concentrations that is needed to progressively specify more-ventral cell types [92].

Although the analysis of floor plate differentiation in avian and mammalian embryos provided a coherent picture of the inductive process, genetic studies in zebrafish revealed that a differentiated notochord is not strictly required for the generation of a floor plate in this vertebrate. Indeed, zebrafish mutants lacking the notochord (*flh*, *momo*, *bozozok*, and *ntl*) and *shh* mutants can develop al least the medial floor plate [93, 94]. In addition to *shh*, zebrafish embryos express two other Hh-related genes, *echidna hedgehog* (*ehh*) and *tiggywinkle hedgehog* (*twhh*), in notochord and floor plate respectively. Therefore, it is reasonable that multiple Hh genes might cooperate in the induction of a floor plate in zebrafish. Conversely, it is likely that only *shh* is responsible for the floor plate differentiation in avian and mammalian embryos. In fact, in chick and mouse embryos the specification of the floor plate and other ventral neuronal progenitors depends on distinct timing and duration of Shh signaling [95]. In a restricted developmental time frame, spanning from gastrulation to early somitogenesis stages, a transient burst of Shh signaling from the notochord is both necessary and sufficient for the specification of floor plate [82, 84, 87]. However, neural progenitors progressively lose their ability to acquire a floor plate identity in response to high levels of Shh. The downregulation of Shh signaling is a prerequisite for the onset of a floor plate identity [95]. Furthermore, it is likely that this mechanism contributes to the restriction of the floor plate to the neural tube midline. The possibility that neuroepithelial cells can generate a floor plate in response to other signaling pathways active within neural tissue cannot be excluded [95]. Notably, concomitant to Shh, signals of the bone morphogenetic protein (BMPs) family coming from the epidermal ectoderm control dorsal neural tube cell fate and modify its response to Shh signaling, by inhibiting the specification of a ventral cell fate [96–98]. In this context, the presence of notochord-derived BMP antagonists (e.g. Noggin, a notochord-secreted signaling molecule that binds and inactivates BMP, therefore playing a role in generating morphogenic gradients) allows to generate a permissive environment for Shh-mediated induction of the floor plate [99]. Notably, together with BMP ligands, other factors may also influence neural cell responsivity to Shh signaling. Interestingly, studies in chick embryos demonstrated that vitronectin, an extracellular matrix protein expressed in the notochord, is able to potentiate the motor neuron inducing activity of Shh through direct binding to Shh ligands [100, 101].

Patterning other ectoderm derivatives

Different literature data suggest that the notochord, together with the ventral diencephalon and the mesenchyme, is involved in the development of the anterior pituitary. During the formation of cephalic tissues, the rostral tip of the notochord is adjacent to the cephalic ectoderm, where the anterior pituitary starts to develop. Indeed, transplantation experiments revealed that the anterior notochord is able induce the outpouching of the head ectoderm [102]. This leads to a partial formation of the Rathke's pouch and the upward invagination of the oral ectoderm, giving rise to the anterior pituitary. Therefore, a close contact between the diencephalon and ectoderm is a prerequisite for the induction of the anterior pituitary [102].

Notochord signals for mesoderm development

The murine notochord, which is present from embryonic day (E) 7.5 until E12.5, forms all cell types of the nucleus pulposus in intervertebral discs (IVDs) [103, 104]. Moreover, temporal removal of Shh ligands from both the notochord and floor plate demonstrated that this signaling pathway is required for the formation of the peri-notochordal sheath and subsequently of the vertebral column [104]. More recently, it has been found that the expression of Shh in the notochord is sufficient to pattern the intervertebral discs and vertebral column. Indeed, removal of Shh from the notochord leads to failed Shh expression in the floor plate and results in the loss of vertebral structures and nuclei pulposi. In contrast, removal of Shh from the floor plate results in phenotypically normal vertebral column and intervertebral discs. These data indicate that the expression of Shh from the notochord is sufficient for patterning the entire vertebral column [105].

Patterning the somites

During vertebrate embryogenesis, the paraxial mesoderm that lies adjacent to the neural tube becomes segmented into paired epithelial somites. Then, each somite differentiates into the ventral sclerotome, from which the skeletal elements of the ribs and vertebral column derive, and the

dorsal dermomyotome. The dermomyotome further differentiates into the dorsal-lateral dermotome, giving rise to dermis and myotome. The myotome is localized between the sclerotome and the dermotome and represents the precursor of axial musculature. Multiple extracellular signals expressed in the surrounding tissues determine the dorsal and ventral somitic cell fates, establishing the number of precursors that will give rise to either cartilage, muscle or dermal cells (for a review, see [106]).

It has been shown that the initiation and maintenance of the sclerotome depends on both Shh and Noggin, a Bmp4 antagonist, which are both expressed in the notochord when the sclerotome formation begins. Shh produced by the notochord and the floor plate is also important for the proliferation and survival of sclerotomal cells [87, 107–111]. Indeed, in mice with ablation of Hh signaling, sclerotome formation is compromised and no vertebral column is formed [84, 112]. Conversely, gain-of-function studies have demonstrated that ectopic expression of Shh induces the expression of the sclerotomal marker Pax1 and inhibits the expression of the dermomyotomal marker Pax3 [108, 113]. Moreover, it has been demonstrated that the activity of notochord-derived Noggin is required for sclerotome differentiation, since Noggin-deficient embryos display defective sclerotome formation [114]. Indeed, Noggin inhibits the repressive activity of BMP signals, thus allowing the Shh-mediated induction of Pax1 in the somitic mesenchyme and the sclerotomal cell growth and differentiation into cartilage [114]. Therefore, it can be assumed that both signals, Shh and Noggin, cooperate during sclerotome formation [115]. In spite of this, studies in the Danforth's short-tail (Sd) mutant mouse, carrying a semi-dominant mutation that affect vertebral column development, challenged the concept that notochord might be required for sclerotome formation. In the Sd mouse model, although the notochord degenerates completely by E9.5, the floor plate is sufficient to maintain the differentiation of somites into sclerotomes and vertebrae [116]. More recently, it has been found that notochord-derived Shh regulates the expression of the chick early B cell factor 1 (cEbf1), a medial sclerotome marker expressed in somite areas close to the notochord that plays a crucial role for sclerotome development and formation of the vertebral body and pedicles [117].

In vitro and in vivo studies demonstrated that notochord-derived Shh promotes the myotome cell fate [118–121]. Mouse embryos lacking Shh or its cell membrane ligand Smoothened display markedly decreased expression of Myf5, a key myogenic regulatory factor [84, 112]. In zebrafish, Shh is required for the differentiation of Pax3/Pax7-expressing dermomyotomal cells into MyoD-positive differentiated myocytes. In the absence of Shh signaling, Pax3/Pax7-expressing cells increase in number, but fail to activate the myogenic program [122, 123]. Even in this context, the Shh concentration gradients work in a morphogen-like fashion to differentially pattern the dorsal–ventral somitic fates [124]. Indeed, different Shh levels elicit distinct responses in somitic cells. Very low Shh levels, combined with Wnt signaling activity, elicit the maintenance of dermomyotomal gene expression (Pax3). Slightly higher Shh levels induce both loss of dermomyotomal marker gene expression (Pax3) and activation of myogenic differentiation (Myf5 and MyoD). Finally, high Shh levels cause the loss of myotomal markers and the activation of sclerotomal gene expression [124].

It is known that dermomyotome progenitors colonizing the myotome first acquire a myocyte identity and subsequently proliferate as Pax7-expressing progenitors, before undergoing terminal differentiation. Recently, it was shown in both avian and mouse embryos that the loss of Shh responsiveness in dermomyotome-derived muscle progenitors is a key mechanism by which the myotome transits from differentiation into expansion [125]. Initially, Shh emanating from the notochord/floor plate through the sclerotome is able to reach the dermomyotome. In the dermomytome Shh both maintains the proliferation of dermomyotome cells and promotes the terminal myogenic differentiation of progenitors colonizing the myotome. Subsequently, when the myotome enters in the growth phase, myogenic progenitors become refractory to differentiation stimuli coming from Shh [125].

Studies in zebrafish revealed that the correct specification of different cell types within the myotome is also dependent on the timing at which they receive the signal from the notochord and on their competence to respond [126]. Initially, the exposure of myotomal precursors to Hh is restricted to adaxial cells, a single cell layer lying close to the embryonic shield. Then, notochord-derived Hh proteins induce adaxial cells to become slow-twitch muscle fibers [127]. The early exposure to Hh ligands seems to be essential for the specification of muscle pioneer precursors, the slow muscle fiber myoblasts that respond to the highest levels of signaling and express *engrailed* genes [128]. A minor component of muscle pioneers become fated to form the superficial slow fibers and move away from the notochord, displacing precursors of the fast twitch fibers. By this time, these cells—called medial fast fibers—are irreversibly committed to the fast lineage; nevertheless they retain the ability to respond to Hh, as evidenced by their activation of *engrailed* expression, though at lower levels than muscle pioneers [127].

Many zebrafish mutants affecting notochord development, such as *flh*, *mom*, *ntl* and *doc*, display a loss of muscle pioneers and of the horizontal myoseptum, the structure that separates somites into a dorsal and a ventral part. Indeed, cell transplantation experiments carried out in

ntl and *doc* mutants showed that somite defects can be rescued by exogenous wild-type notochord cells [31, 41, 50, 129]. Moreover, *flh* mutant embryos display the transdifferentiation of notochord to muscle [33], and an ectopic induction of both *myf5* and *myoD* in midline cells, especially in caudal somites. Indeed, abolishment of notochord-derived signals in *flh* mutants leads to extensive slow myogenesis, indicating that the combined action of floor plate-derived Twhh and notochord-derived Shh are sufficient to support non-pioneer slow myogenesis [33]. However, Twhh and Shh are unable to maintain and reinitiate MRF expression in adaxial cells during late stages of development. In fact, complete loss of ventral midline signals results in the absence of caudal slow muscle fibers and the formation of fast muscle fibers. Taken together, these data suggest that Shh released from the notochord is required for the maintenance of MRF expression. The additional exposure to midline signals reinitiates MRF expression and delays slow muscle fibers formation in *flh* and *ntl* mutants [130].

Patterning other mesodermal tissues

Notochord signaling is also important for the development of heart and vasculature. Previous studies in zebrafish showed that the anterior end of the notochord normally suppresses cardiogenic fate, by delimiting the expression of Nkx2.5, the earliest marker of presumptive myocardial cell fate [131]. Furthermore, the notochord is involved in the specification of the cardiac left–right asymmetry. Actually, when the notochord is surgically ablated or when it is absent in mutant embryos (such as *ntl* and *flh* zebrafish mutants and *no turning* mice mutants), asymmetric markers of lateral plate mesoderm are either randomized or bilaterally expressed [132–134]. Recently, it has been demonstrated that Hh signaling is required for the earliest steps of specification, differentiation and proliferation of endocardial progenitors in the zebrafish embryo. The Hh signaling is cell-autonomously activated within endocardial progenitors, and the notochord is likely a source of this Hh signal [135].

Concerning the vasculature specification, the notochord seems to have distinct roles in different species and developmental stages. The endothelial precursor cells or angioblasts originate from the mesoderm and then disperse throughout all embryonic tissues [136, 137]. The axial vessels of the trunk form in close proximity to the notochord and the endoderm. The dorsal aorta is normally just ventral to the notochord, whereas the axial vein is just below the dorsal aorta and above the endoderm. Studies in zebrafish indicate that the differentiated notochord is strongly required for the development of the dorsal aorta [138]. In fact, a fully developed notochord is needed for the expression of the vascular endothelial growth factor receptor (VEGFR2) in this axial artery and for the normal vessel assembly [138]. Conversely, the notochord seems less important for the development of the axial vein [139]. Indeed, in both *flh* and *ntl* mutants the dorsal aorta fails to form, while formation of the axial vein is less affected [138, 139]. The less severe vascular phenotype observed in *ntl* mutants may be caused by residual notochord signaling or alternatively by floor plate signals, which share many inductive properties with the notochord and could compensate for notochord loss [138, 139]. Experimental analysis showed that during somatogenesis notochord-derived Hh signals regulate the expression of *vegfa*, coding for vascular endothelial growth factor A (VEGF-A) in the somitic mesoderm. In turn, VEGF-A acts on endothelial cells to drive arterial differentiation [140]. During early avian development, blood vessels develop in the embryonic disc, except in a midline region surrounding the notochord. Indeed, notochord-derived BMP antagonists, including noggin and chordin, are responsible for the generation and maintenance of this midline avascular region by preventing endothelial cells differentiation, migration, and network formation [141]. The combination of these inhibitory cues ensures that blood vessels are excluded from the midline until the paired dorsal aorta fuse.

A narrow strip of tissue located between the paraxial and lateral plate mesoderm, called the intermediate mesoderm, gives raise to the vertebrate kidney. During embryogenesis, three sets of structures (pronephros, mesonephros and metanephros) emerge from the nephric cord within the intermediate mesoderm in an antero-posterior direction. It has been demonstrated that the notochord and floor plate-derived Shh ligands are dispensable for nephrogenesis but required for the correct positioning of the bilateral kidney primordia [142]. Actually, ablation of the notochord and floor plate in mice displays no effect on nephrogenesis but leads to kidney fusion [142]. A recent study on the temporal analysis of Shh function—using a tamoxifen-inducible gene recombination system—indicated that midline-derived Shh is essential to regulate the number of mesonephric tubules [143].

Notochord signals for endoderm development

The endoderm germ layer gives rise to the epithelium of the pharynx and of the respiratory and gastrointestinal tracts, including thyroid, thymus, lung, esophagus, stomach, intestine, liver and pancreas. Thus, determining how the endoderm is patterned is crucial for understanding the development of many internal organs.

The pancreas forms from the fusion of distinct dorsal and ventral buds. Embryonic manipulation in chick provided strong evidence that early signals released from the

notochord to the endoderm permit dorsal pancreatic morphogenesis [144]. Moreover, these signals initiate and maintain the expression of different genes required for pancreatic development. In contrast ventral pancreas, which does not directly contact the notochord, develops normally in the absence of a notochord. In vitro recombination experiments suggest that notochord provides a permissive, rather that instructive, signal to the endoderm for the specification of a pancreatic fate. Indeed, pancreatic gene expression can be initiated and maintained only in prepancreatic chick endoderm cultured with notochord cells, whereas non-pancreatic endoderm does not express pancreatic genes when recombined with the same notochord [144]. Moreover, grafting experiments demonstrated that activin-βB and fibroblast growth factor 2 (FGF2) expressed by the notochord repress endodermal Shh, thereby permitting pancreatic development [145]. Indeed, notochord removal before the onset of the notochord/endoderm molecular interactions leads to ectopic Shh expression in the pancreatic anlage, abnormal pancreatic morphogenesis, and prevents gene expression required for endocrine and exocrine compartments differentiation. Conversely, the inhibition of Shh in isolated prepancreatic endoderm is sufficient to induce specific pancreatic gene expression [145].

Embryological manipulations in amphibians demonstrated that the notochord plays a critical role in the development of the hypochord, a transient, endoderm-derived structure that lies immediately ventral to the notochord in the amphibian and fish embryo. During early neural stages, signals arising from the notochord instruct cells in the underlying endoderm to reach a hypochord fate, whereas further notochord signals are dispensable for the maintenance of this structure [146]. For example, in *flh* and *ntl* zebrafish mutants, the hypochord does not develop or it is severely disrupted [33]. However, in zebrafish *gup*, *bal*, *dop* and *sny* mutants, which are defective in late notochord development, the hypochord appears normal as assayed by the expression of the *co2a1* marker [129]. Removal of the notochord during early neurulation leads to a complete failure of hypochord development and to the loss of *vegf* expression. Grafting experiments demonstrate that higher levels of notochord-derived signaling can expand the number of *vegf*-expressing cells, increasing the size of the differentiated hypochord [146].

Recently, using spatio-temporal manipulation of Noggin conditional alleles during foregut development, it has been demonstrated that during early notochord development the action of Noggin results in BMP signaling attenuation, which in turn is required for the correct separation of the notochord cells from the dorsal foregut endoderm [147]. Importantly, this event appears to be a prerequisite for foregut compartmentalization. Indeed, mice lacking the BMP antagonist Noggin have esophageal atresia with tracheoesophageal fistula, as well as defects in lung branching [148]. This phenotype appears to correlate with abnormal morphogenesis of the notochord. In particular, defective separation of the notochord from the definitive endoderm leads to hypocellularization of the foregut just before the critical period of compartmentalization [147].

Role of extracellular matrix proteins in notochord patterning activity

In order to activate different embryonic differentiation programs, the Hh signals arising from the developing notochord must pass through the extracellular matrix surrounding notochord cells. Laminins are found in the peri-notochordal BM around forming somites, and later on around myotomes including vertical myosepta [22]. The source of notochord-derived Shh has an essential role in controlling laminin α1 gene expression. As laminin 111 (also called laminin-1) is necessary and sufficient to initiate BM formation, these studies revealed that Shh plays a key role in this process [149]. In other systems (e.g. in vitro embryonic stem cells) it is known that Smad4, a BMP mediator, controls BM deposition through a dual control of metalloproteinase and laminin α1 synthesis [150]. In zebrafish *sly* mutants, which carry a mutation in the gene encoding for laminin γ1 thus preventing the formation of laminin 111, Hh signaling is not affected, as revealed by normal expression levels for *ptc*, a gene that is transcriptionally regulated by this signaling pathway [151]. Indeed, these mutants display ectopic BMP activity in the myotome [152]. These findings suggest that a complex feedback mechanism between Shh, BMP and laminin 111 is responsible for the control of BM deposition and myogenesis.

Another example of mutual interaction between peri-notochordal BM deposition and notochord-related signaling activity has been revealed by zebrafish collagen XV depleted embryos [25]. Morpholino-mediated knockdown of *col15a1* revealed that this peri-notochordal sheath protein is required for notochord differentiation, axon guidance and differentiation of functional muscle fibers. The authors proposed that the loss of BM integrity due to ablation of collagen XV may lead to an increased diffusion of Hh ligands from the notochord, resulting in an ectopic differentiation of medial fast fibers. The distinctive expansion of medial fast fibers in this model correlates with the onset of collagen XV expression after the Shh-mediated induction of adaxial and muscle pioneer cells [25].

Studies in *puff daddy* (*pfd*), a zebrafish mutant yielded by a forward genetic screen for mutants exhibiting notochord sensitivity to lysyl oxidase inhibition, demonstrated that fibrillin-2 has an essential role in zebrafish notochord

and vascular morphogenesis [71]. Although the notochord distortion observed in *pfd* mutants results from structural defects, the vascular phenotypes appear to rely at least in part upon altered cell signaling pathways. As genetic interaction between fibrillin-2 and bone morphogenetic protein-7 (BMP-7) has been demonstrated in fibrillin-2 knockout mice [153], Bmp-7-related signals or other morphogens may be required for endothelial cell branching and venous plexus morphogenesis in zebrafish. Moreover, treating zebrafish *pfd* mutant embryos with losartan, a specific inhibitor of the transforming growth factor (TGFβ) signaling pathway, does not rescue their vascular phenotype [154], thus indicating that TGFβ signaling is not involved in the caudal vein abnormalities observed in fibrillin-2 depleted embryos [71].

Recent in vitro and in vivo studies indicate that the peri-notochordal sheath protein Emilin3 modulates the availability of Hh ligands by interacting with the permissive factor Scube2 in the notochord sheath [27]. Scube2 acts non-cell autonomously in the release of lipidated Shh from producing cells [155, 156]. Intriguingly, Emilin3 was shown to interact with the EGF repeats of Scube2, supporting the hypothesis that this extracellular matrix protein may be important for targeting Scube2 to the correct sites, thus tuning its activity in the extracellular milieu. Emilin3 deficiency disturbs notochord sheath formation and may cause an abnormal localization and/or activity of Scube2, leading to increased Hh signals. In agreement with this, expression of *ptc1* and other Hh-responsive genes was shown to be consistently upregulated in Emilin3 depleted zebrafish embryos [27].

Role of the notochord in intervertebral disc formation and in spine morphogenesis

During late embryonic development, the peri-notochordal BM exhibits a metameric pattern of more and less condensed zones that give rise to the outer and inner annulus and the vertebrae [157]. While the notochord completely regresses in the correspondence of the vertebral bodies or centra, small areas of notochord tissue persist in the center of the intervertebral discs and notochord cells condense to form the nucleus pulposus [158, 159]. Thus, in chordate embryos, the nucleus pulposus is the only tissue that is completely derived from the notochord [103]. In zebrafish, vertebrae and IVDs become distinct from each other by 15 days post fertilization. The IVDs contain vacuolated cells of the nucleus pulposus surrounded by smaller cells of the anulus fibrosus [160].

Several gene products regulate intervertebral disc development. Mutant mice lacking collagen type II, which is synthesized by the notochord and deposited into the peri-notochordal sheath, lack intervertebral discs and are unable to remove the notochord. This defect is associated with an enlargement of vertebral bodies and the deposition of abnormal collagen fibrils [159]. Two highly related transcription factors, Sox5 and Sox6, which are expressed in sclerotome-derived cells and in the notochord [161] are required for peri-notochordal sheath formation, cell survival, and late development of the nucleus pulposus. Indeed, the peri-notochordal BM fails to form in *Sox5*/*Sox6* double mutant mice, leading to the subsequent impairment of axial skeleton formation [162]. These findings suggest that a mechanically and structurally intact peri-notochordal sheath is required for inducing notochord reorganization, formation of the intervertebral disc and dismantling of the notochord. Two other paired box transcription factors expressed in the sclerotome, *Pax1* and *Pax9*, regulate vertebral body development. In the corresponding mutant mice, the notochord forms normally but it is not removed from the vertebral bodies, thereby compromising the formation of the nucleus pulposus [163, 164].

The vertebrate notochord plays a critical role in spine morphogenesis and bone ossification during late developmental stages. The link between notochord cells and spine morphogenesis has been deeply analyzed in the Atlantic salmon [165], but in the last years the zebrafish model has become a useful tool to understand the mechanisms underlying the formation of bone matrix of the vertebrae. In teleosts, the notochord directs centrum bone synthesis in vivo, where individual rings of bone centra are deposited within the notochord sheath, leading to the subsequent formation of mature segmented vertebrae [165, 166]. An in vivo study focused on the development of the zebrafish vertebral column revealed that laser ablation of notochord cells at defined periodic locations prevents the development of the correspondent centrum [167]. These findings suggest that the notochord might have an inherent periodicity that imparts segmental patterning to the vertebral column. Moreover, it has been demonstrated that the fully inflated vacuoles of notochord cells mechanically antagonize the pushing force of invading osteoblasts during vertebral bone formation. Zebrafish mutants lacking fully vacuolated cells or with fragmented vacuoles developed kinks in the spine during ossification [16]. These findings identify a novel role for notochord vacuoles in spine morphogenesis. Different works support the model of notochord-dependent vertebral column formation [16, 66, 167, 168]. Thus, it is reasonable to suppose that the patterns of vertebral alterations and scoliosis can be a common consequence of malformations or injury to embryonic notochord tissues. Further studies will help elucidating the mechanisms underlying vertebral column ossification.

As the intervertebral disc matures, the composition of the nucleus pulposus changes: the large vacuolated cells

with notochordal origin decrease in number, whereas smaller chondrocyte-like cells, of a different embryonic origin, increase. Indeed, there is a controversy regarding the embryonic origin of the cells populating the mature nuclei pulposi. Some authors' stated that notochord cells die during spine morphogenesis and then are replaced by a new population of cells migrating from adjacent tissues [169]. Other authors, however, argued that the smaller adult nucleus pulposus cells, despite their distinct morphology, derive from the original population of larger notochord cells [105]. Some recent reports unveiled the possibility that a notochord-derived population of adult nucleus pulposus cells coexists with another cell population having a different ontogeny (for extensive review on this topic see [170]).

Role of the notochord in the onset of chordomas

A number of animal models of intervertebral disc degeneration were generated [171–176]. However, in these models the fate of the notochord cells, as well as their involvement in functional maintenance of the intervertebral disc in postnatal life, remains poorly defined. For example, few dormant notochord cells persist in the adult vertebral body and give rise to chordomas [103]. Chordomas are rare primary tumors of the axial skeleton, localized mainly in the sacrococcygeal and sphenooccipital regions [177]. These tumors are both sporadic and hereditary and appear to occur more frequently after the fourth decade of life. However, modern technologies have increased the detection of pediatric chordomas. They are traditionally considered to be slow growing, locally invasive neoplasms with a low tendency to metastasize and a high potential for recurrence. Complete surgical removal of the tumor, whenever possible, is the standard of care, usually in combination with radiation therapy. In fact this tumor is known to be highly chemoresistant towards the few proven systemic therapies available for patients with unresectable tumors or distant metastases [178].

The current concept is that chordomas arise from the remnants of the notochord after embryogenesis. Lineage-tracing experiments in mouse models allowed to clarify that during embryogenesis, as the ossification of the spine proceeds and vertebral bodies form, the embryonic notochord directly gives rise to all cell types present in the nucleus pulposus of the intervertebral discs. Additionally, rare isolated embryonic notochord cells were also found to reside in the vertebrae between the intervertebral discs. The location in which these cells are found is characteristic of the "notochordal remnants", which in humans have been proposed to give rise to chordoma [103]. Other observations support the notochordal origin of chordomas. Between notochordal remnants and the histopathology exhibited by chordomas there is a morphological similarity at light and electron microscope levels [179, 180], and both share a similar immunophenotype [177, 181, 182]. Histologically, chordomas are composed of physaliphorous cells expressing a particular low-molecular-weight cytokeratin protein embedded in a mucomyxoid background. They are divided into classical (or conventional), chondroid, and dedifferentiated types. The chondroid variety may have a more favorable prognosis than other chordomas [183].

Actually, chordomas do not only have microscopic features resembling the embryonic notochord, but also express the transcription factor T (referred to as *brachyury* henceforth), the founding member of the T-box family of transcription factors, which is required for the specification of mesodermal identity [184] and regulates notochord formation. Duplication of the *brachyury* locus was reported in rare cases with genetic predisposition to familial chordoma [185], along with amplification of *brachyury* in some sporadic chordomas [186]. Moreover, an extensive genotyping study of individuals with sporadic chordoma revealed recurrent single nucleotide polymorphisms (SNPs) in the *brachyury* DNA-binding domain. These SNPs alter the DNA-binding properties of the transcription factor, suggesting that misregulation of some of the genes controlled by *brachyury* could be a mechanism underlying the genesis of chordoma [187]. A recent study using integrated functional genomics identified several target genes of *brachyury* involved in the regulation of the cell cycle, in the production of extracellular matrix and cytokines, and in glycosaminoglycan binding, all of which are pertinent to the notochord and chordomas [188]. At a functional level, in vitro suppression of *brachyury* halts cell proliferation in two different chordoma cell lines [186, 189]. It was also shown that overexpression of *brachyury* leads to enhanced proliferation, motility, and invasiveness in a *brachyury*-depleted cell line [190]. Altogether, these findings implicate *brachyury* in the pathogenesis of chordoma and suggest that this transcription factor is a crucial molecular driver in the initiation and propagation of this cancer. In agreement with this, several studies have postulated that *brachyury* represents a novel discriminating biomarker for chordomas. In particular, when combined with cytokeratin staining, the specificity for chordoma detection achieves 100 % [177, 191, 192].

Chordomas were also identified on the basis of their immunoreactivity for the S-100 protein, the epithelial MUC1 membrane glycoprotein and cytokeratins. Another genetic marker of chordomas is chondroitin sulfate proteoglycan 4 (CSPG4 or NG2/MCSP), which has been also targeted for immunotherapy. However, this antigen is expressed only by a fraction (62 %) of these tumors [193] and may lead to false negative diagnoses. Additional studies underlined the importance of some other notochord-related

factors (such as Shh, Wnt, galectin-3 and NCAM) in the pathophysiology of chordoma. For example, the Wnt signaling pathway and the closely related cadherins appear to play a role in different cellular processes that take place in chordomas (for review, see [194]). Moreover, Shh has been found to be overexpressed in some clinical cases of chordoma, although Shh should not be considered a specific and selective marker for this tumor as anti-Shh antibodies also react in 50 % of the notochordal cases and in 81 % of chondrosarcoma cases [195]. In addition, the transcription factor Sox9, which is required for the maintenance of notochord integrity [196], is also expressed in chondrosarcoma samples [191]. These limitations underline the need for the improvement of chordoma diagnosis with new and more distinctive chordoma markers.

In addition, a gene expression profile of human chordoma samples revealed that different genes involved in extracellular matrix synthesis and control were upregulated [197]. These findings suggest that the inhibition of matrix-modifying proteases may prevent the local growth and distant spread of these tumors, by inhibiting the escape of cells from the extracellular matrix. Moreover, blocking proteins important for cell mobilization and cell–matrix interaction may be a reasonable alternative approach to the conventional therapeutic treatments.

In spite of these diverse findings, genetic studies did not reveal mutations that can be therapeutically targeted in chordomas. Studies of human chordoma samples have suggested activation of the EGFR-PI3 K-AKT-mTOR pathway [198, 199], and treatment of the chordoma cell line U-CH1 with mTORC1 and PI3 K inhibitors induces apoptosis [193]. Clinical trials have been carried out with a variety of receptor tyrosine kinase inhibitors, as well as with the mTOR inhibitor rapamycin [178]. Although partial responses have been observed in some patients, there is a pressing need for high-throughput preclinical models to direct targeted therapies in patients with this relatively rare tumor. Recently, it was reported the first in vivo genetic model for chordoma, based on stable notochord-specific expression of H-Ras^{Val12} in zebrafish [200]. This model generates a reproducible tumor phenotype, ultimately leading to larval death. These tumors are highly similar to the human chordoma based on histological, ultrastructural and immunohistochemical features. The rapid onset of the tumor phenotype in this zebrafish chordoma model is well suited for screening for new pharmacological agents that can suppress tumor proliferation or induce tumor cell death. Indeed, the mTORC1 inhibitor rapamycin was shown to delay the onset of tumor formation and improve survival of tumor-bearing fish. Consequently, the zebrafish model of chordoma could enable high-throughput screening of potential therapeutic agents for the treatment of this refractory cancer [200].

The nucleus pulposus is thought to be required for the maintenance of the structural integrity of intervertebral discs and is the first structure to be affected during disc degeneration [201]. In this clinical context, notochord cells are proposed to display an important protective role, since in vitro and in vivo studies have suggested that notochord cells may represent the most effective cell population for repopulating the degenerate nucleus pulposus. Therefore, notochord cells may be the ideal type of cells able to repair a degenerated disc. Moreover, previous in vitro studies have highlighted the stimulatory effect of the conditioned medium of notochord cells on native intervertebral discs [202, 203]. A recent study pointed out the effect of notochord cell-derived conditioned media on mesenchymal stem cell differentiation toward a potentially nucleus pulposus-like phenotype, with some characteristics of the developing intervertebral discs [204]. These findings have important implications to understand fundamental biological processes acting on this complex structure not only in disc homeostasis, but more importantly in intervertebral disc degeneration and back pain.

Concluding remarks

The notochord is one of the earliest distinguishable hallmarks of the developing vertebrate embryo, directing essential patterning and structural activities. A broad number of studies provided insights into the molecular and mechanistic processes involved in notochord formation and homeostasis during embryonic development. Overall, these findings reinforce the concept that structure and function of the notochord are strictly linked, highlighting the signals that the peri-notochordal BM imparts to notochord cells. Besides providing valuable information on vertebrate biology and development, the available data indicate that the study of notochord development is helpful for throwing light on the origin and pathogenesis of chordoma, a rare and malignant bone cancer that originates from notochord remnants. The increasing knowledge on the genetic markers and molecular targets of chordomas is of high interest for devising new and effective therapies for this type of malignant cancer. We also discussed the role of notochord cells in forming the nucleus pulposus portion of the intervertebral discs, a feature that makes notochord cells a promising target for clinical approaches aimed at intervertebral disc repair and back pain treatment.

Acknowledgments The authors are supported by grants from the University of Padova and the Italian Ministry of University and Research. We wish to thank Enrico Moro for the helpful comments and critical reading and Giacomo Cavaliere for the expert image assistance.

Conflict of interest The authors declare no conflict of interest.

References

1. Kowalevsky A (1866) Entwicklungsgeschichte der einfachen Ascidien. Mem l'Acad St Petersbourg Ser 7:11–19
2. Kowalevsky A (1866) Entwicklungsgeschichte des Amphioxus lanceolatus. Mem l'Acad St Petersbourg Ser 7:1–17
3. Satoh N, Tagawa K, Takahashi H (2012) How was the notochord born? Evol Dev 14:56–75. doi:10.1111/j.1525-142X.2011.00522.x
4. Satoh N, Rokhsar D, Nishikawa T (2014) Chordate evolution and the three-phylum system. Proc Biol Sci 281:20141729. doi:10.1098/rspb.2014.1729
5. Hejnol A, Lowe CJ (2014) Animal evolution: Stiff or squishy notochord origins? Curr Biol 24:R1131–R1133. doi:10.1016/j.cub.2014.10.059
6. Lauri A, Brunet T, Handberg-Thorsager M, Fischer A, Simakov O, Steinmetz P, Tomer R, Keller PJ, Arendt D (2014) Development of the annelid axochord: Insight into notochord evolution. Science 345:1365–1368. doi:10.1126/science.1253396
7. Harlan R, Gerhart J (1997) Formation and function of Spemann's organizer. Anuu Rev Cell Dev Biol 13:611–667
8. Spemann H, Mangold H (1924) Induction of embryonic primordia by implantation of organizers from a different species. Roux's Arch Entw Mech 100:599–638
9. Shih J, Fraser SE (1996) Characterizing the zebrafish organizer: microsurgical analysis at the early-shield stage. Development 122:1313–1322
10. Saúde L, Woolley K, Martin P, Driever W, Stemple DL (2000) Axis-inducing activities and cell fates of the zebrafish organizer. Development 127:3407–3417
11. Yan YL, Hatta K, Riggleman B, Postlethwait JH (1995) Expression of a type II collagen gene in the zebrafish embryonic axis. Dev Dyn 203:363–376
12. Yamamoto M, Morita R, Mizoguchi T, Matsuo H, Isoda M, Ishitani T, Chitnis AB, Matsumoto K, Crump JG, Hozumi K, Yonemura S, Kawakami K, Itoh M (2010) Mib-Jag1-Notch signalling regulates patterning and structural roles of the notochord by controlling cell-fate decisions. Development 137:2527–2537. doi:10.1242/dev.051011
13. Leeson TS, Leeson CR (1958) Observations on the histochemistry and fine structure of the notochord in rabbit embryos. J Anat 92:278–285
14. Bancroft M, Bellairs R (1976) The development of the notochord in the chick embryo, studied by scanning and transmission electron microscopy. J Embryol Exp Morphol 35:383–401
15. Adams DS, Keller R, Koehl MA (1990) The mechanics of notochord elongation, straightening and stiffening in the embryo of Xenopus laevis. Development 110:115–130
16. Ellis K, Bagwell J, Bagnat M (2013) Notochord vacuoles are lysosome-related organelles that function in axis and spine morphogenesis. J Cell Biol 200:667–679
17. Inoue S (1989) Ultrastructure of basement membranes. Int Rev Cytol 117:57–98
18. Damjanov I (1990) Heterogeneity of basement membranes in normal and pathologically altered tissues. Virchowa Arch A Pathol Anat Histopathol 416:185–188
19. Erickson AC, Couchman J (2000) Still more complexity in mammalian basement membranes. J Histochem Cytochem 48:1291–1306
20. Timpl R, Brown JC (1996) Supramolecular assembly of basement membranes. BioEssays 18(2):123–132
21. Camón J, Degollada E, Verdú J (1990) Ultrastructural aspects of the production of extracellular matrix components by the chick embryonic notochord in vitro. Acta Anat (Basel) 137:114–123
22. Parsons MJ, Pollard SM, Saude L, Feldman B, Coutinho P, Hirst EM, Stemple DL (2002) Zebrafish mutants identify an essential role for laminins in notochord formation. Development 129:3137–3146
23. Scott A, Stemple DL (2005) Zebrafish notochordal basement membrane: signaling and structure. Curr Top Dev Biol 65:229–253
24. Stemple DL (2005) Structure and function of the notochord: an essential organ for chordate development. Development 132:2503–2512
25. Pagnon-Minot A, Malbouyres M, Haftek-Terrau Z, Kim HR, Sasaki T, Thisse C, Thisse B, Ingham PW, Ruggiero F, Le Guellec D (2008) Collagen XV, a novel factor in zebrafish notochord differentiation and muscle development. Developmental Biology 316:21–35
26. Mangos S, Lam P, Zhao A, Liu Y, Mudumana S, Vasilyev A, Liu A, Drummond IA (2010) The ADPKD genes pkd1a/b and pkd2 regulate extracellular matrix formation. Dis Model Mech 3:354–365. doi:10.1242/dmm.003194
27. Corallo D, Schiavinato A, Trapani V, Moro E, Argenton F, Bonaldo P (2013) Emilin3 is required for notochord sheath integrity and interacts with Scube2 to regulate notochord-derived Hedgehog signals. Development 140:4594–4601. doi:10.1242/dev.094078
28. Buisson N, Sirour C, Moreau N, Denker E, Le Bouffant R, Goullancourt A, Darribère T, Bello V (2014) An adhesome comprising laminin, dystroglycan and myosin IIA is required during notochord development in *Xenopus laevis*. Development 141:4569–4579. doi:10.1242/dev.116103
29. Theiler K (1988) Vertebral malformations. Adv Anat Embryol Cell Biol 112:1–99
30. von Dassow G, Schmidt JE, Kimelman D (1993) Induction of the Xenopus organizer: expression and regulation of Xnot, a novel FGF and activin-regulated homeo box gene. Genes Dev 7:355–366
31. Talbot WS, Trevarrow B, Halpern ME, Melby AE, Farr G, Postlethwait JH, Jowett T, Kimmel CB, Kimelman D (1995) A homeobox gene essential for zebrafish notochord development. Nature 378:150–157
32. Knezevic V, Ranson M, Mackem S (1995) The organizer-associated chick homeobox gene, Gnot1, is expressed before gastrulation and regulated synergistically by activin and retinoic acid. Dev Biol 171:458–470
33. Halpern ME, Thisse C, Ho RK, Thisse B, Riggleman B, Trevarrow B, Weinberg ES, Postlethwait JH, Kimmel CB (1995) Cell-autonomous shift from axial to paraxial mesodermal development in zebrafish floating head mutants. Development 121:4257–4264
34. Kimmel CB, Kane DA, Walker C, Warga RM, Rothman MB (1989) A mutation that changes cell movement and cell fate in the zebrafish embryo. Nature 337:358–362
35. Ho RK, Kane DA (1990) Cell-autonomous action of zebrafish spt-1 mutation in specific mesodermal precursors. Nature 348:728–730
36. Gont LK, Fainsod A, Kim SH, De Robertis EM (1996) Overexpression of the homeobox gene Xnot-2 leads to notochord formation in Xenopus. Dev Biol 174:174–178
37. Yasuo H, Lemaire P (2001) Role of Goosecoid, Xnot and Wnt antagonists in the maintenance of the notochord genetic programme in Xenopus gastrulae. Development 128:3783–3793

38. Abdelkhalek HA, Beckers A, Schuster-Gossler K, Pavlova MN, Burkhardt H, Lickert H, Rossant J, Reinhardt R, Schalkwyk LC, Müller I, Herrmann BG, Ceolin M, Rivera-Pomar R, Gossler A (2004) The mouse homeobox gene Not is required for caudal notochord development and affected by the truncate mutation. Genes Dev 18:1725–1736
39. Yamanaka Y, Mizuno T, Sasai Y, Kishi M, Takeda H, Kim CH, Hibi M, Hirano T (1998) A novel homeobox gene, dharma, can induce the organizer in a non-cell-autonomous manner. Genes Dev 12:2345–2353
40. Fekany K, Yamanaka Y, Leung T, Sirotkin HI, Topczewski J, Gates MA, Hibi M, Renucci A, Stemple D, Radbill A, Schier AF, Driever W, Hirano T, Talbot WS, Solnica-Krezel L (1999) The zebrafish bozozok locus encodes Dharma, a homeodomain protein essential for induction of gastrula organizer and dorsoanterior embryonic structures. Development 126:1427–1438
41. Odenthal J, Haffter P, Vogelsang E, Brand M, van Eeden FJ, Furutani-Seiki M, Granato M, Hammerschmidt M, Heisenberg CP, Jiang YJ, Kane DA, Kelsh RN, Mullins MC, Warga RM, Allende ML, Weinberg ES, Nüsslein-Volhard C (1996) Mutations affecting the formation of the notochord in the zebrafish, Danio rerio. Development 123:103–115
42. George EL, Georges-Labouesse EN, Patel-King RS, Rayburn H, Hynes RO (1993) Defects in mesoderm, neural tube and vascular development in mouse embryos lacking fibronectin. Development 119:1079–1091
43. Chiu CH, Chou CW, Takada S, Liu YW (2012) Development and fibronectin signaling requirements of the zebrafish interrenal vessel. PLoS ONE 7:e43040. doi:10.1371/journal.pone.0043040
44. Davidson LA, Hoffstrom BG, Keller R, DeSimone DW (2002) Mesendoderm extension and mantle closure in *Xenopus laevis* gastrulation: combined roles for integrin α5β1, fibronectin, and tissue geometry. Dev Biol 242:109–129
45. Davidson LA, Marsden M, Keller R, Desimone DW (2006) Integrin α5β1 and fibronectin regulate polarized cell protrusions required for Xenopus convergence and extension. Curr Biol 16:833–844
46. George EL, Baldwin HS, Hynes RO (1997) Fibronectins are essential for heart and blood vessel morphogenesis but are dispensable for initial specification of precursor cells. Blood 90:3073–3081
47. Georges-Labouesse EN, George EL, Rayburn H, Hynes RO (1996) Mesodermal development in mouse embryos mutant for fibronectin. Dev Dyn 207:145–156
48. Marsden M, DeSimone DW (2001) Regulation of cell polarity, radial intercalation and epiboly in Xenopus: novel roles for integrin and fibronectin. Development 128:3635–3647
49. Trinh LA, Stainier DY (2004) Fibronectin regulates epithelial organization during myocardial migration in zebrafish. Dev Cell 6:371–382
50. Halpern ME, Ho RK, Walker C, Kimmel CB (1993) Induction of muscle pioneers and floor plate is distinguished by the zebrafish no tail mutation. Cell 75:99–111
51. Schulte-Merker S, van Eeden FJ, Halpern ME, Kimmel CB, Nüsslein-Volhard C (1994) no tail (ntl) is the zebrafish homologue of the mouse T (Brachyury) gene. Development 120:1009–1015
52. Kispert A, Herrmann BG (1994) Immunohistochemical analysis of the Brachyury protein in wild-type and mutant mouse embryos. Dev Biol 161:179–193
53. Kispert A, Ortner H, Cooke J, Herrmann BG (1995) The chick Brachyury gene: developmental expression pattern and response to axial induction by localized activin. Dev Biol 168:406–415
54. Kispert A, Hermann BG (1993) The Brachyury gene encodes a novel DNA binding protein. EMBO J 12:4898–4899
55. Conlon FL, Sedgwick SG, Weston KM, Smith JC (1996) Inhibition of Xbra transcription activation causes defects in mesodermal patterning and reveals autoregulation of Xbra in dorsal mesoderm. Development 122:2427–2435
56. Wilkinson DG, Bhatt S, Hermann BG (1990) Expression pattern of the mouse T gene and its role in mesoderm formation. Nature 343:657–659
57. Smith JC, Price BM, Green JB, Weigel D, Herrmann BG (1991) Expression of a Xenopus homolog of Brachyury (T) is an immediate-early response to mesoderm induction. Cell 67:79–87
58. Schulte-Merker S, Ho RK, Herrmann BG, Nüsslein-Volhard C (1992) The protein product of the zebrafish homologue of the mouse T gene is expressed in nuclei of the germ ring and the notochord of the early embryo. Development 116:1021–1032
59. Wilson V, Manson L, Skarnes WC, Beddington RS (1995) The T gene is necessary for normal mesodermal morphogenetic cell movements during gastrulation. Development 121:877–886
60. Melby AE, Kimelman D, Kimmel CB (1997) Spatial regulation of floating head expression in the developing notochord. Dev Dyn 209:156–165
61. Colognato H, Yurchenco PD (2000) Form and function: the laminin family of heterotrimers. Dev Dyn 218:213–234
62. Smyth N, Vatansever HS, Murray P, Meyer M, Frie C, Paulsson M, Edgar D (1999) Absence of basement membranes after targeting the LAMC1 gene results in embryonic lethality due to failure of endoderm differentiation. J Cell Biol 144:151–160
63. Pollard SM, Parsons MJ, Kamei M, Kettleborough RNW, Thomas KA, Van Pham N, Bae M, Scott A, Weinstein BM, Stemple DL (2006) Essential and overlapping roles for laminin α chains in notochord and blood vessel formation. Dev Biol 289:64–76
64. Fratzl P (2008) Collagen: structure and mechanics. Springer, New York (ISBN 0-387-73905-X)
65. Gansner JM, Gitlin JD (2011) Essential role for the alpha 1 chain of type VIII collagen in zebrafish notochord formation. Dev Dyn 237:3715–3726. doi:10.1002/dvdy.21779
66. Christiansen HE, Lang MR, Pace JM, Parichy DM (2009) Critical early roles for col27a1a and col27a1b in zebrafish notochord morphogenesis, vertebral mineralization and postembryonic axial growth. PLoS ONE 4:e8481
67. Gansner JM, Mendelsohn BA, Hultman KA, Johnson SL, Gitlin JD (2007) Essential role of lysyl oxidases in notochord development. Dev Biol 307:202–213
68. Mendelsohn BA, Yin C, Johnson SL, Wilm TP, Solnica-Krezel L, Gitlin JD (2006) Atp7a determines a hierarchy of copper metabolism essential for notochord development. Cell Metab 4:155–162
69. Menkes JH (1988) Kinky hair disease: twenty five years later. Brain Dev 10:77–79
70. Madsen EC, Gitlin JD (2008) Zebrafish mutants calamity and catastrophe define critical pathways of gene-nutrient interactions in developmental copper metabolism. PLoS Genet 4:e1000261. doi:10.1371/journal.pgen.1000261
71. Gansner JM, Madsen EC, Mecham RP, Gitlin JD (2008) Essential role for fibrillin-2 in zebrafish notochord and vascular morphogenesis. Dev Dyn 237:2844–2861. doi:10.1002/dvdy.21705
72. Liu X, Zhao Y, Gao J, Pawlyk B, Starcher B, Spencer JA, Yanagisawa H, Zuo J, Li T (2004) Elastic fiber homeostasis requires lysyl oxidase-like 1 protein. Nat Genet 36:178–182
73. Coutinho P, Parsons MJ, Thomas KA, Hirst EM, Saúde L, Campos I, Williams PH, Stemple DL (2004) Differential requirements for COPI transport during vertebrate early development. Dev Cell 7:547–558

74. Nickel W, Brügger B, Wieland FT (2002) Vesicular transport: the core machinery of COPI recruitment and budding. J Cell Sci 115:3235–3240
75. Kelsh RN, Brand M, Jiang YJ, Heisenberg CP, Lin S, Haffter P, Odenthal J, Mullins MC, van Eeden FJ, Furutani-Seiki M, Granato M, Hammerschmidt M, Kane DA, Warga RM, Beuchle D, Vogelsang L, Nüsslein-Volhard C (1996) Zebrafish pigmentation mutations and the processes of neural crest development. Development 123:369–389
76. Ekker SC, Larson JD (2001) Morphant technology in model developmental systems. Genesis 30:89–93
77. Pickart MA, Klee EW, Nielsen AL, Sivasubbu S, Mendenhall EM, Bill BR, Chen E, Eckfeldt CE, Knowlton M, Robu ME et al (2006) Genome-wide reverse genetics framework to identify novel functions of the vertebrate secretome. PLoS ONE 1:e104
78. Robu ME, Larson JD, Nasevicius A, Beiraghi S, Brenner C, Farber SA, Ekker SC (2007) p53 activation by knockdown technologies. PLoS Genet 3:e78
79. Kok FO, Shin M, Ni CW, Gupta A, Grosse AS, van Impel A, Kirchmaier BC, Peterson-Maduro J, Kourkoulis G, Male I, DeSantis DF, Sheppard-Tindell S, Ebarasi L, Betsholtz C, Schulte-Merker S, Wolfe SA, Lawson ND (2015) Reverse genetic screening reveals poor correlation between morpholino-induced and mutant phenotypes in zebrafish. Dev Cell 32:97–108. doi:10.1016/j.devcel.2014.11.018
80. Cleaver O, Krieg PA (2001) Notochord patterning of the endoderm. Dev Biol 234:1–12
81. Briscoe J, Ericson J (1999) The specification of neuronal identity by graded Sonic Hedgehog signalling. Semin Cell Dev Biol 10:353–362
82. Placzek M, Yamada T, Tessier-Lavigne M, Jessell T, Dodd J (1991) Control of dorsoventral pattern in vertebrate neural development: induction and polarizing properties of the floor plate. Development Suppl 2:105–122
83. Yamada T, Placzek M, Tanaka H, Dodd J, Jessell TM (1990) Control of cell pattern in the developing nervous system: Polarizing activity of the floor plate and notochord. Cell 64:635–647
84. Chiang C, Litingtung Y, Lee E, Young KE, Corden JL, Westphal H, Beachy PA (1996) Cyclopia and defective axial patterning in mice lacking Sonic hedgehog gene function. Nature 383:407–413
85. Ericson J, Muhr J, Placzek M, Lints T, Jessell TM, Edlund T (1995) Sonic hedgehog induces the differentiation of ventral forebrain neurons: a common signal for ventral patterning within the neural tube. Cell 81:747–756
86. Martí E, Takada R, Bumcrot DA, Sasaki H, McMahon AP (1995) Distribution of Sonic hedgehog peptides in the developing chick and mouse embryo. Development 121:2537–2547
87. Roelink H, Porter JA, Chiang C, Tanabe Y, Chang DT, Beachy PA, Jessell TM (1995) Floor plate and motor neuron induction by different concentrations of the amino-terminal cleavage product of sonic hedgehog autoproteolysis. Cell 81:445–455
88. Ericson J, Briscoe J, Rashbass P, van Heyningen V, Jessell TM (1997) Graded sonic hedgehog signaling and the specification of cell fate in the ventral neural tube. Cold Spring Harb Symp Quant Biol 62:451–466
89. Echelard Y, Epstein DJ, St-Jacques B, Shen L, Mohler J, McMahon JA, McMahon AP (1992) Sonic hedgehog, a member of a family of putative signaling molecules, is implicated in the regulation of CNS polarity. Cell 75:1417–1430
90. Placzek M, Jessell TM, Dodd J (1992) Induction of floor plate differentiation by contact-dependent, homeogenetic signals. Development 117:205–218
91. Yamada T, Pfaff SL, Edlund T, Jessell TM (1992) Control of cell pattern in the neural tube: motor neuron induction by diffusible factors from notochord and floor plate. Cell 73:673–686
92. Chamberlain CE, Jeong J, Guo C, Allen BL, McMahon AP (2008) Notochord-derived Shh concentrates in close association with the apically positioned basal body in neural target cells and forms a dynamic gradient during neural patterning. Development 135:1097–1106
93. Odenthal J, van Eeden FJM, Haffter P, Ingham PW, Nusslein-Volhard C (2000) Two distinct cell populations in the floor plate of the zebrafish are induced by different pathways. Dev Biol 219:350–363
94. Schauerte HE, van Eeden FJ, Fricke C, Odenthal J, Strahle U, Haffter P (1998) Sonic hedgehog is not required for the induction of medial floor plate cells in the zebrafish. Development 125:2983–2993
95. Ribes V, Balaskas N, Sasai N, Cruz C, Dessaud E, Cayuso J, Tozer S, Yang LL, Novitch B, Marti E, Briscoe J (2010) Distinct Sonic Hedgehog signaling dynamics specify floor plate and ventral neuronal progenitors in the vertebrate neural tube. Genes Dev 24:1186–1200. doi:10.1101/gad.559910
96. Liem KF, Tremml G, Roelink H, Jessell TM (1994) Dorsal differentiation of neural plate cells induced by BMP-mediated signals from epidermal ectoderm. Cell 82:969–979
97. Lee KJ, Jessell TM (1998) The specification of dorsal cell fates in the vertebrate central nervous system. Annu Rev Neurosci 22:261–294
98. Tozer S, Le Dréau G, Marti E, Briscoe J (2013) Temporal control of BMP signalling determines neuronal subtype identity in the dorsal neural tube. Development 140:1467–1474. doi:10.1242/dev.090118
99. Patten I, Placzek M (2002) Opponent activities of Shh and BMP signaling during floor plate induction in vivo. Curr Biol 12:47–52
100. Martinez-Morales JR, Barbas JA, Martí E, Bovolenta P, Edgar D, Rodriguez-Tébar A (1997) Vitronectin is expressed in the ventral region of the neural tube and promotes the differentiation of motor neurons. Development 124:5139–5147
101. Pons S, Trejo JL, Martinez-Morales JR, Martí E (2001) Vitronectin regulates Sonic hedgehog activity during cerebellum development through CREB phosphorylation. Development 128:1481–1492
102. Gleiberman AS, Fedtsova NG, Rosenfeld MG (1998) Tissue interactions in the induction of anterior pituitary: role of the ventral diencephalon, mesenchyme, and notochord. Dev Biol 213:340–353
103. Choi KS, Cohn MJ, Harfe BD (2008) Identification of nucleus pulposus precursor cells and notochordal remnants in the mouse: implications for disk degeneration and chordoma formation. Dev Dyn 237:3953–3958. doi:10.1002/dvdy.21805
104. Choi KS, Harfe BD (2011) Hedgehog signaling is required for formation of the notochord sheath and patterning of nuclei pulposi within the intervertebral discs. Proc Natl Acad Sci USA 108:9484–9489. doi:10.1073/pnas.1007566108
105. Choi KS, Lee C, Harfe BD (2012) Sonic hedgehog in the notochord is sufficient for patterning of the intervertebral discs. Mech Dev 129:255–262. doi:10.1016/j.mod.2012.07.003
106. Christ B, Ordahl CP (1995) Early stages of chick somite development. Anat Embryol (Berl) 191:381–396
107. Fan CM, Tessier-Lavigne M (1994) Patterning of mammalian somites by surface ectoderm and notochord: evidence for sclerotome induction by a hedgehog homolog. Cell 79:1175–1186
108. Johnson RL, Laufer E, Riddle RD, Tabin C (1994) Ectopic expression of Sonic hedgehog alters dorsal-ventral patterning of somites. Cell 79:1165–1173
109. Fan CM, Porter JA, Chiang C, Chang DT, Beachy PA, Tessier-Lavigne M (1995) Long-range sclerotome induction by sonic hedgehog: direct role of the amino-terminal cleavage product and modulation by the cyclic AMP signaling pathway. Cell 81:457–465

110. Teillet M, Watanabe Y, Jeffs P, Duprez D, Lapointe F, Le Douarin NM (1998) Sonic hedgehog is required for survival of both myogenic and chondrogenic somitic lineages. Development 125:2019–2030
111. Buttitta L, Mo R, Hui CC, Fan CM (2003) Interplays of Gli2 and Gli3 and their requirement in mediating Shh-dependent sclerotome induction. Development 130:6233–6243
112. Zhang XM, Ramalho-Santos M, McMahon AP (2001) Smoothened mutants reveal redundant roles for Shh and Ihh signaling including regulation of L/R symmetry by the mouse node. Cell 106:781–792
113. Borycki AG, Mendham L, Emerson CP (1998) Control of somite patterning by Sonic hedgehog and its downstream signal response genes. Development 125:777–790
114. McMahon JA, Takada S, Zimmerman LB, Fan CM, Harland RM, McMahon AP (1998) Noggin-mediated antagonism of BMP signaling is required for growth and patterning of the neural tube and somite. Genes Dev 12:1438–1452
115. Dockter JL (2000) Sclerotome induction and differentiation. Curr Top Dev Biol 48:77–127
116. Ando T, Semba K, Suda H, Sei A, Mizuta H, Araki M, Abe K, Imai K, Nakagata N, Araki K, Yamamura K (2011) The floor plate is sufficient for development of the sclerotome and spine without the notochord. Mech Dev 128:129–140. doi:10.1016/j.mod.2010.11.005
117. El-Magd MA, Allen S, McGonnell I, Mansour AA, Otto A, Patel K (2014) Shh regulates chick Ebf1 gene expression in somite development. Gene 554:87–95. doi:10.1016/j.gene.2014.10.028
118. Borycki AG, Brunk B, Tajbakhsh S, Buckingham M, Chiang C, Emerson CP (1999) Sonic hedgehog controls epaxial muscle determination through Myf5 activation. Development 126:4053–4063
119. Gustafsson MK, Pan H, Pinney DF, Liu Y, Lewandowski A, Epstein DJ, Emerson CP (2002) Myf5 is a direct target of long-range Shh signaling and Gli regulation for muscle specification. Genes Dev 16:114–126
120. McDermott A, Gustafsson M, Elsam T, Hui CC, Emerson CP Jr, Borycki AG (2005) Gli2 and Gli3 have redundant and context-dependent function in skeletal muscle formation. Development 132:345–357
121. Münsterberg AE, Kitajewski J, Bumcrot DA, McMahon AP, Lassar AB (1995) Combinatorial signaling by Sonic hedgehog and Wnt family members induces myogenic bHLH gene expression in the somite. Genes Dev 9:2911–2922
122. Feng X, Adiarte EG, Devoto SH (2006) Hedgehog acts directly on the zebrafish dermomyotome to promote myogenic differentiation. Dev Biol 300:736–746
123. Hammond CL, Hinits Y, Osborn DP, Minchin JE, Tettamanti G, Hughes SM (2007) Signals and myogenic regulatory factors restrict pax3 and pax7 expression to dermomyotome-like tissue in zebrafish. Dev Biol 302:504–521
124. Cairns DM, Sato ME, Lee PG, Lassar AB, Zeng L (2008) A gradient of Shh establishes mutually repressing somitic cell fates induced by Nkx3.2 and Pax3. Dev Biol 323:152–165. doi:10.1016/j.ydbio.2008.08.024
125. Kahane N, Ribes V, Kicheva A, Briscoe J, Kalcheim C (2013) The transition from differentiation to growth during dermomyotome-derived myogenesis depends on temporally restricted hedgehog signaling. Development 140:1740–1750. doi:10.1242/dev.092726
126. Wolff C, Roy S, Ingham PW (2003) Multiple muscle cell identities induced by distinct levels and timing of hedgehog activity in the zebrafish embryo. Curr Biol 13:1169–1181
127. Ingham PW, Kim HR (2005) Hedgehog signalling and the specification of muscle cell identity in the zebrafish embryo. Exp Cell Res 306:336–342
128. Hatta K, Bremiller R, Westerfield M, Kimmel CB (1991) Diversity of expression of engrailed-like antigens in zebrafish. Development 112:821–832
129. Stemple DL, Solnica-Krezel L, Zwartkruis F, Neuhauss SC, Schier AF, Malicki J, Stainier DY, Abdelilah S, Rangini Z, Mountcastle-Shah E, Driever W (1996) Mutations affecting development of the notochord in zebrafish. Development 123:117–128
130. Coutelle O, Blagden CS, Hampson R, Halai C, Rigby PW, Hughes SM (2001) Hedgehog signalling is required for maintenance of myf5 and myoD expression and timely terminal differentiation in zebrafish adaxial myogenesis. Dev Biol 236:136–150
131. Goldstein AM, Fishman MC (1998) Notochord regulates cardiac lineage in zebrafish embryos. Dev Biol 201:247–252
132. Danos MC, Yost HJ (1996) Role of notochord in specification of cardiac left–right orientation in zebrafish and Xenopus. Dev Biol 177:96–103
133. Lohr JL, Danos MC, Yost HJ (1997) Left–right asymmetry of a nodal-related gene is regulated by dorsoanterior midline structures during Xenopus development. Development 124:1465–1472
134. Melloy PG, Ewart JL, Cohen MF, Desmond ME, Kuehn MR, Lo CW (1998) No turning, a mouse mutation causing left–right and axial patterning defects. Dev Biol 193:77–89
135. Wong KS, Rehn K, Palencia-Desai S, Kohli V, Hunter W, Uhl JD, Rost MS, Sumanas S (2012) Hedgehog signaling is required for differentiation of endocardial progenitors in zebrafish. Dev Biol 361:377–391. doi:10.1016/j.ydbio.2011.11.004
136. Noden DM (1989) Embryonic origins and assembly of blood vessels. Am Rev Res Dis 140:1097–1103
137. Risau W, Flamme I (1995) Vasculogenesis. Annu Rev Cell Dev Biol 11:73–91
138. Sumoy L, Keasey JB, Dittman TD, Kimelman D (1997) A role for notochord in axial vascular development revealed by analysis of phenotype and the expression of VEGR-2 in zebrafish flh and ntl mutant embryos. Mech Dev 63:15–27
139. Fouquet B, Weinstein BM, Serluca FC, Fishman MC (1997) Vessel patterning in the embryo of the zebrafish: guidance by notochord. Dev Biol 183:37–48
140. Lawson ND, Vogel AM, Weinstein BM (2002) Sonic hedgehog and vascular endothelial growth factor act upstream of the Notch pathway during arterial endothelial differentiation. Dev Cell 3:127–136
141. Reese DE, Hall CE, Mikawa T (2004) Negative regulation of midline vascular development by the notochord. Dev Cell 6:699–708
142. Tripathi P, Guo Q, Wang Y, Coussens M, Liapis H, Jain S, Kuehn MR, Capecchi MR, Chen F (2010) Midline signaling regulates kidney positioning but not nephrogenesis through Shh. Dev Biol 340:518–527. doi:10.1016/j.ydbio.2010.02.007
143. Murashima A, Akita H, Okazawa M, Kishigami S, Nakagata N, Nishinakamura R, Yamada G (2014) Midline-derived Shh regulates mesonephric tubule formation through the paraxial mesoderm. Dev Biol 386:216–226. doi:10.1016/j.ydbio.2013.12.026
144. Kim SK, Hebrok M, Melton DA (1997) Notochord to endoderm signaling is required for pancreas development. Development 124:4243–4252
145. Hebrok M, Kim SK, Melton DA (1998) Notochord repression of endodermal Sonic hedgehog permits pancreas development. Genes Dev 12:1705–1713
146. Cleaver O, Seufert DW, Krieg PA (2000) Endoderm patterning by the notochord: development of the hypochord in Xenopus. Development 127:869–879
147. Fausett SR, Brunet LJ, Klingensmith J (2014) BMP antagonism by Noggin is required in presumptive notochord cells for

mammalian foregut morphogenesis. Dev Biol 391:111–124. doi:10.1016/j.ydbio.2014.02.008
148. Que J, Choi M, Ziel JW, Klingensmith J, Hogan BL (2006) Morphogenesis of the trachea and esophagus: current players and new roles for noggin and Bmps. Differentiation 74:422–437
149. Anderson C, Thorsteinsdóttir S, Borycki AG (2009) Sonic hedgehog-dependent synthesis of laminin alpha1 controls basement membrane assembly in the myotome. Development 136:3495–3504. doi:10.1242/dev.036087
150. Costello I, Biondi CA, Taylor JM, Bikoff EK, Robertson EJ (2009) Smad4-dependent pathways control basement membrane deposition and endodermal cell migration at early stages of mouse development. BMC Dev Biol 9:54. doi:10.1186/1471-213X-9-54
151. Concordet JP, Lewis KE, Moore JW, Goodrich LV, Johnson RL, Scott MP, Ingham PW (1996) Spatial regulation of a zebrafish patched homologue reflects the roles of sonic hedgehog and protein kinase A in neural tube and somite patterning. Development 122:2835–2846
152. Dolez M, Nicolas JF, Hirsinger E (2011) Laminins, via heparan sulfate proteoglycans, participate in zebrafish myotome morphogenesis by modulating the pattern of Bmp responsiveness. Development 138:97–106. doi:10.1242/dev.053975
153. Arteaga-Solis E, Gayraud B, Lee SY, Shum L, Sakai L, Ramirez F (2001) Regulation of limb patterning by extracellular microfibrils. J Cell Biol 154:275–281
154. Habashi JP, Judge DP, Holm TM, Cohn RD, Loeys BL, Cooper TK, Myers L, Klein EC, Liu G, Calvi C, Podowski M, Neptune ER, Halushka MK, Bedja D, Gabrielson K, Rifkin DB, Carta L, Ramirez F, Huso DL, Dietz HC (2006) Losartan, an AT1 antagonist, prevents aortic aneurysm in a mouse model of Marfan syndrome. Science 312:117–121
155. Creanga A, Glenn TD, Mann RK, Saunders AM, Talbot WS, Beachy PA (2012) Scube/You activity mediates release of dually lipid-modified Hedgehog signal in soluble form. Genes Dev 26:1312–1325. doi:10.1101/gad.191866.112
156. Tukachinsky H, Kuzmickas RP, Jao CY, Liu J, Salic A (2012) Dispatched and scube mediate the efficient secretion of the cholesterol-modified hedgehog ligand. Cell Rep 2:308–320. doi:10.1016/j.celrep.2012.07.010
157. Schaffer J (1910) In von Mollendorff's "Handbuch der Mikroskopischen Anatomie des Menschen". Springer, Berlin, pp 31–44
158. Rufai A, Benjamin M, Ralphs JR (1995) The development of fibrocartilage in the rat intervertebral disc. Anat Embryol (Berl) 192:53–62
159. Aszodi A, Chan D, Hunziker E, Bateman JF, Fassler R (1998) Collagen II is essential for the removal of the notochord and the formation of intervertebral discs. J Cell Biol 143:1399–1412
160. Haga Y, Dominique VJ 3rd, Du SJ (2009) Analyzing notochord segmentation and intervertebral disc formation using the twhh:gfp transgenic zebrafish model. Transgenic Res 18:669–683. doi:10.1007/s11248-009-9259-y
161. Lefebvre V (2002) Toward understanding the functions of the two highly related Sox5 and Sox6 genes. J Bone Miner Metab 20:121–130
162. Smits P, Lefebvre V (2003) Sox5 and Sox6 are required for notochord extracellular matrix sheath formation, notochord cell survival and development of the nucleus pulposus of intervertebral discs. Development 130:1135–1148
163. Wallin J, Wilting J, Koseki H, Fritsch R, Christ B, Balling R (1994) The role of Pax-1 in axial skeleton development. Development 120:1109–1121
164. Peters H, Wilm B, Sakai N, Imai K, Maas R, Balling R (1999) Pax1 and Pax9 synergistically regulate vertebral column development. Development 126:5399–5408
165. Grotmol S, Kryvi H, Nordvik K, Totland GK (2003) Notochord segmentation may lay down the pathway for the development of the vertebral bodies in the Atlantic salmon. Anat Embryol (Berl) 207:263–272
166. Dale RM, Topczewski J (2011) Identification of an evolutionarily conserved regulatory element of the zebrafish col2a1a gene. Dev Biol 357:518–531
167. Fleming A, Keynes R, Tannahill D (2004) A central role for the notochord in vertebral patterning. Development 131:873–880
168. Grey RS, Wilm TP, Smith J, Bagnat M, Dale RM, Topczewski J, Johnson SL, Solnica-Krezel L (2014) Loss of col8a1a function during zebrafish embryogenesis results in congenital vertebral malformations. Dev Biol 386:72–85. doi:10.1016/j.ydbio.2013.11.028
169. Butler WF (1989) Comparative anatomy and development of the mammalian disc. In: Gosh P (ed) The biology of the intervertebral disc. CRC Press, Boca Raton, pp 84–108
170. Rodrigues-Pinto R, Richardson SM, Hoyland JA (2014) An understanding of intervertebral disc development, maturation and cell phenotype provides clues to direct cell-based tissue regeneration therapies for disc degeneration. Eur Spine J 23:1803–1814. doi:10.1007/s00586-014-3305-z
171. Frick SL, Hanley EN, Meyer RA, JrRamp WK, JrChapman TM (1994) Lumbar intervertebral disc transfer. A canine study. Spine 19:1826–1834
172. Lotz JC, Colliou OK, Chin JR, Duncan NA, Liebenberg E (1998) Compression-induced degeneration of the intervertebral disc: an in vivo mouse model and finite-element study. Spine 23:2493–2506
173. Iatridis JC, Mente PL, Stokes IA, Aronsson DD, Alini M (1999) Compression-induced changes in intervertebral disc properties in a rat tail model. Spine 24:996–1002
174. Hutton WC, Ganey TM, Elmer WA, Kozlowska E, Ugbo JL, Doh ES, Whitesides TE Jr (2000) Does long-term compressive loading on the intervertebral disc cause degeneration? Spine 25:2993–3004
175. Kadoya K, Kotani Y, Abumi K, Takada T, Shimamoto N, Shikinami Y, Kadosawa T, Kaneda K (2001) Biomechanical and morphologic evaluation of a three-dimensional fabric sheep artificial intervertebral disc: in vitro and in vivo analysis. Spine 26:1562–1569
176. Kawchuk GN, Kaigle AM, Holm SH, Rod FO, Ekstrom L, Hansson T (2001) The diagnostic performance of vertebral displacement measurements derived from ultrasonic indentation in an in vivo model of degenerative disc disease. Spine 26:1348–1355
177. Vujovic S, Henderson S, Presneau N, Odell E, Jacques TS, Tirabosco R, Boshoff C, Flanagan AM (2006) Brachyury, a crucial regulator of notochordal development, is a novel biomarker for chordomas. J Pathol 209:157–165
178. Walcott BP, Nahed BV, Mohyeldin A, Coumans JV, Kahle KT, Ferreira MJ (2012) Chordoma: current concepts, management, and future directions. Lancet Oncol 13:e69–e76. doi:10.1016/S1470-2045(11)70337-0
179. Persson S, Kindblom LG, Angervall L (1991) Classical and chondroid chordoma: a light-microscopic, histochemical, ultrastructural and immunohistochemical analysis of the various cell types. Pathol Res Pract 187:828–838
180. Yamaguchi T, Suzuki S, Ishiiwa H, Ueda Y (2004) Intraosseous benign notochordal cell tumours: overlooked precursors of classical chordomas? Histopathology 44:597–602
181. Takahiko N, Iwamoto Y, Shinohara N, Chuman H, Fukui M, Tsuneyoshi M (1997) Cytokeratin subtyping in chordomas and the fetal notochord: an immunohistochemical analysis of aberrant expression. Mod Pathol 10:545–551
182. Salisbury JR (1993) The pathology of the notochord: review article. J Pathol 171:153–155

183. Mirra JM, Nelson SD, Della Rocca C, Mertens F (2002) Notochordal tumours. In: Fletcher KK, Mertens F (eds) Pathology and genetics of tumours of soft tissue and bone. IARC Press, Lyon, pp 315–317
184. Showell C, Binder O, Conlon FL (2004) T-box genes in embryogenesis. A review. Dev Dyn 229:202–218
185. Yang XR, Ng D, Alcorta DA, Liebsch NJ, Sheridan E, Li S, Goldstein AM, Parry DM, Kelley MJ (2009) T (brachyury) gene duplication confers major susceptibility to familial chordoma. Nat Genet 41:1176–1178
186. Presneau N, Shalaby A, Ye H, Pillay N, Halai D, Idowu B, Tirabosco R, Whitwell D, Jacques TS, Kindblom LG et al (2011) Role of the transcription factor T (brachyury) in the pathogenesis of sporadic chordoma: a genetic and functional-based study. J Pathol 223:327–335. doi:10.1002/path.2816
187. Pillay N, Plagnol V, Tarpey PS, Lobo SB, Presneau N, Szuhai K, Halai D, Berisha F, Cannon SR, Mead S, Kasperaviciute D, Palmen J, Talmud PJ, Kindblom LG, Amary MF, Tirabosco R, Flanagan AM (2012) A common single-nucleotide variant in T is strongly associated with chordoma. Nat Genet 44:1185–1187. doi:10.1038/ng.2419
188. Nelson AC, Pillay N, Henderson S, Presneau N, Tirabosco R, Halai D, Berisha F, Flicek P, Stemple DL, Stern CD, Wardle FC, Flanagan AM (2012) An integrated functional genomics approach identifies the regulatory network directed by brachyury (T) in chordoma. J Pathol 228(3):274–285. doi:10.1002/path.4082
189. Hsu W, Mohyeldin A, Shah SR, Ap Rhys CM, Johnson LF, Sedora-Roman NI, Kosztowski TA, Awad OA et al (2011) Generation of chordoma cell line JHC7 and the identification of Brachyury as a novel molecular target. J Neurosurg 115:760–769. doi:10.3171/2011.5.JNS11185
190. Fernando RI, Litzinger M, Trono P, Hamilton DH, Schlom J, Palena C (2010) The T-box transcription factor Brachyury promotes epithelial-mesenchymal transition in human tumor cells. J Clin Invest 120:533–544. doi:10.1172/JCI38379
191. Oakley GJ, Fuhrer K, Seethala RR (2008) Brachyury, SOX-9, and podoplanin, new markers in the skull base chordoma vs chondrosarcoma differential: a tissue microarray-based comparative analysis. Mod Pathol 21:1461–1469. doi:10.1038/modpathol.2008.144
192. Sangoi AR, Karamchandani J, Lane B, Higgins JP, Rouse RV, Brooks JD, McKenney JK (2011) Specificity of brachyury in the distinction of chordoma from clear cell renal cell carcinoma and germ cell tumors: a study of 305 cases. Mod Pathol 24:425–429. doi:10.1038/modpathol.2010.196
193. Schwab J, Antonescu C, Boland P, Healey J, Rosenberg A, Nielsen P, Iafrate J, Delaney T, Yoon S, Choy E, Harmon D et al (2009) Combination of PI3K/mTOR inhibition demonstrates efficacy in human chordoma. Anticancer Res 29:1867–1871
194. Yakkioui Y, van Overbeeke JJ, Santegoeds R, van Engeland M, Temel Y (2014) Chordoma: the entity. Biochim Biophys Acta 1846:655–669. doi:10.1016/j.bbcan.2014.07.012
195. Cates JM, Itani DM, Coffin CM, Harfe BD (2010) The sonic hedgehog pathway in chordoid tumours. Histopathology 56:978–979. doi:10.1111/j.1365-2559.2010.03572.x
196. Barrionuevo F, Taketo MM, Scherer G, Kispert A (2006) Sox9 is required for notochord maintenance in mice. Dev Biol 295:128–140
197. Schwab JH, Boland PJ, Agaram NP, Socci ND, Guo T, O'Toole GC, Wang X, Ostroumov E, Hunter CJ, Block JA, Doty S, Ferrone S, Healey JH, Antonescu CR (2009) Chordoma and chondrosarcoma gene profile: implications for immunotherapy. Cancer Immunol Immunother 58:339–349. doi:10.1007/s00262-008-0557-7
198. Han S, Polizzano C, Nielsen GP, Hornicek FJ, Rosenberg AE, Ramesh V (2009) Aberrant hyperactivation of akt and Mammalian target of rapamycin complex 1 signaling in sporadic chordomas. Clin Cancer Res 15:1940–1946. doi:10.1158/1078-0432.CCR-08-2364
199. Presneau N, Shalaby A, Idowu B, Gikas P, Cannon SR, Gout I, Diss T, Tirabosco R, Flanagan AM (2009) Potential therapeutic targets for chordoma: PI3 K/AKT/TSC1/TSC2/mTOR pathway. Br J Cancer 100:1406–1414. doi:10.1038/sj.bjc.6605019
200. Burger A, Vasilyev A, Tomar R, Selig MK, Nielsen GP, Peterson RT, Drummond IA, Haber DA (2014) A zebrafish model of chordoma initiated by notochord-driven expression of HRASV12. Dis Model Mech 7:907–913. doi:10.1242/dmm.013128
201. Sive JI, Baird P, Jeziorsk M, Watkins A, Hoyland JA, Freemont AJ (2002) Expression of chondrocyte markers by cells of normal and degenerate intervertebral discs. Mol Pathol 55:91–97
202. Erwin WM, Inman RD (2006) Notochord cells regulate intervertebral disc chondrocyte proteoglycan production and cell proliferation. Spine 31:1094–1099
203. Cappello R, Bird JL, Pfeiffer D, Bayliss MT, Dudhia J (2006) Notochordal cell produce and assemble extracellular matrix in a distinct manner, which may be responsible for the maintenance of healthy nucleus pulposus. Spine 31:873–882
204. Korecky CL, Taboas JM, Tuan RS, Iatridis JC (2010) Notochordal cell conditioned medium stimulates mesenchymal stem cell differentiation toward a young nucleus pulposus phenotype. Stem Cell Res Ther 1:18. doi:10.1186/scrt18

References

Adams, D. S., Keller, R. and Koehl, M. A. (1990). The mechanics of notochord elongation, straightening and stiffening in the embryo of Xenopus laevis. *Development* **110**, 115–130.

Adams, J. C. and Watt, F. M. (1993). Regulation of development and differentiation by the extracellular matrix. *Development* **117(4)**, 1183-1198.

Astorga, J. and Carlsson, P. (2007). Hedgehog induction of murine vasculogenesis is mediated by Foxf1 and Bmp4. *Development* **134(20)**, 3753-3761.

Astrof, S., Crowley, D. and Hynes, R.O. (2007). Multiple cardiovascular defects caused by the absence of alternatively spliced segments of fibronectin. *Dev Biol*. **311(1)**, 11-24.

Berrier, A. L. and Yamada, K. M. (2007). Cell–matrix adhesion. *J. Cell. Physiol*. **213**, 565-573.

Beachy, P. A., Karhadkar, S. S. and Berman, D. M. (2004). Tissue repair and stem cell renewal in carcinogenesis. *Nature* **432(7015)**, 324-331.

Blagden C. S., Currie P. D., Ingham P. W. and Hughes S. M. (1997). Notochord induction of zebrafish slow muscle mediated by Sonic hedgehog. *Genes Dev*. **11**, 2163-2175.

Borel, A., Eichenberger, D., Farjanel, J., Kessler, E., Gleyzal, C., Hulmes, D.J., Sommer, P. and Font, B. (2001). Lysyl oxidase-like protein from bovine aorta. Isolation and maturation to an active form by bone morphogenetic protein-1. *J. Biol. Chem*. **276**, 48944–48949.

Bornemann, D. J., Duncan, J. E., Staatz, W., Selleck, S. and Warrior, R. (2004). Abrogation of heparan sulfate synthesis in Drosophila disrupts the Wingless, Hedgehog and Decapentaplegic signaling pathways. *Development* **131(9)**, 1927-1938.

Braghetta, P., Ferrari, A., de Gemmis, P., Zanetti, M., Volpin, D., Bonaldo, P., and Bressan, G. M. (2002). Expression of the EMILIN-1 gene during mouse development. *Matrix Biol*. **21**, 603–609.

Braghetta, P., Ferrari, A., de Gemmis, P., Zanetti, M., Volpin, D., Bonaldo, P. and Bressan, G. M. (2004). Overlapping, complementary and site-specific expression pattern of genes of the EMILIN/Multimerin family. *Matrix Biol* **22**, 549–556.

Brand, M., Heisenberg, C. P., Warga, R. M., Pelegri, F., Karlstrom, R. O., Beuchle, D., Picker, A., Jiang, Y. J., Furutani-Seiki, M., van Eeden, F. J., Granato, M.,

Haffter, P., Hammerschmidt, M., Kane, D. A., Kelsh, R. N., Mullins, M. C., Odenthal, J. and Nüsslein-Volhard, C. (1996). Mutations affecting development of the midline and general body shape during zebrafish embryogenesis. *Development* **123**, 129-142.

Brodsky, B. and Persikov, A.V. (2005). Molecular structure of the collagen triple helix. *Adv Protein Chem*. **70**, 301–39.

Broekelmann T. J., Kozel B. A., Ishibashi H., Werneck C. C., Keeley F. W., Zhang L. and Mecham R. P. (2005). Tropoelastin interacts with cell-surface glycosaminoglycans via its COOH-terminal domain. *J. Biol. Chem*. **280**, 40939–40947.

Buglino, J. A. and Resh, M. D. (2008). Hhat is a palmitoylacyltransferase with specificity for N-palmitoylation of Sonic Hedgehog. *J. Biol. Chem*. **283(32)**, 22076-22088.

Burke, R., Nellen, D., Bellotto, M., Hafen, E., Senti, K. A., Dickson, B. J. and Basler, K. (1999). Dispatched, a novel sterol-sensing domain protein dedicated to the release of cholesterol-modified hedgehog from signaling cells. *Cell* **99(7)**, 803-815.

Cain, S. A., Baldock, C., Gallagher, J., Morgan, A., Bax, D. V., Weiss, A. S., Shuttleworth, C. A. and Kielty C. M. (2005). Fibrillin-1 interactions with heparin. Implications for microfibril and elastic fiber assembly. *J. Biol. Chem*. **280(34)**, 30526-30537.

Camenisch, T. D., Spicer, A. P., Brehm-Gibson, T., Biesterfeldt, J., Augustine, M. L., Calabro, A. Jr, Kubalak, S., Klewer, S. E. and McDonald, J. A. (2000). Disruption of hyaluronan synthase-2 abrogates normal cardiac morphogenesis and hyaluronan-mediated transformation of epithelium to mesenchyme. *J Clin Invest*. **106(3)**, 349-360.

Chamoun, Z., Mann, R. K., Nellen, D., von Kessler, D. P., Bellotto, M., Beachy, P. A. and Basler, K. (2001). Skinny hedgehog, an acyltransferase required for palmitoylation and activity of the hedgehog signal. *Science* **293(5537)**, 2080-2084.

Chen, C.H, von Kessler, D.P., Park, W., Wang, B., Ma, Y. and Beachy, P.A. (1999). Nuclear trafficking of Cubitus interruptus in the transcriptional regulation of Hedgehog target gene expression. *Cell* **98**, 305–316.

Chen, J. N., van Bebber, F., Goldstein, A. M., Serluca, F. C., Jackson, D., Childs, S., Serbedzija, G., Warren, K. S., Mably, J. D., Lindahl, P., Mayer, A., Haffter, P.

and Fishman, M. C. (2001). Genetic steps to organ laterality in zebrafish. *Comp Funct Genomics*. **2(2)**, 60-68.

Choudhry, Z., Rikani, A. A., Choudhry, A. M., Tariq, S., Zakaria, F., Asghar, M. W., Sarfraz, M. K., Haider K., Shafiq A. A. and Mobassarah N. J. (2014). Sonic hedgehog signalling pathway: a complex network. *Annals of neurosciences* **21(1)**, 28–31. doi:10.5214/ans.0972.7531.210109.

Christian, S., Ahorn, H., Novatchkova, M., Garin-Chesa, P., Park, J., Weber, G., Eisenhaber, F., Rettig, W. J. and Lenter, M. C. (2001). Molecular cloning and characterization of EndoGlyx-1, an EMILIN-like multisubunit glycoprotein of vascular endothelium. *J. Biol. Chem*. **276 (51)**, 48588-48595.

Christiansen H. E., Lang M. R., Pace J. M. and Parichy D. M. (2009). Critical early roles for col27a1a and col27a1b in zebrafish notochord morphogenesis, vertebral mineralization and post-embryonic axial growth. *PLoS ONE* **4**,e8481.

Christoffels, A., Koh, E. G., Chia, J. M., Brenner, S., Aparicio, S. and Venkatesh, B. (2004). Fugu genome analysis provides evidence for a whole-genome duplication early during the evolution of ray-finned fishes. *Mol Biol Evol* **21**, 1146–1151.

Cohen, M. M. Jr. (2003). The hedgehog signalling network. *Am J Med Genet* **123**, 5–28.

Colognato, H. and Yurchenco, P. D. (2000). Form and function: the laminin family of heterotrimers. *Dev. Dyn.* **218**, 213-234.

Colombatti, A., Doliana, R., Bot, S., Canton, A., Mongiat, M., Mungiguerra, G., Paron-Cilli, S. and Spessotto, P. (2000). The EMILIN protein family. *Matrix Biol.* **19**, 289–301. http://dx.doi.org/10.1016/S0945-053X(00)00074-3.

Corallo, D., Schiavinato, A., Trapani, V., Moro, E., Argenton, F., and Bonaldo, P. (2013). Emilin3 is required for notochord sheath integrity and interacts with Scube2 to regulate notochord-derived Hedgehog signals. *Development* **140(22)**, 4594–4601. doi:10.1242/dev.094078.

Corallo, D., Trapani, V. and Bonaldo, P. (2015). The notochord: structure and functions. *CMLS*. **72(16)**, 2989-3008. doi:10.1007/s00018-015-1897-z.

Corbin, J. G., Gaiano, N., Juliano, S. L., Poluch, S., Stancik, E. and Haydar, T. F. (2008). Regulation of neural progenitor cell development in the nervous system. *J Neurochem*. **106(6)**, 2272-2287.

Coutinho, P., Parsons, M. J., Thomas, K. A., Hirst, E. M., Saúde, L., Campos, I., Williams, P. H. and Stemple, D. L. (2004). Differential requirements for COPI transport during vertebrate early development. *Dev Cell*. **7(4)**, 547-558.

Currie, P. D. and Ingham, P. W. (1996). Induction of a specific muscle cell type by a hedgehog-like protein in zebrafish. *Nature* **382**, 452-455.

Danussi, C., Del Bel Belluz, L., Pivetta, E., Modica, T. M., Muro, A., Wassermann, B., Doliana, R., Sabatelli, P., Colombatti, A. and Spessotto, P. (2013). EMILIN1/alpha9beta1 integrin interaction is crucial in lymphatic valve formation and maintenance. *Mol. Cell. Biol.* **33**, 4381–4394.

Danussi, C., Petrucco, A., Wassermann, B., Pivetta, E., Modica, T.M., Del Bel Belluz, L., Colombatti, A. and Spessotto, P. (2011). EMILIN1-alpha4/alpha9 integrin interaction inhibits dermal fibroblast and keratinocyte proliferation. *J. Cell Biol.* **195**, 131–145.

Danussi, C., Spessotto, P., Petrucco, A., Wassermann, B., Sabatelli, P., Montesi, M., Doliana, R., Bressan, G. M. and Colombatti, A. (2008). Emilin1 Deficiency Causes Structural and Functional Defects of Lymphatic Vasculature. *Mol. Cell Biol* **28(12)**, 4026–4039. doi:10.1128/MCB.02062-07

Davis, E. C. and Mecham, R. P. (1998). Intracellular trafficking of tropoelastin. *Matrix Biol*. **17(4)**, 245-254.

Davis, R. L. and Kirschner, M. W. (2000). The fate of cell in the tailbud of Xenopus laevis. *Development* **127(2)**, 255-67.

DeSimone, D. W., Norton, P. A. and Hynes, R. O. (1992). Identification and characterization of alternatively spliced fibronectin mRNAs expressed in early Xenopus embryos. *Dev Biol.* **149(2)** 357-369.

Discher, D.E., Mooney, D.J. and Zandstra, P.W. (2009). Growth factors, matrices, and forces combine and control stem cells. *Science* **324**, 1673– 1677.

Doi, M., Nagano, A. and Nakamura, Y. (2004). Molecular cloning and characterization of a novel gene, EMILIN-5, and its possible involvement in skeletal development. *Biochem. Biophys. Res. Comm*. **313**, 888-893.

Doliana, R., Bot, S., Bonaldo, P. and Colombatti, A. (2000a). EMI, a novel cysteine-rich domain of EMILINs and other extracellular proteins, interacts with the gC1q domains and participates in multimerization. *FEBS Lett.* **484**, 164-168.

Doliana, R., Canton, A., Bucciotti, F., Mongiat, M., Bonaldo, P. and Colombatti, A. (2000b). Structure, Chromosomal Localization and Promoter Analysis of the Human Elastin Microfibril Interface located protein (EMILIN). *Gene. J. Biol. Chem*. **275**, 785-792

Doliana, R., Bot, S., Mungiguerra, G., Canton, A., Cilli, S. and Colombatti, A. (2001). Isolation and characterization of EMILIN-2, a new component of the

growing EMILINs family and a member of the EMI domain-containing superfamily. *J. Biol. Chem*. **276 (15)**, 12003-12011.

Drapeau, P., Saint-Amant, L., Buss, R. R., Chong, M., McDearmid, J. R. and Brustein, E. (2002). Development of the locomotor network in zebrafish. *Prog Neurobiol*. **68(2)**, 85-111.

Du, S. J., Devoto, S. H., Westerfield, M. and Moon, R. T. (1997). Positive and negative regulation of muscle cell identity by members of the hedgehog and TGF-β gene families. *J. Cell Biol*. **139**, 145-156.

Dupont, S., Morsut, L., Aragona, M., Enz,o E., Giulitti, S., Cordenonsi, M., Zanconato, F., Le Digabel, J., Forcato, M., Bicciato, S., Elvassore, N. and Piccolo, S. (2011). Role of YAP/TAZ in mechanotransduction. *Nature* **474**, 179-183.

Ekker, S. C., Ungar, A. R., Greenstein, P., von Kessler, D. P., Porter, J. A., Moon, R. T. and Beachy, P. A. (1995). Patterning activities of vertebrate hedgehog proteins in the developing eye and brain. *Curr Biol*. **5(8)**, 944-955.

Ellis, K., Bagwell, J. and Bagnat, M. (2013). Notochord vacuoles are lysosome-related organelles that function in axis and spine morphogenesis. *J. Cell Biol.* **200**, 667–679.

Engel, J. (1989). EGF-like domains in extracellular matrix proteins: localized signals for growth and differentiation? *FEBS letters* **251 (1-2)**, 1-7.

Ericson, J., Morton, S., Kawakami, A., Roelink, H. and Jessell, T. M. (1996). Two critical periods of Sonic Hedgehog signaling required for the specification of motor neuron identity. *Cell* **87(4)**, 661-673.

Ffrench-Constant, C. and Hynes, R. O. (1989). Alternative splicing of fibronectin is temporally and spatially regulated in the chicken embryo. *Development* **106(2)**, 375-88

Gansner, J. M. and Gitlin, J. D. (2011). Essential role for the alpha 1 chain of type VIII collagen in zebrafish notochord formation. *Dev. Dyn.* **237**, 3715–3726. doi:10.1002/dvdy.21779

Gansner J. M., Madsen E. C., Mecham R. P. and Gitlin J. D. (2008). Essential role for fibrillin-2 in zebrafish notochord and vascular morphogenesis. *Dev. Dyn.* **237**, 2844–2861. doi:10.1002/dvdy. 21705

Gansner, J. M., Mendelsohn, B. A., Hultman, K. A., Johnson, S. L. and Gitlin, J. D. (2007). Essential role of lysyl oxidases in notochord development. *Dev. Biol.* **307**, 202-213.

Geiger, B., Spatz, J. and Bershadsky, A. (2009). Environmental sensing through focal adhesions. *Nat Rev Mol Cell Biol*. **10 (1)**, 21-33.

Gibson, M. A., Hatzinikolas, G., Davis, E. C., Baker, E., Sutherland, G. R. and Mecham, R. P. (1995). Bovine latent transforming growth factor beta 1-binding protein 2: molecular cloning, identification of tissue isoforms, and immunolocalization to elastin-associated microfibrils. *Mol Cell Biol*. **15(12)**, 6932-6942.

Giltay, R., Kostka, G. and Timpl, R. (1997). Sequence and expression of a novel member (LTBP-4) of the family of latent transforming growth factor-beta binding proteins. *FEBS Lett*. **411(2-3)**, 164-168.

Gordon, M. K. and Hahn, R. A. (2010) Collagens. *Cell Tissue Res*. **339(1)**, 247-257.

Gustafsson, M. K., Pan, H., Pinney, D. F., Liu, Y., Lewandowski, A., Epstein, D. J. and Emerson, C. P. Jr. (2002). Myf5 is a direct target of long-range Shh signaling and Gli regulation for muscle specification. *Genes Dev*. **16(1)**, 114-126.

Hallikas, O., Palin, K., Sinjushina, N., Rautiainen, R., Partanen, J., Ukkonen, E. and Taipale, J. (2006). Genome-wide prediction of mammalian enhancers based on analysis of transcription-factor binding affinity. *Cell* **124(1)**, 47-59.

Han, C., Belenkaya, T. Y., Wang, B. and Lin, X. (2004). Drosophila glypicans control the cell-to-cell movement of Hedgehog by a dynamin-independent process. *Development* **131(3)**, 601-611.

Hardingham, T. E., Bayliss, M. T., Rayan, V. and Noble, D. P. (1992). Effects of growth factors and cytokines on proteoglycan turnover in articular cartilage. *Br J Rheumatol*. **31** Suppl 1:1-6

Harlan, R., and Gerhart, J. (1997). Formation and function of Spemann's organizer. *Annu Rev Cell Dev Biol* **13**, 611–667.

Hatta, K., Bremiller, R., Westerfield, M. and Kimmel, C. B. (1991). Diversity of expression of engrailed-like antigens in zebrafish. *Development* **112(3)**, 821-832.

Hatzinikolas, G. and Gibson, M. A. (1998). The exon structure of the human MAGP-2 gene. Similarity with the MAGP-1 gene is confined to two exons encoding a cysteine-rich region. *J. Biol. Chem*. **273(45)**, 29309-29314.

Hay, E. D. (1981). Extracellular matrix. *J Cell Biol*. **91(3 Pt 2)**, 205s-223s

Hayward, C. P., Hassell, J. A., Denomme, G. A., Rachubinski, R. A., Brown, C. and Kelton, J. G. (1995a). The cDNA sequence of human endothelial cell multimerin. A unique protein with RGDS, coiled-coil, and epidermal growth factor-like

domains and a carboxyl terminus similar to the globular domain of complement C1q and collagens type VIII and X. *J. Biol. Chem.* **270**, 18246-18251.

Hubmacher, D. and Apte, S. S. (2013). The biology of the extracellular matrix: novel insights. *Curr Opin Rheumatol.* **25(1)**, 65-70. doi: 10.1097/BOR.0b013e32835b137b

Hynes, R. (2002). Integrins: bidirectional, allosteric signaling machines. *Cell*, **110 (6)**, 673-87.

Hynes, R. (2009). The Extracellular Matrix: Not Just Pretty Fibrils. *Science* **326(5957)**, 1216-1219.

Ingham, P. W. and McMahon, A. P. (2001). Hedgehog signaling in animal development: paradigms and principles. *Genes Dev.* **15(23)**, 3059-3087.

Jacob, J. and Briscoe J. (2003). Gli proteins and the control of spinal-cord patterning. *EMBO Rep*. **4(8)**, 761-765.

Kantola, A. K., Keski-Oja J. and Koli K. (2008). Fibronectin and heparin binding domains of latent TGF-beta binding protein (LTBP)-4 mediate matrix targeting and cell adhesion. *Exp Cell Res*. **314(13)**, 2488-2500.

Karlstrom, R. O., Talbot, W. S. and Schier, A. F. (1999). Comparative synteny cloning of zebrafish you-too: mutations in the Hedgehog target gli2 affect ventral forebrain patterning. *Genes Dev*. **13(4)**, 388-393.

Krauss, S., Concordet, J.P. and Ingham, P.W. (1993). A functionally conserved homolog of the Drosophila segment polarity gene hh is expressed in tissues with polarizing activity in zebrafish embryos. *Cell* **75**, 1431-1444.

Latimer, A. and Jessen, J. R. (2010). Extracellular matrix assembly and organization during zebrafish gastrulation. *Matrix. biol.* **29**, 89-96.

Laufer, E., Nelson, C. E., Johnson, R. L., Morgan, B. A. and Tabin, C. (1994). Sonic hedgehog and Fgf-4 act through a signaling cascade and feedback loop to integrate growth and patterning of the developing limb bud. *Cell* **79**, 993-1003.

Lausen, M., Lynch, N., Schlosser, A., Tornoe, I., Saekmose, S. G., Teisner, B,. Willis, A. C., Crouch, E., Schwaeble, W. and Holmskov, U. (1999). Microfibril-associated protein 4 is present in lung washings and binds to the collagen region of lung surfactant protein D. *J. Biol. Chem.* **274**, 32234-32240.

Lee, J. D. and Treisman, J. E. (2001) Sightless has homology to transmembrane acyltransferases and is required to generate active Hedgehog protein. *Curr Biol.* **11**, 1147-1152.

Legate, K., Wickström, S. and Fässler, R. (2009). Genetic and cell biological analysis of integrin outside-in signaling. *Genes Dev.* **23**, 397-418.

Leimeister, C., Steidl, C., Schumacher, N., Erhard, S. and Gessler, M. (2002). Developmental expression and biochemical characterization of Emu family members. *Dev. Biol.* **249**, 204-218.

Lewis, K. E., Currie, P. D., Roy, S., Schauerte, H., Haffter, P. and Ingham, P. W. (1999). Control of muscle cell-type specification in the zebrafish embryo by Hedgehog signalling. *Dev. Biol.* **216**, 469-480.

Lewis, K. E. and Eisen, J. S. (2001). Hedgehog signaling is required for primary motoneuron induction in zebrafish. *Development* **128**, 3485-3495.

Lewis, P. M., Dunn, M. P., McMahon, J. A., Logan, M., Martin, J. F., St-Jacques, B. and McMahon, A. P. (2001). Cholesterol modification of Sonic hedgehog is required for long-range signalling activity and effective modulation of signalling by Ptc1. *Cell* **105**, 599-612.

Li, Y., Zhang, H., Litingtung, Y. and Chiang, C. (2006). Cholesterol modification restricts the spread of Shh gradient in the limb bud. *Proc. Natl. Acad. Sci. U. S. A.* **103**, 6548-6553.

Lucero, H. A. and Kagan, H. M. (2006). Lysyl oxidase: an oxidative enzyme and effector of cell function. *Cell. Mol. Life Sci.* **63**, 2304-2316.

Lum, L., Yao, S., Mozer, B., Rovescalli, A., Von Kessler, D., Nirenberg, M. and Beachy, P. A. (2003). Identification of Hedgehog pathway components by RNAi in Drosophila cultured cells. *Science* **299**, 2039-2045.

Mangos, S., Lam, P., Zhao, A., Liu, Y., Mudumana, S., Vasilyev, A., Liu, A. and Drummond, I. A. (2010). The ADPKD genes *pkd1a/b* and *pkd2* regulate extracellular matrix formation. *Dis. Model. Mech*. **3**, 354-365.

McCawley, L. J. and Matrisian, L. M. (2001). Matrix metalloproteinases: they're not just for matrix anymore! *Curr. Opin. Cell. Biol.* **13**, 534-540.

Mecham, R. P. and Gibson, M. A. (2015). The microfibril-associated glycoproteins (MAGPs) and the microfibrillar niche. *Matrix Biol.* **47**, 13-33.

Milanetto, M., Tiso, N., Braghetta, P., Volpin, D., Argenton, F. and Bonaldo, P. (2008). Emilin genes are duplicated and dynamically expressed during zebrafish embryonic development. *Dev. Dyn.* **237**, 222-232.

Mohammadi, M., Olsen, S. and Goetz, R. (2005). A protein canyon in the FGF-FGF receptor dimer selects from an *à la carte* menu of heparan sulfate motifs. *Curr. Opin. Struct. Biol.* **15**, 506-516.

Mongiat, M., Ligresti, G., Marastoni, S., Lorenzon, E., Doliana, R. and Colombatti, A. (2007). Regulation of the extrinsic apoptotic pathway by the extracellular matrix glycoprotein EMILIN2. *Mol. Cell. Biol.* **27**, 7176-7187.

Mongiat, M., Marastoni, S., Ligresti, G., Lorenzon, E., Schiappacassi, M., Perris, R., Frustaci, S. and Colombatti, A. (2010). The extracellular matrix glycoprotein elastin microfibril interface located protein 2: a dual role in the tumor microenvironment. *Neoplasia* **12**, 294-304.

Mongiat, M., Mungiguerra, G., Bot, S., Mucignat, M. T., Giacomello, E., Doliana, R. and Colombatti, A. (2000). Self-assembly and supramolecular organization of EMILIN. *J. Biol. Chem.* **275**, 25471-25480.

Naba, A., Hoersch, S. and Hynes, R. O. (2012). Towards definition of an ECM parts list: an advance on GO categories. *Matrix Biol.* **31**, 371-372.

Nagase, H. and Woessner, J. F. Jr (1999). Matrix metalloproteinases. *J. Biol. Chem.* **274**, 21491-2144.

Nakano, Y., Kim, H. R., Kawakami, A., Roy, S., Schier, A. F. and Ingham, P. W. (2004). Inactivation of dispatched 1 by the chameleon mutation disrupts Hedgehog signalling in the zebrafish embryo. *Dev Biol.* **269**, 381-392.

Ochi, H., Pearson, B. J., Chuang, P. T., Hammerschmidt, M. and Westerfield, M. (2006). Hhip regulates zebrafish muscle development by both sequestering Hedgehog and modulating localization of Smoothened. *Dev. Biol.* **297**, 127-140.

Oliver, T. G., Grasfeder, L. L., Carroll, A. L., Kaiser, C., Gillingham, C. L., Lin, S. M., Wickramasinghe, R., Scott, M. P. and Wechsler-Reya, R. J. (2003). Transcriptional profiling of the Sonic hedgehog response: a critical role for N-myc in proliferation of neuronal precursors. *Proc. Natl. Acad. Sci. U. S. A.* **100**, 7331-7336.

Pagnon-Minot, A., Malbouyres, M., Haftek-Terrau, Z., Kim, H. R., Sasaki, T., Thisse, C., Thisse, B., Ingham, P. W., Ruggiero, F. and Le Guellec, D. (2008). Collagen XV, a novel factor in zebrafish notochord differentiation and muscle development. *Dev. Biol.* **316**, 21-35.

Papke, C. L. and Yanagisawa, H. (2014). Fibulin-4 and fibulin-5 in elastogenesis and beyond: Insights from mouse and human studies, *Matrix Biol.* **37**, 142-149.

Parsi, M. K., Adams, J. R., Whitelock, J. and Gibson, M. A. (2010). LTBP-2 has multiple heparin/heparan sulfate binding sites. *Matrix Biol.* **29**, 393-401.

Parsons, M. J., Pollard, S. M., Saude, L., Feldman, B., Coutinho, P., Hirst, E. M. and Stemple, D. L. (2002). Zebrafish mutants identify an essential role for laminins in notochord formation. *Development* **129**, 3137-3146.

Pierani, A., Brenner-Morton, S., Chiang, C. and Jessell, T. M. (1999). A sonic hedgehog- independent, retinoid-activated pathway of neurogenesis in the ventral spinal cord. *Cell* **97**, 903-915.

Pola, R., Ling, L. E., Silver, M., Corbley, M. J., Kearney, M., Blake Pepinsky, R., Shapiro, R., Taylor, F. R., Baker, D. P., Asahara, T. and Isner, J. M. (2001). The morphogen Sonic hedgehog is an indirect angiogenic agent upregulating two families of angiogenic growth factors. *Nat. Med.* **7**, 706-711.

Porter, J. A., Ekker, S. C., Park, W. J., von Kessler, D. P., Young, K. E., Chen, C. H., Ma, Y., Woods, A. S., Cotter, R. J., Koonin, E. V. and Beachy, P. A. (1996). Hedgehog patterning activity: role of a lipophilic modification mediated by the carboxy-terminal autoprocessing domain. *Cell* **86**, 21-34.

Richard-Blum, S. (2011). The Collagen Family. *Cold Spring Harb. Perspect. Biol.* **3**, 1–19.

Rider, C. (2006). Heparin/heparan sulphate binding in the TGF-beta cytokine superfamily. *Biochem. Soc. Trans.* **34**, 458-460.

Roy, S., Wolff, C. and Ingham, P. W. (2001). The u-boot mutation identifies a Hedgehog-regulated myogenic switch for fiber-type diversification in the zebrafish embryo. *Genes Dev.* **15**, 1563-1576.

Rozario, T. and DeSimone, D. W. (2010). The extracellular matrix in development and morphogenesis: a dynamic view. *Dev. Biol.* **341**, 126-140.

Sakai, L., Keene, D. and Engvall, E. (1986). Fibrillin, a new 350-kD glycoprotein, is a component of extracellular microfibrils. *J. Cell Biol.* **103**, 2499-2509.

Saùde, L., Woolley, K., Martin, P., Driever, W. and Stemple, D. L. (2000). Axis-inducing activities and cell fates of the zebrafish organizer. *Development* **127**, 3407-3417.

Schauerte, H. E., van Eeden, F. J., Fricke, C., Odenthal, J., Strähle, U. and Haffter, P. (1998). Sonic hedgehog is not required for the induction of medial floor plate cells in the zebrafish. *Development* **125**, 2983-2993.

Schenk, S., Hintermann, E., Bilban, M., Koshikawa, N., Hojilla, C., Khokha, R. and Quaranta, V. (2003). Binding to EGF receptor of a laminin-5 EGF-like fragment liberated during MMP-dependent mammary gland involution. *J. Cell Biol.* **161**, 197-209.

Schiavinato, A., Becker, A. K., Zanetti, M., Corallo, D., Milanetto, M., Bizzotto, D., Bressan, G., Guljelmovic, M., Paulsson, M, Wagener, R., Braghetta, P. and Bonaldo, P. (2012). EMILIN-3, peculiar member of elastin microfibril interface-located protein (EMILIN) family, has distinct expression pattern, forms oligomeric assemblies, and serves as transforming growth factor β (TGF-β) antagonist. *J. Biol. Chem.* **287**, 11498-11515.

Schwarzbauer, J. E. and DeSimone, D. W. (2011). Fibronectins, their fibrillogenesis, and *in vivo* functions. *Cold Spring Harb. Perspect. Biol.* **3**, a005041.

Scott, J. E. (2001). Structure and function in extracellular matrices depend on interactions between anionic glycosaminoglycans. *Pathol. Biol. (Paris)* **49**, 284-289.

Sekimizu, K., Nishioka, N., Sasaki, H., Takeda, H., Karlstrom, R. O. and Kawakami, A. (2004). The zebrafish iguana locus encodes Dzip1, a novel zinc-finger protein required for proper regulation of Hedgehog signaling. *Development* **131**, 2521-2532.

Shi, Y. and Massagué, J. (2003). Mechanisms of TGF-beta signaling from cell membrane to the nucleus. *Cell* **113**, 685-700.

Shih, J. and Fraser, S. E. (1996). Characterizing the zebrafish organizer: microsurgical analysis at the early-shield stage. *Development* **122**, 1313-1322.

Silbert, J. E. and Sugumaran, G. (1995). Intracellular membranes in the synthesis, transport, and metabolism of proteoglycans. *Biochim. Biophys. Acta* **1241**, 371-384.

Smits, P. and Lefebvre, V. (2003). Sox5 and Sox6 are required for notochord extracellular matrix sheath formation, notochord cell survival and development of the nucleus pulposus of intervertebral discs. *Development* **130** ,1135-1148.

Spessotto, P., Cervi, M., Mucignat, M. T., Mungiguerra, G., Sartoretto, I., Doliana, R. and Colombatti, A. (2003). β1 Integrin-dependent Cell Adhesion to EMILIN-1 is mediated by the gC1q Domain. *J. Biol. Chem.* **278**, 6160-6167

Spicer, A. P., Tien, J. L., Joo, A. and Bowling Jr, R. A. (2002). Investigation of hyaluronan function in the mouse through targeted mutagenesis. *Glycoconj. J.* **19**, 341-345.

Stemple, D. L. (2005). Structure and function of the notochord: an essential organ for chordate development. *Development* **132**, 2503-2512.

Swindle, C. S., Tran, K. T., Johnson, T. D., Banerjee, P., Mayes, A. M., Griffith, L. and Wells, A. (2001). Epidermal growth factor (EGF)-like repeats of human tenascin-C as ligands for EGF receptor. *J. Cell. Biol.* **154**, 459-468.

Teglund, S. and Toftgård, R. (2010). Hedgehog beyond medulloblastoma and basal cell carcinoma. *Biochim. Biophys. Acta* **1805**, 181-208

Tenzen, T., Allen, B. L., Cole, F., Kang, J. S., Krauss, R. S. and McMahon, A. P. (2006). The cell surface membrane proteins Cdo and Boc are components and targets of the Hedgehog signaling pathway and feedback network in mice. *Dev. Cell.* **10**, 647-656.

Toole, B. P., Wight, T. N. and Tammi, M. I. (2002). Hyaluronan-cell interactions in cancer and vascular disease. *J. Biol. Chem.* **277**, 4593-4596.

Tsang, K. Y., Cheung, M. C., Chan, D. and Cheah, K. S. (2010). The developmental roles of the extracellular matrix: beyond structure to regulation. *Cell. Tissue Res*. **339**, 93-110.

Van Eeden, F. J., Granato, M., Schach, U., Brand, M., Furutani-Seiki, M., Haffter, P., Hammerschmidt, M., Heisenberg, C. P., Jiang, Y. J., Kane, D. A., Kelsh, R. N., Mullins, M. C., Odenthal, J., Warga, R. M., Allende, M. L., Weinberg, E. S. and Nüsslein-Volhard, C. (1996). Mutations affecting somite formation and patterning in the zebrafish, *Danio rerio*. *Development* **123**, 153-164.

Varjosalo, M. and Taipale, J. (2008). Hedgehog: functions and mechanisms. *Genes. Dev.* **22**, 2454-2472.

Vokes, S. A., Ji, H., McCuine, S., Tenzen, T., Giles, S., Zhong, S., Longabaugh, W. J., Davidson, E. H., Wong, W. H. and McMahon, A. P. (2007). Genomic characterization of Gli-activator targets in sonic hedgehog-mediated neural patterning. *Development* **134**, 1977-1989.

Wagenseil, J. E., Mecham, R. P. (2007). New insights into elastic fiber assembly. *Birth Defects Res. C Embryo Today* **81** 229-240.

Whittaker, C., Bergeron, K. F., Whittle, J., Brandhorst, B., Burke, R. and Hynes, R. (2006). The echinoderm adhesome. *Dev. Biol.* **300**, 252-266..

Wilson, V., Olivera-Martinez, I. and Storey, K. G. (2009). Stem cells, signals and vertebrate body axis extension. *Development* **136**, 1591-1604.

Wise, S. G. and Weiss, A. S. (2009). Tropoelastin. *Int. J. Biochem. Cell. Biol.* **41**, 494-497.

Wolff, C., Roy, S. and Ingham, P. W. (2003). Multiple muscle cell identities induced by distinct levels and timing of hedgehog activity in the zebrafish embryo. *Curr. Biol.* **13**, 1169-1181.

Wolff, C., Roy, S., Lewis, K. E., Schauerte, H., Joerg-Rauch, G., Kirn, A., Weiler, C., Geisler, R., Haffter, P. and Ingham, P. W. (2004). Iguana encodes a novel zinc-finger protein with coiled-coil domains essential for Hedgehog signal transduction in the zebrafish embryo. *Genes Dev.* **18**, 1565-1576.

Woods, I. G. and Talbot, W. S. (2005). The you gene encodes an EGF-CUB protein essential for Hedgehog signaling in zebrafish. *PLoS Biol.* **3**, e66

Xu, J., Srinivas, B. P., Tay, S. Y., Mak, A., Yu, X., Lee, S. G., Yang, H., Govindarajan, K. R., Leong, B., Bourque, G., Mathavan, S. and Roy, S. (2006). Genomewide expression profiling in the zebrafish embryo identifies target genes regulated by Hedgehog signaling during vertebrate development. *Genetics* **174**, 735-752.

Yao, S., Lum, L. and Beachy, P. (2006). The iHog cell-surface proteins bind Hedgehog and mediate pathway activation. *Cell* **125**, 343-357

Yurchenco, P. D. (2011). Basement membranes: cell scaffoldings and signaling platforms. *Cold Spring Harb. Perspect. Biol.* **3**, a004911.

Zacchigna, L., Vecchione, C., Notte, A., Maretto, S., Cifelli, G., Dupont, S., Ferrari, A., Maffei, A., Marino, G., Cordenonsi, M., Selvetella, G., Aretini, A., Colonnese, C., Bettarini, U., Russo, G., Fabbro, C., Soligo, S., Adorno, M., Braghetta, P., Bonaldo, P., Volpin, D., Piccolo, S., Lembo, G. and Bressan G. M. (2006). Emilin-1, a cysteine-rich glycoprotein of elastic fibers, is required for blood pressure homeostasis by regulation TGF-β maturation. *Cell* **124**, 929-942.

Zanetti, M., Braghetta, P., Sabatelli, P., Mura, I., Doliana, R., Colombatti, A., Volpin, D., Bonaldo, P. and Bressan, G. M. (2004). EMILIN-1 deficiency induces elastogenesis and vascular cell defects. *Mol. Cell. Biol.* **24**, 638-650.

Zeng, X., Goetz, J. A., Suber, L. M., Scott, W. J. Jr, Schreiner, C. M. and Robbins, D. J. (2001). A freely diffusible form of sonic hedgehog mediates long-range signalling. *Nature* **411**, 716-720.

Zhang, H., Apfelroth, S. D., Hu, W., Davis, E. C., Sanguineti, C., Bonadio, J., Mecham, R. P. and Ramirez, F. (1994). Structure and expression of fibrillin-2, a novel microfibrillar component preferentially located in elastic matrices. *J. Cell. Biol.* **124**, 855-863.

Chapter II

1. Introduction

1.1. Collagen VI

Collagen VI is an extracellular matrix (ECM) protein forming a microfilamentous network in several tissues, such as skeletal muscle, skin, cornea, lung, blood vessels, tendons, intervertebral disks, peripheral nerves, lungs, heart, adipose tissue, skin and cartilages (Kuo *et al*., 1997, Keene *et al*., 1988, for detailed review see Cescon *et al.*, 2015).

1.1.1. Collagen VI chain structure

Originally, three genetically distinct Collagen VI chains, named α1(VI), α2(VI) and α3(VI), were identified (Colombatti and Bonaldo, 1987; Colombatti *et al*., 1995), respectively encoded by the *COL6A1*, *COL6A2* and *COL6A3* genes in humans (Lampe and Bushby, 2005). The *COL6A1* and *COL6A2* genes are organized in a head-to-tail fashion on chromosome 21q22.3, while the *COL6A3* gene maps to chromosome 2q37 (Lampe and Bushby, 2005). Biochemical studies showed that Collagen VI contains α1(VI), α2(VI) and α3(VI) chains, which assemble into a triple helical monomer in a 1:1:1 stoichiometric ratio (Engel *et al*., 1985; Colombatti *et al*., 1987, 1995; Colombatti and Bonaldo, 1987; Chu *et al*., 1990). More recently, genomic database analysis has led to the identification of three other genes encoding Collagen VI chains (Fitzgerald *et al*., 2008; Gara *et al*., 2008). As these additional Collagen VI

chains had a strong sequence homology and shared domain structure with α3(VI), they were annotated as *COL6A4*, *COL6A5* and *COL6A6* genes respectively, located in tandem on chromosome 3q21 (Fitzgerald *et al*., 2008; Gara *et al*., 2008). In humans, the *COL6A4* gene is not functional due to a large chromosome inversion, and it is cleaved into two segments that probably are transcribed as non-processed pseudogenes (Gara *et al*., 2008). The expression pattern of the new chain is restricted to defined tissue. Due to their similar structure, these novel chains could replace the α3(VI) chain forming α1(VI)α2(VI)α4(VI), α1(VI)α2(VI)α5(VI) and α1(VI)α2(VI)α6(VI) triple helical monomers, thus increasing the structural and functional versatility of Collagen VI (Gara *et al*., 2008) and showing different roles in tissue homeostasis or disease (Gara *et al*., 2011).

All Collagen VI chains comprise a relatively short central triple helical regions of 335–336 amino acids, which are flanked by large N- and C-terminal globular regions which are constituted of about 200 amino acid motifs that share similarity with the von Willebrand factor type A (vWF-A) module (Bernardi and Bonaldo, 2008). The α1(VI) and α2(VI) chains are approximately 130 – 150 kDa in size, extend for nearly 1,000 amino acids and contain one N-terminal (N1) and two C-terminal (C1 and C2) vWF-A modules (Bonaldo *et al*., 1989). Conversely, α3(VI), α4(VI), α5(VI) and α6(VI) are much larger, spanning from around 220 kDa to over 300 kDa. Though they share structural similarity at the N-terminal end, which comprises up to seven (N1 to N7 in α4, α5 and α6 chains) or up to ten N-terminal vWF-A modules (N1 to N10 in α3 chain), at the C- terminus they present two C-terminal vWF-A modules (C1 and C2), followed by unique regions (C3–C5) (Bernardi and Bonaldo, 2008; Bonaldo *et al*., 1990). The C3 domain contains a proline-rich sequence that in the α6(VI) chain also represents the C-terminal end. In the α3(VI) chain, C4 is a fibronectin-type-III domain, and C5 is a Kunitz-like domain (Bonaldo *et al*., 1990). The murine α4(VI) chain presents a short stretch of 17 amino acid residues at the C-terminal end (C4) that is similar to a partial Kunitz domain. The C-terminus of α5(VI) comprises a third vWF-A domain (C4), followed by another unique domain (C5) (Colombatti and Bonaldo *et al*., 1987, 1990; Bonaldo and Colombatti, 1989; Fitzgerald *et al*., 2008; Gara *et al*., 2008; Sabatelli *et al*., 2011; Sabatelli *et al*., 2012). It has been demonstrated that the α3(VI) C5 domain is cleaved when collagen VI is deposited in the ECM (Aigner *et al*., 2002; Nanda *et al*., 2004), but its function remains to be clarified. Several alternatively spliced variants that involve some of the vWF-A modules have also been described for the α3(VI) and α2(VI) chains. For instance, in

the α3(VI) chain, the domains N10, N9 and N7 are subjected to alternative splicing in mouse tissues, and transcript variants missing one or more of these N-terminal domains have also been described in mouse tissue and human cells (Doliana *et al*., 1990; Dziadek *et al*., 2002). Conversely, alternative splicing of the human α2(VI) transcript was found to generate three different protein variants, called α2C2, α2C2a and α2C2a′ (Saitta *et al*., 1990).

1.1.2. Collagen VI structure and assembly

Collagens represent important components of the ECM and are often reported as a superfamily, which is classified into subtypes depending on the supramolecular assemblies (Myllyharju and Kivirikko, 2004). Contrary to other collagens, Collagen VI presents unique supramolecular assembly, which is guided by a distinct multi-step process, which also implicates extensive disulfide bond interactions. After translation and entry of the three α(VI) chains within the endoplasmic reticulum, the three α-chains associate in a 1:1:1 stoichiometric ratio to form a triple-helical monomer (~500 kDa). Then, before secretion, monomers assembly into disulfide-bonded antiparallel dimers (~ 1000 kDa), which then align to form large tetramers that are also stabilized by disulfide bonds (~ 2000 kDa) (Engel *et al*., 1985; Colombatti *et al*., 1987, 1995; Colombatti and Bonaldo, 1987; Chu *et al*., 1990). Finally, tetramers are secreted and, within the extracellular space, they associate end-to-end through non-covalent bonds to form the distinctive beaded microfilaments network in the ECM, with a beaded repeat of 105 nm, as revealed with electron microscopy (Furthmayr *et al*., 1983; Knupp *et al*., 2006; Bernardi and Bonaldo, 2008). As already mentioned, the similar structure of α4(VI), α5(VI) and α6(VI) chains with α3(VI) suggests that they represent alternative polypeptides for the assembly of Collagen VI chains into α1–α2–αX triple-helix monomers (where αX is either α3, α4, α5 or α6) (Fitzgerald *et al*., 2008; Gara *et al*., 2008).

1.1.3. Collagen VI functions and tissue distribution

Collagen VI exerts different functions in the tissues where it is expressed, ranging from mechanical roles, which are typical of collagen components of the ECM, to more specific cytoprotective roles; these comprise inhibition of apoptosis and oxidative damage (Irwin *et al*., 2003; Cheng *et al*., 2009; Cheng *et al*., 2011), the promotion of tumor growth and progression (Iyengar *et al*., 2005), the regulation of cell differentiation and autophagic machinery (Grumati *et al*., 2010), and maintenance of cell stemness by fine-tuning the local stiffness (Urciuolo *et al*., 2013).

Thanks to its complex structure and domains' variety, Collagen VI is able to bind different components of the ECM, therefore linking cells to the surrounding connective tissue and arranging the 3D tissue architecture of skeletal muscles, tendons, bone and cartilage. Moreover, Collagen VI allows the creation of a physical connection between muscle cells and ECM, by binding collagen IV and perlecan in the basal lamina (Kuo *et al*., 1997). Moreover, interactions with other collagens have been described, comprising collagen type I (Bonaldo *et al*., 1990), type II (Bidanset *et al*., 1992) and type XIV (Brown *et al*., 1994). Studies propose that some ECM interacting molecules, such as biglycan and von Willebrand A domain-related protein (WARP), play a role in stabilizing and regulating Collagen VI secretion and assembly in the extracellular space (Hansen *et al*., 2012), whereas absence of Collagen VI has been reported to alter fibronectin deposition (Sabatelli *et al*., 2001). Interactions between Collagen VI and microfibril-associated MAGP1 glycoprotein (Finnis and Gibson, 1997), matrilin-1 (Wiberg *et al*., 2001), fibulin-2 (Sasaki *et al*., 1995), lumican (Takahashi *et al*., 1993), heparin, hyaluronan (Specks *et al*., 1992) and the small leucine-rich-repeat proteoglycan decorin (Bidanset *et al*., 1992) have also been described. Moreover, *in vitro* studies identified several cell surface receptors that are capable of binding Collagen VI, which are implicated in intracellular signaling pathways. For instance, integrin α1β1, α2β1, α3β1, α10β1 and αvβ3 integrins (Doane *et al*., 1992; Pfaff *et al*., 1993; Tulla *et al*., 2001) as well as the chondroitin sulfate proteoglycan-4 (CSPG4; also known as NG2) (Marcelino and McDevitt, 1995; Doane *et al*., 1998; Petrini *et al*., 2005) were found to interact with collagen VI and transduce signals by acting on cytoskeleton, regulating cell adhesion, proliferation and modulating integrin activity (Pfaff *et al*., 1993; Burg *et al*., 1996; Midwood and Salter, 2001; Stallcup, 2002).

1.1.3.1. Collagen VI function in skeletal muscle

Collagen VI is one of the major components of muscle ECM and, therefore is implicated in establishing the basement membrane of myofiber endomysium (Bonnemann, 2011). The major cell type responsible for Collagen VI deposition are interstitial fibroblasts, whereas myogenic cells only contain factors that can influence Collagen VI secretion, though they do not express it (Braghetta *et al*., 2008; Zou *et al*., 2008).

The essential role of Collagen VI in skeletal muscle homeostasis is underlined by the fact that altered expression or mutations in the genes encoding Collagen VI chains have a causative role in several human disorders, collectively known as

"Collagen VI-related myopathies". These include two major clinical forms of inherited human muscle diseases, including Ullrich congenital muscular dystrophy (UCMD [MIM 254090]) and Bethlem myopathy, (BM [MIM 158810]), but also include some limb girdle and the myosclerosis myopathy [MIM 255600] (Jobsis *et al*., 1996; Camacho Vanegas *et al*., 2001; Merlini *et al*., 2008).

Ullrich congenital muscular dystrophy is characterized by an early-onset, severe, generalized and rapidly progressive muscle weakness and wasting, with proximal limb contractures, coexisting distal joint hyperlaxity, rigid spine and rare ability to walk. The rapid progression of UCMD clinical symptoms usually leads to early death in the first or second decade of life, largely as a result of respiratory failure since the diaphragm is severally compromised (Mercuri and Longman, 2005; Briñas *et al*., 2010). Usually, the muscle biopsies from UCMD patients present a marked decrease or complete absence of Collagen VI (Lampe and Bushby 2005).

Slowly progressive, axial and proximal muscle wasting and weakness, associated with finger flexion contractures, characterize Bethlem myopathy. Although it shows interfamilial variability and different clinical onset, from prenatal to mid-adulthood, usually the pathology is mild with slow progression of the symptoms (Pepe *et al*., 2002) therefore affected individuals can live over 50 years of age requiring aids for outdoor mobility. Possibly, respiratory insufficiency can occur in ambulatory patients (Lampe and Bushby 2005). In Bethlem myopathy patients, mutations can affect any of the three Collagen VI genes, even though the expression of Collagen VI appears normal or mildly reduced in the endomysium of most patients (Lampe and Bushby 2005).

Both Ullrich congenital muscular dystrophy and Bethlem myopathy can be caused by either recessive or dominant mutations in Collagen VI genes (Gualandi *et al*., 2009). The incidence has been estimated as 0.1:100,000 for Ullrich congenital muscular dystrophy and 0.5:100,000 for Bethlem myopathy (Lampe and Bushby 2005).

Myosclerosis is a severe and rare myopathy characterized by early, diffuse, and progressive contractures resulting in a "woody consistency" of muscle and in severe limitation of movement of axial, proximal, and distal joints. It is primary due to a mutation in the *COL6A2* gene (Merlini *et al*., 2008).

The wide spectrum of mutation associated of the Collagen VI genes were associated either with UCMD or with BM revealed an important role of the protein in muscle not only on the basis of its amount, but also depending on qualitatively

alterations. Actually, several mechanisms were reported, including: (a) loss of function with alteration of triple helix formation, assembly or secretion; (b) mutations that give rise to abnormal polypeptides that act as dominant-negative form secreted in the matrix; (c) the mechanism of haploinsufficiency is proposed for mutations affecting mRNA stability, causing a reduced synthesis of normal protein (Sasaki *et al*., 2000; Zhang *et al*., 2002).

1.1.3.1.1. Collagen VI null mouse model and therapeutic approaches to ameliorate muscle phenotype

In order to investigate *in vivo* the role of Collagen VI, in 1998 the team of Prof. Bonaldo generated a Collagen VI (*Col6a1*$^{-/-}$) knockout mouse model. *Col6a1*$^{-/-}$ mice were obtained by a targeted inactivation of the second exon of the *Col6a1* gene, through an interruption of the coding sequence after the signal peptide sequence, therefore leading to the complete absence of the α1(VI) chain. Although α2(VI) and α3(VI) chains are normally transcribed and translated, in *Col6a1*$^{-/-}$ mice the absence of α1(VI) prevents the formation of Collagen VI monomers, consequentially the assembly and secretion of the entire Collagen VI protein do not occur and *Col6a1*$^{-/-}$ mice completely lack the protein in their tissues (Bonaldo *et al*., 1998). *Col6a1* null mice have contributed to disclose some *in vivo* roles for Collagen VI, thus throwing new light on the importance of this major matrix component, and also of the ECM in general, in regulating several key cellular pathways.

Although *Col6a1*$^{-/-}$ mice have normal development, are fertile and do not display any obvious anatomical alteration, they are affected by an early onset of myophatic disease, characterized by histological alteration of skeletal muscle tissue, including myofiber degeneration, centrally nucleated fibers and variability in myofiber cross-sectional areas (Bonaldo *et al*., 1998). Additionally, *Col6a1*$^{-/-}$ muscles display a loss of contractile strength associated with ultrastructural alterations of sarcoplasmic reticulum and mitochondria, and spontaneous apoptosis (Irwin *et al*., 2003). *Ex vivo* studies show the presence of a latent mitochondrial dysfunction that affects *Col6a1*$^{-/-}$ myofibers (Irwin *et al*., 2003). Indeed, *Col6a1*$^{-/-}$ mitochondria are not able to maintain their membrane potential because of the increased sensibility to opening of the permeability transition pore (PTP), therefore leading also to the release of cytochrome *c*, a strong inductor of apoptosis (Irwin *et al*., 2003*). In vivo* treatment with cyclosporin A, an inhibitor of the cyclophilin D that desensitizes PTP opening, was able to rescue the apoptotic and mitochondrial defects and, importantly, also the myopathic phenotype of *Col6a1*$^{-/-}$ muscles. Independent studies in muscle

biopsies and muscle cell cultures from BM and UCMD patients revealed the same pathomolecular defects in human collagen VI myopathies. As for *Col6a1*$^{-/-}$ mice, cyclosporin A treatment, as well as by adhesion onto native collagen VI as a substrate, were able to rescue the latent mitochondrial dysfunction and spontaneous apoptosis of patients' muscle cultures (Irwin *et al*., 2003; Angelin *et al*., 2007). Taken together, these studies in *Col6a1*$^{-/-}$ mice disclosed a cytoprotective role for Collagen VI (Irwin *et al*., 2003).

Further mechanistic studies demonstrated that the presence of dysfunctional organelles in *Col6a1*$^{-/-}$ muscle is due to defects in the regulation of the autophagic pathway (Grumati *et al*., 2010). Autophagy is the process by which portions of cytoplasm are sequestered by double-membraned vesicles called autophagosomes and delivered to lysosomes for degradation and subsequent recycling (Galluzzi *et al*., 2015). In particular, lack of Collagen VI causes a defective regulation of the autophagic flux. Actually, muscles of *Col6a1*$^{-/-}$ mice display lower lipidation of microtubule-associated protein-1 light chain 3 (LC3)-II, which is generated during autophagosome formation. Moreover, the lower induction of Beclin-1 and Bnip3, which are key effectors in the initiation of autophagy, and lack of autophagosomes after starvation, revealed that those alteration are linked to a defective autophagy rather than excessive vesicle exhaustion (Grumati *et al*., 2010). Consequentially, *Col6a1*$^{-/-}$ muscles have a detrimental accumulation of dysfunctional and damaged organelles. Interestingly, reactivation of autophagy in *Col6a1*$^{-/-}$ mice by genetic, pharmacological or nutritional methods rescued the myopathic phenotype and restored muscle homeostasis and strength (Grumati *et al*., 2010).

The scientific impact of these studies on human Collagen VI diseases was very high, since the cellular and molecular features displayed by Collagen VI null mice were also confirmed in Bethlem and Ullrich patients. Indeed, analysis of muscle biopsies and primary muscle cultures of Ullrich and Bethlem patients revealed a spontaneous apoptosis and mitochondrial dysfunction (Angelin *et al*., 2007), associated with decrease levels of Beclin-1 and Bnip3, thus confirming a defect in autophagy regulation in the presence of mutated Collagen VI (Grumati *et al*., 2010). These findings indicate that *Col6a1*$^{-/-}$ mice are a valuable model for clarifying the pathogenesis of Collagen VI-related myopathies and investigating novel therapeutic approaches.

Further studies demonstrated that Collagen VI is a key component of the niche adult muscle stem cells (or satellite cells) and is involved in the proper regulation of

muscle stiffness. Actually, *Col6a1*$^{-/-}$ satellite cells display impaired self-renewal capabilities and defective muscle regeneration (Urciuolo *et al*., 2013).

Despite all these important discoveries, it remains to be elucidated how Collagen VI extracellular signals are transduced – likely through specific cell receptors – within muscle fibers, thus accounting for its effects on specific cell-survival pathways, such as apoptosis and autophagy.

1.1.3.2. Collagen VI function in nervous system

Although the phenotype of patients with Collagen VI deficiencies and of the *Col6a1*$^{-/-}$ mouse model clearly underline the critical role of this ECM component in skeletal muscles, Collagen VI has a broad distribution in the body and likely exerts multiple functions in different tissues. Actually, different studies have demonstrated that Collagen VI is expressed in the central and peripheral nervous system. Initially, Collagen VI deposition in the brain was described in meningeal cells (Sievers *et al*., 1994). Subsequently, it has been reported an hippocampal expression of Collagen VI that was higher in the samples affected by the Alzheimer's disease mutation, in particular in the granule cells of the dentate gyrus, identifying a link between Collagen VI expression and Alzheimer's disease (Cheng *et al*., 2009). Moreover, it has been proposed a neuroprotective role for Collagen VI against Aβ-peptide toxicity, mechanism involved in the etiology of Alzheimer's disease (Cheng *et al*., 2009). In another study, addition of Collagen VI to the medium of neuron cultures was able to rescue UV-induced apoptosis and limited dendrite reduction, suggesting again an anti-apoptotic role for Collagen VI in the nervous system (Cheng *et al*., 2011). These observations not only provided new insights into the function of Collagen VI in the central nervous system, but also offered new perspectives for the potential role of this ECM component in regulating neuronal survival processes. Interestingly, even though its pathogenic role has not been clearly demonstrated yet, a recent study has reported a disease-segregating mutation in the *COL6A2* gene in a consanguineous family affected by progressive myoclonus epilepsy (Karkheiran *et al*., 2013). More recently, in three families with early-onset segmental isolated dystonia it has been identified disease-segregating compound heterozygous mutations in *COL6A3*, highlighting biallelic mutations of this gene as an autosomal-recessive cause of isolated dystonia (Zech *et al*., 2015). Furthermore, the authors showed that *COL6A3* is broadly expressed in neurons, with relevant mRNA levels detectable throughout the adult mouse brain, including motor regions thought to have a central role in the pathogenesis of dystonia, and indicating neurons as its cellular source (Zech *et al*.,

2015). Interestingly, although the specific mechanisms by which *COL6A3* mutations cause isolated dystonia remain to be clarified, it has been observed that all isolated dystonia-related *COL6A3* mutations occurred in the C-terminal tail of the α3 (VI) chain, whereas myopathy-causing mutations cluster in the N-terminal and triple helical segments. It is important to remind that previous work indicate that a portion of the α3(VI) C-terminal end is proteolytically cleaved, suggesting microfibril-independent functions for this region (Aigner *et al*., 2002). Moreover, the Fibronectin type III (FN-III) motif of other ECM proteins has been linked in axonal outgrowth of neurons, thus regulating long-term potentiation in the hippocampus (Strekalova *et al*., 2002).

In the peripheral nervous system, Collagen VI is abundantly expressed by Schwann cells and is present in the connective tissue of the endo-, peri- and epineurium (Braghetta *et al*., 1996; Chen *et al*., 2014a). It has been previously shown that activation of *Col6a1* transcription is accounted for the molecular program underlying Schwann cell differentiation and is regulated by axonal signals. Actually, immature Schwann cells express Collagen VI in a neuregulin-dependent manner when they start differentiating from the neural crest cells into myelinating cells, than the Schwann cell precursors acquired the competence of transcribing the *Col6a1* gene independently from neuregulins (Vitale *et al*., 2001). Recently, studies in *Col6a1*$^{-/-}$ mice have uncovered that Collagen VI has a role in maintaining proper peripheral nervous system myelination and function in the sciatic nerves (Chen *et al*., 2014a). Indeed, in the absence of Collagen VI, hypermyelination was observed, resulting in altered Remak bundles (fibers responsible for sensory transmission), in deficits of motor and sensory functions, and in decreased nerve conduction velocities. Moreover, Collagen VI deficiency in peripheral nerves was accompanied by higher phosphorylation levels of focal adhesion kinase (FAK), Akt, extracellular-signal-regulated kinase (ERK) and p38 MAP (Mitogen-activated protein) kinases – all of which are known signaling pathways involved in axon myelination – whereas phosphorylation of c-Jun N-terminal kinase (JNK) is decreased in *Col6a1*$^{-/-}$ sciatic nerves (Chen *et al*., 2014a). Additional studies revealed that Collagen VI has a critical role in peripheral nerve regeneration, together with macrophage recruitment and polarization. This is in agreement with previous studies that described the regulated expression and secretion of Collagen VI from macrophages (Schnoor *et al*., 2008). Indeed, injury-induced nerve regeneration is impaired in Collagen VI null mice due

to a failure in recruiting polarized macrophages to the injury site (Chen *et al*., 2014b).

1.1.4. Collagen VI in zebrafish animal model

In last years, zebrafish models with different forms of mutated collagen VI chains were obtained by the injection of morpholino oligonucleotides (Telfer *et al.*, 2010; Zech *et al*., 2015; Ramanoudjame *et al*., 2015).

In 2010, Telfer and colleagues used the antisense morpholino technology to generated zebrafish models for collagen VI myopathies. One morpholino was designed to target exon 9 of *col6a1*, resulting in an in-frame deletion of the N-terminal part of the triple helical domain that mimics one of the dominant mutations of Ullrich patients. Another morpholino was designed to target exon 13 and resulted in an in-frame deletion of the C-terminal part of the triple helical domain, mimicking a dominant mutation of Bethlem patients affected by a milder myopathy with late-onset motor deficits. *col6a1* exon 9 morphant zebrafish had a severe myopathy with early-onset development motor deficits, increased cell death and mitochondrial swelling. Treatment with cyclosporin A, an inhibitor of the cyclophilin D that desensitizes PTP opening previously shown to be effective in the *Col6a1*$^{-/-}$ mouse model (Irwin *et al*., 2003), was able to decreased apoptosis, improved mitochondrial shape and overall motor function but failed to reverse the sarcolemmal damage (Telfer *et al*., 2010).

The well known immunosuppressive effects of cyclosporin A rise several concerns for the long-term treatment of patients affected by Collagen VI-related myopathies, especially for those affected by respiratory insufficiency, which can be exacerbated by pulmonary infections (Merlini *et al*., 2008). Therefore, a study investigated the effects of N-methyl-4-isoleucine-cyclosporin (NIM811), a cyclophilin D inhibitor that desensitizes the PTP to Ca^{2+} without affecting calcineurin (Waldmeier *et al*., 2002), in zebrafish morphants for *col6a1* exon 9 (Zulian *et al*., 2014). The results of this study showed that NIM811 seems to be more effective than cyclosporin A in zebrafish mutants for Collagen VI, with recovery of motor deficits and normalization of muscle structure (Zulian *et al*., 2014), which were not observed after cyclosporin A treatment (Telfer *et al*., 2010). The different effects of NIM811 and cyclosporin A are likely due to the roles of calcineurin in skeletal muscle differentiation, regeneration and fiber type specification, all functions that are crucial to muscle development, metabolism and functional adaptation (Sakuma *et al*., 2010).

Recently, to support the human genetics data of patients affected by isolated dystonia caused by mutation of the *COL6A3* gene, Zech and colleagues induced a series of in-frame deletions in exon 41 of the zebrafish ortholog for *COL6A3*. The disruption of this exon caused deficits in axonal outgrowth in developing zebrafish embryos, supporting the hypothesis that loss-of-function mutations affecting exon 41 cause recessive isolated dystonia with underlying neurodevelopmental deficits. Moreover, these data highlight the brain ECM as a contributor to dystonia pathogenesis (Zech *et al*., 2015).

In another recent study in zebrafish, two novel Collagen VI long chains were identified and characterized (Ramanoudjame *et al*., 2015). Even though in databases there are sequences that were predicted as *col6a6* and *col6a4* from the zebrafish genome assembly, the authors proposed that these genes are homologous to the mammalian α4(VI) chain – in light of their higher homology with murine α4(VI) – thus naming them *col6a4a* and *col6a4b*, respectively. By RT-qPCR at different developmental stages, they described the unique temporal and spatial expression kinetics of *col6a4b*, which appears delayed compared with those of *col6a4a* and the *col6a3*. Using *in situ* hybridization, they reported a strong signal of *col6a4a/b* transcripts in myotome, as well as in the eye. Then, the authors created models of α4(VI) deficiency in zebrafish, using antisense morpholinos oligonucleotide. In parallel, they also generated loss-of-function of *col6a2* gene, a chain already implicated in Collagen VI-related myopathy. Notably, knockdown of *col6a4a* and *col6a4b* also caused defects in muscle organization and ultrastructure, leading to impaired motility. Moreover, while apoptosis was not drastically increased, autophagy induction was defective in all these morphants. Furthermore, motor neuron axon growth was abnormal in these morphants, similarly to the axonal growth defects recently reported in *col6a3* zebrafish models reproducing mutations identified in patients with dystonia (Zech *et al*., 2015). Overall, these results further confirm the importance of Collagen VI in zebrafish muscle development and may provide new insights on potential human phenotypes associated with deficiency of the recently described "novel" α(VI) chains (Ramanoudjame *et al*., 2015).

Although the above studies in zebrafish provided useful information concerning the effects of Collagen VI ablation in tissues such as skeletal muscle and nervous system, the morpholino-mediated knockdown only allowed the study of transient phenotypes in embryos up to 2 days post-fertilization (dpf). For this reason, a transcription activator-like effector nuclease (TALEN) was recently exploited to

generate a stable mutant *col6a1*^{ama605003}-line, which carries a mutation disrupting an essential splice site in intron 14 of the *col6a1* gene, resulting in an in-frame skipping of exon 14 coding for the N-terminal portion of the collagenous domain of the α1(VI) chain (Radev *et al*., 2015). In this way, the authors reproduced in zebrafish a co-dominant mutation frequently reported in Bethlem patients, which prevents the assembly of Collagen VI dimers and tetramers and inhibits secretion of tetramers into the ECM (Bertini *et al*., 2002, Lampe and Bushby, 2005; Lampe *et al*., 2008). Analysis of homozygous and heterozygous mutant larvae and 3 months post-fertilization (mpf) fish at histological and ultrastructural levels revealed abnormal myofibers with disorganized myofibrils, abnormal dilation of the sarcoplasmic reticulum, altered mitochondria and misaligned adjacent sarcomeres. These symptoms worsened with ageing, similarly to what described in patients with collagen VI deficiency (Radev *et al*., 2015).

1.2. The CRISPR/Cas9 genome editing technology

Nowadays, the use of genome editing tools allows designing targeted mutations in zebrafish and other model organisms, by DNA double-strand breaks and error-prone repair through non-homologous end joining. In the past years, genome editing was mostly carried out with zinc-finger nucleases (ZFNs) or transcription activator-like effector nucleases (TALENs) (Hruscha *et al*., 2013). First adopted in 1996, ZFNs require a pair of DNA-binding zinc fingers and the restriction endonuclease domain Fokl to create double-strand breaks and DNA modification. ZFNs can work very efficiently in zebrafish, however the assembly, development and optimization of custom proteins for the recognition of target DNA sequences is complicated, time-consuming and expensive (Carroll, 2011; Kim and Kim, 2014; Jo *et al*., 2015). TALENs first appeared in 2010, with some improvements compared to ZFNs. This technique requires DNA-binding proteins called transcription activator-like effectors (TALEs) that are combined with a DNA cleavage domain such as Fokl. TALENs are easy to design, although requiring laborious cloning steps (Joung and Sander, 2013) and they tend to have a much higher success rate and average mutation rate than ZFNs (Kim and Kim, 2014). However, TALENs have limitations similar to those of ZFNs in terms of developing and optimizing the custom proteins (Kim and Kim, 2014; Jo *et al*., 2015). In this context, the prokaryotic machinery based on clustered, regularly interspaced, short palindromic repeats (CRISPR) and the CRISPR-associated system (Cas) (CRISPR/Cas system) is a very appealing alternative, since it is the only genome engineering tool described so far that relies on Watson-Crick base pairing rather than the potentially less specific protein-DNA interaction (Gaj *et al*., 2013).

The CRISPR/Cas system is an adaptive defence mechanism found in Bacteria and Archaea, which use small RNAs and Cas endonuclease to target and cleave invading foreign DNAs, thus protecting their genome against invading bacteriophages and exogenous plasmids (Wiedenheft *et al*., 2012). Several groups have demonstrated that CRISPR/Cas9 a type II CRISPR/Cas system from *Streptococcus pyogenes*, is especially useful for targeted genome modifications in mammalian cells (Cong *et al*., 2013; Mali *et al*., 2013). Briefly, the *Streptococcus pyogenes* endonuclease Cas9 enzyme uses two small RNAs: *i)* a target-recognizing CRISPR RNA (crRNA), which directs cleavage through its complementarity to 20 bases of genomic DNA sequence, and *ii)* an auxiliary *trans*-activating crRNA (tracrRNA), which induces sequence-specific double-strand breaks in 20 bp DNA target sequence followed by an NGG

trinucleotide known as the protospacer adjacent motif (PAM). Other studies showed that a synthetic single-guide chimeric RNA (sgRNA) that mimics the crRNA (the sequence complementary to the target at its 5' end) and the tracrRNA complex (the Cas9-interaction interface structure at its 3' end) is able to guide Cas9 endonuclease for site-directed cleavage of target DNA (Jinek *et al*., 2012). This simplified system has been implemented in a variety of *in vivo* settings, resulting in efficient mutagenesis by introduction of small insertions or deletions (indels) during the repair of cleaved DNA by nonhomologous end joining (NHEJ), often causing frameshifts and premature stop codons (Mali *et al*., 2013; Cong *et al*., 2013; Wang *et al*., 2013; Hwang *et al*., 2013).

A first advantage of the CRISPR/Cas9 tool is the greater ease by which it can be designed and implemented. The CRISPR/Cas9 tool consists of two components, the sgRNA and the Cas9 nuclease (Jinek *et al*., 2012). In this system the mutagenesis can be redirected to diverse genomic locations by simply customizing the design of sgRNAs, changing the 20-base-long sequence, without the need to reengineer the Cas9 enzyme, thus simplifying the design and lowering the cost of gene targeting compared with the protein-based target recognition platforms. Contrary, ZFNs and TALENs require some protein engineering and regulation of protein-DNA binding strength that can often be demanding. This distinct feature makes CRISPR/Cas9 suitable for multiple genome modifications. It has been shown that high-efficiency multiplex genome editing can be achieved using CRISPR/Cas by simply combining Cas9 with multiple sgRNAs (Cong *et al*., 2013; Jao *et al*., 2013; Chang, *et al*., 2013; Mali *et al*., 2013). The potential to direct double-strand breaks to multiple *loci* at the same time proves especially beneficial when single indel mutations are not sufficient for *locus* disruption. Multiplex capability of the CRISPR/Cas9 technology allows a high-throughput genetic engineering tool (Jo *et al*., 2015), since multiplex genome editing using several ZFN or TALEN pairs carries the risk of exacerbating off-target effects by the cross reaction between nuclease pairs (Sollu *et al*., 2010).

The second advantage of CRISPR/Cas is its comparable or greater genome-editing efficiencies than that of ZFNs or TALENs. In general, CRISPR/Cas functions with greater consistency, efficacy, and less toxicity than lab-produced ZFNs (Cornu *et al*., 2008; Maeder *et al*., 2008; Ramirez *et al*., 2008), and they are likely to be more effective at targeting methylated genomic sites compared to TALENs (Hsu *et al*., 2013).

Moreover, Watson–Crick base pairing in the CRISPR/Cas9 system tends to result in a higher precision and sequence specificity for a target DNA sequence than ZFNs and TALENs (Kim and Kim, 2014; Ain *et al*., 2015). Greater sequence specificity of sgRNA enables better recognition and initiation of double-strand breaks at targeted sites with fewer off-target effects (Wu *et al*., 2014). Therefore, many researchers have studied factors that may determine the sequence specificity and binding interaction between target DNA and the sgRNA‑Cas9 complex. However, one sequence restriction for the design of sgRNAs is the requirement of a three-nucleotide spacer sequence (namely protospacer adjacent motif, PAM) in the target DNA just outside the region of RNA-DNA hybridization. As mentioned above, the most widely used Cas9 is derived from *Streptococcus pyogenes*, which prefers NGG as PAM sequence and a guide RNA with 20 nucleotides of homology to the target site. Therefore a typical target site consists of a N_{21}-GG consensus. Cleavage by Cas9 normally occurs just upstream the PAM sequence, beside the complementary bases in the target locus (Auer *et al*., 2014; Farboud *et al*., 2015). The 3' end sequence of the sgRNA sequence seems to play a crucial role in base pairing since it conforms to its complementary PAM sequence of the target DNA sequence. That said, mismatches are generally better tolerated at 5' end of the target site, but not at the 3' end "seed" sequence (8‑12 bp upstream of the PAM) (Semenova *et al*., 2011; Wiedenheft *et al*., 2011). Therefore, the basic step to secure a high rate of on-site genetic modification via CRISPR/ Cas9 technology is to optimize the complementarity of the sgRNA strand to the target sequence, especially at the seed sequence. While the seed sequence is sensitive to even single mismatches, the rest of the molecule can tolerate several mismatches. This means that a zebrafish genome may contain many thousands of these off-target sites and some of them may be located in essential parts of the genome, whose cleavage may obscure the effects of the desired mutations or even induce additional phenotypes. Yet, many tools can predict the possible off-target sites for each identified sgRNA in the input sequence and often provide a specificity score based on the predicted off-target sites (Prykhozhij *et al*., 2015).

1.2.1. Generation of loss-of-function frameshift mutations in zebrafish using CRISPR/Cas9

Either by disruption of an open reading frame by indel mutations (due to NHEJ mediated DNA repair) or deletion of whole loci from the genome (by chromosomal deletion), the CRISPR/Cas9 system represents an essential new tool for the future

generation of loss-of-function alleles and for the in depth analysis of resulting phenotypes. Nonetheless, some DNA sequence modifications such as *locus*-specific insertion of reporter genes or tagging of open reading frames are highly desirable for many purposes. Since its first application, this system has been used for the targeted insertion of short DNA sequences. Site-specific DNA integration was demonstrated in mouse and zebrafish, by co-injection of single-stranded oligonucleotides bearing sequences flanking the cleaved target (Bedell *et al*., 2012; Chang *et al*., 2013; Hwang *et al*., 2013a; Wang *et al*., 2013).

1.2.1.1. Cas9 modification

The most studied and commonly implemented version of Cas9 endonuclease used for CRISPR/Cas genome editing is *Streptococcus pyogenes* Cas9 (SpCas9). However, because of the innate differences in cellular contexts between prokaryotic and eukaryotic systems, this bacterial Cas9 has been modified for *in vivo* eukaryotic experimentation (Cong *et al*., 2013; Mali *et al*., 2013). Moreover, one or more commonly used nuclear localization signals (NLS), such as the SV40 NLS, were added to one or both sequence *termini* of the Cas9 protein to facilitate endonuclease entrance into the eukaryotic nucleus (Hwang *et al*., 2013). Once obtained the Cas9-containing plasmid, it should be linearized by the appropriate restriction enzyme and then *in vitro* transcribed to produce Cas9 mRNA. Most Cas9 plasmids contain either a T7 or SP6 promoter upstream the Cas9 sequence to allow *in vitro* transcription. The mRNAs should have a 50-cap and a 30-poly(A) tail in order to be translated efficiently in zebrafish embryos (Gonzales *et al*., 2014). Though most published papers to date implemented CRISPR/Cas in zebrafish by co-injecting Cas9 mRNA and sgRNA together into zebrafish embryos, it has recently been argued that the direct injection of preformed Cas9 protein–sgRNA complexes may be more advantageous because it does not require Cas9 translation before CRISPR/Cas can start functioning (Gagnon *et al*., 2014).

1.2.1.2. Single-guide RNA design

To ensure that an introduced indel generate a deleterious frameshift alleles disrupting almost the entire protein, a constitutive exon (present in all transcript isoforms) situated 3' from the exon containing the initiation codon should be targeted. Most suitable exons for targeting should also correspond to functionally important domains of proteins, conserved during evolution. Ideally, the length of targeted exons should be more than 100 bp to ensure identification of successful

sites. As already mentioned, the sgRNA is a ~100 bp sequence in which the first 20 nucleotides interact with the complementary strand of the target site, while the remaining portion interacts with SpCas9 (Hwang *et al*., 2013). The sgRNA vectors should have a T7 or SP6 promoter, from which the sgRNA is usually transcribed *in vitro* and then microinjected in order to be expressed in early stage zebrafish embryos. The sgRNA should not have a 5'-cap or a 3'-poly(A) tail. The transcribed sgRNA can recognize any DNA target in a 5'-GG-N_{18}-NGG-3' format, with the 5'-GG required for T7-driven transcription, while the NGG being the *S. pyogenes* PAM. Initially, some authors proposed to loosen the constraint of the T7 promoter, which would enable targeting of sequences made of 5'-(G/A)(G/A)-N_{18}-NGG-3' (Hwang *et al*., 2013). Nonetheless, a recent report by Gagnon and colleagues suggests that any change to the 5'-GG can reduce sgRNA efficiency. This result is likely due to T7-driven transcription errors because in all three cases tested, the 5'-GA sgRNAs transcribed by the SP6 promoter showed similar activities to their 5'-GG sgRNA counterparts (Gagnon *et al*., 2014). Therefore, the SP6 promoter may be more flexible than the T7 promoter, tolerating a G→A change at the second position from the transcription start site (Helm *et al*., 1999; Imburgio *et al*., 2000; Kuzmine, Gottlieb and Martin, 2003). At least two studies have proposed guidelines for choosing sgRNA sequences that are more likely to be effective (Gagnon *et al*., 2014; Wang *et al*., 2014). Together, these studies suggest that the last 1–4 nucleotides of the spacer region should preferably be purines. In addition, the GC content of the spacer region near the PAM should be >50%, but not too high. Upon choosing a sgRNA target site, complementary oligonucleotides containing the designed sgRNA spacer region can be synthesized, annealed, and inserted into plasmids for cloning, restriction linearization, and subsequent T7 or SP6 *in vitro* transcription. In addition, there are now published cloning-free methods for sgRNA synthesis that may make sgRNA production quicker (Cho *et al*., 2013; Gagnon *et al*., 2014; Hruscha *et al*., 2013).

Rapid and efficient identification of target sites immediately preceding PAM sites, quantification of off-target sites and predictions of cutting efficiency are some of the features where computational tools play critical roles in CRISPR/Cas9 applications. Some online tool permits to have a global view of the possible sgRNAs in several different exons of the input target gene. For example, CHOPCHOP on line tool (https://chopchop.rc.fas.harvard.edu/) visualizes all candidate sgRNAs within the gene and it also provides help in genotyping assay design, such as primer and

restriction enzyme sites overlapping the Cas9 cut sites. Moreover, this tool has sufficient flexibility in target definition parameters and predicts specificity using an algorithm that searches the genome for off-target sites (Gonzales *et al*., 2014).

1.2.1.3. In vivo introduction and identification of Cas9–sgRNA-induced Indels

After designing and synthetizing the appropriate Cas9 and sgRNA(s) for a given target, CRISPR/Cas genome editing can be applied *in vivo* by zebrafish embryo microinjections. To facilitate homogenous distribution of CRISPR/Cas components among all future daughter cells, zebrafish eggs must be harvested and immediately injected at the one-cell stage before the first round of cellular mitosis (Gagnon *et al*., 2014; Gonzales *et al*., 2014).

A very important point concerns the techniques that allow rapid and cost-effective Cas9 induced mutation detection as well as genotyping of fish carrying mutations in the next generation (Prykhozhij *et al*., 2015). The simplest tools for mutation detection are mismatch-sensitive nucleases such as T7 endonuclease I (T7EI) and CEL-1 (Surveyor). These endonucleases recognize the structure of the double-stranded DNA and cut when there are distortions due to mismatches or bulges due to the presence of indels. In this method, PCR amplicons of targeted genomic *loci* are denatured and gradually cooled to allow partial hybridization between indel-containing single-stranded DNA fragments. These partially hybridized PCR strands will contain mismatched regions at the designed target sites that may be cleaved by T7EI to produce two fragments of predictable lengths. Upon electrophoresis, the percentage of cleaved PCR products can be measured, as well as the estimated NHEJ percentage rates (Guschin *et al*., 2010). Their advantage is that they offer a simple and rapid way to check any sgRNA for efficacy, but in turn they become quite problematical and expensive for genotyping small indels in subsequent generations of fish. In addition, false positives due to genetic polymorphisms surrounding the target site should be carefully controlled. Moreover, in case of uncertain results sequencing of the PCR products should be considered, rising the cost of the analysis. Finally, it is worth to consider that these methods can detect mutations only when the wild-type version of the PCR product is also present in the sample, while homozygous mutant fish cannot be detected (Prykhozhij *et al*., 2015).

Another cost-effective and quicker approach for genotyping mutations is the restriction fragment length polymorphism (RFLP) analysis to detect mutations.

Clearly, this method requires finding a suitable restriction enzyme site overlapping 4–6 bp immediately preceding the PAM sequence. Indeed, such a restriction site will most probably be disrupted by most indel mutations. Ideally, this site should be present only once in the PCR amplicon used for genotyping purposes or mutating this site should have a strong effect on the pattern of restriction fragments after digestion. As already mentioned, CHOPCHOP and many DNA sequence editors support the design of genotyping assays based on restriction enzyme disruption. However, this method restricts a lot the number of available target sites and, furthermore, assaying for lack of a restriction site in a PCR product could be complicated to interpret (Prykhozhij *et al*., 2015).

The heteroduplex mobility assay (HMA) is another technique that can detect heteroduplexes PCR products in samples containing mutations by much slower migration through 8%–15% polyacrylamide gels during electrophoresis (Ota *et al*., 2014; Kotani *et al*., 2015). However, the polyacrylamide gel electrophoresis of DNA is a more laborious than the agarose gel electrophoresis. Furthermore, the pattern of bands of different samples could be difficult to analyse (Prykhozhij *et al*., 2015).

High-resolution melt (HRM) analysis is another method of mutation detection that relies on the idea that when mutations are present in the samples the melting curves of quantitative PCR amplicons significantly differ. HRM can be applied both for an initial evaluation of sgRNA efficacy and for subsequent genotyping analysis (Thomas *et al*., 2014). HRM seems to be both scalable and cost-effective and the only potential drawback is the requirement for specialized software and equipment (Prykhozhij *et al*., 2015).

Chapter II

2. Materials and methods

2.1. Database searches and bioinformatic analysis

Collagen VI chain sequence were identified in the zebrafish genome (assembly version Zv9) at the NCBI (http://www.ncbi.nlm.nih.gov) and Ensembl (http://www.ensembl.org/Danio_rerio/) web sites. Multiple sequence comparison and phylogenetic tree building were carried out with the ClustalW program (http://www.ebi.ac.uk/Tools/msa/clustalo/). Chromosomal localization and flanking genes were derived from NCBI and Ensembl annotations. The conserved synteny was analysed using the Synteny Database program (http://syntenydb.uoregon.edu/synteny_db/). The domain organization of the zebrafish Collagen VI protein were analysed with the SMART (http://smart.embl-heidelberg.de Simple Modular Architecture Research Tool).

2.2. Zebrafish husbandry and embryo manipulations

Wild-type or transgenic (*e.g. Tg(mnx1: GFP; Tg(7xtcf-Xla.siam:nlsmcherry)ia4; Tg(2xID1BRE:nlsmcherry)ia17*), zebrafish were raised and maintained at approximately 28.5 °C in embryo medium (0.5 mM NaH_2PO_4, 0.5 mM Na_2HPO_4, 1.5 g Instant Ocean in deionized water), under a photoperiod of 14 hours of light and 10 hours of dark. Embryos were obtained by natural mating and subsequently cultured

in the same conditions. Embryos were staged by morphological features, and developmental stages were indicated as hours post fertilization (hpf), accordingly to Kimmel *et al.* (1995). The night before the microinjection, males and females were put in breeding tank separated by a partition. At the onset of the light cycle, males and females were put together, generally initiate breeding behaviour that results in the laying and fertilization of eggs. Then the eggs were collected pouring the water through the strainer. Then, the strainer was inverted over a Petri dish to transfer them into the dish.

2.3. Microinjection

Injection needles were pulled to form thin walled glass capillaries (World Precision Instruments) with a pipette puller. Before injection, embryos were collected and placed aligned against a clean glass slide in the lid of a Petri dish. Injections were performed on a dissecting microscope using a micromanipulator attached to a microinjector controlled by a pedal to inject the desired amount of reagent. The samples (morpholinos oligonucleotides, mRNA and DNA) were loaded with tips into the injection needles. Then, the tip of injection needles was broken with dissection forceps. Samples were injected into the yolk sack of 1 or 2-cell stage embryos. After injection, embryos were incubated in fish water and kept at 28.5 °C in an incubator. Injected embryos were raised to the desired stages for observations or collected for further analysis. Live embryos were observed under a Leica DMR compound/ Nomarski microscope equipped with a Leica DC500 digital camera. Images of representative fish, anesthetized with tricaine and mounted in 2% methylcellulose, were acquired.

2.3.1. Morpholino oligonucleotides

Morpholino oligonucleotides were designed and synthesized by Gene Tools, Philomath, OR, USA (www.gene-tools.com), targeting the 3' splice sites between the third exon and the third intron of zebrafish *col6a1* (*col6a1*-MO) and the 5’ splice site of the exon 9 of zebrafish *col6a1* (*col6a1* ex9-MO). Morpholino oligonucleotides were delivered as a prequantitated, sterile, salt-free, lyophilized solid in a glass vial. The stock solution (8 mg/ml) was prepared with nuclease-free water, as advised by Gene Tool’s protocols, and kept at room temperature. Morpholino working solutions were prepared diluting stock solutions in sterile water, Danieau buffer 10× (50 mM NaCl, 0.7 mM KCl, 0.4 mM $MgSO_4$, 0.6 mM $Ca(NO_3)_2$, 5 mM HEPES pH 7.6), and 0.1%

phenol red to facilitate visualization during microinjection. Standard control morpholino was likewise prepared.

Morpholino sequences are as follows:

col6a1-MO — 5’ - ATGTCAGAATTCACATACGCTCTGA - 3' —.

col6a1 ex9-MO — 5’ - GAGAGCGGAAGACGAACCTTCATTC - 3' —

Standard Control — 5' - CCT CTT ACC TCA GTT ACA ATT TAT A - 3' —.

Morpholinos were heated at 65 °C for 5 minutes before injection. The *col6a1*-MO and *col6a1* ex9-MO were injected into one to two-cell embryos at 6 and 2 ng/embryo concentration, respectively. The verification of the knockdown was assessed by the amplification flanking the targeted splice site with the following primers, normalized to *β-actin* housekeeping gene:

primerexon3FOR CCTGTGATCGCGATGTGACA

primerexon4REV CTCTGGTCAGGTGAGATGGC

*β-actin*FOR TGTTTTCCCCTCCATTGTTGG

*β-actin*REV TTCTCCTTGATGTCACGGAC

2.3.2. *In vitro* mRNA synthesis

Zebrafish *col6a1* mRNA was transcribed from DNA plasmid pCS2-z*fcol6a1* after linearization with NotI, a restriction enzyme downstream of the insert. The product was then transcribed using the mMESSAGE mMACHINE kit (Ambion): 1 µg linear template DNA, 10 µl 2× NTP/CAP, 2 µl 10× Reaction Buffer, 2 µl Enzyme Mix and Nuclease-free Water to a final volume of 20 µl. The reaction mix was incubated at 37 °C for 2 hours. Then, 1 µl of TURBO DNAse was added to remove the template DNA, leaving the reaction for 15 min at 37 °C. The transcription was stopped adding 15 µl Ammonium Acetate Stop Solution in 115 µl Nuclease-free Water. To purify the transcript, the RNA was precipitated by adding 200 µl of isopropanol. The mixture was chilled for at least 1 hour at –80 °C, and then centrifuged at 4 °C for 30 minutes at 15,000 rcf to pellet the RNA. After removing the supernatant, the pellet was washed with 500 µl of 70% ethanol followed by another centrifugation at 4 °C for 5 min at 15,000 rcf. The RNA was resuspended in 100 µl of water and 30 µl of sodium acetate. After an overnight at –80 °C, the sample was centrifuged at 4 °C for 30 min at maximum speed and washed in 500 µl of 70% ethanol. Finally, the pellet was resuspended in 15 µl of milliQ water, quantified using Thermoscientific Nanodrop and stored at –80 °C. For mRNA injection, the zebrafish *col6a1* mRNA was dissolved in distilled H_2O to a final concentration of 100 ng/µl. Moreover, 0.1% phenol red was added to the mRNA solution to facilitate visualization during microinjection.

2.4. Plasmid constructions

Zebrafish total RNA was isolated from 56 hpf embryos using TRIZOL reagent (Invitrogen) and reverse transcribed with SuperScript II Reverse Transcriptase (Life Technologies) as already described. Using 1 µl of cDNA, full-length zebrafish *col6a1* was PCR amplified with Phusion High-Fidelity DNA Polymerase (Bio-Rad) using following primers in order to add a BamHI restriction site at 5' end and a XbaI restriction site at 3' end by PCR amplification:

zf*col6a1*BamHIFOR: GGATCCATGGCGCTTAATGGATATATATTGA

Zf*col6a1*XbaIREV: TCTAGATCACCCTCTCGTCTCCAGG

The PCR product was cloned into pCR-Blunt II-TOPO (Invitrogen). Then we moved the insert to pCS2 backbone in order to have the SVpolyA at the 3'. pCR-Blunt II-TOPO – zf*col6a1*BamHI/XbaI was digested with BamHI and XbaI to release the insert, and pCS2 was digested with BamHI and XbaI as well. The linearized pCS2BamHI/XbaI vector was dephosphorylated using the Calf Intestinal Alkaline Phosphatase (Promega). To separate the insert zf*col6a1*BamHI/XbaI from the vector, the obtained solutions were loaded in a 0.8% preparative agarose gel. The fragments of pCS2BamHI/XbaI vector and the insert zf*col6a1*BamHI/XbaI were isolated and purified by Wizard® SV Gel and PCR Clean-Up System. Based on the quantification, the volume of the ligation mix was calculated, in order to reach the ratio vector/insert at 1:1. The sticky-sticky ligation proceeded overnight at 16°C. Then DH5α *E. coli* were transformed with the ligation mix. The plasmid DNA was isolated from *E. coli* to obtain the final construct pCS2-zf*col6a1*.

2.4.1. Agarose gel electrophoresis

DNA samples, obtained from PCR reactions, miniprep, or enzymatic digestion, were analysed by agarose gel electrophoresis. According to their presumptive size, samples were loaded on 0.8 or 1% agarose gel in TAE 1× (4.86 g/l Tris base; 0.744 g/l EDTA; 1.142 ml glacial acetic acid) containing GelRed™ diluted 1:50. Also the 1 Kb Plus DNA Ladder 1 mg/ml (Invitrogen) was loaded, in order to determine the molecular weights of different fragments. The resulting bands were photographed in a UV chamber supplemented with a camera.

2.4.2. Restriction digestion

All the restriction enzymes were purchased from Promega. The reaction mix usually contains between 5 and 15 U of restriction endonuclease, depending on the amount of DNA to be cut, usually from 1 to 10 µg. The restriction digests were

performed assembling the following components: DNA (1 to 10 µg), 10× Restriction Enzyme Buffer, 100× Acetylated BSA, 5-15 U of the Restriction Enzyme and milliQ water to the final volume. Then the mix was incubated at the enzyme's optimum temperature (usually at 37 °C) for 2 hours.

2.4.3. Dephosphorylation

To prevent re-circularization and re-ligation of linearized cloning vehicle DNA, the Calf Intestinal Alkaline Phosphatase (CIAP, Promega) was used, removing phosphate groups from both 5'-*termini*. The following reaction has been set up: 30 µl of digested DNA, 5 µl of CIAP 10× Reaction Buffer (50 mM Tris-HCl pH 9.3, 1 mM $MgCl_2$, 0.1 mM $ZnCl_2$ and 1 mM spermidine), 3 µl of enzyme and milliQ water to a final volume of 50 µl. This mix was incubated at 37 °C for 30 minutes. Then, another aliquot of CIAP was added, and the incubation continued for other 30 minutes.

2.4.4. Column DNA purification

To purify through column system, the Wizard® SV Gel and PCR Clean-Up System was used, as described below.

2.4.4.1. DNA extraction from agarose gel

First of all, using a long-wavelength UV lamp, DNA fragment of interest has been excised using a clean razor blade. For each 10 mg of agarose gel slice 10 µl of Membrane Binding Solution (4.5 M guanidine isothiocyanate, 0.5 M potassium acetate pH 5.0) has been added. This mixture was incubated at 50–65 °C for 10 minutes, until the gel slice is completely dissolved, mixing every few minutes. Then, the DNA has been purified by centrifugation.

2.4.4.2. Purification of DNA by Centrifugation

After a brief spin, the dissolved gel mixture or prepared PCR product has been transferred to the SV Minicolumn assembly and incubated for 1 minute at room temperature. Then, the SV Minicolumn assembly has been centrifuged in a microcentrifuge at 16,000 rcf for 1 minute. The column was washed by adding 700 µl of Membrane Wash Solution, (10 mM potassium acetate pH 5.0, 80% ethanol, 16.7 µM EDTA pH 8.0) and centrifuging for 1 minute at 16,000 rcf. This wash step was repeated with 500 µl of Membrane Wash Solution and centrifuged again for 5 minutes at 16,000 rcf. To allow evaporation of any residual ethanol the column assembly was re-centrifuged for 1 minute. Finally the SV Minicolumn was transferred to a new, sterile 1.5 ml microcentrifuge tube, and eluted the plasmid DNA by adding 50 µl of Nuclease-Free Water to the column incubating at room

temperature for 1 minute and centrifuging at maximum speed for 1 minute. The purified plasmid DNA was quantified by Thermoscientific Nanodrop and stored at –20 °C.

2.4.5. Ligation

To perform DNA ligations has been combined the digested plasmid vector DNA and the DNA fragment to be inserted in a total volume of 5-10 µl. The vector/ insert ratio used was 1:3 or 1:1. To calculate the appropriate amount of DNA fragments to include in the ligation reaction, we used the following equation:

$$\left(\frac{lengh_insert\,(KB)}{lenght_vector}\right) \times ng\ of\ vector = ng\ of\ insert\ needed\ for\ a\ 1{:}1\ ratio$$

Then one volume of Ligation Mix (5-10 µl) was added to the DNA solution and incubated at 16 °C over night. The ligation reaction mixture was used directly to transform *E. coli* DH5α competent bacteria.

2.4.6. Heat shock transformation

Competent DH5α *E. coli* bacteria were taken off –80 °C freezer and kept on ice. The solution containing the plasmid was added and bacteria were incubated on ice for 30 minutes. Then, they were put into water bath at 42 °C for 1 minute for the heat shock transformation, and back on ice for 1 minutes. After that, 300 µl of Luria Broth (LB) were added without antibiotic addition and tubes were left for 1 hour at 37 °C on a shaking incubator. The resulting culture was spread on LB plates with appropriate antibiotic resistance (Ampicillin or Kanamycin) and left growing overnight at 37 °C.

2.4.7. Purification of plasmid DNA

2.4.7.1. MiniPrep

For the isolation of plasmid DNA from *E. coli* hosts the Wizard® Plus SV Minipreps DNA Purification System has been used. First of all, a single, well-isolated colony from a fresh Luria Bertani (LB) agar plate (containing antibiotic) has been used to inoculate 5 ml of LB medium (containing the same antibiotic) and incubated overnight at 37 °C in a shaking incubator. Then, 2-5 ml of bacterial culture was harvested by centrifugation for 5 minutes at 10,000 rcf in a table top centrifuge. The pellet was resuspended in 250 µl of Cell Resuspension Solution (50 mM Tris-HCl pH 7.5, 10 mM EDTA, 100 µg/ml RNase A) and then lysed by adding 250 µl of Cell Lysis Solution (0.2 M NaOH, 1% SDS). When the cell suspension cleared, 10 µl of Alkaline Protease Solution has been added and incubated for 5 minutes at room temperature.

Alkaline protease inactivates endonucleases and other proteins released during the lysis of the bacterial cells that can adversely affect the quality of the isolated DNA. After the addition of 350 µl of Neutralization Solution (4.09 M guanidine hydrochloride, 759 mM potassium acetate, 2.12 M glacial acetic acid pH 4.2) the bacterial lysate was centrifuged at maximum speed (around 14,000 rcf) in a microcentrifuge for 10 minutes at room temperature. The cleared lysate supernatant (approximately 850 µl) was transferred to the prepared Spin Column by decanting and centrifuged at maximum speed in a microcentrifuge for 1 minute at room temperature. Then the column has been washed adding 750 µl of Column Wash Solution (60% ethanol, 60 mM potassium acetate, 8.3 mM Tris-HCl, 0.04 mM EDTA) and centrifuged again at maximum speed in a microcentrifuge for 1 minute at room temperature. This wash has been repeated adding 250 µl of Column Wash Solution and centrifuging at maximum speed in a microcentrifuge for 2 minutes at room temperature. Finally, the Spin Column was transferred to a new, sterile 1.5ml microcentrifuge tube, and the plasmid DNA was eluted by adding 50 µl of Nuclease-Free Water to the Spin Column and centrifuging at maximum speed for 1 minute at room temperature in a microcentrifuge. The purified plasmid DNA was quantified by Thermoscientific Nanodrop and stored at –20 °C.

2.5. Quantitative RT-PCR (qRT-PCR).

RNA extraction was performed by adding 1 ml TRIzol Reagent (Life Technologies) directly on anesthetized embryos and following the manufacturer's protocol. RNA was quantified using a Nanodrop ND-1000 instrument (Nanodrop Technologies) and 1 µg total RNA was retrotranscribed using the SuperScript III First-Strand Synthesis System for RT-PCR (Life Technologies), following manufacturer's instructions. Resulting cDNAs were used to perform quantitative real time PCR using Rotor-Gene SYBR Green PCR Kit mastermix (Qiagen) with the RotorGeneQ instrument (Qiagen). Primer sequences are shown below.

primer	Forward	Reverse
qPCRzf*col6a1*(1)	CATCAAGACCCTGACCGACC	GCACAGCACGTTTAATGGCA
qPCRzf*col6a1*(2)	CAAACGCTCTCAACTTCGCC	TGCTCCACGGCTTTCTCAAT
qPCRzf*col6a2* (1)	CGGTGCCCTGGATATTGTGT	GTTGAGTCGAATGGCCTGGA
qPCRzf*col6a2* (2)	CTGTGCTTTGTCCGGATCCT	AAGACCAGATCAACAGGCCG
qPCRzf*col6a3*(1)	CATCCTCGCCACTTGAAGGT	CCAACCGCCATCACCACTAT
qPCRzf*col6a3*(2)	GGACTTCTGTGCCCCTGATC	TGGTGGGATCTCTTCGGTCT
qPCRzf*col6a4*(1)	AACAGGGACATAGGGCAAGC	AGCCTCGATTCACTCTCCGA
qPCRzf*col6a4*(2)	CGGAGAGTGAATCGAGGCTC	AACCTGCATTGCTCGTCTCA

qPCRz*fcol6a6*(1)	GCGCCGACTTTGAAGATGTG	TGAAGAGTGGGATTGCGGTC
qPCRz*fcol6a6*(2)	CACTTCAAATCGCCGCAACA	TCCTCAGAGCAATGACCCCA
qPCRz*fef1a*	CTGGAGGCCAGCTCAAACAT	ATCAAGAAGAGTAGTACCGCTAGCATTAC
qPCR*mCherry*	GAAGGTGACCAAGGGCGGCC	CTGGGTCACGGTCACCACGC

2.6. Whole-mount *in situ* hybridization

Wild type or morpholinos injected embryos were analysed by whole mount *in situ* hybridization for collagen VI chains transcripts and reporter gene expression respectively.

2.6.1. Preparation of antisense digoxigenin (DIG) labelled RNA probes

The plasmid for the preparation of probes were generated amplifying ~700 bp of the transcript of interest with Phusion High-Fidelity DNA Polymerase (Bio-Rad) and then cloned into pCR-Blunt II-TOPO (Invitrogen). The primer used are listed below:

Probe	Forward	Reverse
z*fcol6a1*	ATCGTGGACAGCTCTGAGAG	TCCGTGAGAAGTCCTTGGTC
z*fcol6a2*	TGTGAAAAGAGATGCGGTGC	GATCCGGACAAAGCACAGTC
z*fcol6a3*	AGGCTTTGCAAACCCGTAAG	TCCTCTAAGAAGCTGCGGAC

The plasmid for *mCherry* probe was already available in the lab. For the preparation of the template, 5 µg of plasmid were linearized using the appropriate restriction enzyme under appropriate conditions of salt and temperature. To check if the linearization is complete, 1 µl was tested on a 1% agarose gel. Then, a phenol/chloroform extraction was used for purifying DNA remove all enzyme and most of the free nucleotides from reactions. Nucleic acids remain in the aqueous phase and proteins separate into the organic phase or lie at the phase interface. First of all, sample was diluted to 100 µl. Then, an equal volume of phenol was added to the tube and mixed vigorously. The tube was centrifuged in a microcentrifuge at top speed for 5 minutes to separate the phases. So, the aqueous phase was transferred to a new tube. The sample has been extract two times adding an equal volume of chloroform, centrifuging and transferring each time the aqueous phase to a new tube. Finally, the nucleic acid has been precipitate adding 1/10 volume of 3 M sodium acetate and 2 volumes of 100% ethanol. The solution was mixed and frozen at least 30 min at –20 °C (or at –80 °C for ten minutes or shortly into liquid nitrogen). Then it was centrifuged at maximum speed in a standard microcentrifuge at 4 °C for 10 minutes. The supernatant was removed and the pellet was washed in

70% ethanol, followed by another centrifugation at 4 °C for 5 min at maximum speed. Supernatant removed, the pellet was dried and resuspended in 10 µl of Nuclease-free water. *In vitro* synthesis of the antisense RNA consist of a 2 hours incubation at 37 °C with the following transcription mix (DIG RNA Labelling kit, Roche): 1 µg of linearized DNA, 2 µl of transcription buffer, 2 µl of DIG-RNA labelling mix, 1 µl of RNase inhibitor RNaseOUT (10 U/µl), 1 µl of 0.1 M DTT, 1 µl of T7 or SP6 RNA polymerase and sterile water up to 20 µl. Following the initial incubation, the DNA template was digested by the addition of 2 µl DNase (Roche) for 15 minutes at 37 °C. Then DNase digestion was stopped by adding 1 µl 0.5 M EDTA pH 8.0. Synthesized RNA was then purified through Quick spin™ (Roche) kit. Firstly, the Quick spin column was centrifuged 1 minute at 1,000 rcf. Then, breaking the base of the column and removing the top, it was placed in a microcentrifuge tube and re-centrifuged for 1 minute at 1,000 rcf to remove the column buffer. Finally, the column was placed in an RNase free vial, added the RNA sample on top of the resin, and centrifuged 4 minutes at 1,000 rcf. The RNA sample was stored at –80 °C. To determine that the procedure was successful, 1 µl of the synthesized RNA was heated at 80 °C for 5 minutes and then visualized on 1% agarose gel.

2.6.2. Preparation of embryos

Embryos were dechorionated by using syringe needle and fixed at the appropriate stage in 4% paraformaldehyde in 1× PBS overnight at 4 °C (or 2 hours at RT). Fixed embryos were then dehydrated progressively in Methanol (MeOH) at room temperature, then stored in 100% Methanol at –20 °C (for at least 2 hours and up to several months) prior to proceeding with *in situ* hybridization experiments.

2.6.3. Pre-hybridization treatments and hybridization

The embryos stored in 100% methanol were rehydrated through a methanol series:

75% MeOH / 25% PBS for 5 minutes;

50% MeOH / 50% PBS for 5 minutes;

25% MeOH / 75% PBS for 5 minutes;

100% PBT (PBS/0.1% Tween-20), 4 times for 5 minutes.

To obtain better permeability of the tissues for RNA probes and antibodies, fixed embryos were treated with Proteinase K (10 µg/ml in PBT) at RT. The length of the digestion was adjusted according to the developmental stage of the embryos. Digestion was stopped by fixing in 4% paraformaldehyde in 1× PBS for 30 minutes.

After this step, samples were washed in PBT (PBS/0.1% Tween-20), 5 times for 5 minutes. Pre-hybridization was performed by incubation in 500 µl of Hybridization Mix (HM) for 2 to 5 h at 65 °C in a water bath. Hybridization Mix (HM) is composed by 65% formamide, 5× SSC, 0.1% Tween-20, Citric acid to adjust HM to pH 6.0 (460 µl of 1 M Citric acid for 50 ml of mix), 50 µg/ml heparin, 500 µg/ml tRNA. Then, the pre-hybridization mix has been replaced with 200 µl of new hybridization mix containing about 200 ng of antisense DIG labelled RNA probe. The hybridization step is carried out overnight at 65 °C in a water bath.

2.6.4. Post-hybridization washes

The embryos were washed in 500 µl of the following high stringency solutions (that remove non specifically hybridized probes) at 65 °C:

100% HM wash (very brief wash; HM wash do not contain tRNA and Heparin);

75% HM wash / 25% 2× SSC for 15 minutes;

50% HM wash / 50% 2× SSC for 15 minutes;

25% HM wash / 75% 2× SSC for 15 minutes;

2× SSC for 15 minutes;

0.2× SSC for 30 minutes.

Then, embryos were progressively moved from 0.2× SSC to 100% PBT (PBS/0.1% Tween-20) by the following incubations at room temperature in slow agitation:

75% 0.2× SSC / 25% PBT (PBS/0.1% Tween-20) for 10 minutes;

50% 0.2× SSC / 50% PBT (PBS/0.1% Tween-20) for 10 minutes;

25% 0.2× SSC / 75% PBT (PBS/0.1% Tween-20) for 10 minutes;

PBT (PBS/0.1% Tween-20) for 15 minutes.

The embryos were blocked for 2 to 5 hours at room temperature in blocking buffer made in PBT (PBS/0.1% Tween-20), 2% Sheep serum and 2 mg/ml BSA. Then they were incubated overnight at 4 °C in antibody solution Anti DIG antibody-alkaline phosphatase Fab fragment (Roche) diluted at 1:3000 in blocking buffer under slow agitation.

2.6.5. Staining

The day after, the antibody solution was collected and the samples were washed 6 times for 15 minutes in PBT (PBS/0.1% Tween-20), and 3 times for 5 minutes in staining buffer (100 mM Tris HCl pH 9.5, 50 mM $MgCl_2$, 100 mM NaCl, 0.1% Tween-20). The samples were then transferred into 24 well plates and staining buffer was

replaced with staining solution containing 200 µl of NBT/BCIP Stock Solution (Roche) in 10 ml of staining buffer. The staining reaction was developed in the dark at room temperature, until the proper staining intensity was reached. The staining was stopped by removing the staining solution and washing the embryos with PBT (PBS/0.1% Tween-20). Labelled embryos were re-fixed in 4% paraformaldehyde in 1× PBS and then stored in PBT (PBS/0.1% Tween-20) at 4 °C.

2.6.6. Imaging

Whole-mount *in situ* hybridization-stained embryos were mounted in 80% glycerol in 1× PBS between slide and coverslip. They were analysed under a Leica DMR compound/Nomarski microscope equipped with a Leica DC500 digital camera.

2.6.7. Vibratome sectioning

Whole-mount *in situ* hybridized embryos were embedded in a solution containing 0.5% gelatin, 30% bovine serum albumin, 20% saccharose, and 1.75% glutaraldehyde. Sections (30 µm) were prepared using a Leica VT1000S Vibratome. Embryos were mounted in glycerol gelatin (Sigma) and analysed under Nomarski microscope equipped with a Leica DC500 digital camera.

2.7. Western blot analysis

De-yolked embryos were lysed in Invitrogen Tissue Extraction Reagent I and proteases inhibitors (Complete EDTA free, Roche). Lysates were then sonicated twice for 15 sec using a Bioruptor (Diagenode) and quantified with the BCA Protein Assay kit (Pierce). SDS-PAGE of protein lysates (20 or 30 µg) was performed using 4-12% polyacrylamide Novex NuPAGE Bis-Tris gels (Invitrogen) and electrotransferred onto PDVF membrane (Millipore). Membranes were blocked for 1 hour in 5% milk in TBST and incubated overnight at 4° C with anti-pSmad1/5/8 primary antibody diluted 1:400 (Cell Signaling) in 2.5% milk. To perform the Ponceau staining for locating protein bands we incubated the membrane for few minutes in Ponceau staining solution with gentle agitation, we rinsed the membrane in distilled water until the background is clean and we took a picture. The stain was completely removed from the protein bands by washing with TBST. Membranes were then washed three times and incubated for 1 hour at room temperature with anti rabbit HRP-conjugated secondary antibodies (Amersham Bioscience) diluted 1:1000 in TBST and 2.5% milk. Detection was performed by SuperSignal West Pico or Dura Chemiluminescent Substrate with CL-X Posure Film (Thermo Scientific).

2.8. Whole mount immunofluorescence

Embryos were fixed at the appropriate stage in 4% paraformaldehyde in 1× PBS. With the exception of the anti-acetylated tubulin antibody staining, the embryos were dehydrated progressively in Methanol (MeOH) at room temperature, and then stored in 100% Methanol at –20 °C. The embryos were permeabilized in acetone for 7 minutes and then washed 3 times for 5 minutes in PBS/1% Triton X-100 (Sigma). Then, they were incubated twice for 1 hour in a blocking solution (PBS/1% Triton X-100, 10% Goat Serum), at room temperature. After, the blocking solution has been replaced with primary antibody, properly diluted in PBS/Triton X-100, 5% goat serum. The antibodies used were the following: rabbit polyclonal anti-laminin (L9393, Sigma; 1:200), anti-slow MyHC and anti-fast MyHC (F59 and F310 respectively, DSHB 1:50), anti-acetylated tubulin (Sigma, 1:1000). These incubations were performed over night at 4 °C on a gentle agitation. Then, embryos were washed 3 times for 10 minutes and then 3 times for 30 minutes in PBS/1% Triton X-100. After that, embryos were incubated with secondary anti-rabbit (Jackson Immuno Research) and/or anti-mouse (Alexa Fluor Goat anti- mouse Invitrogen) antibodies, both diluted 1:500 in PBS/1% Triton X-100, 5% Goat Serum, for 3 hours at room temperature. The rhodamine-coniugated α-bungarotoxin (αBTX, Invitrogen) was used to stain acetylcholine receptor clusters diluted 1:200 together with secondary antibodies. After brief washes, the embryos were incubated with Hoechst (1:10) to visualize nuclei. Then embryos were mounted in melted 1.5 % agarose low melting placing a coverslip on the sample. The images were acquired on Leica SP5, Nikon C2 or Zeiss LSM 700 confocal microscope and images were analysed by ImageJ/Fiji software.

2.9. Birefringence assay

Muscle birefringence was analysed by placing anesthetized embryos on a glass polarizing filter and covering with a second polarizing filter on a Leica DMR microscope. Embryos were photographed with a Leica DC500 digital camera. The top filter was twisted until it was possible to see the light refracting through the striated muscle. Pixel intensity in the trunk region was measured with ImageJ software. Values were expressed as the percentage to WT.

2.10. Evans blue dye (EBD) injection

Evans blue dye (Sigma) was injected at 0.1 mg/ml directly into the pre-cardiac sinuous of anaesthetised embryos, allowing the dye circulate through the cardiovascular system before analysis under confocal microscopy.

2.11. Analysis of motor axons defects

Tg(mnx1:GFP), which express GFP in ventrally projecting motor neurons, were used for Ctrl-MO, *col6a1*-MO and *col6a1*-ex9-MO morpholinos and zf*col6a1* mRNA injections. After injections, at 48 and 72 hpf the phenotype was analysed, visualizing and acquiring images of the GFP^+ motoneurons in live anesthetized HB9:GFP^+ under a 20× objective of Nikon C2 confocal microscopy. We used a scoring system of the hemisegment phenotypes similar to those previously used by others (Sleigh *et al.*, 2014; Ramanoudjame *et al.*, 2015). In detail, each image was analysed using ImageJ software and, for each embryo, 7-8 hemisegments were scored according to this classification: (0) for a hemisegment without a ventral motor axon; (1) for a hemisegment with a motor axon that cannot reach the horizontal myoseptum; (2) for a heamisgment with a motor axon, longer than half myoseptum, which bifurcates and shows extensive lateral branches; (3) for a hemisegment with a wild-type-like ventral motor axon. The relative percentage of hemisegment that display each phenotype is reported, together with the mean score hemisegment for each condition.

2.12. CRISPR/Cas9-mediated mutagenesis protocol

2.12.1. Target site selection

To aid in target site selection, we use an online web tool named CHOPCHOP (https://chopchop.rc.fas.harvard.edu/), which allows easy visualization of candidate Cas9 target sites within the gene, and predicts specificity using an algorithm that searches the genome for off-target sites. The system searches in the sequence of the target gene these basic characteristics: (G/A)(G/A)-N_{19}-GG, and >50% G/C content downstream of the empirically- or algorithmically-determined start codon

2.12.2. Generation of sgRNA

We used a cloning-independent generation of sgRNAs protocol published by Gagnon and colleagues. In particular, was ordered a 60 bp “gene-specific

oligonucleotide" containing: a SP6 promoter for *in vitro* transcription (shown in blue below), the 20 base spacer region specific to the target site, and an overlap region that anneals to the constant oligonucleotide (shown in grey below). The *col6a1*-specific oligo sequence using SP6 has the sequence shown below:

ATTTAGGTGACACTATAGGAGCGGGAGTTGTCTGCAGGTTTTAGAGCTAGAAATAGCAA
G

Moreover the 80 base "constant oligonucleotide" was ordered as well. The constant oligonucleotide, regardless of promoter or target gene choice, has this sequence:

AAAAGCACCGACTCGGTGCCACTTTTTCAAGTTGATAACGGACTAGCCTTATTTTAACTT
GCTATTTCTAGCTCTAAAAC

We order standard desalted oligos from Life Technologies, with no additional purification.

Then we used this protocol to anneal oligos:

Gene-specific oligo (100 µM)	1.5 µl
Constant oligonucleotide (100 µM)	1.5 µl
Water	7 µl
Total:	10 µl

95 °C	5 minutes
95 °C -> 85 °C	–2 °C/second
85 °C -> 25 °C	–0.1 °C/second
4 °C	hold

Next, T4 DNA polymerase was added in the reaction to fill in and the mix was incubated for 20 minutes at 12 °C:

dNTPs (10 mM)	2.5 µl
10× NEB buffer 2	2 µl
100× NEB BSA	0.2 µl
T4 NEB DNA polymerase	0.5 µl
Water	4.8 µl
Total	10 µl

The template was purified using a PCR clean up column, and eluting in 30 µl of water, and to verify a product of ~120 bp we run a sample on an agarose gel.

Subsequently, we transcribe sgRNA using Ambion MEGAscript T7/SP6 Kit, following the reagent amount below and incubate the mix for 2-4 hours at 37°C.

ATP	1 µl
GTP	1 µl
CTP	1 µl
UTP	1 µl
10x buffer	1 µl
T7/SP6 enzyme mix	1 µl
Water	2.5 µl
Template (400 ng)	1.5 µl
Total:	5 µl

Then, 14 µl of water and 1 µl of TURBO DNase were added and the mix was incubated for 15 minutes at 37 ˚C. Finally, we cleaned up sgRNA transcription reaction with the standard ethanol/ammonium acetate protocol, detailed below.

10 µl of 5 M ammonium acetate and 60 µl of 100% ethanol were added and the mix was frozen in liquid nitrogen. The samples were pelleted for 15 minutes at 4 ˚C, at maximum speed and then washed with 1 ml 70% ethanol. The pellet was dried at room temperature for a few minutes and then resuspended in 50 µl water. The RNA concentration was determined with Nanodrop.

2.12.3. Generation of Cas9 mRNA

To generate Cas9 mRNA we used the pCS2-Cas9 plasmid – (http://www.addgene.org/Alex_Schier/). The plasmid was used to transform DH5α that were grown in liquid LB/ampicillin under standard conditions, and the DNA was prepared using a standard miniprep protocol. pCS2-Cas9 was linearized with NotI restriction enzyme and purified using standard DNA column purification protocol. Capped Cas9 mRNA was transcribed with SP6 polymerase using Ambion mMessage mMachine as already described. The reaction mix was incubated at 37 ˚C for 4 hours, then 1 µl TURBO DNase was added and then incubated for 15 minutes at 37 ˚C. The transcription reaction was cleaned up using standard ethanol/ammonium acetate precipitation as described above. RNA concentration was quantified using Nanodrop, and a sample was run on an agarose gel with a DNA ladder. The Cas9 mRNA was stored in aliquots at –80 ˚C.

2.12.4. Injection of Cas9 mRNA and sgRNA

The injection mix was prepared on the day of injection:

sgRNA (750ng/µl)	0.4 µl
Cas9 mRNA (500ng/µl)	2 µl
phenol red injection dye	0.3 µl
Danieu buffer 10×	0.3 µl
	3 µl

The injection mix was loaded into the needle and microinjected 1 nl into the cell (not the yolk) of zygotes using standard zebrafish injection protocols.

2.12.5. Determination of somatic indel frequency

At 24-72 hpf, we prepared single embryo genomic DNA using the HotSHOT protocol (Meeker *et al.*, 2007). For fin clip lysates, adult fish (1 month post fertilization) were anesthetized with 0.5 mg/mL tricaine buffered with sodium bicarbonate and biopsies from the caudal fin removed with a sharp blade. Briefly, we added 50 µl of 50 mM NaOH to single embryo or fin clip biopsies, we incubated for 20 minutes at 95 ˚C, cooled to 4 ˚C and finally added 5 µl of 1 M Tris HCl pH 7.5. Subsequently, we amplified the genomic region surrounding the target exon using the following primers:

Primerintron4FOR TGTTTTGCTTTTCTTTCATCCC

Primerintron5REV CTTTTGATCAATTGAACGCATC

Next, the amplicons were digested with PstI restriction enzyme to analyse restriction fragment length polymorphism (RFLP) for induction of mutations. Selected PCR sample were purified with ExoSAP and then sequenced by BMR Genomics Company, and chromatograms were analysed with 4Peaks program and PolyPeakParser web-based tool (http://yosttools.genetics.utah.edu/PolyPeakParser/) to deconstruct chromatograms with double peaks into wild type and alternative allele sequences.

Alternatively, the genomic samples were analysed by High resolution melting. In particular, PCR, denaturation and melting were performed the RotorGeneQ instrument (Qiagen) with the primers, reagents (LightScanner® Master Mix from Idaho Technology) and program described below:

primerexon5HRMFOR: TTCCCAGGACACCAGACTGT

primerexon5HRMREV: CATGTGGATGATGGAGCGTA

Genomic DNA (20-80 ng)	1 µl
Master Mix	2.5 µl
Primer forward	0.5 µl
Primer reverse	0.5 µl
$MgCl_2$	0.1 µl
Water	5.4 µl
Total	10 µl

1) 95 ˚C	2 minutes
2) 95 ˚C	20 seconds
3) 72 ˚C -> 67 ˚C	20 seconds (–0.5 ˚C/cycle)
4) 72 ˚C	20 seconds
5) Go to 2) 12 times with the touchdown in the annealing step	
6) 95 ˚C	30 seconds
7) 67 ˚C	30 seconds (–0.5 ˚C/cycle)
8) 72 ˚C	30 seconds
9) Go to 6) 24 times	
10) 95 ˚C	hold for 3 minutes
11) 25 ˚C	hold for 20 minutes
12) 65 ˚C -> 95 ˚C	melting step (+0.4 ˚C/step) and acquire fluorescence

Chapter II

3. Results

3.1. Characterization of the zebrafish genes coding for collagen VI chains

Sequence comparisons and BLAST searches of the GenBank and Ensembl databases using sequences coding for mammalian collagen VI chains against the zebrafish genome, allowed me to identify single orthologs for *col6a1*, *col6a2, col6a3, col6a4* and *col6a6* genes in the zebrafish genome (*col6a1* NCBI database: Gene ID 569755, Transcript Reference Sequence XM_009306169.1, Protein Reference Sequence XP_009304444.1; Ensembl database: Gene ID ENSDARG00000074908, Transcript ID ENSDART00000110608 5637, Protein ID ENSDARP00000103794.3. *col6a2* NCBI database: Gene ID 567771, Transcript Reference Sequence XM_009306168.1 or XM_691072.6, Protein Reference Sequence XP_009304443.1 or XP_696164.2; Ensembl database: Gene ID ENSDARG00000061436 Transcript ID ENSDART00000087597, Protein ID ENSDARP00000082031.4. *col6a3* NCBI database: Gene ID 556874, Longest Transcript Isoform Reference Sequence XM_009304692.1, Longest Protein Isoform Reference Sequence XP_009302967.1; Ensembl database: Gene ID ENSDARG00000077139, Transcript ID

ENSDART00000138754, Protein ID ENSDARP00000123601.2. *col6a4* NCBI database: Gene ID: 100535278, Transcript Reference Sequence XM_009307580.1; Protein Reference Sequence XP_009305855.1. *col6a6* NCBI database: Gene ID: 564005 Transcript Reference Sequence XM_687365.7 Protein Reference Sequence XP_692457.6 Ensembl database: Gene ID ENSDARG00000079752, Transcript ID ENSDART00000109703, Protein ID ENSDARP00000103549.3.)

Interestingly, I did not detect any ortholog for the mammalian gene coding for α5(VI) in *Danio rerio* or in *Takifugu rubripes* genomes, suggesting that this gene originated later during vertebrate evolution (**Fig. 1A**).

3.1.1. Conserved synteny for zebrafish Collagen VI genes

Next, I analysed synteny, *i.e.* the conserved flanking genes between zebrafish and mammalian genomes, using the Synteny Database software (http://syntenydb.uoregon.edu/synteny_db/). Like the mammals orthologs, the *col6a1* and *col6a2* genes are in the same chromosome (zebrafish chromosome 11, Dre11), flanking one each other in a head-to-tail orientation. The *col6a3* gene displayed strong synteny with its mammalian homologue, as the portion of zebrafish chromosome 9 (Dre9) that contains *col6a3* displays other four genes that are orthologous with the genes in the corresponding portion of murine chromosome 1 (Mmu1) that contains *Col6a3*. At difference from their mammalian orthologs, the *col6a4* and *col6a6* genes are not in tandem in the same chromosome, and the *pik3r4* gene, which is located downstream both genes in mammals, flanks the *col6a6* gene in zebrafish (**Fig. 1B**).

3.1.2. Zebrafish collagen VI chains share high structural similarities with their mammalian counterparts

Next, I analysed the domain organization of the zebrafish Collagen VI chains with the SMART (Simple Modular Architecture Research Tool) web tool in comparison with their murine counterparts. This analysis showed that the overall domain structure of zebrafish Collagen VI chains is similar to that of the corresponding mammalian chains and display common features of all Collagen VI chains, such as a short collagenous domain with [Gly-X-Y] repeats flanked by large globular regions with a variable number of vWFA modules. The zebrafish α3(VI) chain, like its mammalian counterpart, contains three additional domains at the carboxyl-terminal end: a characteristic unique domain, one fibronectin type III module and a Kunitz-like module. Interestingly, when compared to their mammalian orthologs, zebrafish α4(VI) and α6(VI) chains display additional vWF-A modules at the N-terminal and bear two Kunitz-like module in C-terminal end (**Fig. 2A**).

Then, the amino acid sequences of zebrafish Collagen VI chains were compared with

those of the corresponding fugu, human and murine orthologs, using multiple sequence alignments with ClustalW software (**Fig. 2B** and data not shown). For each zebrafish protein, the highest value of amino acid identities matches the corresponding fugu human and murine ortholog, with the exception of the zebrafish α6 chain that seems to be more similar to the murine α4(VI) chain (38.46%) instead of murine α6(VI) chain (37.22%). Furthermore, to study the evolutionary relationships among Collagen VI genes, a phylogenetic analysis was inferred using the ClustalW software (data not shown). This analysis showed that the genes coding for these proteins appeared in lower chordates and expanded during vertebrate evolution. Notably, zebrafish α4(VI) and α6(VI) chains are highly similar and their genes seem both phylogenetically closer to murine *Col6a4* than to either murine *Col6a3*, *Col6a5* or *Col6a6*. This suggests that these two genes represent the ancestors of mammalian *Col6a4-Col6a6* genes. Multiple sequence alignments between human, mouse and zebrafish α1(VI)–α6(VI) proteins are presented in *Appendix*.

3.2. Expression pattern of zebrafish Collagen VI chains during development

For the initial *in vivo* analysis of Collagen VI expression in zebrafish embryos, I examined the spatio-temporal expression pattern and distribution of Collagen VI chains at different developmental stages by real-time quantitative PCR (RT-qPCR) and whole mount *in situ* hybridization. Gene-specific primer sets were designed to span exons separated by one or more introns, thus allowing detect any contaminating genomic DNA as larger amplicons. Simultaneous detection of the expression of the *ef1a* gene (a housekeeping gene coding for the translation elongation factor EF-1α) was used to normalize the expression levels of Collagen VI transcripts. For the comparison of differences in gene expression over time, all values were adjusted to the stage with the lowest expression level, corresponding to *col6a1* expression at 24 hpf, which was set at an arbitrary value of 1. During zebrafish embryogenesis, Collagen VI transcripts were first detected at 24 hpf. Of note, *col6a1* and *col6a2* transcript levels were the most abundant at all developmental stages included in the analysis. Among the transcripts encoding the longer chains, *col6a3* and *col6a6* expression gradually increased between 24 and 72 hpf, whereas *col6a4* levels were barely detectable before 72 hpf, then increased between 72 and 96 hpf (**Fig. 3A**). To further investigate the spatio-temporal expression of *col6a1*, *col6a2* and *col6a3* mRNAs during zebrafish development, *in situ* hybridization was performed on embryos and larvae from 24 hpf to 72 hpf, using digoxigenin-labeled antisense mRNA probes (**Fig. 3B**). At 24 hpf, Collagen VI transcripts were restricted to the precursors of slow muscle fibers

(adaxial cells) and to the pectoral fin buds. At 48 hpf, strong signals for Collagen VI transcripts were localized throughout the myotome, in the myotendineous junctions (MTJ), in the pectoral fins, in the axial vasculature and in the gut. Expression of Collagen VI genes was also detected in lens and sclera at 48 and 72 hpf, whereas expression in the branchial arches was only detectable at 72 hpf (**Fig. 3B**).

3.3. Knockdown of *col6a1* gene leads to developmental defects

3.3.1. Efficacy of morpholinos-mediated knock-down of *col6a1* gene in zebrafish embryos

The above data provided the basis for functional studies in zebrafish aimed at understanding the role of Collagen VI during development. Toward this aim, I designed gene-specific antisense morpholino oligonucleotides targeting the acceptor splice site between the third exon and third intron of the *col6a1* pre-mRNA (*col6a1*-MO) (**Fig. 4A**). This was designed to induce the retention of third intron in the mature mRNA, thus altering the translation reading frame with the introduction of a premature stop codon. RT-PCR analysis with specific primers flanking the splice site in total RNA extracted from 24 hpf embryos confirmed decreased levels of *col6a1* transcripts in *col6a1*-MO-injected embryos, and the size of the mis-spliced product was consistent with the retention of the third intron. In addition, I also used an exon skipping morpholino oligonucleotide targeting exons 9 of *col6a1*, which encodes a portion of the N-terminal triple helical domain, a common site for dominant mutations in Ullrich patients (Telfer *et al*., 2010). Injection of *col6a1* exon 9 skipping morpholino into 1–2-cell stage embryos resulted in the reduction of the normal *col6a1* transcript and in the appearance of a novel truncated transcript, with deletion of exon 9 (**Fig. 4B**). This was predicted to function as a dominant negative mutant that generates an Ullrich-like phenotype (Telfer *et al*., 2010). The rationale behind *col6a1* knockdown was to obtain morphant embryos deficient in the α1(VI) chain, which is know to be essential for Collagen VI biosynthesis and secretion (Colombatti *et al*., 1987, 1995). A control morpholino with no biological target was injected as a control for specificity.

3.3.2. Analysis of macroscopic phenotypic alterations of *col6a1* morphants

I first examined *col6a1* morphant embryos for morphologic alterations, using live light microscopy. As reported above (§ 3.2) in wild-type embryos *col6a1* mRNA was first detected from 24 hpf, a time when muscle differentiation is completed. From 24 hpf,

col6a1 morphant embryos displayed a macroscopic phenotype characterized by a moderate curvature of the tail and trunk. As shown in **Figure 5A**, in the trunk region of *col6a1* embryos with a more severe phenotype, somites presented a "U-shape" morphology, rather the typical "chevron" shape seen in control-MO injected embryos. These defects in the midbody and tail, which are mainly constituted of skeletal muscles, were previously reported in other zebrafish models with muscle development defects or myopathic phenotype (Bassett *et al*., 2003; Hall *et al*., 2007; Guyon *et al*., 2009; Charvet *et al*., 2013; Telfer *et al*., 2010). In *col6a1* morphants, these muscular defects were frequently combined with anterior defects, such as in the developing brain and eye, and caudally they displayed an enlarged caudal vein plexus (**Fig. 5A**). At 48 hpf, *col6a1* MO-injected embryos displayed a reduced pigmentation, in addition to shorter, curved trunk, cardiac edema and smaller eyes, phenotypes which were not observed in control MO-injected embryos (**Fig. 5B**).

To further confirm that the phenotype of *col6a1* morphants was specific to *col6a1* knockdown, I carried out rescue experiments where zebrafish *col6a1* mRNA (zf*col6a1* mRNA) was co-injected with the *col6a1*-MO. Notably, 79% of co-injected embryos displayed a phenotype similar to control morphants, confirming the specificity of MO-mediated knockdown (**Fig. 5A-C**).

3.3.3. Muscle development is affected in collagen VI morphant embryos

3.3.3.1. Knockdown of col6a1 interferes with muscle integrity

The birefringence of the trunk muscle, *i.e.* the reflected appearance of muscle below polarized light, is a normal property of undamaged muscle with a correct myofibers organization. The measurement of the birefringence is commonly used to quantify the level of myofibers integrity and muscle damage in zebrafish (Sztal *et al*., 2012). Birefringence is easily measured by quantifying the mean intensity of a fixed portion of the embryo (Berger *et al*., 2012). Reduced birefringence has been reported in several zebrafish models of muscular dystrophy (Bassett *et al*., 2003; Guyon *et al*., 2009; Charvet *et al*., 2013; Telfer *et al*., 2010). As measured at 48 hpf, the percentage of birefringence was significantly reduced in all morphants compared with control-MO injected embryos. The reduction of birefringence in larvae injected with Collagen VI morpholinos suggests a disorganization of muscle fibers (**Fig. 6A-B**). When normalized respect to control-MO injected embryos birefringence (100%±5.6% SEM), exon 9 morphants had an average birefringence intensity of 23%±5% SEM (n=18, p<0.000001) and *col6a1*-morphant embryos of 56% ± 3% SEM (n=19, p<0.00001) (**Fig. 6B**). Importantly, the average

birefringence intensity of embryo co-injected with zebrafish *col6a1* mRNA (zf*col6a1* mRNA) and the *col6a1*-MO was of 89%±12% SEM, not significantly different from the birefringence of control-MO injected embryos (**Fig. 6A-B**).

It is known from literature that morpholinos can cause off-target phenotypic effects, due to a nonspecific activation of the tumor suppressor p53-induced apoptosis (Robu *et al*., 2007). Therefore, I injected *col6a1* morpholinos in the *tp53*^{zdf1} zebrafish line, which expresses an autosomal-dominant p53 mutation (Berghmans *et al*., 2005). The presence of *p53* mutation background failed to eliminate the morphant phenotypes, confirming that these were target-related and not caused by off-target p53-induced apoptosis (**Fig. 6C**).

3.3.3.2. Collagen VI ablation affects myofibers and myosepta development

Next, to assess whether *col6a1* knockdown resulted in defective specification and patterning of slow and/or fast muscle fibers, I performed an immunofluorescence staining of *col6a1* morphant embryos with the F59 and F310 antibodies, which label slow and fast myosin isoforms, respectively. Slow muscle fibers were still present after *col6a1* knockdown, although myofibers density appeared lower (**Fig. 7A**). However, whereas in control embryos the fibers were well organized and the myotomal segments were V-shaped and regularly spaced, the slow muscles of morphant embryos looked highly disorganized, with wavy and twisted myofibrils. Some muscle fibers were missing or detached from the myosepta, leading to cell-free spaces in *col6a1* morphants. Detachment primary occurred in the slow muscle layer at the periphery of the myotome, which are the first fibers in the embryo to differentiate and function. Conversely, the deeper fast muscle seems to be less affected, although somewhat irregular and wavy (**Fig. 7A**). Taken together, these data indicate that although slow and fast muscle fibers were still present and in the correct positions within the somites, myofiber organization was disrupted in *col6a1* morphant embryos.

To further evaluate the myosepta defects, I performed whole-mount double immunofluorescence with an antibody against laminin, a basement membrane component, and with the slow muscle fibers F59 antibody, in order to examine whether laminin epitopes also retracted with detached fiber (**Fig. 7B**). Laminin antibody primarily stained the myotendineous junction (MTJ) of control embryos, whereas in *col6a1*-MO this basement membrane component retracted with detached fiber ends (**Fig. 7B**). These data suggest that Collagen VI depletion modifies the interactions between muscle basement membrane and collagen fibrils at MTJ, making the embryo susceptible to muscle fibers detachment.

3.3.3.3. col6a1 knockdown causes contraction-induced myofibers detachment

Evans blue dye (EBD) is a small-molecular-weight dye that fluoresces in the red channel under UV light and widely used *in vivo* as a useful vital stain to assess plasma membrane permeability and myofibers integrity. Actually, once EBD reaches the larval circulatory system through precardiac sinus injection, this dye is selectively uptaken by cells with loss of sarcolemma integrity, while the sarcolemma of normal cells is impermeable to EBD. This technique has previously been used to reveal sites of membrane permeability and to investigate whether sarcolemmal integrity is affected in zebrafish models of muscular dystrophy (Bassett *et al*., 2003; Hall *et al*., 2007; Lo *et al*., 2015). EBD analysis revealed that the dye accumulates in a number of muscle fibers of *col6a1* morphants, indicating loss of sarcolemmal integrity in response of contraction (**Fig. 7C**). Moreover, EBD fluorescence was observed in the interfiber myotomal lesions generated by fiber retraction (**Fig. 7C**). The loss of sarcolemmal integrity in *col6a1* morphants could be exacerbated by increasing the mechanical strain, through incubation of the larvae in a highly viscous medium (e.g. 3% methylcellulose) (Hall *et al*., 2007; Lo *et al*., 2015).

3.3.4. Neuromuscular development is affected in collagen VI morphant embryos

3.3.4.1. col6a1 knockdown leads to primary motor neuron defects and abnormal AchRs patterning

Recent work from the team of Prof. Bonaldo highlighted a role for Collagen VI in the peripheral and central nervous system (Chen *et al*., 2014a; Cescon *et al*., under revision). To investigate whether Collagen VI plays a role in motor neuron development, I carried out *col6a1* knockdown in a zebrafish transgenic line, *Tg(mnx1:GFP*) (also known as *Tg(mHB9:GFP)*), in which motor neuron are labelled by GFP. Analysis at 30, 48 and 72 hpf showed that while in control embryos the motor neurons completed their migration toward the myotome, *col6a1*-MO and *col6a1* ex9-MO injected embryos displayed defective motor neuron pathfinding, branching and extension (**Fig. 8A**). In particular, at 24 hpf, axons frequently failed to extend and migrate along the common path, resulting in absent or very short ventral axons. Then later, at 48 hpf, morphant embryos display axons with excessive branching. Injected embryos were scored based on their motor neuron abnormalities, which included pathfinding errors, failure to extend and abnormal branching (**Fig. 8A**). The severity of these defects was ranked according both to the extent of growth with respect to the horizontal myoseptum, and to the degree of branching

(Sleigh *et al*., 2013; Ramanoudjame *et al*., 2015). Overall, up to 48% of *col6a1* deficient embryos displayed the most severe defects in motor axon outgrowth, classified as hemisegments motor axon scores 0 and 1 (*i.e.* no growth or growth arrest before the horizontal myoseptum). Moreover, between 37% (*col6a1*-MO, *n*=31) and 48% (*col6a1* ex9-MO, *n*=31) of morphants embryos displayed abnormally branched motor axons (hemisegments motor axon score 2). Notably, these phenotype were rescued by co-injecting the *col6a1*-MO together with zf*col6a1* mRNA (81% of motoraxons were classified as normal, *n*=6) (**Fig. 8C**). The same results were obtained by calculating the mean hemisegments motor axon score for each condition. Indeed, while in control embryo the mean hemisegment motor axon score was near to 3 (2.94±0.03 SEM, *n*=21), in collagen VI morphants the hemisegments score was significantly reduced to half (*col6a1*-MO: score 1.61±0.09 SEM, *n*=31; *col6a1* ex9-MO: score 1.38±0.05 SEM, *n*=31; $p<0.0001$), and co-injection of zf*col6a1* mRNA partially rescued the phenotype of morphant embryos (score recovered to 2.62±0.12, *n*=6, **Fig. 8D**). These data indicate that *col6a1* knockdown affects primary motor axon branching.

To analyse the neuromuscular junction (NMJ) compartment in control and morphant embryos at 48 hpf, I labelled post-synaptic AchRs clusters of NMJs with alpha-bungarotoxin together with an antibody against acetylated tubulin, which that label motor neurons. This analysis revealed that together with the motor neuron outgrowth defects, AchR clusters also appear affected in Collagen VI morphant embryos (**Fig. 8B**).

3.3.5. Collagen VI knockdown results in alterations of Wnt and BMP signaling pathways

In order to investigate which signaling pathways are affected by ablation of Collagen VI, I injected morpholinos against *col6a1* in different zebrafish signaling reporter lines, *i.e.* transgenic biosensor animals expressing fluorescent proteins under the control of signaling pathway-responsive *cis*-elements.

First of all, I injected *col6a1* morpholinos in the Wnt reporter line *Tg(7xtcf-Xla.siam:nlsmcherry)ia4* (Moro *et al*., 2012). At 24 hpf, strong reporter expression was detected in the tail, while the gradient distribution was more clearly visible along the trunk. Positive cells were visible also in the fronto-nasal ectoderm and midbrain-hindbrain boundary. At 48 hpf, reporter expression was detected in the hypothalamus, tectum, pectoral fin, jaw cartilages, midbrain-hindbrain boundary and heart. Interestingly, both Collagen VI morphants display an increased Wnt reporter expression (**Fig. 9A-B**).

In addition, I injected *col6a1* morpholinos in the BMP reporter line *Tg(2xID1BRE:nlsmcherry)ia17* (Schiavone *et al*., 2014). At 24 hpf, fluorescent protein

expression was observed in the developing somites, heart, otic vesicle, pharyngeal arches, dorsal eye, lens, pineal, and other brain regions, as well as sporadic cells in the hatching gland. At 48 hpf, expression persisted in the developing heart, gut, somites, dorsal eye and lens, nascent jaw, and gill arches, and within the midbrain–hindbrain boundary of the brain. In this reporter line, I observed a decreased expression of the reporter transgene in *col6a1* morphants, especially in the trunk region (**Fig. 9C**), paralleled by a decreased detection of pSmad1/5/8, the downstream effector of this pathway (**Fig. 9D**).

Notably, knockdown of Collagen VI in *col6a1* morphants did not lead to any detectable difference in transgene expression for other transgenic reporter lines, such as the *Tg(12xCAGA:EGFP)ia16* line, reporter for TGF-β signaling, the *Tg(12xGli-HSV.Ul3:EGFP)ia11* line, reporter for Hedgehog signaling, and the *Tg(12xNRE:EGFP)* line, reporter for Notch signaling (data not shown).

3.4. Generation of a *col6a1* null zebrafish line with CRISPR/Cas9 technology

In parallel, I exploited the innovative CRISPR/Cas9 technology of site-specific mutagenesis to generate a zebrafish Collagen VI null line, in order to extend the above results obtained by morpholino-mediated knockdown. Toward this aim, I followed the previously described protocol for *in vivo* genome editing via CRISPR/Cas9 (Gagnon *et al*., 2014). Briefly, in order to generate a null *col6a1* allele via Non Homologous End Joining (NHEJ)-generated indels, I selected target sites in *col6a1* exons matching the (G/A)(G/A)-N_{19}-GG sequence and displaying >50% G/C content. As an aid for target site selection, I used the CHOPCHOP online webtool (https://chopchop.rc.fas.harvard.edu/), which allows easy visualization of candidate Cas9 target sites within the gene of interest and predicts specificity using an algorithm that searches the genome for off-target sites. Then, based on the ranking of the possible target sequence, I had chosen the most suitable one, located on the exon 5 of *col6a1* gene (**Fig. 10A**). The reason of this choice is that the selected sequence bears, just upstream the PAM sequence (i.e. the region that is more frequently mutated by the Cas9 nuclease) a site that is recognized and cut by restriction enzyme PstI. This was extremely useful to detect the fish that have a mutation in that site. The target specific sgRNAs and Cas9 mRNA were microinjected in 1-2 cell embryos (**Fig. 10B**), and then injected and uninjected embryos were analyzed between 24 and 72 hpf for genome modifications of the target locus. Towards this aim, I extracted genomic DNA from tail of injected fish, amplified a region that includes the target site, and analysed the PCR product by restriction fragment length polymorphism (RFLP) for induction of mutations (Schmid

et al., 2013). As illustrated in **Figure 10C**, while the wild type amplicon was digested by PstI into two faster migrating bands, some amplicons from the tails of injected fish could not be cut efficiently by the restriction enzyme, suggesting that a mutations occurred in that region. Sequence analyses were used to confirm that the loss of the respective restriction site was due to mutations at the target sites in the sgRNA/Cas9-injected embryos. Indeed, downstream the target sequence, double peaks were present, indicating an alteration in that region (**Fig. 10D**). Once selected F0 fish were grown to fertile adults, I outcrossed these putative founders and screened the offspring for genome modification in the target locus. In particular, I cut the tail to determine the heterozygous individuals (**Fig. 11A**). By RFLP analysis of amplicon and subsequent Sanger sequencing, I could identify different mutations. Some mutations did not generate a null allele, as they corresponded to 3-nucleotide deletion or 12-nucleotide insertion, but others (namely the insertion or deletion of 7 nucleotides) caused a frameshift leading to a premature stop codon (**Fig. 11B** and data not shown). To rapidly and efficiently detect nuclease-derived mutation, I applied High Resolution Melting (HRM) analysis. HRM is a fluorescence-based method that measures the amount of double stranded DNA at different temperatures, thus revealing the temperature of melting (Tm) of a particular PCR product. This analysis confirmed that the analysed F1 animals were heterozygous, as they displayed an homoduplex product with a specific Tm, together with a heteroduplex product with an additional much lower Tm (**Fig. 11C**).

Concurrently, I crossed the heterozygous ins7/+ F1 fish with a BMP reporter fish line, in order to obtain heterozygous fish in the BMP reporter background, which were then intercrossed (**Fig. 12B**). By selecting the fluorescent larvae among the F2 offspring, I analysed the intensity of fluorescence of this pool of embryos, made of wild type (expected ¼), heterozygous (expected ½) and homozygous (expected ¼). Similarly to *col6a1* morphant embryos (**Fig. 12A**), I observed a reduced BMP signaling in the majority of larvae (**Fig. 12C**), suggesting that a reduction – in heterozygous fish – or a complete depletion – in homozygous animals – of Collagen VI leads to a substantial reduction of BMP signaling.

Chapter II

4. Discussion

Collagen VI is an ECM protein playing a key role in different tissues (Cescon *et al*., 2015). In particular, it is critical for proper skeletal muscle structure and function. Indeed, inherited mutations of the genes coding for the Collagen VI subunits cause different forms of myopathies and muscular dystrophies in humans (Merlini *et al*., 2008). The generation of a Collagen VI null mouse model, carried out by Prof. Bonaldo's team, provided a valuable tool for investigating the *in vivo* roles of Collagen VI (Bonaldo *et al*., 1998). These studies revealed that Collagen VI has several cytoprotective effects, which extend from counteracting apoptosis and oxidative damage to the regulation of autophagy and cell differentiation (Bonaldo *et al*., 1998; Irwin *et al*., 2003; Grumati *et al*., 2010, Urciuolo *et al*., 2013). Nonetheless, the function of this ECM protein during development and its specific regulatory effects on intracellular signaling pathways are largely unknown. *Danio rerio* is a powerful model organism for studying vertebrate development. Moreover, the availability of transgenic biosensor lines makes zebrafish an ideal tool for *in vivo* analysis of signaling pathways and tissue development. My project arose from these premises, with the aim of throwing light into the signaling pathways and tissues affected by the absence of this major ECM component, using zebrafish as a model organism.

Although a zebrafish morphant mimicking Collagen VI-related myopathies was previously generated (Telfer *et al*., 2010), no studies on the structure, expression and function of the different Collagen VI genes in zebrafish were yet performed. In

the present work, I first characterized the structure, genetic organization and expression of zebrafish Collagen VI chains. First of all, the GenBank and Ensembl databases analysis and sequence comparison allowed me to identify single orthologs for *col6a1*, *col6a2*, *col6a3*, *col6a4* and *col6a6* genes in zebrafish genome. Interestingly, no ortholog for the mammalian gene coding for α5(VI) chain was identified, suggesting that this gene originated later during vertebrate evolution. Furthermore, these analyses revealed that the domain organization and amino acid motifs of the zebrafish Collagen VI proteins were similar to the corresponding mammalian ortologs, with a noticeable exception, as the zebrafish α4(VI) and α6(VI) chains display additional vWF-A modules at the N-terminal end and two Kunitz-like domains in C-terminal end. The presence of Kunitz-like domains at the C-terminal end of zebrafish α4(VI) and α6(VI) chains and their higher degrees of similarity with murine α4(VI) suggest that the annotated zebrafish *col6a4* and *col6a6* genes are instead two paralogs of the mammalian *col6a4* gene. A recent report also supported this concept, changing the name of zebrafish *col6a4* and *col6a6* genes in *col6a4b* and *col6a4a*, respectively (Ramanoudjame *et al*., 2015). In this work, it was suggested that the *col6a4* ancestor gene underwent duplication in fish, as happened to many genes in the teleost genomes, giving rise to *col6a4a* and *col6a4b* that evolved differently (Ramanoudjame *et al*., 2015). Actually, it is worth to underline a slight difference between zebrafish and mammalian collagen VI "novel" chains, not yet reported in full. In mammals, α4(VI) and α6(VI) proteins are more diversified and their genes lie in the same chromosome (*e.g.* mouse chromosome 9). Conversely, these two chains have similar domain structure in zebrafish, making them more related one to the other, but their genes are in different chromosomes (chromosome 13 and 16, respectively). Notably, the gene *pik3r4*, located downstream the genes coding for the α6(VI) and α5(VI) chains in mammals (human chromosome 3, *PIK3R4-COL6A6-COL6A5*; mouse chromosome 9, *Pik3r4-Col6a6-Col6a5-Col6a4*), flanks the zebrafish *col6a6* gene on chromosome 16. By analysing in more detail the amino acid sequence conservation, I observed that if the first extra N-terminal domain (named in this work N7') was excluded from the alignment, the percentage of amino acid identities between zebrafish and murine α6(VI) chains markedly increases (detailed alignment are presented in *Appendix*). These data suggest that more analyses are needed to classify these two genes as paralogs or different orthologs. Undoubtedly, these findings open new interesting views on how Collagen VI genes behave during vertebrate evolution. One hypothesis is that an ancestor

gene was amplified during the evolution, through duplication or triplication. Subsequently, the resulting genes underwent divergence, giving rise to the mammalian *Col6a4-Col6a6* genes, which encode for different Collagen VI chains with distinctive expression patterns.

For the initial *in vivo* analysis, I characterized the temporal expression of Collagen VI transcripts. During zebrafish embryogenesis, Collagen VI transcripts were first detected at 24 hpf. Remarkably, *col6a1* and *col6a2* transcripts are expressed at higher levels throughout zebrafish development, in agreement with the requirement of α1(VI) and α2(VI) for the 1:1:1 stoichiometric association with one of the longer chains (α3, α4 or α6). Notably, the combination of the expression patterns of the transcripts coding for the three long chains results in a quantity that is comparable to those of the transcripts coding for the shorter α1(VI) and α2(VI) chains. This is in line with the fact that Collagen VI chains assembly into α1–α2–αX triple-helical monomers, where αX is one of the three long chains (Fitzgerald *et al*., 2008; Gara *et al*., 2008). Moreover, the expression of *col6a4* appears delayed compared with that of *col6a6* and *col6a3*, suggesting that this chain may be present in different late developing structures with respect the other two long chains, thus perhaps playing a distinct role. By *in situ* hybridization analysis, *col6a1*, *col6a2* and *col6a3* transcripts could be detected in myotome, developing cartilage as well as in the eye and gut, where mammalian Collagen VI is known to be expressed (Braghetta *et al*., 1996). In a recent study, expression of *col6a4* and *col6a6* was detected in myotome and in the eyes by *in situ* hybridization (Ramanoudjame *et al*., 2015). Interestingly, the murine α4(VI) protein is not found, in muscle but is restricted to the intestinal smooth muscle, ovary and testis. Conversely, the α5(VI) and α6(VI) chains are differentially expressed in skeletal muscle: α5(VI) is detected at the myotendineous junction (MTJ), while the α6(VI) is found in the endomysium and perimysium of skeletal muscle, with a partial co-localization with α3(VI) (Sabatelli *et al*., 2012). In addition, α5(VI) shows a unique, strong expression in the basal lamina of NMJs and in the perineurium of intramuscular peripheral nerves (Gara *et al*., 2008, Gara *et al*., 2011). It would be interesting to analyse in more detail the expression patterns of zebrafish *col6a4* and *col6a6* transcripts, determining if they are similar to those of the mammalian long chains.

In order to carry out functional studies for Collagen VI in zebrafish, I performed loss-of-function of the *col6a1* gene, which encodes for one of the crucial chains present in all Collagen VI isoforms. In particular, I designed gene-specific antisense

morpholino that lead to the retention of the third intron and thus altering the translation reading frame with the introduction of a premature stop codons. In addition, I used another morpholino that causes an in-frame skipping of zebrafish *col6a1* exon 9 (corresponding to human exon 10, which encodes a portion of the N-terminal triple helical domain) and thus functions as a dominant negative form that generates an Ullrich-like phenotype (Telfer *et al*., 2010). The data presented in this thesis indicate that knockdown of *col6a1* results in a gross phenotype similar to those previously reported for other zebrafish models with muscle developmental defects or myopathic phenotypes. The defects I detected in *col6a1* morphant embryos include abnormal trunk curvature, misshapen vertical myosepta, reduction of myofibers density, defects in muscle organization with abnormal orientation and decreased alignment of myofibers. Interestingly, all these phenotypes were more severe in the exon 9 skipping morphants, suggesting that this dominant negative mutation of *col6a1* is more deleterious than mutations causing the absence of gene product. Moreover, the depletion of Collagen VI makes the embryo more susceptible to muscle fibers detachment, with loss of sarcolemmal integrity in response of contraction. It will be interesting to understand if the loss of sarcolemmal integrity in *col6a1* morphants could be exacerbated by increasing the mechanical strain, through incubation of the larvae in a highly viscous medium (3% methylcellulose) (Hall *et al*., 2007; Lo *et al*., 2015). Importantly, the majority of the defects observed in *col6a1* morphant embryos were rescued by co-injection with zebrafish full-length *col6a1* mRNA, thus confirming that these defects were caused by Collagen VI depletion. The rescue with the injection of the *col6a1* mRNA was not performed with the exon 9 skipping morpholino, as this dominant negative mutation would adversely affects the normal, wild-type gene product.

Besides muscles, Collagen VI is also abundant in adult peripheral nerves, where it is produced by Schwann cells and endoneurial/perineural cells but not by neural crest and axons (Braghetta *et al*., 1996; Vitale *et al*., 2001; Chen *et al*., 2014a). Actually, studies in the *Col6a1 null* mouse model showed that Collagen VI prevents Schwann cell myelination with functional impairment of peripheral nerves (Chen *et al*., 2014a). Interactions between nerve cell projections and molecules of the ECM are essential for the axons reaching their targets (Hynes and Lander, 1992). The importance of ECM molecules in axon guidance has been previously reported in zebrafish (Bernhard and Schachner, 2000; Pagnon-Minot *et al.*, 2008). For instance, chondroitin sulfates, which are present in zebrafish at the interface between

notochord and somites, are involved in axon growth (Bernhard and Schachner, 2000). Collagen XV is also located at the interface between notochord and somites in zebrafish and lack of collagen XV affects motor axon growth (Pagnon-Minot *et al.*, 2008). In this work, through Collagen VI morpholino-mediated knockdown in motor neurons of the transgenic reporter zebrafish line *(Tg(mnx1:GFP)* (also known as *Tg(mHB9:GFP)*) I found that *col6a1* knockdown affect primary motor axon growth and branching. In the *Col6a1* null mouse model NMJ alterations were observed, in particular in AChR pre-patterning, *i.e.* the accumulation of AChRs in the centre of muscle cells, where the first synapses will form (Cescon and Bonaldo, unpublished data). Actually, in *col6a1* morphant embryos AChR clusters appear affected, in parallel with motor neuron outgrowth defects. These findings are perfectly in line with the primary motor neurons guidance defects reported in *col6a4a* and *col6a4b* (*i.e. col6a6* and *col6a4*) morphants (Ramanoudjame *et al*., 2015). A similar, although less severe, axonal growth defects were recently reported in new *col6a3* zebrafish models reproducing mutations identified in patients with dystonia (Zech *et al*., 2015). The mechanism of action of Collagen VI in motor axon growth and branching is unclear. Collagen VI may serves as a guide to axon navigation in the ECM from the spinal cord to their muscle targets, or alternatively could be important in the AChR pre-patterning, both essential processes in the formation of neuromuscular synapses. Interestingly, it is known that Wnt-induced trafficking of the muscle-specific kinase (MuSK) receptor initiates a signaling cascade that is crucial for AChR accumulation at future synaptic sites (Gordon *et al*., 2012). In this sense, it will be interesting to determine whether in *col6a1* depleted embryos there is a correlation between neuromuscular development and Wnt signaling pathway alterations. Moreover, it remains to be determined whether these primary motor neurons growth defects are either a consequence or a cause of the muscle defects.

To assess whether Collagen VI depletion affects signaling pathways involved in embryonic development, I carried out collagen VI morpholino-mediated knockdown in zebrafish reporter lines for different signaling pathways. Interestingly, these experiments revealed an opposite variation in Wnt and BMP signaling pathways, suggesting a potential correlation between developmental defects and signaling pathway alterations, which has to be further investigated. With the aim of confirming and extending the above results, I exploited the CRISPR/Cas9 technology of site-specific mutagenesis to generate a zebrafish Collagen VI *null* line. According to the guidelines for choosing sgRNA sequences that are more likely to be effective

and with the help of the CHOPCHOP web tool, I selected the suitable target sequence to knockout the *col6a1* gene. In particular, I chose a sequence on exon 5 that displays a site recognized and cut by the restriction enzyme PstI. This site is just upstream the PAM sequence, in the so-called "seed" region that is more frequently mutated by the Cas9 nuclease. In this way, I could apply a genotyping assay based on restriction enzyme disruption to detect mutations occurring in that region. By screening the F1 generation, I detected heterozygous fish for mutations causing a frameshift leading to premature stop codons, namely an insertion and a deletion of 7 nucleotides. Moreover, I checked that frameshift and stop codons appearance would occur even in the case of cryptic splice site activation and joining of downstream exons, as these latters have a different reading frame to exon 5. In order to obtain a preliminary analysis regarding the effect of Collagen VI ablation in BMP signaling, heterozygous fish, one of which already in BMP reporter background, were crossed to analyse the F2 generation. Interestingly, these embryos display a severe reduction of BMP signaling. I am currently corroborating these findings by single embryo DNA and RNA extraction, by which it will be possible to verify the genotype of these embryos. Having these *col6a1* mutated lines together with reporter lines for signaling pathways involved in embryonic development, further experiments will be performed in the next future to understand in detail which signaling pathways and tissues are affected by ablation of collagen VI.

In conclusion, in this PhD work I first characterized the structure, the gene organization and the expression of Collagen VI chains in zebrafish. Knockdown of Collagen VI during embryogenesis allowed me to identify alterations of muscle fibers development and axonal growth defects of motor neurons in morphant embryos. In addition, I also detected variations in Wnt and BMP signals in Collagen VI morphant embryos. Finally, through the CRISPR/Cas9 site-specific mutagenesis technology, I generated a zebrafish *col6a1* VI null line, which represents a valuable tool for the thorough understanding of the functions of Collagen VI during development and in regulating signaling pathways. These studies are of particular significance, since they will allow unveiling previously unknown connections between molecular and signalling defects and Collagen VI deficiency, a relevant field of study considering the range of disorders linked to mutations of Collagen VI genes in humans.

Chapter II

Figures

Figure 1. Identification of single orthologs of zebrafish collagen VI chains. (A) The table reports the chromosome and chromosomal position of each zebrafish gene, derived from the GenBank annotations, and their synteny, *i.e.*, the conserved flanking genes for each zebrafish collagen VI chain. Syntenic genes whose murine ortholog is also flanking the corresponding murine collagen VI chain are underlined. **(B)** Graphical rapresentation of conserved genomic synteny around the collagen VI genes in zebrafish and mouse. The analysis was performed with the Synteny Database program (http://syntenydb.uoregon.edu/synteny_db/) with a sliding window size of 50 genes. Synteny analysis shows that the portion of zebrafish chromosome 9 (Dre9) that contains *col6a3* posses other four genes that are orthologous to the genes in the portion of murine chromosome 1 (Mmu1) that contains *Col6a3*. The figure depicts the relative location of genes, drawn as squares, but not to physical scale. Orange lines connect presumed paralogs within chromosome groups.

Figure 1

A

Gene	Chromosomal localization	Flanking genes
col6a1	Chr. 11, pos. 34.83 Mb	*PHKA2, col6a2, tdo2b, ATP13A3*
col6a2	Chr. 11, pos. 34.75 Mb	*nxph2b, PHKA2, col6a1, tdo2b*
col6a3	Chr. 9, pos. 24.94 Mb	*asb18, cops8, cxcr7, mlph, prlh, lrrfip1a*
col6a4	Chr. 13, pos. 46.26 Mb	*rhd, tmem57b, ldlrap1b, fndc5α, olig4*
col6a6	Chr.16, pos. 38.05 Mb	*ptrub, ptru, pik3r4, decr1, calb1, pnp4b*

B

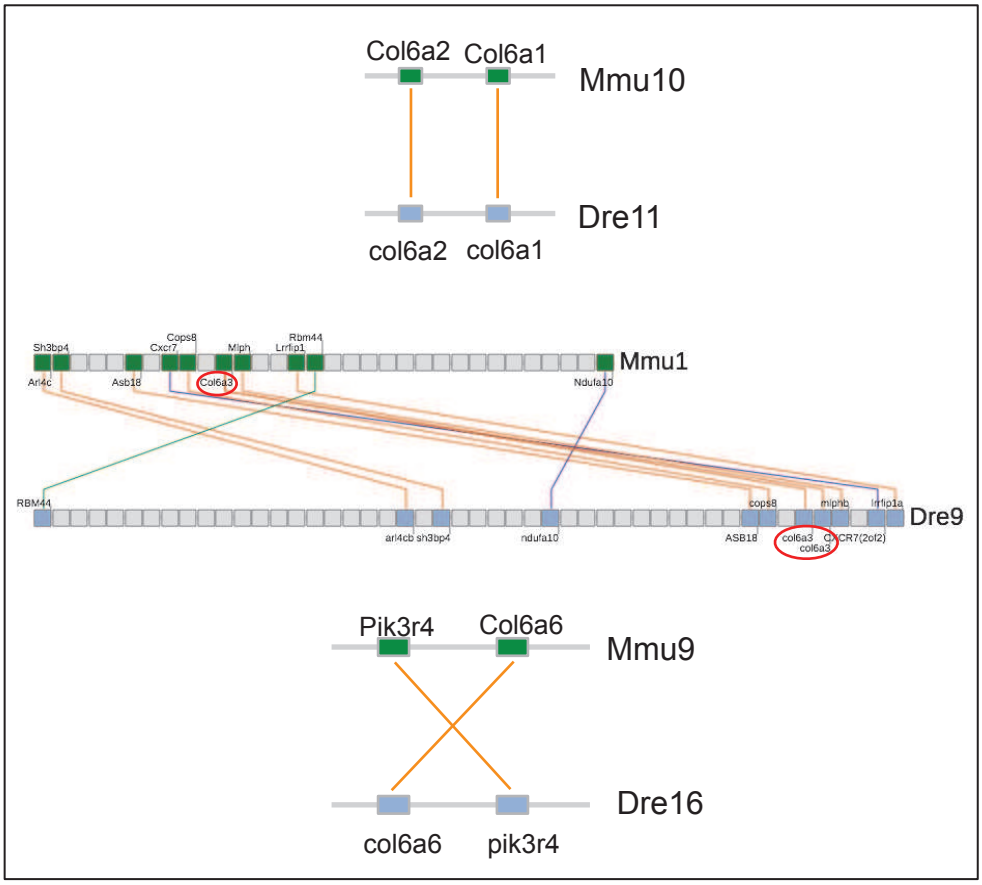

Figure 2. Zebrafish collagen VI chains presents the overall structure of its mammalian counterparts. (A) Schematic diagram of the domain structure of collagen VI subunits in mouse and zebrafish. Each chain is made of a short collagenous (COL) region flanked by a variable number of von Willebrand factor type A (vWF-A) modules. Bioinformatic tools showed that the domain structure of zebrafish collagen VI chains largely resembles that of their mammalian counterparts. However, in comparison with their mammalian ortholog, the zebrafish α4 and α6 collagen VI chains display additional vWF-A modules at the N-terminal and possess two Kunitz domains in C-terminal. **(B)** Percentage of amino acid sequence identities between zebrafish and murine collagen VI chains, obtained by multiple sequence alignments with ClustalW program of entire protein sequences from *Danio rerio* (Dr) and *Mus musculus* (Mm). For each zebrafish genes, the highest value matches the corresponding murine ortholog, except for the α6(VI) chain that seem to be more similar to the murine α4(VI) chain instead of the α6(VI) chain.

Figure 2

A

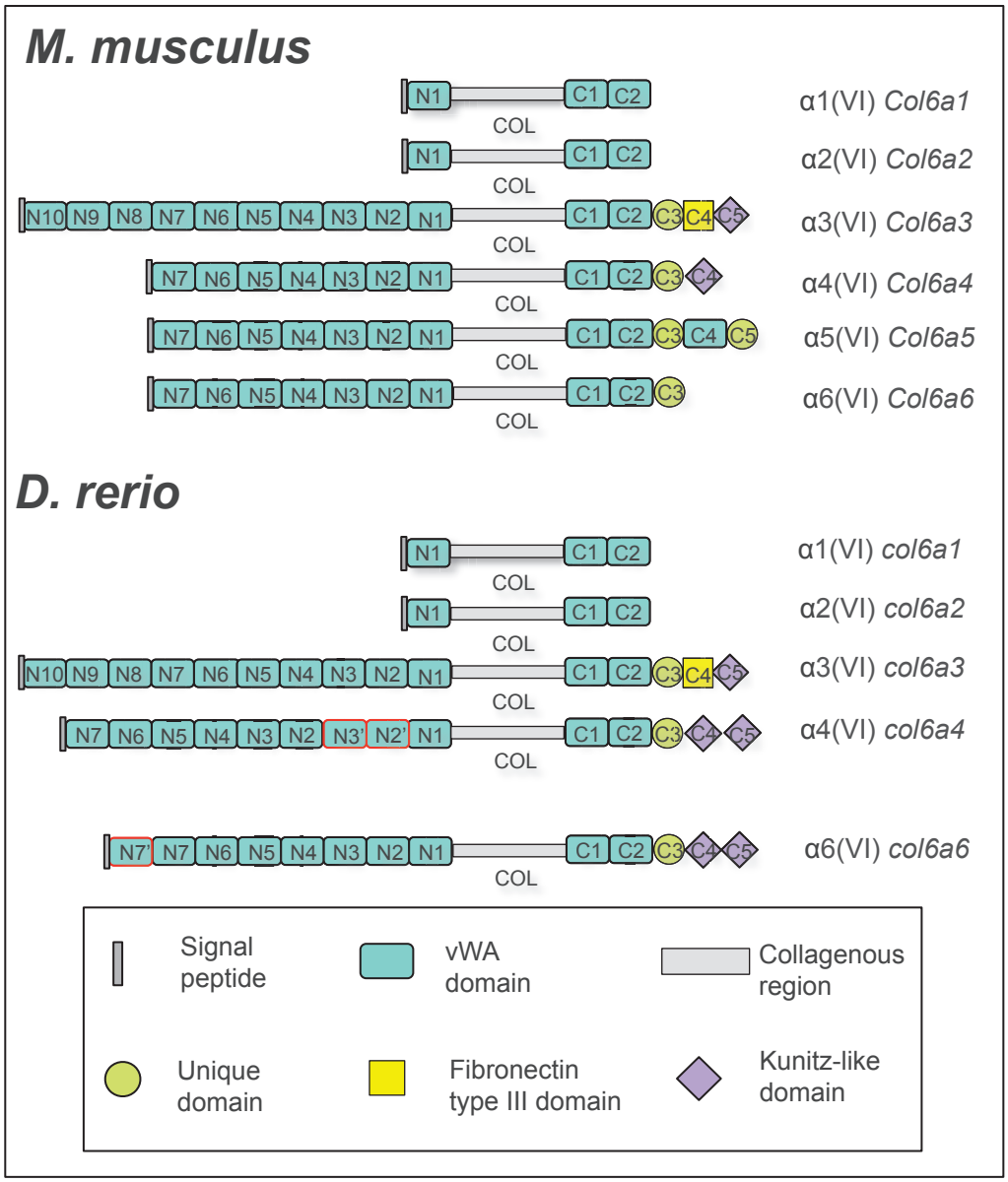

B

M. musculus / *D. rerio*	*Col6a1*	*Col6a2*	*Col6a3*	*Col6a4*	*Col6a5*	*Col6a6*
col6a1	**56.34%**	35.44%	28.57%	28.48%	25.26%	26.16%
col6a2	36.53%	**62,04 %**	28,5%	29.33%	26.00%	28.36%
col6a3	28.28%	27.55%	**43.02%**	32.03%	28.73%	30.43%
col6a4	25.00%	25.68%	32.18%	**38.79%**	32.00%	35.07%
col6a6	24.66%	25.26%	30.32%	**38.46%**	33.86%	37.22%

Figure 3. Spatio-temporal expression pattern of zebrafish collagen VI genes. (A) The graph shows the relative expression of collagen VI transcripts in whole zebrafish embryos, from 12 to 96 hpf, as determined by qRT-PCR. These data indicate that collagen VI transcripts are first detected at 24 hpf and increase throughout early development. **(B)** Whole-mount *in situ* hybridization (WISH) analyses of the expression pattern of collagen VI genes at different developmental stages. At 24 hpf, *col6a1*, *col6a2* and *col6a3* mRNAs became restricted in two lines of adaxial cells and in the pectoral fin buds. At 48 hpf, strong signals for collagen VI transcripts were detected in myotendineous junctions, pectoral fins, branchial arches, heart, axial vasculature and gut. lat, lateral views; dors, dorsal views; sc, spinal cord; no, notochord; fb, fin buds; ey, eye; mtj, myotendineous junction.

Figure 3

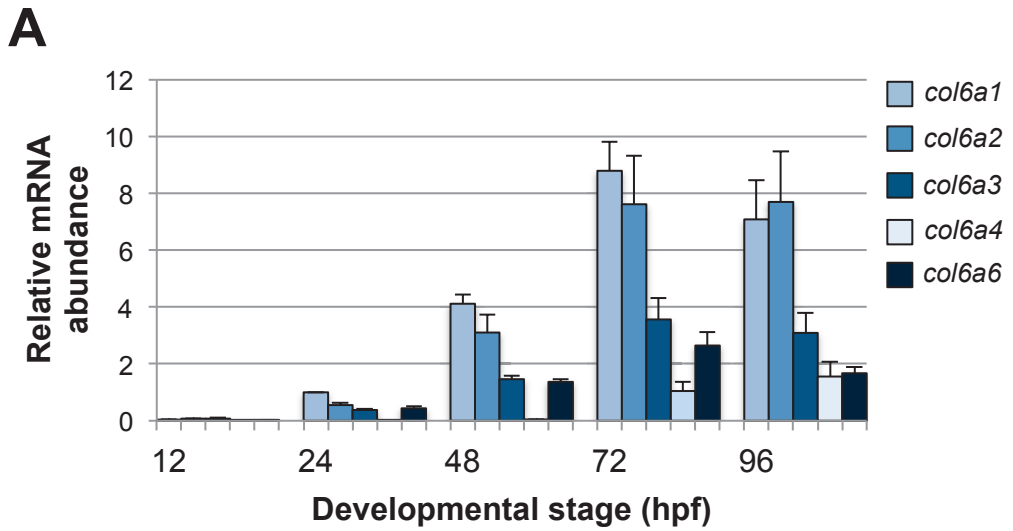
A
Relative mRNA abundance
12
10
8
6
4
2
0
12
24
48
72
96
Developmental stage (hpf)
col6a1
col6a2
col6a3
col6a4
col6a6

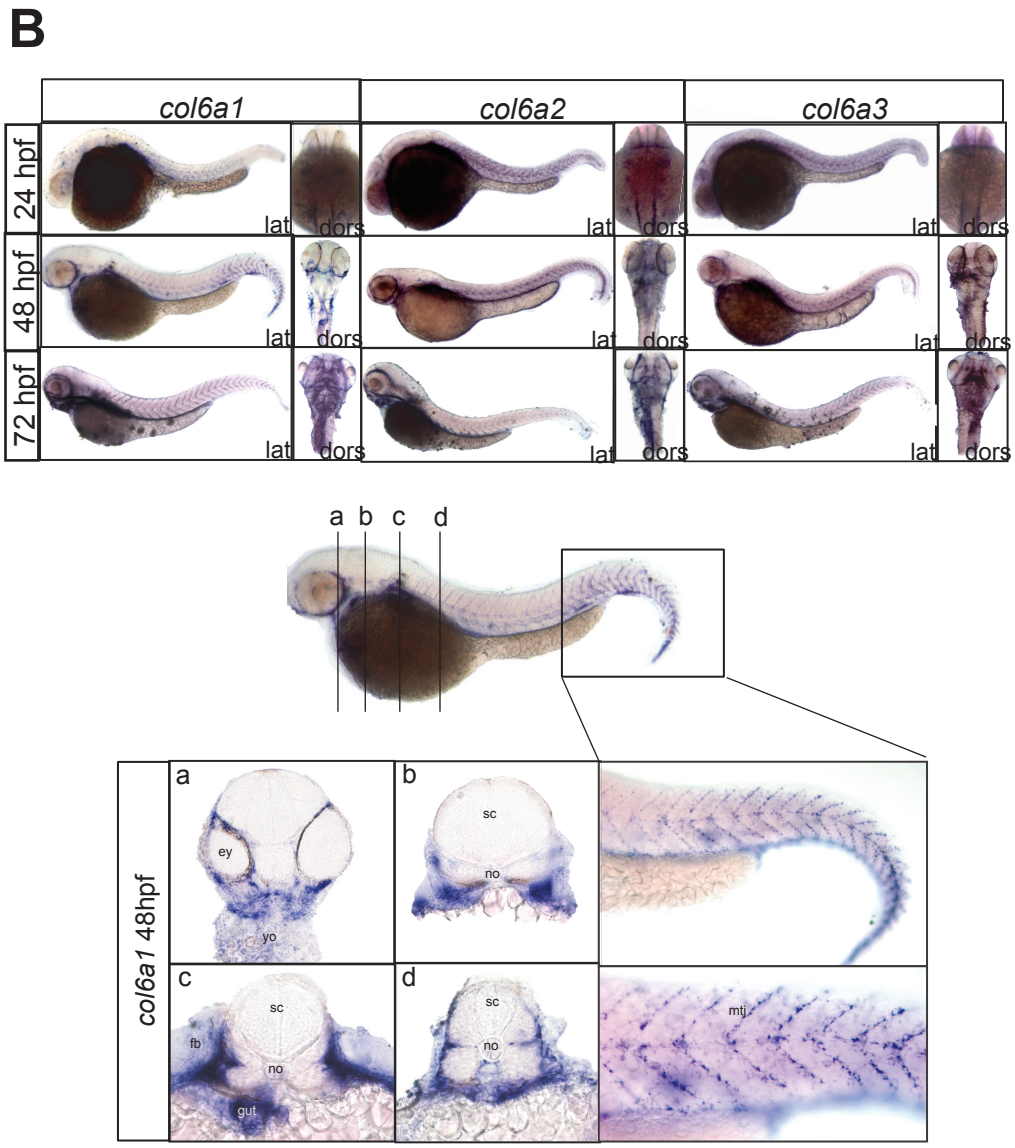
B
col6a1
col6a2
col6a3
24 hpf
48 hpf
72 hpf
lat
dors
a b c d
col6a1 48hpf
a
b
c
d
ey
yo
sc
no
fb
gut
mtj

Figure 4. Effectiveness of morpholinos-mediated knock-down of *col6a1* gene in zebrafish embryos. (A) We designed a morpholino antisense oligonucleotide that causes the retention of the third intron of *col6a1* transcript, leading to the insertion of multiple premature stop codons and transcript degradation, as confirmed by RT-PCR analysis. **(B)** In parallel, we used another morpholino, designed to skip exon 9 of *col6a1* (Telfer *et al.*, 2010). Injection of this morpholino leads to decreased levels of the normal *col6a1* transcript and the appearance of a truncated transcript (arrow) that should acts as a dominant negative, generating a Ullrich congenital muscular dystrophy (UCMD)-like phenotype. Ctrl MO, control morpholino; *col6a1*-MO, morpholino for *col6a1* 3rd intron retention; *col6a1* ex9-MO, morpholino for exon 9 skipping of *col6a1*.

Figure 4

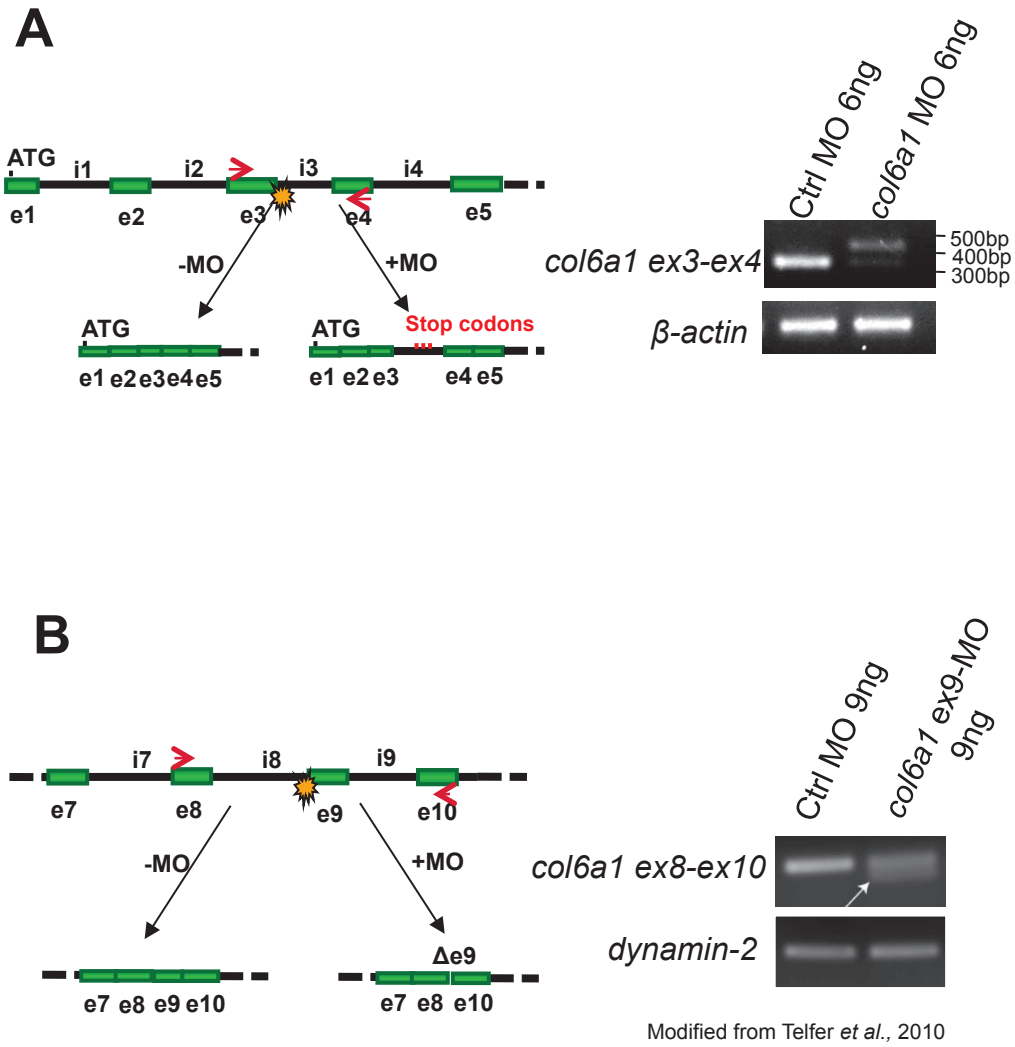

Modified from Telfer *et al.*, 2010

Figure 5. Macroscopic phenotypic alteration of *col6a1* morphants. 24 hpf **(A)** or 48 hpf **(B)** embryos injected with control (Ctrl-MO), collagen VI morpholinos (*col6a1*-MO and *col6a1* ex9-MO), or co-injected with *col6a1*-MO and full length zebrafish *col6a1* mRNA (*col6a1*-MO + zf*col6a1* mRNA) are classified according to a mild or severe phenotype, as seen in the trunk and tail, but also in eye and heart. **(C)** Graph of phenotypic repartition of Control-MO injected embryos (*n*=25), collagen VI morpholinos-injected embryos (*n*=37, 34 for *col6a1*-MO and *col6a1* ex9-MO, respectively) and *col6a1*-MO and full length zebrafish *col6a1* mRNA co-injected embryos (*n*=27) at 48 hpf. Blue: no phenotype; Green: severe phenotype; Red: mild phenotype.

Figure 5

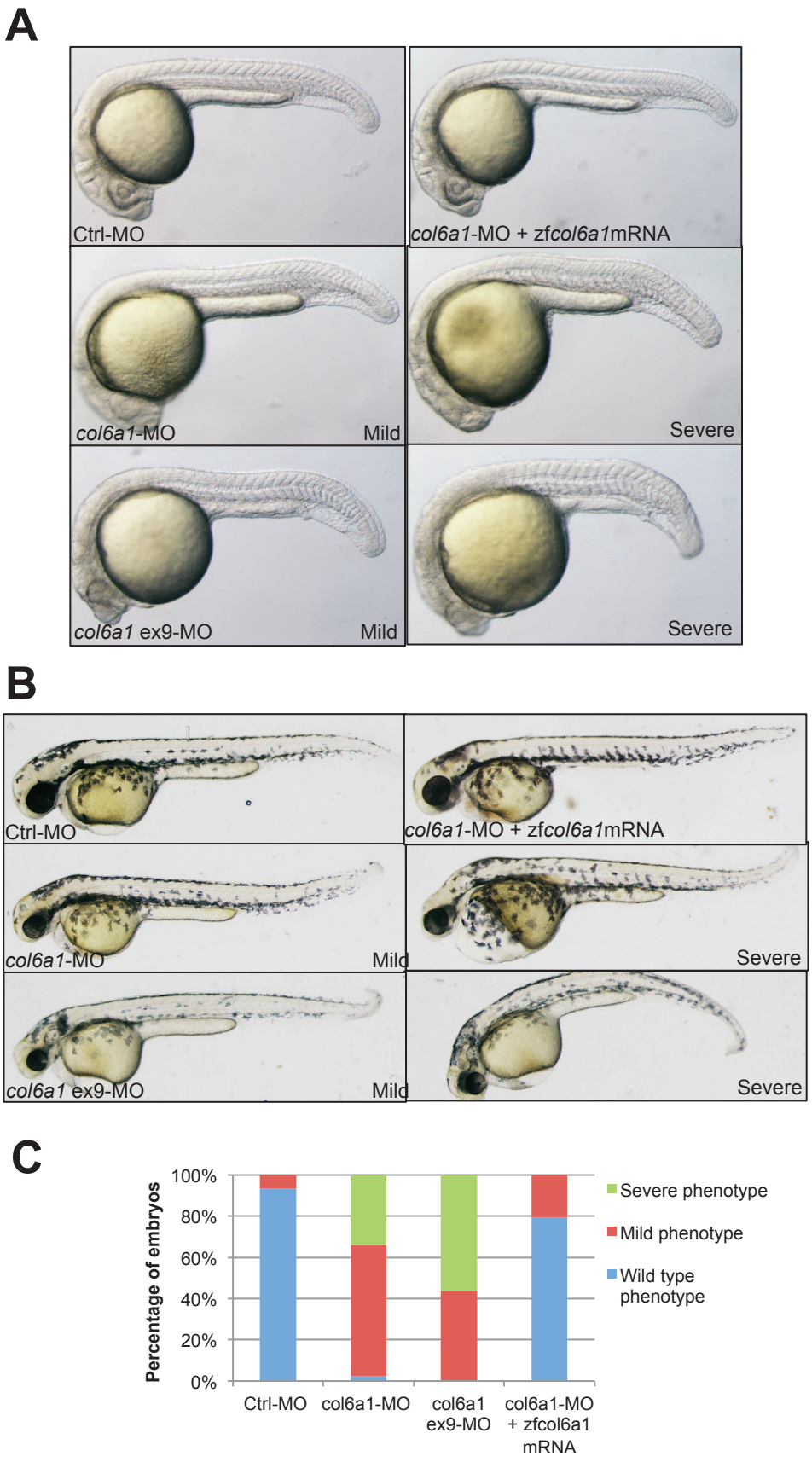
A
Ctrl-MO
col6a1-MO + zfcol6a1mRNA
col6a1-MO
Mild
Severe
col6a1 ex9-MO
Mild
Severe
B
Ctrl-MO
col6a1-MO + zfcol6a1mRNA
col6a1-MO
Mild
Severe
col6a1 ex9-MO
Mild
Severe
C
Percentage of embryos
100%
80%
60%
40%
20%
0%
Ctrl-MO
col6a1-MO
col6a1 ex9-MO
col6a1-MO + zfcol6a1 mRNA
Severe phenotype
Mild phenotype
Wild type phenotype

Figure 6. Muscle integrity of *col6a1* morphant embryos is affected at 48 hpf as seen by birefringence analysis. (A) Representative images under normal and polarized light of 48 hpf live embryos injected with the indicated morpholinos. The phenotypic defects of collagen VI morphants embryos, including birefringence, are rescued by co-injection with zebrafish *col6a1* mRNA. **(B)** Quantification of embryo trunk muscles birefringence shows a severe and statistically significant reduction in collagen VI morphants (*col6a1*-MO 55.7%±3.2% SEM and *col6a1*ex9-MO 23%±4.9% SEM, $p<0.0001$). Muscle birefringence resulted statistically increased when *col6a1* morpholino was co-injected with zebrafish *col6a1* mRNA. (Ctrl-MO $n=25$, for *col6a1*-MO $n=37$, *col6a1* ex9-MO $n=34$, *col6a1*-MO+zf*col6a1* mRNA $n=27$). **(C)** Comparison of WT and *tp53*^{zdf1} zebrafish embryos injected with indicated morpholinos. The presence of *p53* mutation background failed to eliminate the morphant phenotypes. Ctrl MO, control morpholino; *col6a1*-MO, morpholino for *col6a1* 3rd intron retention; *col6a1* ex9-MO, morpholino for exon 9 skipping of *col6a1*; zf*col6a1* mRNA, full length zebrafish *col6a1* mRNA.

Figure 6

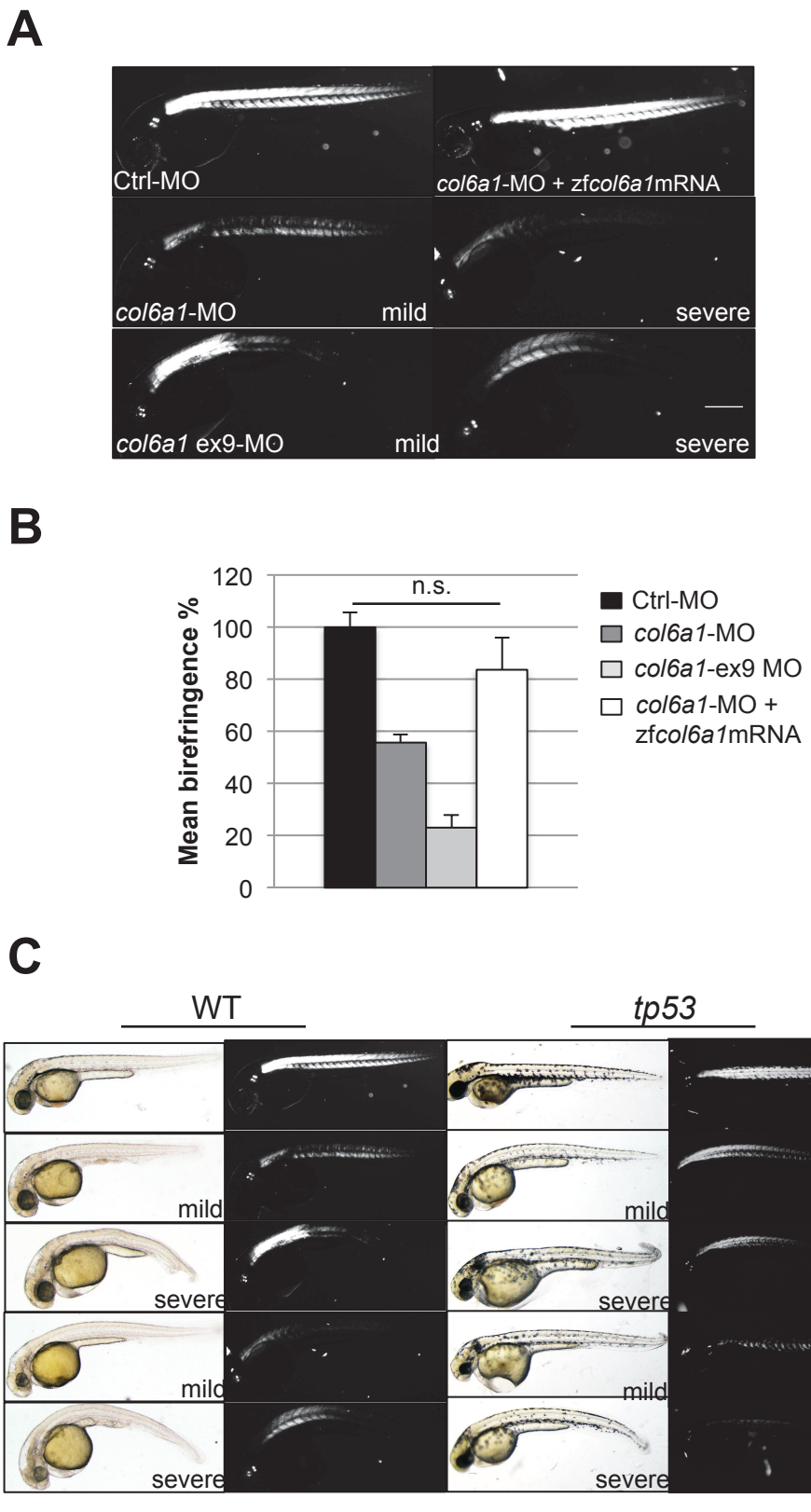
A
Ctrl-MO
col6a1-MO + zfcol6a1mRNA
col6a1-MO
mild
severe
col6a1 ex9-MO
mild
severe
B
Mean birefringence %
120
100
80
60
40
20
0
n.s.
Ctrl-MO
col6a1-MO
col6a1-ex9 MO
col6a1-MO + zfcol6a1mRNA
C
WT
tp53
Ctrl-MO
col6a1-MO
mild
severe
col6a1 ex9-MO
mild
severe
mild
severe

Figure 7. Myofibers are affected in collagen VI morphant embryos. (A) 24 and 48 hpf embryos injected with control morpholino (Ctrl-MO) and collagen VI morphants (*col6a1*-MO and *col6a1* ex9-MO) were stained with F59 antibody to detect slow muscle fibers and with F310 antibody to visualize fast muscle fibers. In collagen VI morphant embryos, myofibrils are not properly organized. Moreover, collagen VI morphants display gaps in myofiber arrangement, and myofibers have a wavy morphology. **(B)** 48 hpf embryos injected with control morpholino (Ctrl-MO) and collagen VI morpholino (*col6a1*-MO and *col6a1* ex9-MO) were stained with anti-laminin (red), F59 (green) antibodies and nuclei were counterstained with Hoescht solution (blue). The images indicate laminin epitope (red) retraction with detached muscle cells (green) in collagen VI morphants. **(C)** Evans blue dye-positive retracted fibers in 72hpf collagen VI morphants. Ctrl MO, control morpholino; *col6a1*-MO, morpholino for *col6a1* 3rd intron retention; *col6a1* ex9-MO, morpholino for exon 9 skipping of *col6a1*.

Figure 7

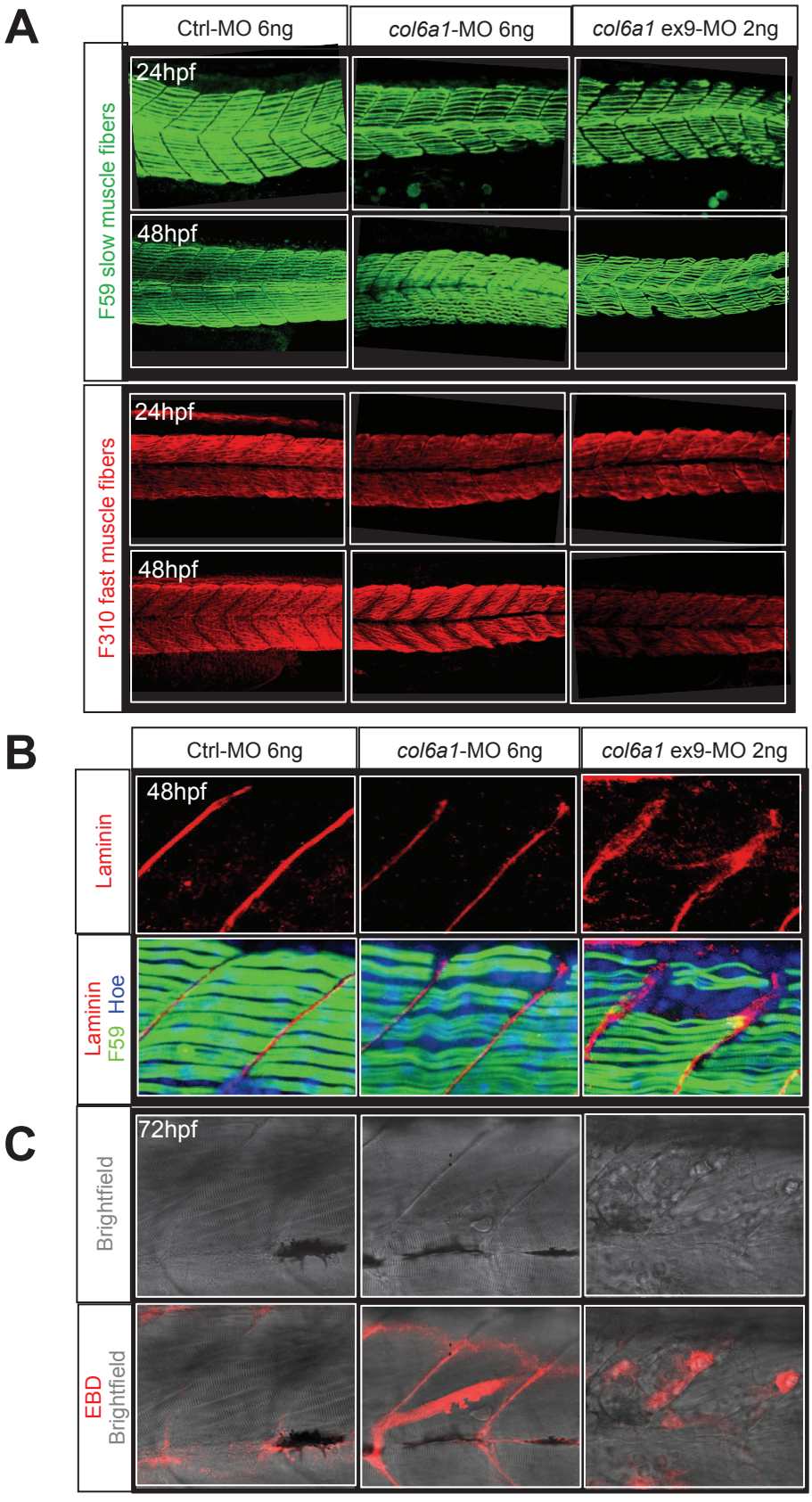
A
Ctrl-MO 6ng
col6a1-MO 6ng
col6a1 ex9-MO 2ng
24hpf
48hpf
F59 slow muscle fibers
F310 fast muscle fibers
B
Laminin
Laminin F59 Hoe
C
72hpf
Brightfield
EBD Brightfield

Figure 8. Neuromuscular development is affected in collagen VI morphant embryos. (A) *col6a1* morpholinos were injected in *Tg(mnx1:GFP)* transgenic line in which motor neuron are labelled in green. While in control embryos the motor neurons have completed their migration toward the myotome, motor neuron pathfinding, branching, and extension errors were observed in *col6a1*-MO and *col6a1* ex9-MO injected embryos at 30, 48 and 72 hpf. **(B)** Representative lateral views of 48 hpf zebrafish embryos, injected with indicated morpholinos, stained with acetylated tubulin antibody (AcTub, in green) and rhodamine coniugated alpha-bungarotoxin (α-Btx, in red). In correspondence of the motorneuron outgrowth defects, AchRs clusters appear affected in collagen VI morphant embryos. **(C)** Graph of phenotypic repartition of motor axons defects considering both to the extent of growth and to the degree of branching. Overall, up to 48% of *col6a1* deficient embryos displayed no motor axons growth (classified as hemisegments motor axon score 0, in red) or growth arrest before the horizontal myoseptum (classified as score 1, in orange). Moreover, between 37% (*col6a1*-MO, *n*=31) and 48% (*col6a1* ex9-MO, *n*=31) of col6a1 morphants presented motor axons that were abnormally branched (score 2, in yellow). Interestingly, these phenotype were rescued co-injecting the *col6a1*-MO together with zf*col6a1* mRNA (81% of motoraxon were classified as normal *n*=6). **(D)** Graphical representation of mean hemisegments motor axon score. While in control embryo the mean hemisegment motor axon score was near to 3 (2.94±0.03 SEM, *n*=21) in collagen VI morphants the score is significantly reduce to half (*col6a1*-MO score 1.61±0.09 SEM *n*=31; *col6a1* ex9-MO score 1.38±0.05 SEM *n*=31; $p<0.0001$), and interestingly the co-injection of zf*col6a1* mRNA partially rescued the morphants phenotype (score recovered to 2.62±0.12, *n*=6). Ctrl MO, control morpholino; *col6a1*-MO, morpholino for *col6a1* 3rd intron retention; *col6a1* ex9-MO, morpholino for exon 9 skipping of *col6a1*; zf*col6a1* mRNA, full length zebrafish *col6a1* mRNA.

Figure 8

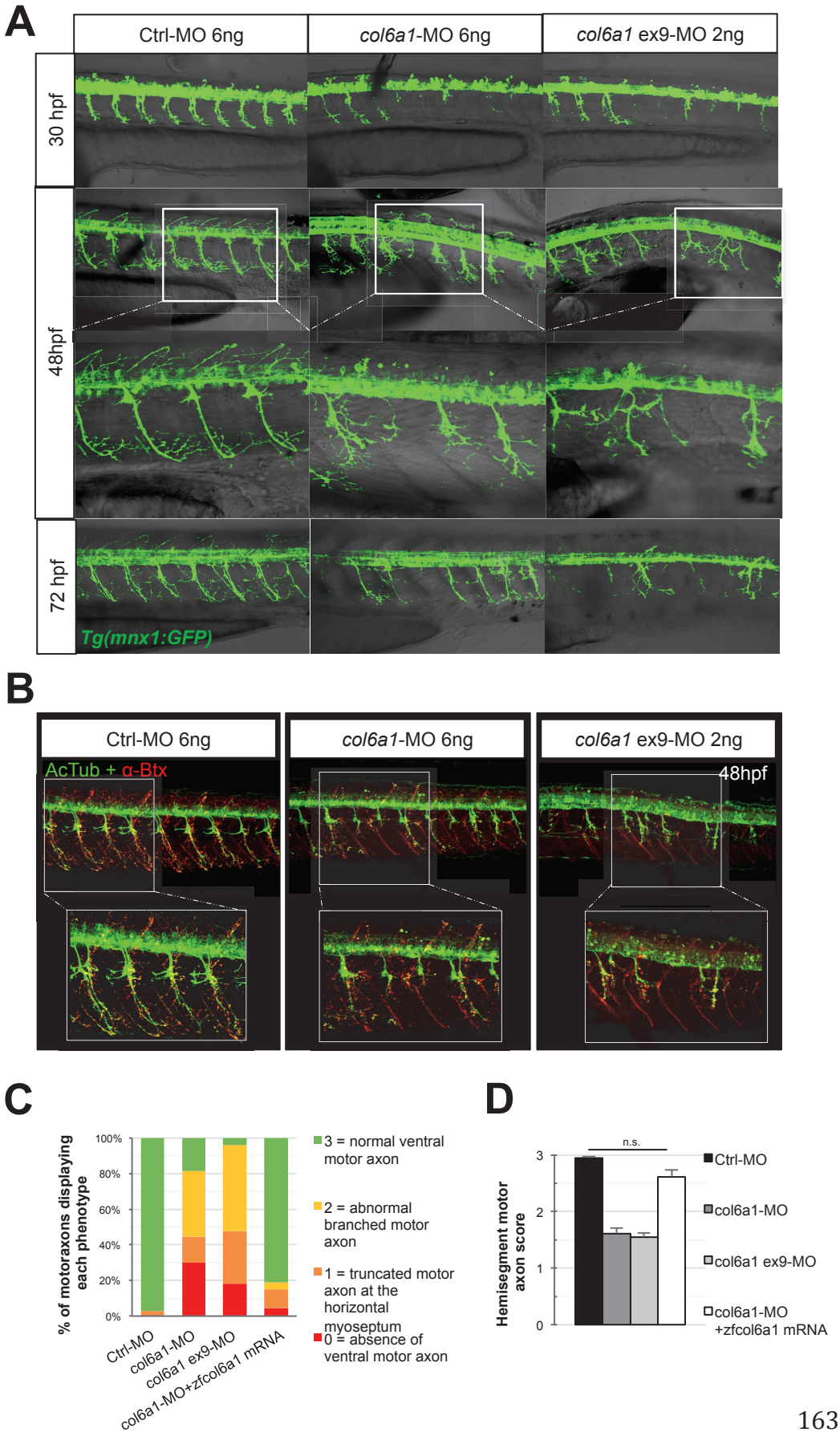
A
Ctrl-MO 6ng
col6a1-MO 6ng
col6a1 ex9-MO 2ng
30 hpf
48hpf
72 hpf
Tg(mnx1:GFP)
B
Ctrl-MO 6ng
col6a1-MO 6ng
col6a1 ex9-MO 2ng
AcTub + α-Btx
48hpf
C
% of motoraxons displaying each phenotype
100%
80%
60%
40%
20%
0%
Ctrl-MO
col6a1-MO
col6a1 ex9-MO
col6a1-MO+zfcol6a1 mRNA
3 = normal ventral motor axon
2 = abnormal branched motor axon
1 = truncated motor axon at the horizontal myoseptum
0 = absence of ventral motor axon
D
Hemisegment motor axon score
n.s.
3
2
1
0
Ctrl-MO
col6a1-MO
col6a1 ex9-MO
col6a1-MO +zfcol6a1 mRNA

Figure 9. Collagen VI knockdown results in alteration of signaling pathways. **(A-B) Wnt signaling is upregulated in collagen VI morphant embryos**. **(A)** *Tg(7xtcf-Xla.siam:nlsmcherry)ia4* embryos were injected with the indicated morpholinos and probed at 24 hpf and 48 hpf by *in situ* hybridization for *mCherry* reporter gene. **(B)** qRT-PCR for *col6a1* and *mCherry* transcripts in collagen VI morphant and control embryos ($p<0.05$). **(C-D) BMP signaling is downregulated in collagen VI morphant embryos**. **(C)** *Tg(2xID1BRE:nlsmcherry)ia17* embryos were injected with the indicated morpholinos and probed at 24 hpf and 48hpf by *in situ* hybridization for *mCherry*. **(D)** qRT-PCR for *col6a1* and *mCherry* transcripts in collagen VI morphant and control embryos ($p<0.05$). Western blot for the BMP signaling downstream effector pSmad1/5/8. Ctrl MO, control morpholino; *col6a1*-MO, morpholino for *col6a1* 3rd intron retention; *col6a1* ex9-MO, morpholino for exon 9 skipping of *col6a1*.

Figure 9

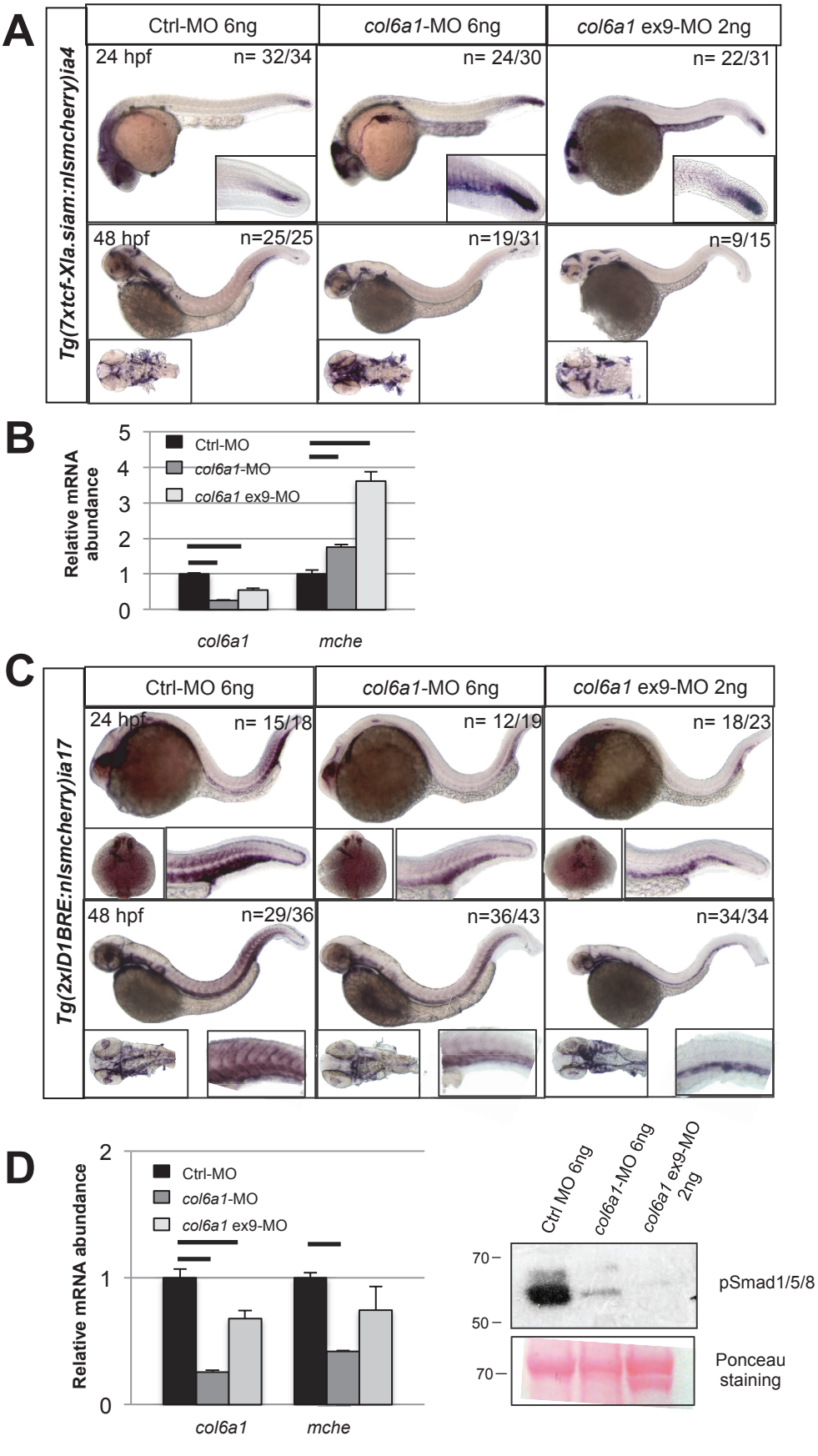
A
Tg(7xtcf-Xla.siam:nlsmcherry)ia4
Ctrl-MO 6ng
col6a1-MO 6ng
col6a1 ex9-MO 2ng
24 hpf
n= 32/34
n= 24/30
n= 22/31
48 hpf
n=25/25
n=19/31
n=9/15
B
Relative mRNA abundance
Ctrl-MO
col6a1-MO
col6a1 ex9-MO
col6a1
mche
C
Tg(2xID1BRE:nlsmcherry)ia17
Ctrl-MO 6ng
col6a1-MO 6ng
col6a1 ex9-MO 2ng
24 hpf
n= 15/18
n= 12/19
n= 18/23
48 hpf
n=29/36
n=36/43
n=34/34
D
Relative mRNA abundance
Ctrl-MO
col6a1-MO
col6a1 ex9-MO
col6a1
mche
Ctrl MO 6ng
col6a1-MO 6ng
col6a1 ex9-MO 2ng
70
50
70
pSmad1/5/8
Ponceau staining

Figure 10. Design and introduction of loss-of-function frameshift mutations in zebrafish *col6a1* gene using CRISPR/Cas9 technology. **(A)** Target sequence selection through CHOPCHOP on line tool. The target sequence selected is located in the exon 5 of *col6a1* gene. Additionally it presents, just upstream the PAM, a sequence that is recognized and cut by the restriction enzyme PstI. **(B)** Schematic representation of the target specific sgRNAs and Cas9 mRNA microinjected in 1-2 cells embryos to generate founder fish that harbour several different mutations (indicated by coloured circles; Hruscha *et al.*, 2014). **(C)** PstI digestion of amplicon from injected and uninjected embryos. While the wild type amplicon was digested by PstI in to two lower bands, some amplicons from the PCR on tails of injected fish could not be cut efficiently by the restriction enzyme, suggesting that a mutations occur in that region. **(D)** Sequence analyses were used to confirm that the loss of the respective restriction site is due to mutations at the target sites in the gRNA/Cas9-injected embryos: downstream the target sequence appear double peaks, indicating an alteration in that region.

Figure 10

A

Ranking	Target sequence	Genomic location	Strand	GC content (%)	Off-targets		
					0	1	2
6	GGAGCGGGAGTTGTCTGCAGCGG	chr11:34895970	+	70	0	0	0

PstI site

No.	Exon / Intron	Start	End	Start Phase	End Phase	Length	Sequence
5	ENSDARE00000815171	33,796,981	33,796,868	0	0	114	GACACCAGACTGTCTGTCATTGCCACAGATATAAACTACAGACAGAACTTCACGGCTGCA GACAACTCCCGCTCCACACAAATGAGCACTATACGCTCCATCATCCACATGATT

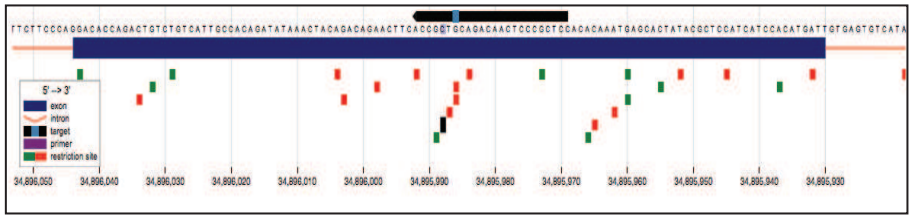

B

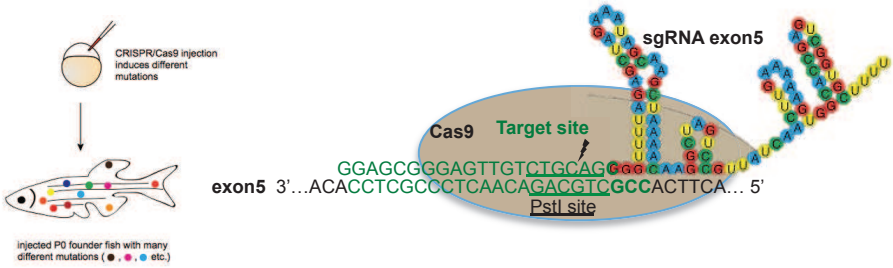

Hruscha *et al.*, 2014

modified from Auer *et al.*, 2014

C

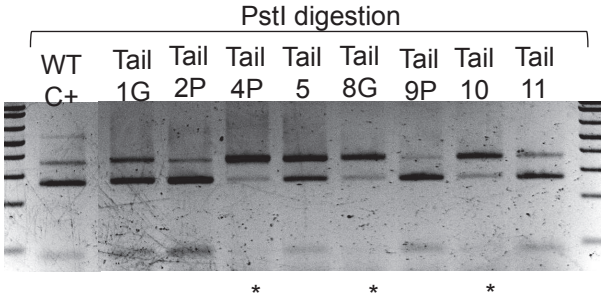

D

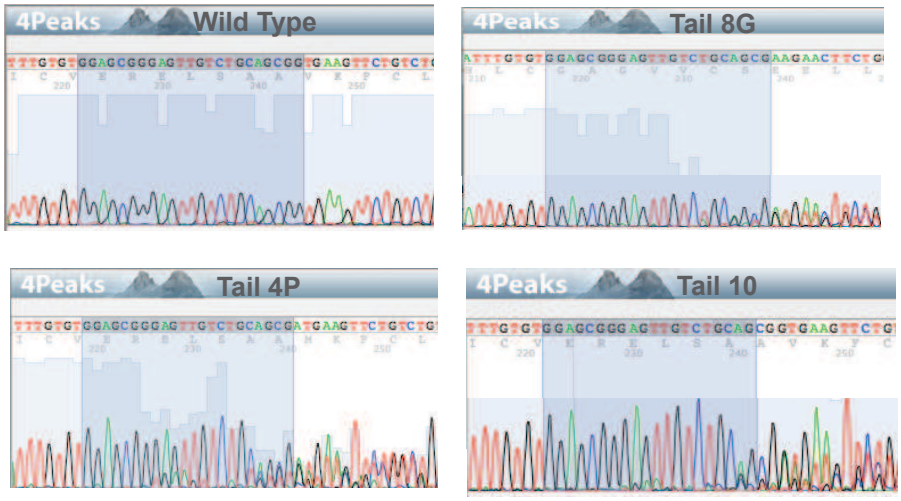

Figure 11. Identification of Cas9–sgRNA-induced Indels (A) Schematic representation of germline transmission of mutations from a mosaic founder fish. Mutations in the germline will be propagated to the F1 offspring. The F1 embryos will be heterozygous for the respective mutation(s) (as indicated by the colors; Hruscha *et al.*, 2014) **(B)** Targeted indel mutations induced by engineered sgRNA:Cas9 at the exon5 of *col6a1* gene. The wild-type sequence is shown at the top with the target site written in orange and the PAM sequence in light blue. Deletions are shown as violet dashes and insertions are written in violet. The net change in length caused by each indel mutation is to the right of each sequence (+, insertion; −, deletion). The frequency by which each mutant allele was isolated is shown in brackets. **(C)** HRM analysis of F1 offspring. This analysis confirmed that F1 animals considered were heterozygous. PCR samples were heated to 95 ℃ and then rapidly cooled, in that way heteroduplex products could be generated in heterozygous sample . These heteroduplex, due to decreased complementarity, have a much lower Tm and appear as the curve profile represented to the left of the homoduplex. HRM curves of wild-type (yellow and red curves), heterozygous insertion of 7bp in genomic DNA samples (pink and blue curves) and heterozygous deletion of 7bp in genomic DNA samples (green curve) generated PCR amplicons that surround the mutation.

Figure 11

A

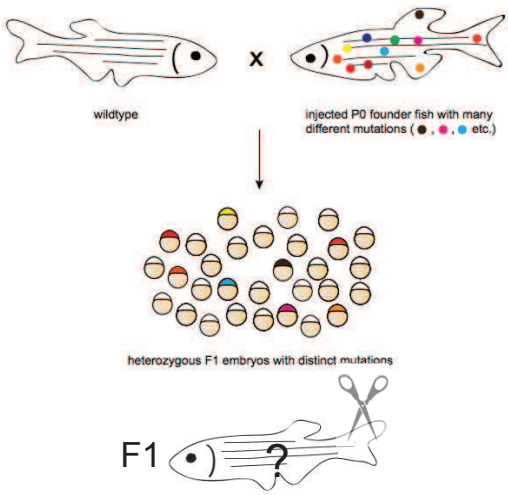

modified from Hruscha *et al.*, 2014

B

WT	ACTTCACCGCTGCAGACAACTCCCGCTCCACACAAATGAGCACTA
F1 Founder #3	ACTTCACCGCT---GACAACTCCCGCTCCACACAAATGAGCACTA -3 (x5)
F1 Founder #2	ACTTCACCGCTGCCAGACCGCGGCCAGACAACTCCCGCTCCACAC +12 (x1)
	ACTTCACCGCTGTGAACTACAGACAACTCCCGCTCCACACAAATG +7 (X4)
	ACTTCACCG--------CAACTCCCGCTCCACACAAATGAGCACTA -7 (X12)
	ACTTCA-------AGACAACTCCCGCTCCACACAAATGAGCACTA -7 (x1)

C

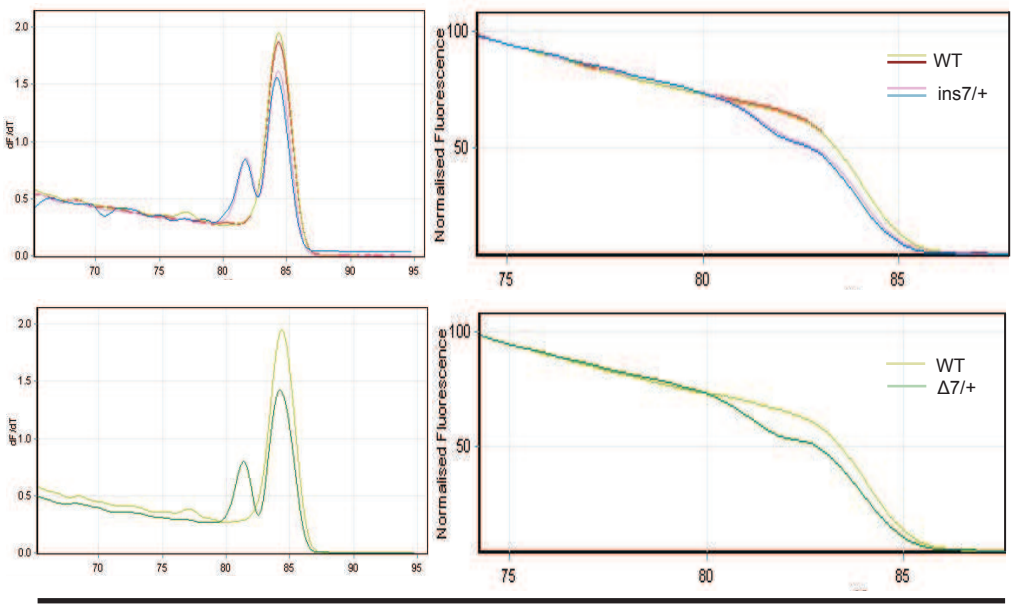

Figure 12. Depletion of collagen VI lead to a substantial reduction of BMP signaling. Like in *col6a1* morphant embryos **(A)**, reduced BMP signaling was observed in the majority of larvae **(C)** derived from ins7/+ heterozygous fish in BMP reporter background crossed with another ins7/+ heterozygous fish **(B)**.

Figure 12

A

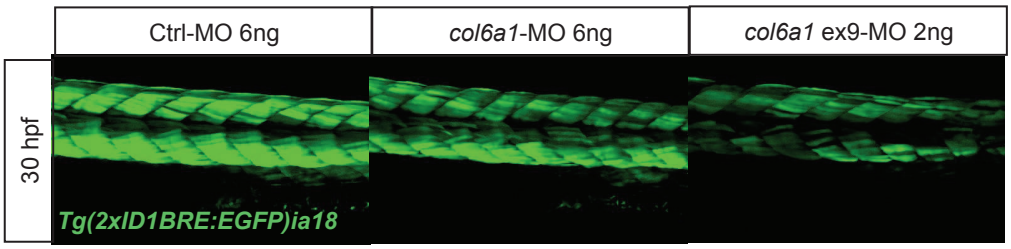

B

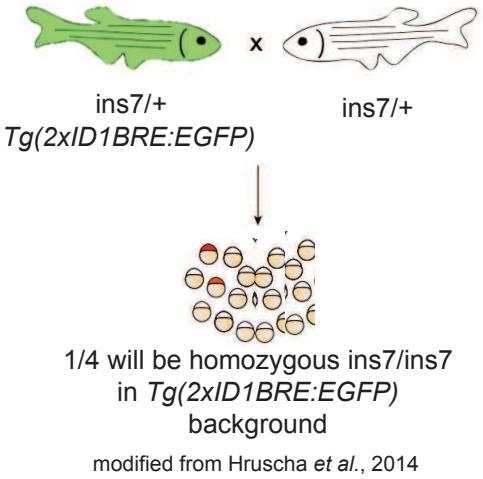

C

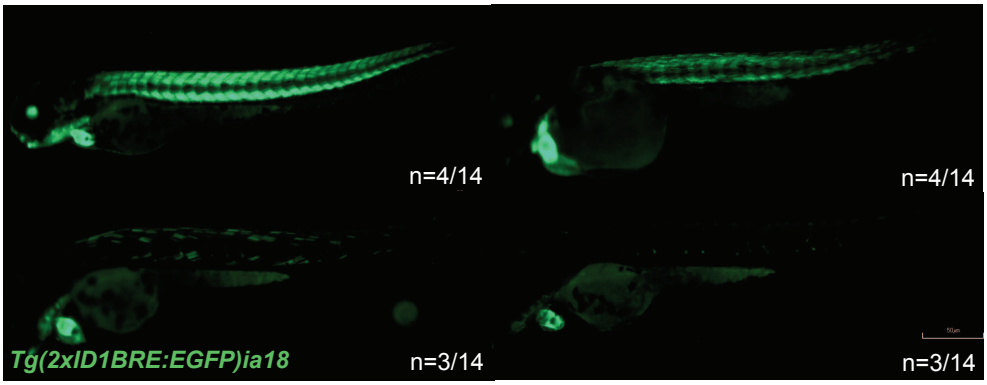

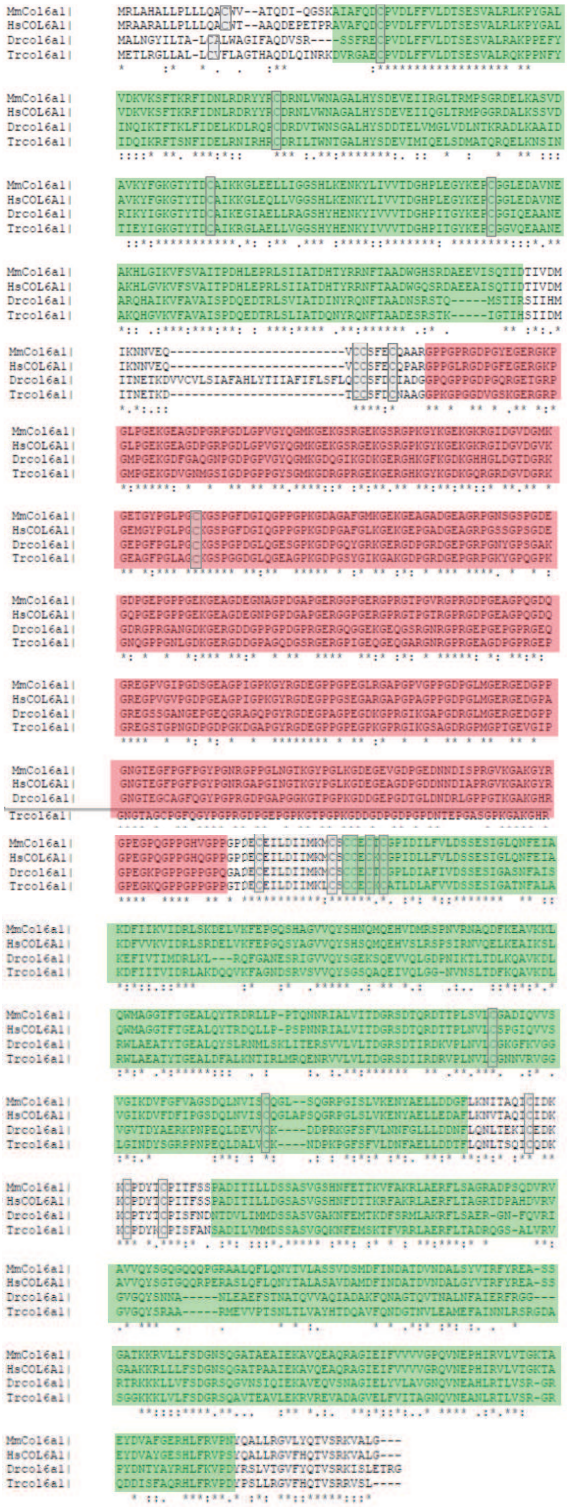

Multiple sequence alignment of human (HS, *Homo sapiens*), mouse (Mm, *Mus musculus*), fugu (Tr, *Takifugu rubripes*) and zebrafish (Dr, *Danio rerio*) collagen VI alpha 1 chain was originated with ClustalW program, using the default parameters. In the alignment, identical residues in all sequences are indicated by '*', while conservative and semi-conservative substitutions are indicated by ':' and '.', respectively. The vWF-A domains are highlighted in green, while the Collagen triple helix is shown in red. The signal peptide cleavage site indicated by the arrow was predicted by SignalP 4.1.

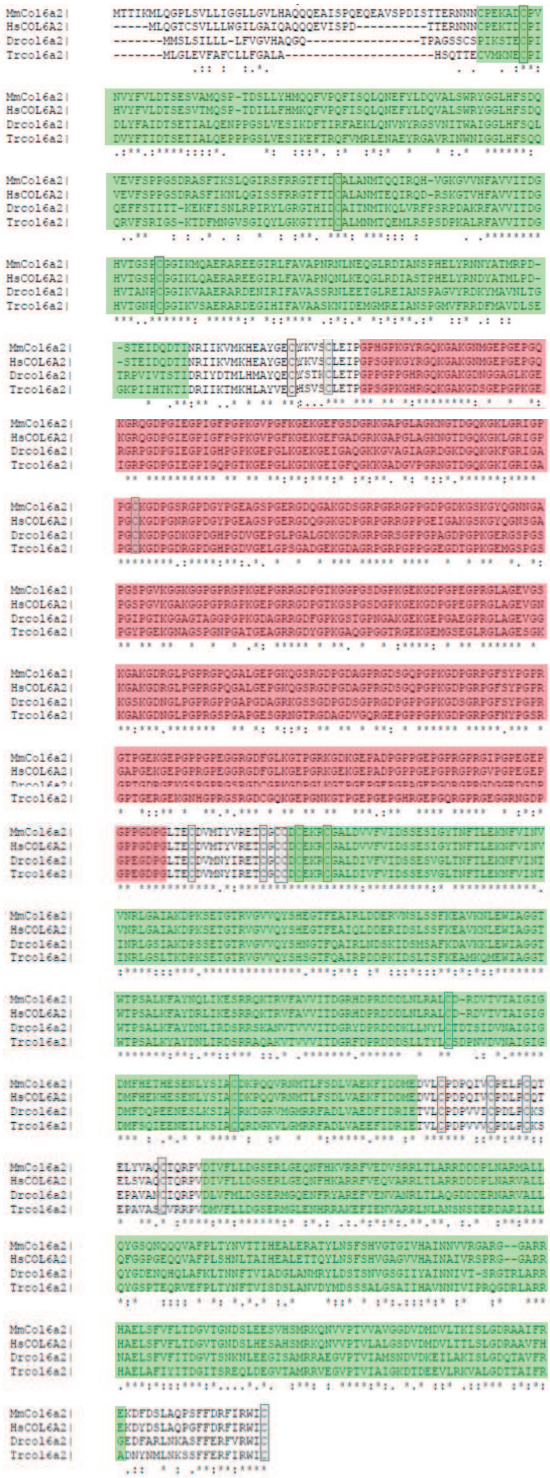

Multiple sequence alignment of human (HS, *Homo sapiens*), mouse (Mm, *Mus musculus*), fugu (Tr, *Takifugu rubripes*) and zebrafish (Dr, *Danio rerio*) collagen VI alpha 2 chain was originated with ClustalW program, using the default parameters. In the alignment, identical residues in all sequences are indicated by '*', while conservative and semi-conservative substitutions are indicated by ':' and '.', respectively. The vWF-A domains are highlighted in green, while the Collagen triple helix is shown in red. The signal peptide cleavage site indicated by the arrow was predicted by SignalP 4.1.

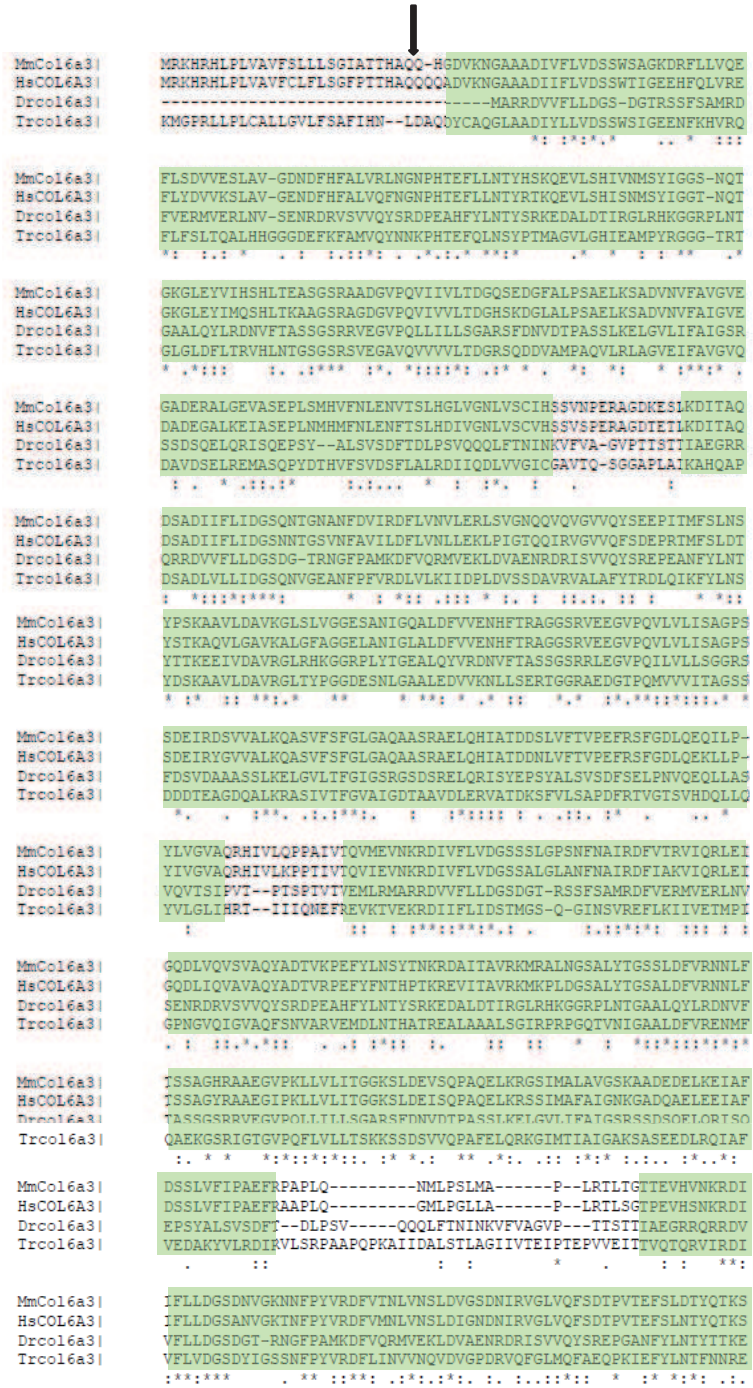
MmCol6a3|
HsCOL6A3|
Drcol6a3|
Trcol6a3|

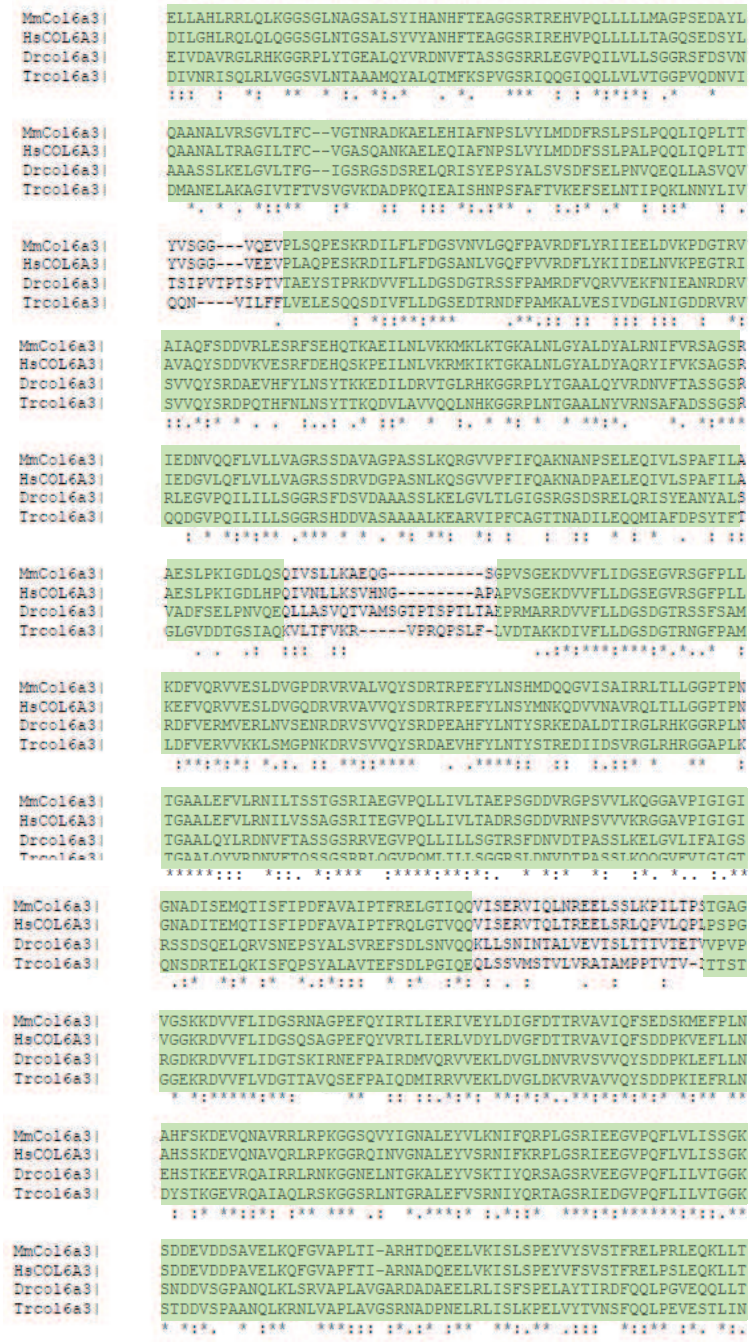
MmCol6a3|
HsCOL6A3|
Drcol6a3|
Trcol6a3|

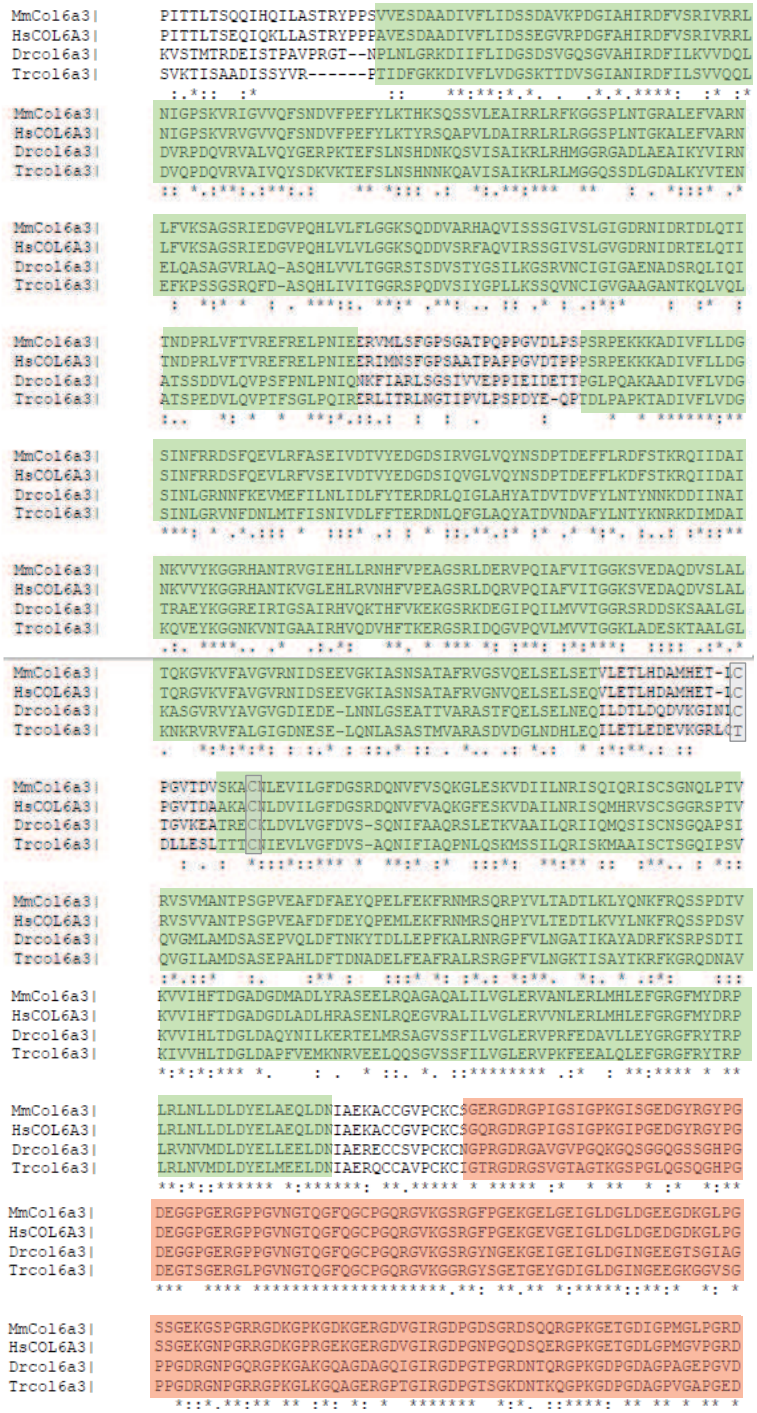
MmCol6a3|
HsCOL6A3|
Drcol6a3|
Trcol6a3|

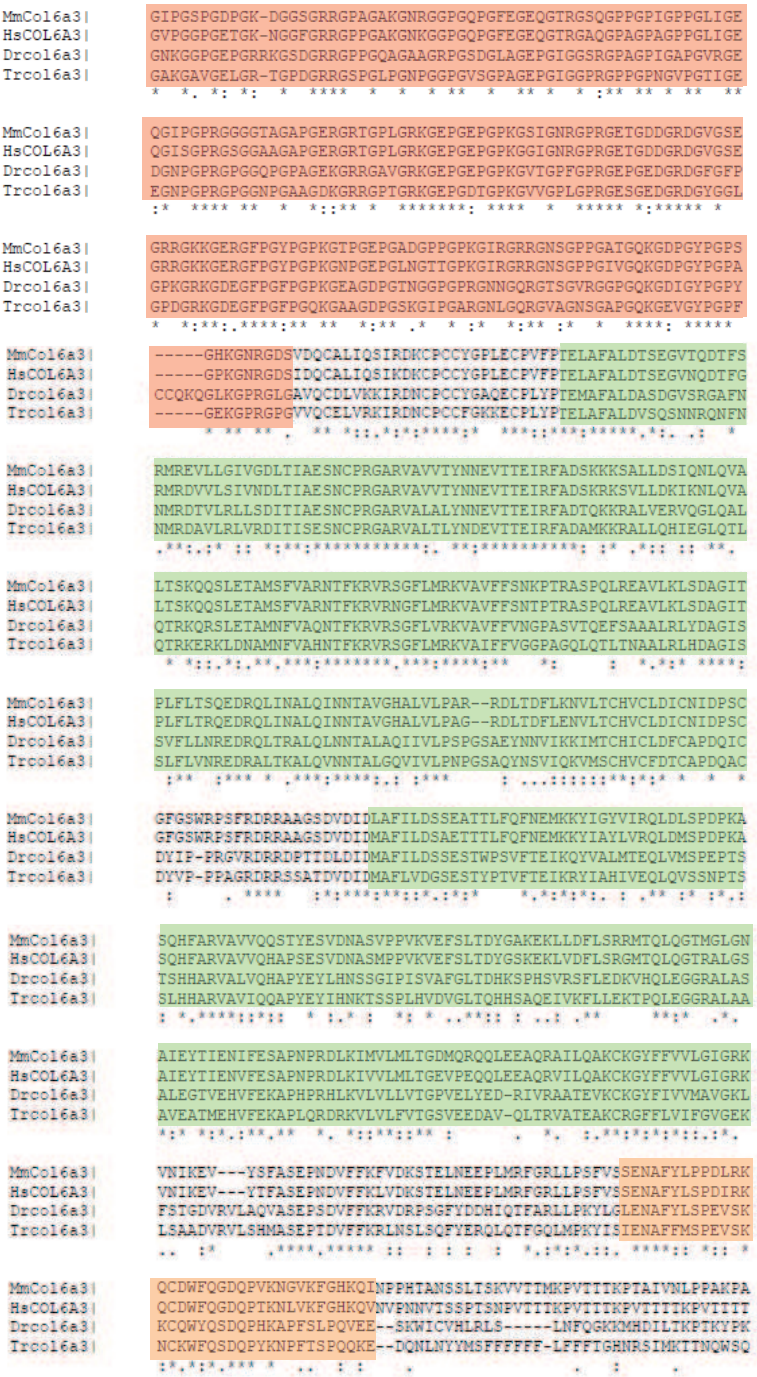
MmCol6a3|
HsCOL6A3|
Drcol6a3|
Trcol6a3|

Multiple sequence alignment of human (HS, *Homo sapiens*), mouse (Mm, *Mus musculus*), fugu (Tr, *Takifugu rubripes*) and zebrafish (Dr, *Danio rerio*) collagen VI alpha 3 chain was originated with ClustalW program, using the default parameters. In the alignment, identical residues in all sequences are indicated by '*', while conservative and semi-conservative substitutions are indicated by ':' and '.', respectively. The N10 domains are highlighted in green, the Collagen triple helix is shown in red and unique domain in orange while the fibronectin type III domain is in violet and Kunitz domain in blu. The signal peptide cleavage site indicated by the arrow was predicted by SignalP 4.1.

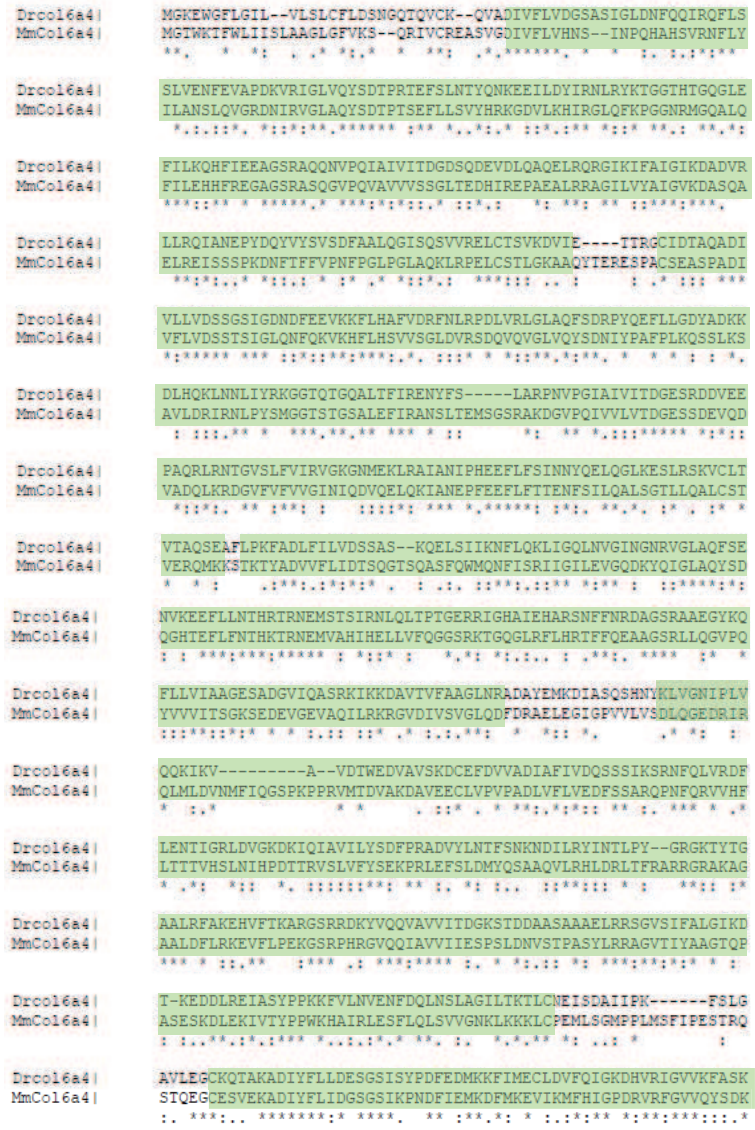
Drcol6a4|
MmCol6a4|

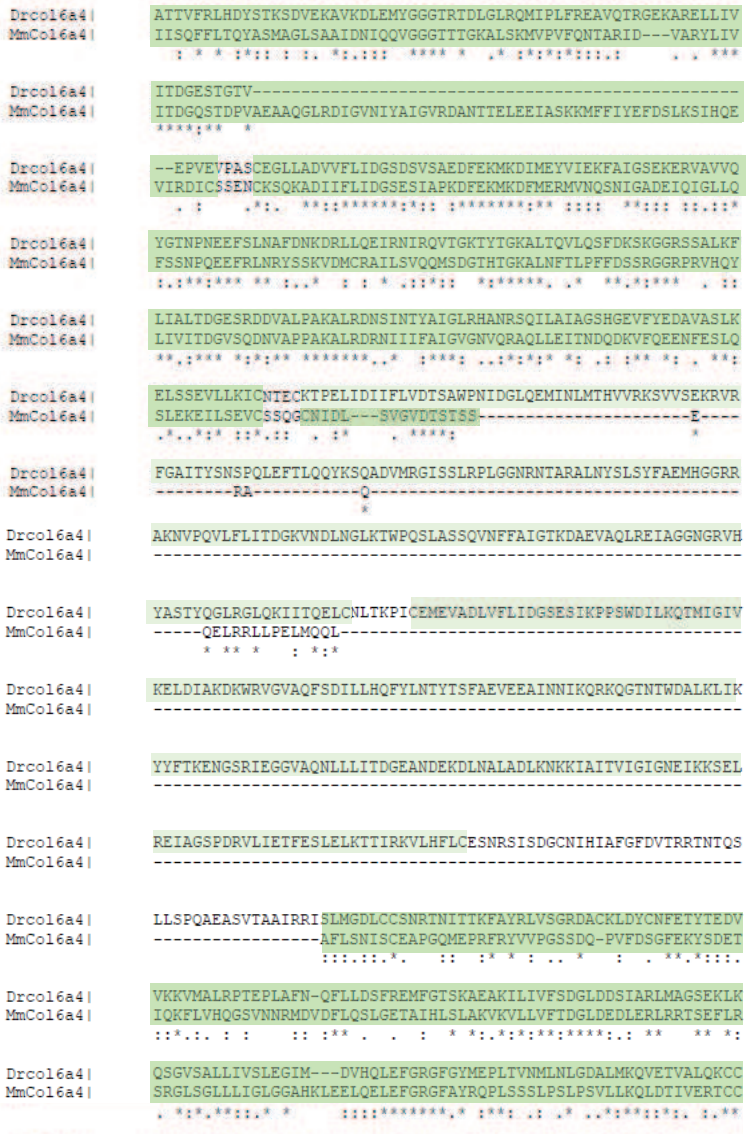
Drcol6a4|
MmCol6a4|

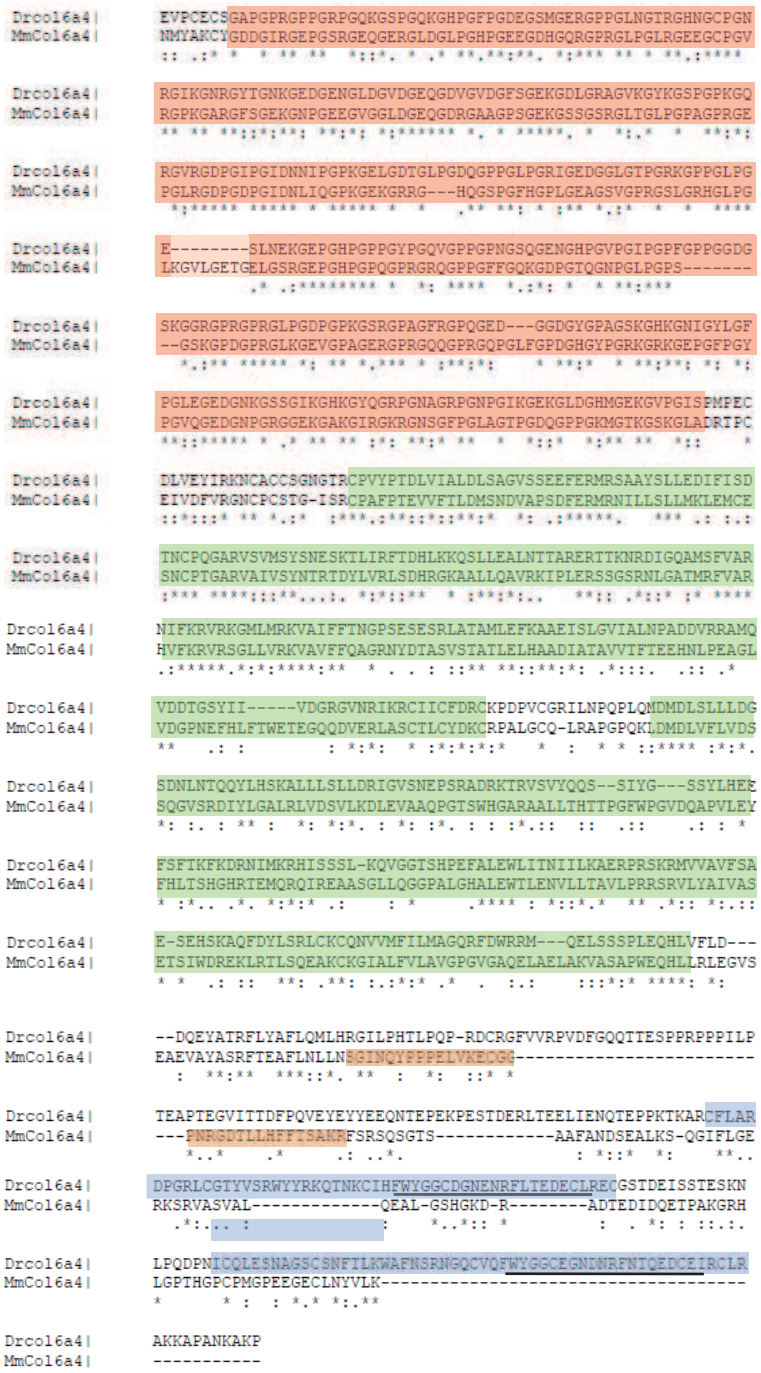

Multiple sequence alignment of human (HS, *Homo sapiens*), mouse (Mm, *Mus musculus*), fugu (Tr*, Takifugu rubripes*) and zebrafish (Dr, *Danio rerio*) collagen VI alpha 4 chain was originated with ClustalW program, using the default parameters. In the alignment, identical residues in all sequences are indicated by '*', while conservative and semi-conservative substitutions are indicated by ':' and '.', respectively. The vWF-A domains are highlighted in green, the Collagen triple helix is shown in red while unique domain is in orange and the Kunitz domains are in blu. The signal peptide cleavage site indicated by the arrow was predicted by SignalP 4.1.

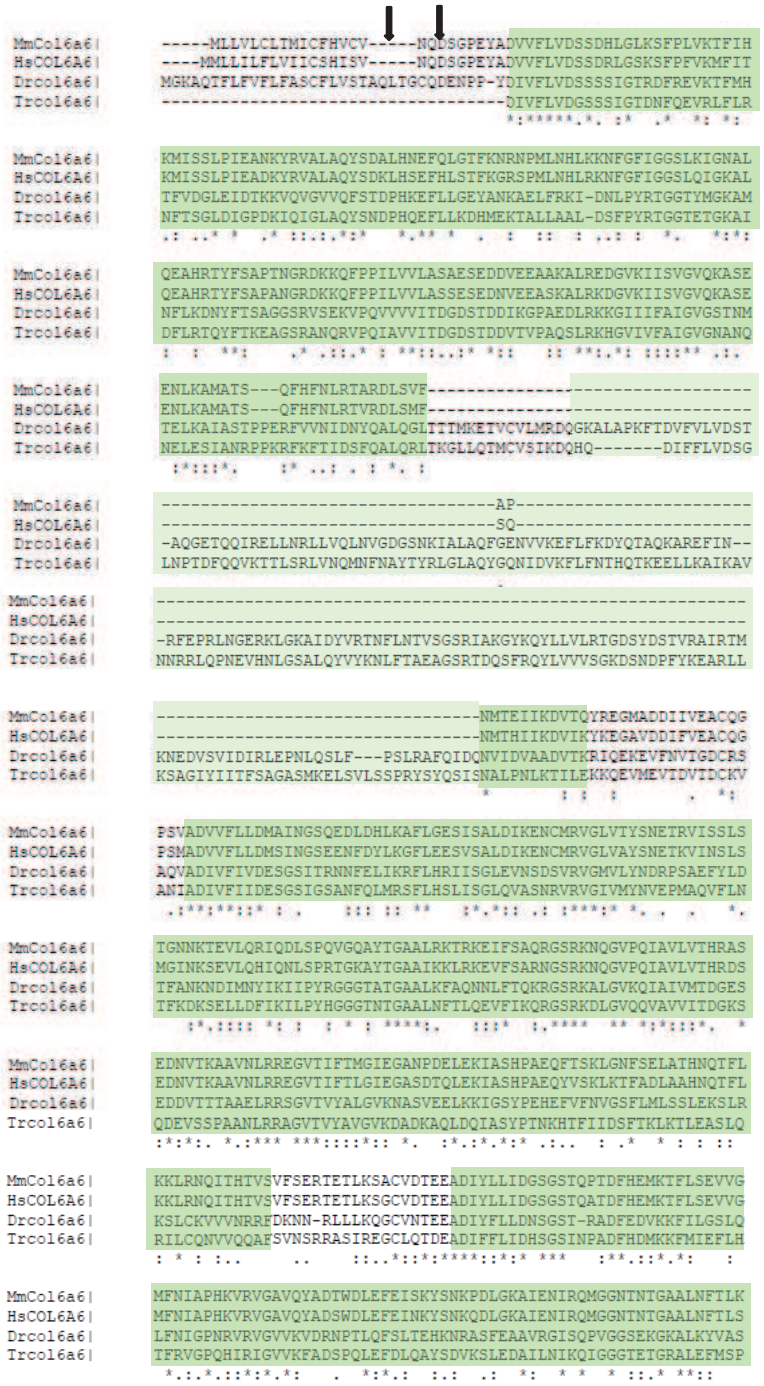
MmCol6a6|
HsCOL6A6|
Drcol6a6|
Trcol6a6|

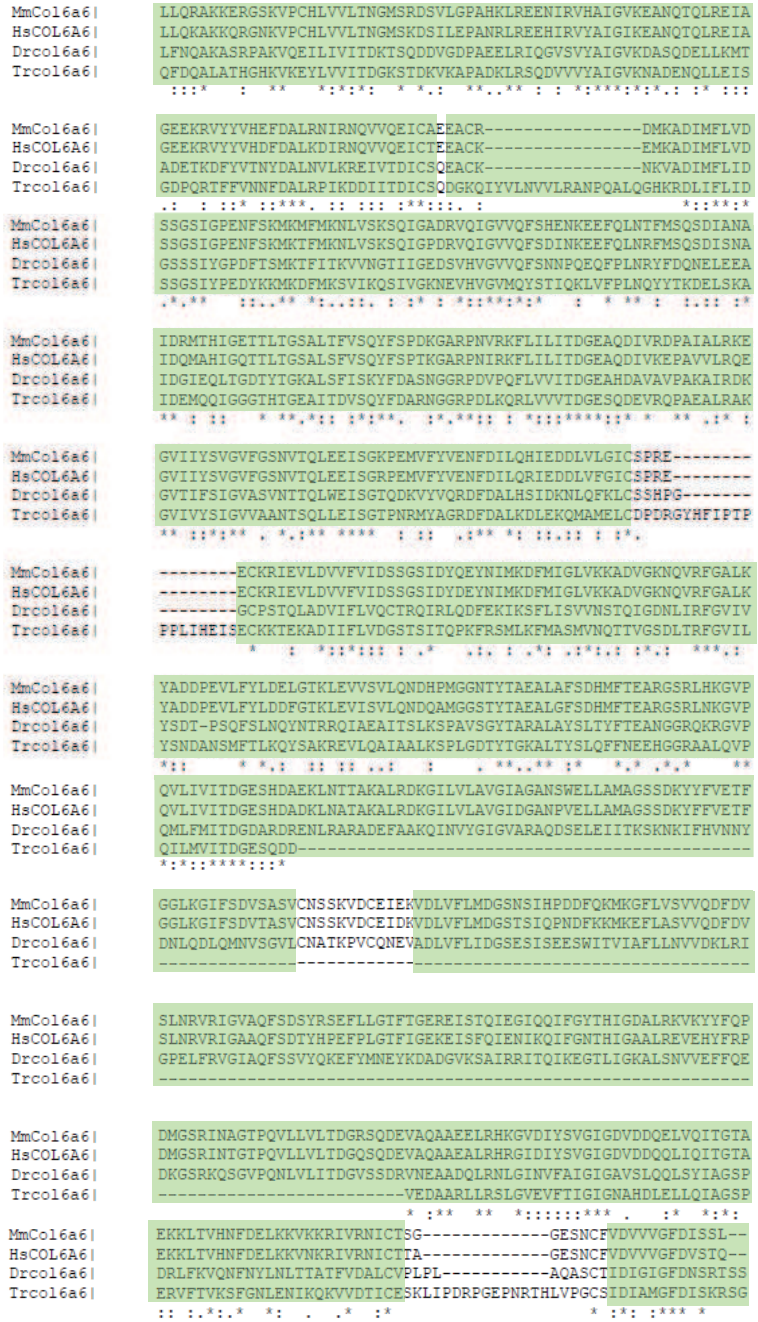
MmCol6a6|
HsCOL6A6|
Drcol6a6|
Trcol6a6|

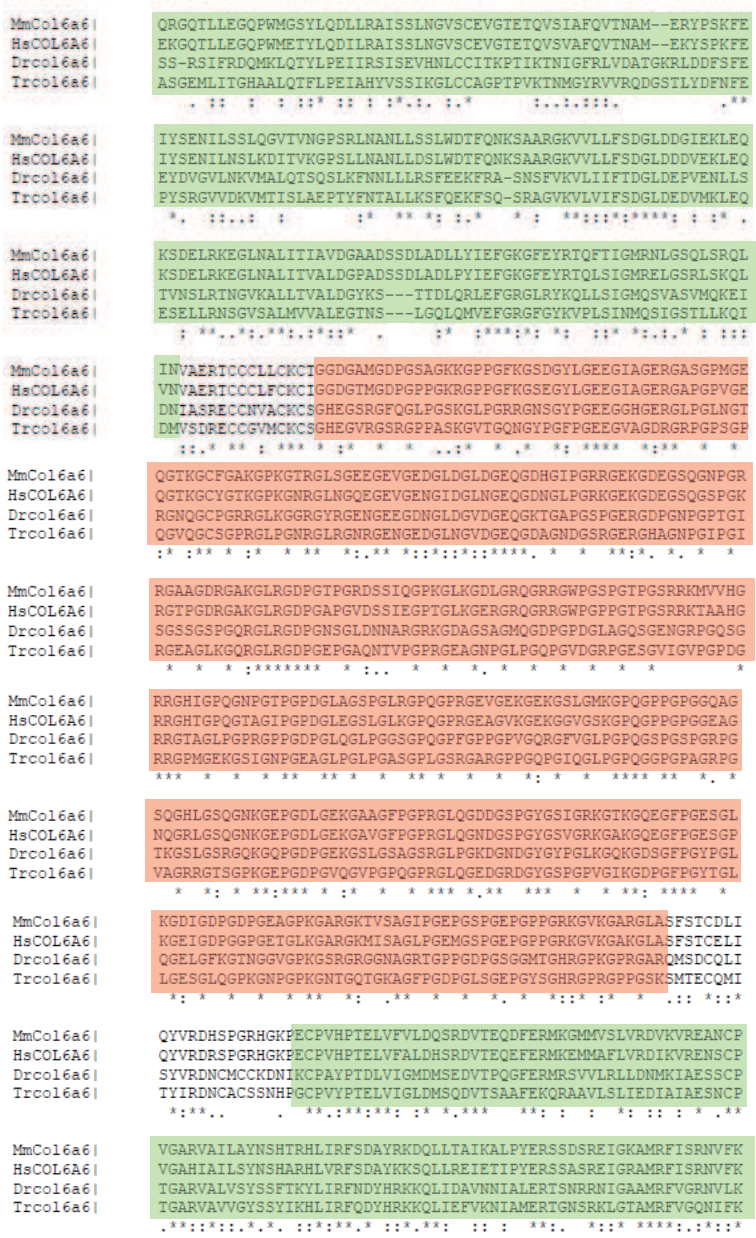
MmCol6a6|
HsCOL6A6|
Drcol6a6|
Trcol6a6|

Multiple sequence alignment of human (HS, *Homo sapiens*), mouse (Mm, *Mus musculus*), fugu (Tr*, Takifugu rubripes*) and zebrafish (Dr, *Danio rerio*) collagen VI alpha 6 chain was originated with ClustalW program, using the default parameters. In the alignment, identical residues in all sequences are indicated by '*', while conservative and semi-conservative substitutions are indicated by ':' and '.', respectively. The vWF-A domains are highlighted in green, the Collagen triple helix is shown in red while unique domain is in orange and the Kunitz domains are in blu. The signal peptide cleavage site indicated by the arrow was predicted by SignalP 4.1.

References

Aigner, T., Hambach, L., Söder, S., Schlötzer-Schrehardt, U. and Pöschl, E. (2002). The C5 domain of *Col6A3* is cleaved off from the Col6 fibrils immediately after secretion. *Biochem. Biophys. Res. Commun.* **290**, 743-748.

Ain, Q. U., Chung, J. Y. and Kim, Y. H. (2015). Current and future delivery systems for engineered nucleases: ZFN, TALEN and RGEN. *J. Control Release* **205**, 120-127.

Angelin, A., Tiepolo, T., Sabatelli, P., Grumati, P., Bergamin, N., Golfieri, C., Mattioli, E., Gualandi, F., Ferlini, A., Merlini, L., Maraldi, N. M., Bonaldo, P. and Bernardi, P. (2007). Mitochondrial dysfunction in the pathogenesis of Ullrich congenital muscular dystrophy and prospective therapy with cyclosporins. *Proc. Natl. Acad. Sci. U. S. A.* **104**, 991-996.

Auer, T. O., Duroure, K., De Cian, A., Concordet, J. P. and Del Bene, F. (2014). Highly efficient CRISPR/Cas9-mediated knock-in in zebrafish by homology-independent DNA repair. *Genome Res.* **24**, 142-153.

Bassett, D. I., Bryson-Richardson, R. J., Daggett, D. F., Gautier, P., Keenan, D. G. and Currie, P. D. (2003). Dystrophin is required for the formation of stable muscle attachments in the zebrafish embryo. *Development* **130**, 5851-5860.

Bedell, V. M., Wang, Y., Campbell, J. M., Poshusta, T. L., Starker, C. G., Krug, R. G. 2nd, Tan, W., Penheiter, S. G., Ma, A. C., Leung, A. Y., Fahrenkrug, S. C., Carlson, D. F., Voytas, D. F., Clark, K. J., Essner, J. J. and Ekker, S. C. (2012). *In vivo* genome editing using a high-efficiency TALEN system. *Nature* **491**, 114-118.

Berger, J., Sztal, T. and Currie, P.D. (2012). Quantification of birefringence readily measures the level of muscle damage in zebrafish. *Biochem. Biophys. Res. Commun.*, **423**, 785-788.

Berghmans, S., Murphey, R. D., Wienholds, E., Neuberg, D., Kutok, J. L., Fletcher, C. D., Morris, J. P., Liu, T. X., Schulte-Merker, S., Kanki, J. P., Plasterk, R., Zon, L. I., and Look A. T. (2005). tp53 mutant zebrafish develop malignant peripheral nerve sheath tumors. *Proc. Natl. Acad. Sci. U. S. A.* **102**, 407-412.

Bernardi, P. and Bonaldo, P. (2008). Dysfunction of mitochondria and sarcoplasmic reticulum in the pathogenesis of collagen VI muscular dystrophies. *Ann. N. Y. Acad. Sci.* **1147**, 303-311.

Bernhardt, R. R. and Schachner, M. (2000). Chondroitin sulfates affect the formation of the segmental motor nerves in zebrafish embryos. *Dev. Biol.* **221**, 206-219.

Bertini, E. and Pepe, G. (2002). Collagen type VI and related disorders: Bethlem myopathy and Ullrich scleroatonic muscular dystrophy. *Eur. J. Paediatr. Neurol.* **6**, 193-198.

Bidanset, D. J., Guidry, C., Rosenberg, L. C., Choi, H. U., Timpl, R. and Hook, M. (1992). Binding of the proteoglycan decorin to collagen type VI. *J. Biol. Chem.* **267**, 5250-5256.

Bonaldo, P. and Colombatti, A. (1989). The carboxyl terminus of the chicken α3 chain of collagen VI is a unique mosaic structure with glycoprotein Ib-like, fibronectin type III, and Kunitz modules. *J. Biol. Chem.* **264**, 20235-20239.

Bonaldo, P., Braghetta, P., Zanetti, M., Piccolo, S., Volpin, D. and Bressan, G. M. (1998). Collagen VI deficiency induces early onset myopathy in the mouse: an animal model for Bethlem myopathy. *Hum. Mol. Genet.* **7**, 2135-2140.

Bonaldo, P., Russo, V., Bucciotti, F., Bressan, G. M. and Colombatti, A. (1989). α1 chain of chick type VI collagen. The complete cDNA sequence reveals a hybrid molecule made of one short collagen and three von Willebrand Factor type A-like domains. *J. Biol. Chem.* **264**, 5575-5580.

Bonaldo, P., Russo, V., Bucciotti, F., Doliana, R. and Colombatti, A. (1990). Structural and functional features of the alpha 3 chain indicate a bridging role for chicken collagen VI in connective tissues. *Biochemistry* **29**, 1245-1254.

Bönnemann, C. G. (2011). The collagen VI-related myopathies: muscle meets its matrix. *Nat. Rev. Neurol.* **7**, 379-390.

Braghetta, P., Fabbro, C., Piccolo, S., Marvulli, D., Bonaldo, P., Volpin, D. and Bressan, G. M. (1996). Distinct regions control transcriptional activation of the alpha1(VI) collagen promoter in different tissues of transgenic mice. *J. Cell Biol.*

135, 1163-1177.

Braghetta, P., Ferrari, A., Fabbro, C., Bizzotto, D., Volpin, D., Bonaldo, P. and Bressan, G. M. (2008). An enhancer required for transcription of the *Col6a1* gene in muscle connective tissue is induced by signals released from muscle cells. *Exp. Cell Res.* **314**, 3508-3518.

Briñas, L., Richard, P., Quijano-Roy, S., Gartioux, C., Ledeuil C., Lacène E., Makri S, Ferreiro A, Maugenre S, Topaloglu H, Haliloglu G, Pénisson-Besnier, I., Jeannet, P. Y., Merlini, L., Navarro, C., Toutain, A., Chaigne, D., Desguerre, I., de Die-Smulders, C., Dunand, M., Echenne, B., Eymard, B., Kuntzer, T., Maincent, K., Mayer, M., Plessis, G., Rivier, F., Roelens, F., Stojkovic, T., Taratuto, A. L., Lubieniecki, F., Monges, S., Tranchant, C., Viollet, L., Romero, N. B., Estournet, B., Guicheney, P. and Allamand V. (2010). Early Onset Collagen VI Myopathies: Genetic and Clinical Correlations. *Ann. Neurol.* **68**, 511-520.

Brown, J. C., Golbik, R., Mann, K. and Timpl, R. (1994). Structure and stability of the triple-helical domains of human collagen XIV. *Matrix Biol.* **14**, 287-295.

Burg, M. A., Tillet, E., Timpl, R. and Stallcup, W. B. (1996). Binding of the NG2 proteoglycan to type VI collagen and other extracel- lular matrix molecules. *J. Biol. Chem.* **271**, 26110-26116.

Camacho Vanegas, O., Bertini, E., Zhang, R. Z., Petrini, S., Minosse, C., Sabatelli, P., Giusti, B., Chu, M. L. and Pepe, G. (2001). Ullrich scleroatonic muscular dystrophy is caused by recessive mutations in collagen type VI. *Proc. Natl. Acad. Sci. U. S. A.* **98**, 7516-7521.

Carroll, D. (2011). Genome engineering with zinc-finger nucleases. *Genetics* **188**, 773-782.

Cescon, M., Gattazzo, F., Chen, P., and Bonaldo, P. (2015). Collagen VI at a glance. *J. Cell Sci.* **128**, 3525-3531.

Chang N., Sun C., Gao L., Zhu D., Xu X., Zhu, X., Xiong, J. W. and Xi, J. J. (2013). Genome editing with RNA-guided Cas9 nuclease in zebrafish embryos. *Cell Res.* **23**, 465-472.

Charvet, B., Guiraud, A., Malbouyres, M., Zwolanek, D., Guillon, E., Bretaud, S., Monnot, C., Schulze, J., Bader, H. L., Allard, B., Koch, M. and Ruggiero, F. (2013). Knockdown of *col22a1* gene in zebrafish induces a muscular dystrophy by disruption of the myotendinous junction. *Development* **140**, 4602-4613.

Chen, P., Cescon, M., Megighian, A. and Bonaldo, P. (2014a). Collagen VI regulates peripheral nerve myelination and function. *FASEB J.* **28**, 1145-1156.

Chen, P., Cescon, M., Zuccolotto, G., Nobbio, L., Colombelli, C., Filaferro, M., Vitale, G., Feltri, M. L. and Bonaldo, P. (2014b). Collagen VI regulates peripheral nerve regeneration by modulating macrophage recruitment and polarization. *Acta Neuropathol.* **129**, 97-113.

Cheng, I. H., Lin, Y. C., Hwang, E., Huang, H. T., Chang, W. H. Liu, Y. L. and Chao, C. Y. (2011). Collagen VI protects against neuronal apoptosis elicited by ultraviolet irradiation via an Akt/phosphatidylinositol 3-kinase signaling pathway. *Neuroscience* **183**, 178-188.

Cheng, J. S., Dubal, D. B., Kim, D. H., Legleiter, J., Cheng, I. H., Yu, G. Q., Tesseur, I., Wyss-Coray, T., Bonaldo, P. and Mucke, L. (2009). Collagen VI protects neurons against Aβ toxicity. *Nat. Neurosci.* **12**, 119-121.

Cho, S. W., Kim, S., Kim, J. M. and Kim, J. S. (2013). Targeted genome engineering in human cells with the Cas9 RNA-guided endonuclease. *Nat. Biotechnol.* **31**, 230-232.

Chu, M. L., Pan, T. C., Conway, D., Saitta, B., Stokes, D., Kuo, H. J., Glanville, R. W., Timpl, R., Mann, K. and Deutzmann, R. (1990). The structure of type VI collagen. *Ann. N. Y. Acad. Sci.* **580**, 55-63.

Colombatti, A. and Bonaldo, P. (1987). Biosynthesis of chick type VI collagen II. Processing and secretion in fibroblasts and smooth muscle cells. *J. Biol. Chem.* **262**, 14461-14466.

Colombatti, A., Bonaldo, P., Ainger, K., Bressan, G. M. and Volpin, D. (1987). Biosynthesis of chick type VI collagen. I. Intracellular assembly and molecular structure. *J. Biol. Chem.* **262**, 14454-14460.

Colombatti, A., Mucignat, M. T. and Bonaldo, P. (1995). Secretion and matrix

assembly of recombinant type VI collagen. *J. Biol. Chem.* **270**, 13105-13111.

Cong, L., Ran, F. A., Cox, D., Lin, S., Barretto, R., Habib, N., Hsu, P. D., Wu, X., Jiang, W., Marraffini, L. A. and Zhang, F. (2013). Multiplex genome engineering using CRISPR/Cas systems. *Science* **339**, 819-823.

Cornu, T. I., Thibodeau-Beganny, S., Guhl, E., Alwin, S., Eichtinger, M., Joung, J. K. and Cathomen, T. (2008). DNA-binding specificity is a major determinant of the activity and toxicity of zinc-finger nucleases. *Mol. Ther.* **16**, 352-358.

Doane, K. J., Howell, S. J. and Birk, D. E. (1998). Identification and functional characterization of two type VI collagen receptors, alpha 3 beta 1 integrin and NG2, during avian corneal stromal development. *Invest. Ophthalmol. Vis. Sci.* **39**, 263-275.

Doane, K. J., Yang, G. and Birk, D. E. (1992). Corneal cell-matrix interactions: type VI collagen promotes adhesion and spreading of corneal fibroblasts. *Exp. Cell Res.* **200**, 490-499.

Doliana, R., Bonaldo, P. and Colombatti, A. (1990). Multiple forms of chicken α3 (VI) collagen chain generated by alternative splicing in type A repeated domains. *J. Cell Biol.* **111**, 2197-2205.

Dziadek, M., Kazenwadel, J. S., Hendrey, J. A., Pan, T. C., Zhang, R.-Z. and Chu, M. L. (2002). Alternative splicing of transcripts for the alpha3 chain of mouse collagen VI: identification of an abundant isoform lacking domains N7–N10 in mouse and human. *Matrix Biol.* **21**, 227-241.

Engel, J., Furthmayr, H., Odermatt, E., Mark, H., Aumailley, M., Fleischmajer, R. and Timpl, R. (1985). Structure and macromolecular organization of type VI collagen. *Ann. N. Y. Acad. Sci.* **460**, 25-37.

Farboud, B., Meyer, B. J. (2015). Dramatic enhancement of genome editing by CRISPR/Cas9 through improved guide RNA design. *Genetics* **199**, 959-971.

Finnis, M. L. and Gibson, M. A. (1997). Microfibril-associated glycoprotein-1 (MAGP-1) binds to the pepsin-resistant domain of the α3(VI) chain of type VI collagen. *J. Biol. Chem.* **272**, 22817-22823.

Fitzgerald, J., Rich, C., Zhou, F. H. and Hansen, U. (2008). Three novel collagen VI chains, alpha4(VI), alpha5(VI), and alpha6(VI). *J. Biol. Chem.* **283**, 20170-20180.

Furthmayr, H., Wiedemann, H., Timpl, R., Odermatt, E. and Engel, J. (1983). Electron-microscopical approach to a structural model of intima collagen. *Biochem. J.* **211**, 303-311.

Gagnon, J. A., Valen, E., Thyme, S. B., Huang, P., Ahkmetova, L., Pauli, A., Montague, T. G., Zimmerman, S., Richter, C. and Schier, A. F. (2014). Efficient mutagenesis by Cas9 protein-mediated oligonucleotide insertion and large-scale assessment of single-guide RNAs. *PLoS One* **9**, e98186.

Gaj, T., Gersbach, C. A. and Barbas, C. F. 3rd (2013). ZFN, TALEN, and CRISPR/Cas-based methods for genome engineering. *Trends Biotechnol.* **31**, 397-405.

Galluzzi, L., Bravo-san Pedro, J. M., Vitale, I., Aaronson, S. A., Abrams J. M., Adam D., Alnemri, E. S., Altucci, L., Andrews, D., Annicchiarico-Petruzzelli, M., Baehrecke, E. H., Bazan, N. G., Bertrand, M. J., Bianchi, K., Blagosklonny, M. V., Blomgren, K., Borner, C., Bredesen, D. E., Brenner, C., Campanella, M., Candi, E., Cecconi, F., Chan, F. K., Chandel, N. S., Cheng, E. H., Chipuk, J. E., Cidlowski, J. A., Ciechanover, A., Dawson, T. M., Dawson, V. L., De Laurenzi, V., De Maria, R., Debatin, K. M., Di Daniele, N., Dixit, V. M., Dynlacht, B. D., El-Deiry, W. S., Fimia, G. M., Flavell, R. A., Fulda, S., Garrido, C., Gougeon, M. L., Green, D. R., Gronemeyer, H., Hajnoczky, G., Hardwick, J. M., Hengartner, M. O., Ichijo, H., Joseph, B., Jost, P. J., Kaufmann, T., Kepp, O., Klionsky, D. J., Knight, R. A., Kumar, S., Lemasters, J. J., Levine, B., Linkermann, A., Lipton, S. A., Lockshin, R. A., López-Otín, C., Lugli, E., Madeo, F., Malorni, W., Marine, J. C., Martin, S. J., Martinou, J. C., Medema, J. P., Meier, P., Melino, S., Mizushima, N., Moll, U., Muñoz-Pinedo, C., Nuñez, G., Oberst, A., Panaretakis, T., Penninger, J. M., Peter, M. E., Piacentini, M., Pinton, P., Prehn, J. H., Puthalakath, H., Rabinovich, G. A., Ravichandran, K. S., Rizzuto, R., Rodrigues, C. M., Rubinsztein, D. C., Rudel, T., Shi, Y., Simon, H. U., Stockwell, B. R., Szabadkai, G., Tait, S. W., Tang, H. L., Tavernarakis, N., Tsujimoto, Y., Vanden Berghe, T., Vandenabeele, P., Villunger, A., Wagner, E. F., Walczak, H., White, E., Wood, W. G., Yuan, J., Zakeri, Z., Zhivotovsky, B., Melino, G. and Kroemer G. (2015). Essential versus Accessory Aspects of Cell Death: Recommendations of the NCCD 2015. *Cell Death Differ.* **22** 58-73.

Gara, S. K., Grumati, P., Squarzoni, S., Sabatelli, P., Urciuolo, A., Bonaldo, P., Paulsson, M. and Wagener, R. (2011). Differential and restricted expression of novel collagen VI chains in mouse. *Matrix Biol.* **30**, 248-257.

Gara, S. K., Grumati, P., Urciuolo, A., Bonaldo, P., Kobbe, B., Koch, M., Paulsson, M. and Wagener, R. (2008). Three novel collagen VI chains with high homology to the alpha3 chain. *J. Biol. Chem.* **283**, 10658-10670.

Gonzales, A. P., Yeh J. R. (2014). Cas9-based genome editing in zebrafish. *Methods Enzymol.* **546**, 377-413.

Gordon, L. R., Gribble, K. D., Syrett, C. M., and Granato, M. (2012). Initiation of synapse formation by Wnt-induced MuSK endocytosis. *Development* **139(5)**, 1023–1033. doi:10.1242/dev.071555

Grumati, P., Coletto, L., Sabatelli, P., Cescon, M., Angelin, A., Bertaggia, E., Blaauw, B., Urciuolo, A., Tiepolo, T., Merlini, L., Maraldi, N. M., Bernardi, P., Sandri, M. and Bonaldo, P. (2010). Autophagy is defective in collagen VI muscular dystrophies, and its reactivation rescues myofiber degeneration. *Nat. Med.* **16**, 1313-1320.

Gualandi, F., Urciuolo, A., Martoni, E., Sabatelli, P., Squarzoni, S., Bovolenta, M., Messina, S., Mercuri, E., Franchella, A., Ferlini, A., Bonaldo, P. and Merlini, L. (2009). Autosomal recessive Bethlem myopathy. *Neurology.* **73**, 1883-1891.

Gupta, A., Hall, V. L., Kok, F. O., Shin, M., McNulty, J. C., Lawson, N. D. and Wolfe, S. A. (2013). Targeted chromosomal deletions and inversions in zebrafish. *Genome Res.* **23**, 1008-1017.

Guschin, D. Y., Waite, A. J., Katibah, G. E., Miller, J. C., Holmes, M. C. and Rebar, E. J. (2010). A rapid and general assay for monitoring endogenous gene modification. *Methods Mol. Biol.* **649**, 247-256.

Guyon, J. R., Goswami, J., Jun, S. J., Thorne, M., Howell, M., Pusack, T., Kawahara, G., Steffen, L. S., Galdzicki, M. and Kunkel, L. M. (2009). Genetic isolation and characterization of a splicing mutant of zebrafish dystrophin. *Hum. Mol. Genet.* **18**, 202-211.

Hall, T. E., Bryson-Richardson, R. J., Berger, S., Jacoby, A. S., Cole, N. J.,Hollway,

G. E., Berger, J. and Currie, P. D. (2007). The zebrafish candyfloss mutant implicates extracellular matrix adhesion failure in laminin alpha2-deficient congenital muscular dystrophy. *Proc. Natl. Acad. Sci. U. S. A.* **104**, 7092-7097.

Hansen, U., Allen, J. M., White, R., Moscibrocki, C., Bruckner, P., Bateman, J. F. and Fitzgerald, J. (2012). WARP interacts with collagen VI-containing microfibrils in the pericellular matrix of human chondrocytes. *PLoS One.* **7**, e52793.

Helm, M., Brule, H., Giege, R. and Florentz, C. (1999). More mistakes by T7 RNA polymerase at the 59 ends of *in vitro*-transcribed RNAs. *RNA.* **5**, 618–621.

Hruscha, A., Krawits, P., Rechenberg, A., Heinrich, V., Hecht, J., Haass, C. and Schmid, B. (2013). Efficient CRISPR/Cas9 genome editing with low off-target effects in zebrafish. *Development* **140**, 4982-4987.

Hsu, P.D., Scott, D. A., Weinstein, J. A., Ran, F. A., Konermann, S., Agarwala, V., Li, Y., Fine, E. J., Wu, X., Shalem, O., Cradick, T. J., Marraffini, L. A., Bao, G. and Zhang, F. (2013). DNA targeting specificity of RNA-guided Cas9 nucleases. *Nat. Biotechnol.* **31**, 827-832.

Hwang, W. Y., Fu, Y., Reyon, D., Maeder, M. L., Kaini, P., Sander, J. D., Joung, J. K., Peterson, R. T. and Yeh, J. R. (2013). Heritable and precise zebrafish genome editing using a CRISPR-Cas system. *PLoS One* **8**, e68708.

Hwang, W. Y., Fu, Y., Reyon, D., Maeder, M. L., Tsai, S. Q., Sander, J. D., Peterson, R. T., Yeh, J. R. and Joung, J. K. (2013). Efficient genome editing in zebrafish using a CRISPR-Cas system. *Nat. Biotechnol.* **31**, 227-229.

Hwang, W. Y., Fu, Y., Reyon, D., Maeder, M. L., Kaini, P., Sander, J. D., Joung, J. K., Peterson, R. T. and Yeh, J. R. (2013a). Heritable and precise zebrafish genome editing using a CRISPR-Cas system. *PLoS One* **8**, e68708.

Hynes, R. O. and Lander, A. D. (1992). Contact and adhesive specificities in the associations, migrations, and targeting of cells and axons. *Cell* **68**, 303-322.

Imburgio, D., Rong, M., Ma, K. and McAllister, W. T. (2000). Studies of promoter recognition and start site selection by T7 RNA polymerase using a comprehensive collection of promoter variants. *Biochemistry* **39**, 10419-10430.

Irwin, W. A., Bergamin, N., Sabatelli, P., Reggiani, C., Megighian, A., Merlini, L., Braghetta, P., Columbaro, M., Volpin, D., Bressan, G. M., Bernardi, P. and Bonaldo, P. (2003). Mitochondrial dysfunction and apoptosis in myopathic mice with collagen VI deficiency. *Nat. Genet.* **35**, 367-371.

Iyengar, P., Espina, V., Williams, T. W., Lin, Y., Berry, D., Jelicks, L. A., Lee, H., Temple, K., Graves, R., Pollard, J., Chopra, N., Russell, R. G., Sasisekharan, R., Trock, B. J., Lippman, M., Calvert, V. S., Petricoin, E.F. 3rd, Liotta, L., Dadachova, E., Pestell, R. G., Lisanti, M. P., Bonaldo, P., Scherer, P.E. (2005). Adipocyte-derived collagen VI affects early mammary tumor progression *in vivo*, demonstrating a critical interaction in the tumor/stroma microenvironment. *J. Clin. Invest.* **115**, 1163-1176.

Jao L. E., Wente S. R. and Chen W. (2013) Efficient multiplex biallelic zebrafish genome editing using a CRISPR nuclease system. *Proc. Natl. Acad. Sci. U. S. A.*, **110**, 13904-13909.

Jinek, M., Chylinski, K., Fonfara, I., Hauer, M., Doudna, J. A. and Charpentier, E. (2012). A programmable dual-RNA-guided DNA endonuclease in adaptive bacterial immunity. *Science* **337**, 816-821.

Jo Y.I., Suresh B., Kim H. and Ramakrishna S. (2015). CRISPR/Cas9 system as an innovative genetic engineering tool: Enhancements in sequence specificity and delivery methods. *Biochim. Biophys. Acta*. **1856**, 234–243.

Jöbsis, G.J., Keizers, H., Vreijling, J.P., de Visser, M., Speer, M.C., Wolterman, R.A., Baas, F. and Bolhuis, P.A. (1996). Type VI collagen mutations in Bethlem myopathy, an autosomal dominant myopathy with contractures. *Nat. Genet.* **14**, 113-115.

Joung, J.K. and Sander, J.D. (2013). TALENs: A widely applicable technology for targeted genome editing. *Nat. Rev. Mol. Cell. Biol.* **14**, 49-55.

Karkheiran, S., Krebs, C. E., Makarov, V., Nilipour, Y., Hubert, B., Darvish, H., Frucht, S., Shahidi, G. A., Buxbaum, J. D. and Paisán-Ruiz, C. (2013). Identification of *COL6A2* mutations in progressive myoclonus epilepsy syndrome. *Hum. Genet.* **132**, 275-283.

Keene, D., Engvall, E. and Glanville, R. (1988). Ultrastructure of type VI collagen in human skin and cartilage suggests an anchoring function for this filamentous network. *J. Cell Biol.,* **107**, 1995-2006.

Kim H. and Kim J. S. (2014). A guide to genome engineering with programmable nucleases. *Nat. Rev. Genet.* **15**, 321 334.

Kimmel, C. B., Ballard, W. W., Kimmel, S. R., Ullmann, B. and Schilling, T. F. (1995) Stages of embryonic development of the zebrafish. *Dev. Dyn.* **203**, 253-310.

Knupp, C., Pinali, C., Munro, P. M., Gruber, H. E., Sherratt, M. J., Baldock, C. and Squire, J. M. (2006). Structural correlation between collagen VI microfibrils and collagen VI banded aggregates. *J. Struct. Biol*. **154**, 312-326.

Kotani, H., Taimatsu, K., Ohga, R., Ota, S. and Kawahara, A. (2015). Efficient Multiple Genome Modifications Induced by the crRNAs, tracrRNA and Cas9 Protein Complex in Zebrafish. *PLoS One* **10**, e0128319.

Kuo, H. J., Maslen, C. L., Keene, D. R. and Glanville, R. W. (1997). Type VI collagen anchors endothelial basement membranes by interacting with type IV collagen. *J. Biol. Chem.* **272**, 26522-26529.

Kuzmine I., Gottlieb P. A. and Martin C. T. (2003). Binding of the priming nucleotide in the initiation of transcription by T7 RNA polymerase. *J. Biol. Chem.* **278**, 2819-2823.

Lampe, A. K., Zou, Y., Sudano, D., O'Brien, K. K., Hicks, D., Laval, S. H., Charlton, R., Jimenez-Mallebrera, C., Zhang, R. Z., Finkel, R. S., Tennekoon, G., Schreiber, G., van der Knaap, M. S., Marks, H., Straub, V., Flanigan, K. M., Chu, M. L., Muntoni, F., Bushby, K. M. and Bönnemann, C. G. (2008). Exon skipping mutations in collagen VI are common and are predictive for severity and inheritance. *Hum. Mutat.* **29**, 809-822.

Lampe, A. K. and Bushby, K. M. D. (2005). Collagen VI related muscle disorders. *J. Med. Genet.*, **42**, 673-685.

Lo, H. P., Nixon, S. J., Hall, T. E., Cowling, B. S., Ferguson, C., Morgan, G. P., Schieber, N. L., Fernandez-Rojo, M. A., Bastiani, M., Floetenmeyer, M., Martel,

N., Laporte, J., Pilch, P. F., Parton, R. G. (2015). The caveolin-cavin system plays a conserved and critical role in mechanoprotection of skeletal muscle. *J. Cell Biol.* **210**, 833-849.

Maeder, M. L., Thibodeau-Beganny, S., Osiak, A., Wright, D. A., Anthony, R. M., Eichtinger, M., Jiang, T., Foley, J. E., Winfrey, R. J., Townsend, J. A., Unger-Wallace, E., Sander, J. D., Müller-Lerch, F., Fu, F., Pearlberg, J., Göbel, C., Dassie, J. P., Pruett-Miller, S. M., Porteus, M. H., Sgroi, D. C., Iafrate, A. J., Dobbs, D., McCray, P. B. Jr., Cathomen, T., Voytas, D. F. and Joung, J. K. (2008). Rapid "open-source" engineering of customized zinc- finger nucleases for highly efficient gene modification. *Mol. Cell* **31**, 294-301.

Mali, P., Yang, L., Esvelt, K. M., Aach, J., Guell, M., DiCarlo, J. E., Norville, J. E. and Church, G. M. (2013) RNA-guided human genome engineering via Cas9. *Science* **339**, 823-826.

Marcelino, J. and McDevitt, C. A. (1995). Attachment of articular cartilage chondrocytes to the tissue form of type VI collagen. *Biochim. Biophys. Acta* **1249**, 180-188.

Meeker, N. D., Hutchinson, S. A., Ho, L., and Trede, N. S. (2007). Method for isolation of PCR-ready genomic DNA from zebrafish tissues. *BioTechniques*, **43(5)**, 610–614.

Mercuri, E., and Longman C. (2005). Congenital Muscular Dystrophy. *Pediatric Annals* **34**, 560-562, 564-568

Merlini, L., Martoni, E., Grumati, P., Sabatelli, P., Squarzoni, S., Urciuolo, A., Ferlini, A., Gualandi, F. and Bonaldo, P. (2008). Autosomal recessive myosclerosis myopathy is a collagen VI disorder. *Neurology* **71**, 1245-1253.

Merlini, L., Martoni, E., Grumati, P., Sabatelli, P., Squarzoni, S., Urciuolo, A., Ferlini, A., Gualandi, F. and Bonaldo, P. (2008). Autosomal recessive myosclerosis myopathy is a collagen VI disorder. *Neurology* **71**, 1245-1253.

Midwood, K. S. and Salter, D. M. (2001). NG2/HMPG modulation of human articular chondrocyte adhesion to type VI collagen is lost in osteoarthritis. *J. Pathol.* **195**, 631-635.

Morgelin, M. and Heinegard, D. (2001). Biglycan and decorin bind close to the n-terminal region of the collagen VI triple helix. *J. Biol. Chem.* **276**, 18947-18952.

Moro, E., Ozhan-Kizil, G., Mongera, A., Beis, D., Wierzbicki, C., Young, R. M., Bournele, D., Domenichini, A., Valdivia, L. E., Lum, L., Chen, C., Amatruda, J. F., Tiso, N., Weidinger, G. and Argenton, F. (2012). *In vivo* Wnt signaling tracing through a transgenic biosensor fish reveals novel activity domains. *Dev. Biol.* **366**, 327-340.

Myllyharju, J. and Kivirikko, K. I. (2004). Collagens, modifying enzymes and their mutations in humans, flies and worms. *Trends Genet.* **20**, 33-43.

Nanda, A., Carson-Walter, E. B., Seaman, S., Barber, T. D., Stampfl, J., Singh, S., Vogelstein, B., Kinzler, K. W. and St Croix, B. (2004). TEM8 interacts with the cleaved C5 domain of collagen alpha 3(VI). *Cancer Res.* **64**, 817-820.

Ota, S., Hisano, Y., Ikawa, Y. and Kawahara, A. (2014). Multiple genome modifications by the CRISPR/Cas9 system in zebrafish. *Genes Cells* **19**, 555-564.

Pagnon-Minot, A., Malbouyres, M., Haftek-Terreau, Z., Kim, H. R., Sasaki, T., Thisse, C., Thisse, B., Ingham, P.W., Ruggiero, F. and Le Guellec, D. (2008). Collagen XV, a novel factor in zebrafish notochord differentiation and muscle development. *Dev. Biol*., **316**, 21–35.

Pepe, G., Bertini, E., Bonaldo, P., Bushby, K., Giusti, B., de Visser, M., Guicheney, P., Lattanzi, G., Merlini, L., Muntoni, F., Nishino, I., Nonaka, I., Yaou, R. B., Sabatelli, P., Sewry, C., Topaloglu, H. and van der Kooi, A. (2002). Bethlem myopathy (BETHLEM) and Ullrich scleroatonic muscular dystrophy: 100th ENMC International Workshop, 23-24 November 2001, Naarden, The Netherlands. *Neuromuscul. Disord.* **12**, 984-993.

Petrini, S., Tessa, A., Stallcup, W. B., Sabatelli, P., Pescatori, M., Giusti, B., Carrozzo, R., Verardo, M., Bergamin, N., Columbaro, M., Bernardini, C., Merlini, L., Pepe, G., Bonaldo, P. and Bertini, E. (2005). Altered expression of the MCSP/NG2 chondroitin sulfate proteoglycan in collagen VI deficiency. *Mol. Cell Neurosci.* **30**, 408-417.

Pfaff, M., Aumailley, M., Specks, U., Knolle, J., Zerwes, H. G. and Timpl, R. (1993).

Integrin and Arg-Gly-Asp dependence of cell adhesion to the native and unfolded triple helix of collagen type VI. *Exp. Cell Res.* **206**, 167-176.

Prykhozhij, S. V., Rajan, V. and Berman, J. N. (2015). A Guide to Computational Tools and Design Strategies for Genome Editing Experiments in Zebrafish Using CRISPR/Cas9. *Zebrafish*. **13(1)**, 70-73.

Radev, Z., Hermel, J. M., Elipot, Y., Bretaud, S., Arnould, S., Duchateau, P., Ruggiero, F., Joly, J. S. and Sohm, F. (2015). A TALEN-Exon Skipping Design for a Bethlem Myopathy Model in Zebrafish. *PLoS One* **10**, e0133986.

Ramanoudjame, L., Rocancourt, C., Lainé, J., Klein, A., Joassard, L., Gartioux, C., Fleury, M., Lyphout, L., Kabashi, E., Ciura, S., Cousin, X. and Allamand, V. (2015). Two novel COLVI long chains in zebrafish that are essential for muscle development. *Hum. Mol. Genet.* **24**, 6624-6639.

Ramirez, C. L., Foley, J. E., Wright, D. A., Muller-Lerch, F., Rahman, S. H., Cornu, T. I., Winfrey, R. J., Sander, J. D., Fu, F., Townsend, J. A., Cathomen, T., Voytas, D. F. and Joung, J. K. (2008). Unexpected failure rates for modular assembly of engineered zinc fingers. *Nat. Methods*, **5**, 374-375.

Robu, M. E., Larson, J. D., Nasevicius, A., Beiraghi, S., Brenner, C., Farber, S. A. and Ekker, S. C. (2007). p53 activation by knockdown technologies. *PLoS Genet.* **3**, e78.

Sabatelli, P., Gara, S. K., Grumati, P., Urciuolo, A., Gualandi, F., Curci, R., Squarzoni, S., Zamparelli, A., Martoni, E., Merlini, L., Paulsson, M., Bonaldo, P. and Wagener, R. (2011). Expression of the collagen VI α5 and α6 chains in normal human skin and in skin of patients with collagen VI-related myopathies. *J. Invest. Dermatol.* **131**, 99-107.

Sabatelli, P., Gualandi, F., Gara, S.K., Grumati, P., Zamparelli, A., Martoni, E., Pellegrini, C., Merlini, L., Ferlini, A., Bonaldo, P., Maraldi, N. M., Paulsson, M., Squarzoni, S. and Wagener, R. (2012). Expression of collagen VI alpha5 and alpha6 chains in human muscle and in Duchenne muscular dystrophy-related muscle fibrosis. *Matrix Biol*. **31**, 187-196.

Saitta, B., Stokes, D. G., Vissing, H., Timpl, R. and Chu, M. L. (1990). Alternative

splicing of the human alpha 2(VI) collagen gene generates multiple mRNA transcripts which predict three protein variants with distinct carboxyl termini. *J. Biol. Chem.* **265**, 6473-6480.

Sakuma, K. and Yamaguchi, A. (2010). The functional role of calcineurinin hypertrophy, regeneration, and disorders of skeletal muscle. *J. Biomed. Biotechnol.* 721219.

Sasaki, T., Göhring, W., Pan, T. C., Chu, M. L. and Timpl, R. (1995). Binding of mouse and human fibulin-2 to extracellular matrix ligands. *J. Mol. Biol.* **254**, 892-899.

Sasaki, T., Hohenester, E., Zhang, R. Z., Gotta, S., Speer, M. C., Tandan, R., Timpl, R. and Chu, M. L. (2000). A Bethlem myopathy Gly to Glu mutation in the von Willebrand factor A domain N2 of the collagen alpha3(VI) chain interferes with protein folding. *FASEB J.* **14**, 761-768.

Schiavone, M., Rampazzo, E., Casari, A., Battilana, G., Persano, L., Moro, E., Liu, S., Leach, S. D., Tiso, N. and Argenton, F. (2014). Zebrafish reporter lines reveal in vivo signaling pathway activities involved in pancreatic cancer. *Dis. Model. Mech.* **7**, 883-894.

Schmid, B., Hruscha, A., Hogl, S., Banzhaf-Strathmann, J., Strecker, K., van der Zee, J., Teucke, M., Eimer, S., Hegermann, J., Kittelmann, M., Kremmer, E., Cruts, M., Solchenberger, B., Hasenkamp, L., van Bebber, F., Van Broeckhoven, C., Edbauer, D., Lichtenthaler, S. F. and Haass, C. (2013). Loss of ALS-associated TDP-43 in zebrafish causes muscle degeneration, vascular dysfunction, and reduced motor neuron axon outgrowth. *Proc. Natl. Acad. Sci. U. S. A.* **110**, 4986-4991.

Schnoor, M., Cullen, P., Lorkowski, J., Stolle, K., Robenek, H., Troyer, D., Rauterberg, J. and Lorkowski, S. (2008). Production of type VI collagen by human macrophages: a new dimension in macrophage functional heterogeneity. *J. Immunol.* **180**, 5707-5719.

Semenova, E., Jore, M.M., Datsenko, K.A., Semenova, A., Westra, E.R., Wanner, B., van der Oost, J., Brouns, S.J. and Severinov, K. (2011). Interference by clustered regularly interspaced short palindromic repeat (CRISPR) RNA is

governed by a seed sequence, *Proc. Natl. Acad. Sci. U. S. A.* **108**, 10098-10103.

Sievers, J., Pehlemann, F. W., Gude, S. and Berry, M. (1994). Meningeal cells organize the superficial glia limitans of the cerebellum and produce components of both the interstitial matrix and the basement membrane. *J. Neurocytol.* **23**, 135-149.

Sleigh, J. N., Barreiro-Iglesias, A., Oliver, P. L., Biba, A., Becker, T., Davies, K. E., Becker, C. G. and Talbot, K. (2014). Chondrolectin affects cell survival and neuronal outgrowth in *in vitro* and *in vivo* models of spinal muscular atrophy. *Hum. Mol. Genet.* **23**, 855-869.

Sollu, C., Pars, K., Cornu, T. I., Thibodeau-Beganny, S., Maeder, M. L., Joung, J. K., Heilbronn, R. and Cathomen, T. (2010). Autonomous zinc-finger nuclease pairs for targeted chromosomal deletion. *Nucleic Acids Res.* **38**, 8269-8276.

Specks, U., Mayer, U., Nischt, R., Spissinger, T., Mann, K., Timpl, R., Engel, J. and Chu, M. L. (1992). Structure of recombinant *N*-terminal globule of type VI collagen alpha 3 chain and its binding to heparin and hyaluronan. *EMBO J*. **11**, 4281-4290.

Stallcup, W.B. (2002). The NG2 Proteoglycan: Past Insights and Future Prospects. *J. Neurocytol.* **31**, 423-435.

Strekalova, T., Sun, M., Sibbe, M., Evers, M., Dityatev, A., Gass, P. and Schachner, M. (2002). Fibronectin domains of extracellular matrix molecule tenascin-C modulate hippocampal learning and synaptic plasticity. *Mol. Cell. Neurosci.* **21**, 173-187.

Sztal, T. E., Sonntag, C., Hall, T. E. and Currie, P. D. (2012). Epistatic dissection of laminin-receptor interactions in dystrophic zebrafish muscle. *Hum. Mol. Genet.* **21**, 4718-4731.

Takahashi, T., Cho, H. I., Kublin, C. L. and Cintron, C. (1993). Keratan sulfate and dermatan sulfate proteoglycans associate with type VI collagen in fetal rabbit cornea. *J. Histochem. Cytochem*. **41**, 1447-1457.

Telfer, W. R., Busta, A. S., Bonnemann, C. G., Feldman, E. L. and Dowling, J. J. (2010). Zebrafish models of collagen VI-related myopathies. Hum. *Mol. Genet.* **19**,

2433-2444.

Thomas, H. R., Percival, S. M., Yoder, B. K., Parant, J. M. (2014). High-Throughput Genome Editing and Phenotyping Facilitated by High Resolution Melting Curve Analysis. *PLoS One* **9**, e114632.

Tulla, M., Pentikainen, O. T., Viitasalo, T., Kapyla, J., Impola, U., Nykvist, P., Nissinen, L., Johnson, M. S. and Heino, J. (2001). Selective binding of collagen subtypes by integrin alpha1I, alpha2I, and alpha10I domains. *J. Biol. Chem.* **276**, 48206-48212.

Urciuolo, A., Quarta, M., Morbidoni, V., Gattazzo, F., Molon, S., Grumati, P., Montemurro, F., Tedesco, F. S., Blaauw, B., Cossu, G., Vozzi, G., Rando, T. A., Bonaldo, P. (2013). Collagen VI regulates satellite cell self-renewal and muscle regeneration. *Nat. Commun.* **4**, 1964.

Vitale, P., Braghetta, P., Volpin, D., Bonaldo, P. and Bressan, G. M. (2001). Mechanisms of transcriptional activation of the *col6a1* gene during Schwann cell differentiation. *Mech. Dev.* **102**, 145-156.

Waldmeier, P. C., Feldtrauer, J. J., Qian, T. and Lemasters, J. J. (2002). Inhibition of the mitochondrial permeability transition by the nonimmunosuppressive cyclosporin derivative NIM811. *Mol. Pharmacol*. **62**, 22-29.

Wang H., Yang H., Shivalila C. S., Dawlaty M. M., Cheng A. W., Zhang, F. and Jaenisch, R. (2013). One-step generation of mice carrying mutations in multiple genes by CRISPR/Cas-mediated genome engineering. *Cell* **153**, 910-918.

Wang, T., Wei, J. J., Sabatini, D. M., Lander, E. S. (2014) Genetic screens in human cells using the CRISPR-Cas9 system. *Science* **343**, 80-84.

Wiberg, C., Hedbom, E., Khairullina, A., Lamande, S. R., Oldberg, A., Timpl, R., Wiedenheft, B., Sternberg, S. H. and Doudna, J. A. (2012). RNA-guided genetic silencing systems in bacteria and archaea. *Nature* **482**, 331-338.

Wiedenheft, B., van Duijn, E., Bultema, J. B., Waghmare, S. P., Zhou, K., Barendregt, A., Westphal, W., Heck, A. J., Boekema, E. J., Dickman, M. J. and Doudna, J. A. (2011). RNA-guided complex from a bacterial immune system enhances target recognition through seed sequence interactions, *Proc. Natl. Acad.*

Sci. U. S. A. **108**,10092-10097.

Wu, X., Kriz, A.J. and Sharp, P.A. (2014). Target specificity of the CRISPR-Cas9 system. *Quant. Biol.* **2**, 59-70.

Zech, M., Lam, D. D., Francescatto, L., Schormair, B., Salminen, A. V., Jochim, A., Wieland, T., Lichtner, P., Peters, A., Gieger, C., Lochmüller, H., Strom, T. M., Haslinger, B., Katsanis, N. and Winkelmann, J. (2015). Recessive mutations in the α3 (VI) collagen gene *COL6A3* cause early-onset isolated dystonia. *Am. J. Hum. Genet.*, **96**, 883-893.

Zhang, R. Z., Sabatelli, P., Pan, T. C., Squarzoni, S., Mattioli, E., Bertini, E., Pepe, G. and Chu, M. L. (2002). Effects on collagen VI mRNA stability and microfibrillar assembly of three *COL6A2* mutations in two families with Ullrich congenital muscular dystrophy. *J. Biol. Chem.* **277**, 43557-43564.

Zou, Y., Zhang, R. Z., Sabatelli, P., Chu, M. L. and Bönnemann, C. G. (2008). Muscle interstitial fibroblasts are the main source of collagen VI synthesis in skeletal muscle: implications for congenital muscular dystrophy types Ullrich and Bethlem. *J. Neuropathol. Exp. Neurol.* **67**, 144-154.

Zulian, A., Rizzo, E., Schiavone, M., Palma, E., Tagliavini, F., Blaauw, B., Merlini, L., Maraldi, N.M., Sabatelli, P., Braghetta, P., Bonaldo, P., Argenton, F. and Bernardi, P. (2014). NIM811, a cyclophilin inhibitor without immunosuppressive activity, is beneficial in collagen VI congenital muscular dystrophy models. *Hum. Mol. Genet*. **23**, 5353-5363.